

NSL 65-16-1  
APRIL 1966

FACILITY FORM 602

NO. 26691	(THRU)
ACCESSION NUMBER	1
70	(CODE)
CC 75041	33
(NASA CR OR TMX OR AD NUMBER)	(CATEGORY)

**FINAL REPORT**

CONTRACT NO. NAS 8-11163

GEORGE C. MARSHALL SPACE FLIGHT CENTER  
NATIONAL AERONAUTICS AND SPACE ADMINISTRATION  
HUNTSVILLE, ALABAMA

**RESEARCH AND DEVELOPMENT  
STUDY ON THERMAL CONTROL  
BY USE OF FUSIBLE MATERIALS**

BY  
E. W. BENTILLA  
K. F. STERRETT  
L. E. KARRE

GPO PRICE \$ \_\_\_\_\_

CFSTI PRICE(S) \$ \_\_\_\_\_

Hard copy (HC) 3.00

Microfiche (MF) ,75

**NORTHROP SPACE LABORATORIES**  
3401 WEST BROADWAY, HAWTHORNE, CALIFORNIA 90250

# 853 July 85

**NORTHROP CORPORATION**

NSL 65-16-1  
APRIL 1966

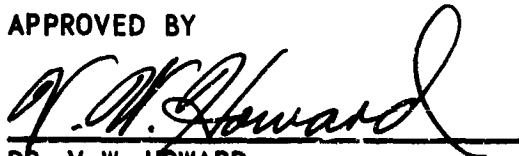
**FINAL REPORT**

CONTRACT NO. NAS 8-11163

GEORGE C. MARSHALL SPACE FLIGHT CENTER  
NATIONAL AERONAUTICS AND SPACE ADMINISTRATION  
HUNTSVILLE, ALABAMA

**RESEARCH AND DEVELOPMENT  
STUDY ON THERMAL CONTROL  
BY USE OF FUSIBLE MATERIALS**

APPROVED BY



DR. V. W. HOWARD  
VICE PRESIDENT  
AND  
MANAGER  
SYSTEMS DEPARTMENT

**NORTHROP SPACE LABORATORIES**  
3401 WEST BROADWAY, HAWTHORNE, CALIFORNIA 90250

**NORTHROP CORPORATION**

## FOREWORD

This report covers a research and development study program conducted from March 1964 to March 1966 for the purpose of developing techniques and design data for the use of fusible materials in the thermal control of spacecraft subsystems.

The study was sponsored by the George C. Marshall Space Flight Center, National Aeronautics and Space Administration, Huntsville, Alabama, under Contract No. NAS 8-11163, and was conducted under the direction of Mr. T. C. Bannister, MSFC Research Project Laboratory, Space Thermodynamics Branch. The study was initiated and continued for a year and one half under the direction of Mr. A. P. Shlosinger, Supervisor of the Temperature and Environmental Control Systems Branch, Systems Engineering Section, Northrop Space Laboratories (NSL). Upon Mr. Shlosinger's termination from Northrop, Mr. E. W. Bentilla of the same engineering group was appointed as principal investigator.

Mr. Bentilla conducted the thermal analysis and experimental verification of the temperature control systems with the support of Mr. C. Cafaro and Mr. W. Woo of the Temperature and Environmental Control Systems Branch, NSL. Mr. R. Dudley of the NSL Structures Department and Mr. G. Larsen of the Norair Manufacturing Research Department supported the design, development, and fabrication of the final fusible material packaging concept. Dr. K. F. Sterrett, Head of the NSL Space Physics and Chemistry Laboratory, conducted the supercooling study, supported by Mr. J. Jones of the NSL Space Materials Laboratory. The experimental investigation of the fusible materials thermophysical properties and the solution and phase equilibria study of binary systems were performed by Mr. L. E. Karre of the NSL Space Materials Laboratory.

This final report was prepared by Messrs. Bentilla, Sterrett, and Karre of Northrop Space Laboratories. The support of Mr. R. Schmaeman in data reduction and presentation is appreciated.

## TABLE OF CONTENTS

<u>Section</u>		<u>Page</u>
	SUMMARY .....	xiii
1	INTRODUCTION .....	1-1
2	TEMPERATURE CONTROL SYSTEMS .....	2-1
3	FUSIBLE MATERIAL SELECTION .....	3-1
	Fusible Materials Selected For Study .....	3-1
	Thermophysical Properties .....	3-2
	Liquefaction and Recrystallization .....	3-2
	Melt Point Control .....	3-3
4	SYSTEM PERFORMANCE ANALYTICAL TECHNIQUES .....	4-1
5	ONE-DIMENSIONAL ADIABATIC SYSTEM .....	5-1
	Thermal Analysis .....	5-1
	Analytical Results .....	5-2
	Parametric Analysis .....	5-2
	Verification Experiment .....	5-3
	Correlation of Analytical and Experimental Results .....	5-4
6	RADIATING FIN WITH ATTACHED FUSIBLE MATERIAL .....	6-1
	Fin Selection Analysis .....	6-1
	Radiating Fin Performance Analysis .....	6-2
	Experimental Verification .....	6-2
	Correlation of Analytical and Experimental Results .....	6-4
7	SYSTEM PERFORMANCE IMPROVEMENT .....	7-1
	Aluminum Wool Filler Materials .....	7-2
	Metallic Foam Filler Materials .....	7-3
	Simplified Analysis of a Foam-Octadecane System .....	7-3
	Metallic Honeycomb Filler Materials .....	7-3
	Model Design and Fabrication .....	7-4
	Experimental Evaluation of System Improvement Models .....	7-6
	Correlation of Test Results .....	7-7
	Analysis of Test Results .....	7-8
	Summary of Experimental Results .....	7-8
	Comparison of Test Results and Simplified Analytical Model .....	7-9
8	SUPERCOOLING .....	8-1
	Fundamental Nucleation Theory .....	8-1
	Effect of Weightlessness .....	8-4
	Experimental Investigation of Supercooling and Nucleation in Paraffins .....	8-6

## TABLE OF CONTENTS (Continued)

<u>Section</u>		<u>Page</u>
9	PHASE EQUILIBRIA STUDY OF BINARY ALIPHATIC HYDROCARBON SYSTEMS . . . . .	9-1
	Experimental Procedure . . . . .	9-1
	Experimental Results . . . . .	9-2
	Discussion of Results . . . . .	9-4
10	CONCLUSIONS AND RECOMMENDATIONS. . . . .	10-1
	Temperature Control Systems . . . . .	10-1
	Crystal Growth Phenomena and the Effects of Zero Gravity. . . . .	10-2
	Applicable Fusible Materials . . . . .	10-3
	REFERENCES . . . . .	11-1

## LIST OF ILLUSTRATIONS

<u>Figure</u>		<u>Page</u>
2-1	Typical Applications of Fusible Materials for Thermal Control . . . . .	2-3
3-1	Energy and Temperature for Solid-Liquid Phase Change and Solid-Solid Transition of n-Paraffins, From C <sub>14</sub> to C <sub>36</sub> . . . . .	3-9
3-2	Density and Specific Heat of Selected n-Paraffins . . . . .	3-10
3-3	Vapor Pressure and Thermal Conductivity of Selected n-Paraffins . . . . .	3-11
4-1	Analytical Models for the Selected Temperature Control Systems . . . . .	4-2
5-1	Simple and One Dimensional Adiabatic System Performance With Four n-Paraffins as Fusible Materials . . . . .	5-6
5-2	Temperature and Melt Thickness Parameters Versus Time Parameter for Melting of Semi-Infinite Slabs . . . . .	5-7
5-3	Metallic Bellows Adiabatic Test Model . . . . .	5-8
5-4	Assembled Simple Adiabatic Test Model . . . . .	5-9
5-5	Three Foot Vacuum Chamber Facility . . . . .	5-10
5-6	Comparison of Analytical and Test Results - Simple Adiabatic Model . . .	5-11
5-7	Temperature History of Metallic Bellows Test Model for Test Run No. 6 . . . . .	5-12
5-8	Power Histogram for Test Run No. 6 - Simple Adiabatic Bellows Model . . . . .	5-13
5-9	Comparison of Test Runs With Equal Power Input - Cold Plate Tempera- ture History . . . . .	5-14
5-10	Comparison of Analytical and Test Results - Thickness of Melted Fusible Material . . . . .	5-15
6-1	Root Temperature History of a Radiating Fin With and Without Attached Fusible Material . . . . .	6-5
6-2	Root Temperature History of a Radiating Fin With and Without Attached Fusible Material at 50 Watts/Ft of Fin Root (164 Watts/m) . . . . .	6-6
6-3	Radiating Fin With Attached Fusible Material Test Model . . . . .	6-7
6-4	Radiating Fin With Attached Fusible Material - Fill and Vent Ports Before and After Filling . . . . .	6-8
6-5	Solid Aluminum Radiating Fin Test Model . . . . .	6-9
6-6	Radiating Fin Test Model Installed in Insulating Glove . . . . .	6-10
6-7	Installation for Two Radiating Fin Models . . . . .	6-11
6-8	Radiating Fin Models After Test . . . . .	6-12
6-9	Resultant Fin Root Temperature History for Two Equal Weight Radiating Fins (One With Attached Fusible Material, One of Solid Aluminum) Ener- gized by Heat Pulses of 25 Watt <sup>2</sup> /Ft of Fin Root With Various Cooling Periods (Run 2) . . . . .	6-13

LIST OF ILLUSTRATIONS (Continued)

<u>Figure</u>		<u>Page</u>
6-10	Resultant Fin Root Temperature History for Two Equal Weight Radiating Fins (One With Attached Fusible Material, One of Solid Aluminum) Energized by Heat Pulses of 50 Watts/Ft of Fin Root With Various Cooling Periods (Run 3) . . . . .	6-16
6-11	Resultant Fin Root Temperature History for Two Equal Weight Radiating Fins (One With Attached Fusible Material, One of Solid Aluminum) Energized by Heat Pulses of 75 Watts/Ft of Fin Root With Various Cooling Periods (Run 4) . . . . .	6-19
6-12	Temperature Distribution for Two Equal Weight Radiating Fins (One With Attached Fusible Material, One of Solid Aluminum) for a 25 Watts/Ft of Fin Root Heat Pulse and a Zero Watt Cooling Period (Run 2, 3rd Heat Pulse) . . . . .	6-21
6-13	Temperature Distribution for Two Equal Weight Radiating Fins (One With Attached Fusible Material, One of Solid Aluminum) for a 25 Watts/Ft of Fin Root Heat Pulse and a 5.9 Watts/Ft Cooling Period (Run 2, 6th Heat Pulse) . . . . .	6-22
6-14	Temperature Distribution for Two Equal Weight Radiating Fins (One With Attached Fusible Material, One of Solid Aluminum) for a 50 Watts/Ft of Fin Root Heat Pulse and a Zero Watt Cooling Period (Run 3, 3rd Heat Pulse) . . . . .	6-23
6-15	Temperature Distribution for Two Equal Weight Radiating Fins (One With Attached Fusible Material, One of Solid Aluminum) for a 50 Watts/Ft of Fin Root Heat Pulse and a 2.9 Watts/Ft Cooling Period (Run 3, 4th Heat Pulse) . . . . .	6-24
6-16	Temperature Distribution for Two Equal Weight Radiating Fins (One With Attached Fusible Material, One of Solid Aluminum) for a 75 Watts/Ft of Fin Root Heat Pulse and a Zero Watt Cooling Period (Run 4, 2nd Heat Pulse) . . . . .	6-25
6-17	Temperature Distribution for Two Equal Weight Radiating Fins (One With Attached Fusible Material, One of Solid Aluminum) for a 75 Watts/Ft of Fin Root Heat Pulse and a 1.5 Watts/Ft Cooling Period (Run 4, 3rd Heat Pulse) . . . . .	6-26
6-18	Comparison of Analytical and Experimental Results for Radiating Fin With Attached Fusible Material . . . . .	6-27
6-19	Comparison of Analytical and Experimental Results for Equal Weight, Solid Aluminum Radiating Fin . . . . .	6-28
7-1	Metallic Wood and Foam Filler Materials Investigated to Improve Thermal Diffusivity . . . . .	7-11
7-2	Aluminum Honeycomb Filler Materials Used to Improve Thermal Diffusivity	7-12
7-3	Adiabatic Test Model Filled With 10% Aluminum Wool . . . . .	7-13
7-4	Adiabatic Test Model Filled With 18% Aluminum Wool . . . . .	7-14
7-5	Aluminum Wool Models . . . . .	7-15
7-6	Test Results of Adiabatic Model Filled With 10% by Volume Aluminum Wool . . . . .	7-16

LIST OF ILLUSTRATIONS (Continued)

<u>Figure</u>		<u>Page</u>
7-7	Test Results of Adiabatic Model Filled With 18% by Volume Aluminum Wool . . . . .	7-17
7-8	Improvement of Adiabatic System Performance; Simplified One-Dimensional Analytical Model; Aluminum Foam and Fusible Material With Infinite Cross Conduction . . . . .	7-18
7-9	Thermophysical Properties Used for the Improved - Adiabatic - System Analysis Incorporating Aluminum Foam . . . . .	7-19
7-10	Weight Estimate for Improved Adiabatic System Incorporating Aluminum Foam and Honeycomb Filler Materials . . . . .	7-19
7-11	Fin Spacing for Regular Hexagonal Honeycomb and Estimated Fin Spacing for Optimum Weight Performance. . . . .	7-20
7-12	Adiabatic Test Models (Dwg. No. 126-00100) With Metallic Foam and Honeycomb Filler Materials . . . . .	7-21
7-13	Ruptured Copper Foam (30 Cells/in.) Model. . . . .	7-22
7-14	Nominal Honeycomb Sheet Thickness and Spacing of the System Improvement - Adiabatic - Test Models . . . . .	7-23
7-15	A System Improvement - Adiabatic - Model Ready for Test. . . . .	7-24
7-16	Installation of System Improvement - Adiabatic - Model in Vacuum Chamber	7-25
7-17	Test Results, Run 1, for an Adiabatic Test Model With a Structural Adhesive. Fusible Material Is Octadecane With Aluminum Honeycomb Filler Material ( t = .0048 cm, .0019 in. ), 10.8% of Total Void Volume . .	7-26
7-18	Test Results, Run 1, for an Adiabatic Test Model With a High Conductivity Adhesive. Fusible Material Is Octadecane With Aluminum Honeycomb Filler Material ( t = .0048 cm, .0019 in. ), 10.8% of Total Void Volume . . . . .	7-27
7-19	Test Results, Run 2, for Two Adiabatic Test Models With Different Adhesives. Fusible Material Is Octadecane With Aluminum Honeycomb Filler Material ( t = .0048 cm, .0019 in. ), 10.8% of Total Void Volume . .	7-28
7-20	Test Results, Run 3, for Two Adiabatic Test Models With Different Adhesives. Fusible Material Is Octadecane With Aluminum Honeycomb Filler Material ( t = .0048 cm, .0019 in. ), 10.8% of Total Void Volume . .	7-29
7-21	Test Results, Run 4, for Two Adiabatic Test Models With Different Adhesives. Fusible Material Is Octadecane With Aluminum Honeycomb Filler Material ( t = .0048 cm, .0019 in. ), 10.8% of Total Void Volume . .	7-30
7-22	Test Results, Run 5, for Two Adiabatic Test Models With Different Adhesives. Fusible Material Is Octadecane With Aluminum Honeycomb Filler Material ( t = .0048 cm, .0019 in. ), 10.8% of Total Void Volume . .	7-31
7-23	Test Results, Run 6, for an Adiabatic Test Model With a Structural Adhesives. Fusible Material Is Octadecane With Aluminum Honeycomb Filler Material ( t = .0048 cm, .0019 in. ), 10.8% of Total Void Volume . .	7-32
7-24	Correlation of Test Results for Two System Improvement - Adiabatic - Test Models With Different Adhesives. Fusible Material - Octadecane, Filler Material - Aluminum Honeycomb ( t = .0048 cm, .0019 in. ), 10.8% of Total Void Volume . . . . .	7-33

LIST OF ILLUSTRATIONS (Continued)

<u>Figure</u>		<u>Page</u>
7-25	Performance Comparison for Various Analytical and Test Adiabatic Models With an Equal Total Energy Input. Fusible Material Is Octadecane . . . . .	7-34
7-26	System Improvement Adiabatic Test Results, Fusible Material - Octadecane, Model 126-00100-1, Mod 1 . . . . .	7-35
7-27	System Improvement Adiabatic Test Results, Fusible Material - Octadecane, Model 126-00100-7, Mod 1 . . . . .	7-36
7-28	System Improvement Adiabatic Test Results, Fusible Material - Octadecane, Model 126-00100-9, Mod 1 . . . . .	7-37
7-29	System Improvement Adiabatic Test Results, Fusible Material - Octadecane, Model 126-00100-13, Mod 1 . . . . .	7-38
7-30	System Improvement Adiabatic Test Results, Fusible Material - Octadecane, Model 126-00100-15, Mod 1 . . . . .	7-39
7-31	System Improvement Adiabatic Test Results, Fusible Material - Octadecane, Model 126-00100-19, Mod 1 . . . . .	7-40
7-32	System Improvement Adiabatic Test Results, Fusible Material - Tetradecane, Model 126-00100-7, Mod 2 . . . . .	7-41
7-33	System Improvement Adiabatic Test Results, Fusible Material - Tetradecane, Model 126-00100-19, Mod 2 . . . . .	7-42
7-34	System Improvement Adiabatic Test Results, Fusible Material - Hexadecane, Model 126-00100-9, Mod 2 . . . . .	7-43
7-35	System Improvement Adiabatic Test Results, Fusible Material - Hexadecane, Model 126-00100-15, Mod 2 . . . . .	7-44
7-36	System Improvement Adiabatic Test Results, Fusible Material - Eicosane, Model 126-00100-11, Mod 1 . . . . .	7-45
7-37	System Improvement Adiabatic Test Results, Fusible Material - Eicosane, Model 126-00100-11, Mod 2 . . . . .	7-46
7-38	System Improvement Adiabatic Test Results, Fusible Material - Eicosane, Model 126-00100-15, Mod 1 . . . . .	7-47
7-39	Correlation of Test Results - System Improvement - Adiabatic Model - Fusible Material Octadecane, Model 126-00100-7, Mod 1 . . . . .	7-48
7-40	Correlation of Test Results - System Improvement - Adiabatic Model - Fusible Material Octadecane, Model 126-00100-9, Mod 1 . . . . .	7-49
7-41	Correlation of Test Results - System Improvement - Adiabatic Model - Fusible Material Octadecane, Model 126-00100-13, Mod 1 . . . . .	7-50
7-42	Correlation of Test Results - System Improvement - Adiabatic Model - Fusible Material Octadecane, Model 126-00100-15, Mod 1 . . . . .	7-51
7-43	Correlation of Test Results - System Improvement - Adiabatic Model - Fusible Material Octadecane, Model 126-00100-19, Mod 1 . . . . .	7-52
7-44	Correlation of Test Results - System Improvement - Adiabatic Model - Fusible Material Tetradecane, Model 126-00100-7, Mod 2 . . . . .	7-53
7-45	Correlation of Test Results - System Improvement - Adiabatic Model - Fusible Material Tetradecane, Model 126-00100-19, Mod 2 . . . . .	7-54

LIST OF ILLUSTRATIONS (Continued)

<u>Figure</u>		<u>Page</u>
7-46	Correlation of Test Results - System Improvement - Adiabatic Model - Fusible Material Hexadecane, Model 126-00100-9, Mod 2 . . . . .	7-55
7-47	Correlation of Test Results - System Improvement - Adiabatic Model - Fusible Material Hexadecane, Model 126-00100-15, Mod 2 . . . . .	7-56
7-48	Correlation of Test Results - System Improvement - Adiabatic Model - Fusible Material Eicosane, Model 126-00100-11, Mod 1 . . . . .	7-57
7-49	Correlation of Test Results - System Improvement - Adiabatic Model - Fusible Material Eicosane, Model 126-00100-11, Mod 2 . . . . .	7-59
7-50	Correlation of Test Results - System Improvement - Adiabatic Model - Fusible Material Eicosane, Model 126-00100-15, Mod 1 . . . . .	7-59
7-51	Performance Comparison of the System Improvement - Adiabatic - Test Models . . . . .	7-60
7-52	Adiabatic System Performance of the Improved Package With Aluminum Honeycomb Core and n - Paraffin Fusible Materials . . . . .	7-62
7-53	Comparison of Test Results and Simplified Analytical Model for the System Improvement Study . . . . .	7-63
8-1	Dilatometers (2) Used in Supercooling Experiments . . . . .	8-9
8-2	Cooling-Heating Cycle Illustrating Supercooling in an Aqueous n-Octadecane Dispersion (Large Dilatometer) . . . . .	8-10
8-3	Cooling-Heating Cycle Illustrating Supercooling in an Aqueous n-Octadecane + Aluminum Wool Dispersion (Large Dilatometer) . . . . .	8-11
8-4	Cooling-Heating Cycle Illustrating Supercooling in an Aqueous n-Octadecane + Aluminum Wool Dispersion (Large Dilatometer) . . . . .	8-12
8-5	Cooling-Heating Cycle Illustrating Supercooling in an Aqueous n-Hexadecane Dispersion (Large Dilatometer) . . . . .	8-13
8-6	Cooling-Heating Cycle Illustrating Supercooling in an Aqueous n-Hexadecane + Aluminum Wool Dispersion (Large Dilatometer) . . . . .	8-14
8-7	Cooling-Heating Cycle Illustrating Supercooling in an Aqueous n-Octadecane Dispersion (Small Dilatometer) . . . . .	8-15
8-8	Cooling-Heating Cycle Illustrating Supercooling in an n-Octadecane Dispersion (Small Dilatometer, Test Rerun (Figure 8-7) . . . . .	8-15
8-9	Cooling-Heating Cycle Illustrating Supercooling in an Aqueous n-Octadecane + Aluminum Wool Dispersion (Small Dilatometer) . . . . .	8-16
8-10	Cooling-Heating Cycle Illustrating Supercooling in an Aqueous n-Octadecane + Colloidal Silica Dispersion (Small Dilatometer) . . . . .	8-17
8-11	Cooling-Heating Cycle Illustrating Supercooling in an Aqueous n-Octadecane + Silica Gel Dispersion (Small Dilatometer) . . . . .	8-17
9-1	Experimental Apparatus for Solution and Phase Equilibria Study . . . . .	9-7
9-2	Heating-Cooling Curves for Pure Octacosane . . . . .	9-8
9-3	Heating-Cooling Curves for Pure Eicosane . . . . .	9-8
9-4	Heating-Cooling Curves for 80% Octacosane - 20% Eicosane Binary System . . . . .	9-9

**LIST OF ILLUSTRATIONS (Continued)**

<u>Figure</u>		<u>Page</u>
9-5	Heating-Cooling Curves for 50% Octacosane - 50% Eicosane Binary System . . . . .	9-9
9-6	Heating-Cooling Curves for 20% Octacosane - 80% Eicosane Binary System . . . . .	9-10
9-7	Heating-Cooling Curves for 8% Octacosane - 92% Eicosane Binary System . . . . .	9-10
9-8	Behavior of Pure Octacosane at One Heating Rate and Two Cooling Rates .	9-11
9-9	Temperature-Composition Phase Diagram for the Octacosane-Eicosane Binary System . . . . .	9-12
10-1	Applications of the Improved Fusible Material - Honeycomb - Adiabatic - Package to Other Passive Temperature Control Techniques. . . . .	10-4
10-2	Applications of the Improved Fusible Material - Honeycomb - Adiabatic - Package to Active Temperature Control Systems to Decrease Temperature Excursions and Allow Systems to Be Designed for Nominal Power Levels . . . . .	10-5

## LIST OF TABLES

<u>Table</u>		<u>Page</u>
3-1	Fusible Materials With a Heat of Fusion Greater than 80 Btu/lb (3.1 watt-min/gm) Listed in Order of Increasing Melt Temperatures From 40° to 150° F (4.4 to 65°C) .....	3-4
3-2	Normal Paraffins (C <sub>14</sub> H <sub>30</sub> to C <sub>40</sub> H <sub>82</sub> ) With an Even Number of Carbon Atoms .....	3-7
7-1	Repeatability of Test Results (Comparison of Results For Tests Repeated on the Same Model) .....	7-10

**BLANK PAGE**

RESEARCH AND DEVELOPMENT STUDY  
ON THERMAL CONTROL BY USE OF FUSIBLE MATERIALS

By E. W. Bentilla, K. F. Sterrett,  
and L. E. Karre

SUMMARY

This report presents the results of a two-year research and development study on the application of the melting and solidification of materials to the thermal control of space vehicle subsystems. The study program has resulted in the selection of fusible materials and the development of system concepts and packaging techniques to the point where this method of temperature control can be incorporated into thermal control subsystems.

During the first phase of the program, four candidate fusible materials (all n-paraffins) were selected. The thermophysical properties of the paraffins necessary for thermal analysis were determined, and the performance of these materials was analyzed with selected temperature control system concepts. The first system studied was adiabatic, with all the waste heat being absorbed by the fusible material. The second system concept was a space radiator with attached fusible material. In this system, the fusible material increases the thermal inertia of the radiator, thus reducing the temperature excursions resulting from high-density heat pulses. Packaging techniques were studied, and experimental verification of the systems studied was initiated. This work was summarized in an interim report (Reference 1).

The verification experiments were completed during the second phase of the program. Packaging techniques were developed and verified by experimental models, with a demonstrated improvement in system performance. This improved system performance was obtained by increasing the thermal diffusivity of the package plus the fusible material. Additional n-paraffins were selected as good candidate fusible materials for use with the developed packaging techniques. Eight n-paraffins are commercially available having a melt point range from 5 to 70°C, with melt point increments between homologues on the order of 6 to 15°C.

A supercooling study was conducted to assist in defining the effects of weightlessness on the melting and solidification process. Techniques were developed to minimize the supercooling of the selected fusible materials.

A detailed solution and phase equilibria study was performed to determine the feasibility of melt point control by mixtures of neighboring members of the homologous series of n-paraffins.

**BLANK PAGE**

## SECTION I

### INTRODUCTION

The use of fusible materials for the bulk cooling of perishables is an old concept. Fusible materials have been considered for the cooling of electronic equipment exposed to high external heat flux rates (Reference 2) and systems at elevated temperature levels (Reference 3). The application of fusible materials to spacecraft and launch vehicle thermal control shows promise for a number of reasons.

Most unmanned spacecraft rely on passive temperature control systems without the use of expendables. All the heat rejected from the vehicle must be thermally radiated at relatively low temperatures. This heat rejection method is usually acceptable on a total integrated energy basis, but temperature control problems are encountered because of the high density power dissipation periods. Fusible materials can be used to store the energy dissipated at the high power conditions at relatively constant temperature. The stored energy can then be radiated to space continuously at the same equipment temperature level.

Another application is the adiabatic system, in which a temperature-sensitive unit having only one duty cycle exceeds a temperature limit when rejecting heat to the structure of the vehicle. A fusible material package could be attached to the component to absorb the waste heat at a constant temperature level.

Long-term missions to planets with cold environments will require the conservation of waste heat to maintain equipment at reasonable temperatures during long dormant periods. This task could be accomplished with an attached fusible material package at a constant temperature level. The package would also serve to reduce the temperature rise during heat dissipation periods.

The enthalpy change that occurs during the melting and solidification of materials having a melt point close to the design environments of electronic equipment, 40 to 150° F (279 to 339°K), was investigated with the above requirements in mind. Such materials, on melting or solidifying, have enthalpy changes in the range of 100 Btu per pound (3.9 watt-min/gm). They can be applied in close contact with the devices requiring temperature control, and will absorb heat when melting or supply heat when solidifying. They can be used in combination with a radiator as a means for increasing thermal mass and thereby permit radiators to be sized for average rather than peak system heat dissipation.

When compared with the heat absorption capabilities of solids (resulting from the product of allowable temperature changes and specific heat), the heat of fusion of paraffins provides a capacity approximately two orders of magnitude higher for equal weight. When compared with liquid-to-vapor phase changes, like boiling of water to the vacuum of space, solid-to-liquid phase changes provide heat capacities an order of magnitude smaller for equal material weight.

The simplicity of the solid-to-liquid phase change system, which is entirely passive, shows a definite advantage over the liquid-to-vapor phase change system, which requires controls, tankage, heat exchangers, etc., when the total integrated energy level is low.

The objective of this study was to develop specific design data for the application of the solid-to-liquid phase change concept to spacecraft temperature control. The technical approach was to select typical temperature control problem areas where the addition or use of fusible materials showed definite advantages.

The temperature control systems (adiabatic and radiating fin) selected for study are discussed in Section 2. The selection of fusible materials (n-paraffins) is discussed in Section 3. The analytical techniques used to analyze the performance of the fusible materials in the selected temperature control system concepts are described in Section 4. Section 5 describes the analytical and experimental evaluation of the performance of these fusible materials in the simple adiabatic system. In Section 6, the performance evaluation (analytical and experimental) of octadecane attached to a radiating fin is described. The adiabatic system was used in Section 7 for developing improved packaging techniques; the filler materials used to improve thermal diffusivity were metallic wool, foam, and honeycomb. The effects of weightlessness on the liquefaction-solidification process are discussed in Section 8, and the solution and phase equilibria study in Section 9. Conclusions and recommendations resulting from this study are presented in Section 10.

In each section, the tables and figures have been grouped immediately after the text, with the tables preceding the figures.

## SECTION 2

### TEMPERATURE CONTROL SYSTEMS

Three systems or techniques using the heat of fusion for temperature control of electronic equipment are presented in Figure 2-1. These systems are all completely passive. In one system, all the waste heat is absorbed by the fusible material package. In the other two systems, fusible materials are used to increase the thermal inertia of a space radiator.

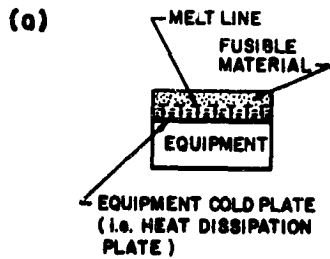
System (a) of Figure 2-1 is assumed to be adiabatic. All the waste heat given off by an electronic package is absorbed by the melting of the solid fusible material; in addition, some sensible heat is absorbed by the melted liquid material.

Systems (b) and (c) of Figure 2-1 use the heat of fusion and thermal radiation for temperature control. The fusible material melts and supplements the radiator only during high equipment heat dissipation periods and solidifies during low heat dissipation periods. System (b) has fusible material attached to the radiator fin, allowing good conductive heat transfer to the surfaces radiating to space. This arrangement allows the maximum heat rejection by radiation directly from the equipment, but decreases the temperature potential at the fin-fusible material interface because of the temperature decay along the fin.

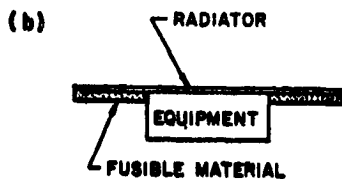
System (c) has fusible material between the equipment heat source and the radiator. The heat rejected by radiation is limited by this technique. The radiator will be at or below the fusible material melt temperature until all the material is melted, with the fusible material acting as an insulator between the heat source and the radiator. The adiabatic system (a) and the radiating fin with attached fusible material (b) were selected for further study.

In order to predict the performance of these two systems by analysis and to proceed to the design, development, and experimental performance verification of thermal control packages, data are required on suitable materials and their pertinent thermophysical properties. The effects on heat transfer of the formation of the layer of molten material which forms during heat addition can be predicted by a transient heat transfer analysis. The adiabatic system can be represented by a one-dimensional adiabatic analytical model, with heat applied at one end representing the electronic equipment. The radiating fin with the attached fusible material system is represented by a two-dimensional analytical model, with heat applied at the fin root.

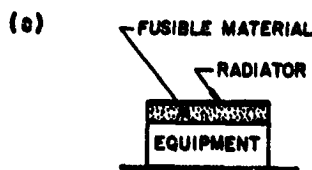
System (c) of Figure 2-1 was not analyzed in this study for the reasons mentioned above. This system, in which the fusible material package is between the heat source and the space radiator, looks promising when combined with the improved packaging technique discussed in Section 7.



All of equipment waste heat absorbed by melting fusible material (at constant temperature of fusion and zero heat exchange with environment). Fusible material selected so that its melting point is below the equipment temperature limit.



Radiator acts as a thermally conductive fin. Addition of fusible material (increased thermal mass), controls the temperature of the equipment by melting during high equipment heat loads and solidifying during low equipment heat loads.



Same as above configuration except that radiator size equals equipment cold plate. Heat must pass through fusible material. The useful amount of fusible material is limited by the trade-off between the amount of heat absorbed by the fusible material and the radiator effectiveness which is reduced due to the temperature drop across the fusible material.

FIGURE 2-1 TYPICAL APPLICATIONS OF FUSIBLE MATERIALS FOR THERMAL CONTROL

## SECTION 3

### FUSIBLE MATERIAL SELECTION

A literature search was conducted to identify fusible materials that were applicable for use in the temperature control systems selected for study. Previous efforts to use fusible materials for temperature control of electronic systems and other equipment (References 2 and 3) were reviewed for the fusible materials considered.

The selected melting temperature range for this study was 40°F to 150°F (278°K to 339°K), which covers the range of heat rejection temperatures required for most electronic equipment. Materials with a heat fusion of less than 80 Btu/lb ( $3.1 \frac{\text{watt-min}}{\text{gm}}$ ) were not considered in order to limit the materials screened to a reasonable number. Also deleted were materials that were obviously not practical for engineering applications because they were explosive, extremely corrosive, melted only under extreme pressure, etc.

The literature search and a preliminary screening resulted in a list of potential candidate fusible materials (Table 3-1). After more extensive evaluation of these materials, the normal (n-) paraffins containing from 14 to 30 carbon atoms were considered as the best candidate materials for this study. Some of the reasons for selecting the normal paraffins are as follows:

1. They have a high heat of fusion.
2. They are chemically inert and stable compounds.
3. They are nontoxic and noncorrosive.
4. Their physical properties, including low vapor pressure and volume reduction during solidification, are conducive to package design.
5. They are a family of compounds with similar properties. Consequently, their thermophysical properties are more predictable than those of other compounds, and packaging design and analytical techniques can be applied to the homologous series.

#### Fusible Materials Selected for Study

Four n-paraffins with an even number of carbon atoms, i. e., tetradecane  $C_{14}H_{30}$ , hexadecane  $C_{16}H_{34}$ , octadecane  $C_{18}H_{38}$ , and eicosane  $C_{20}H_{42}$ , were selected for further

study. The freezing temperature and heat of fusion for the n-paraffins are presented in Figure 3-1. Note that some of the paraffins also have a solid-solid crystal transition just below the freezing point. The materials selected for detailed study, containing 14, 16, 18, and 20 carbon atoms, have a heat of fusion on the order of 100 Btu/lb ( $3.9 \frac{\text{watt-min}}{\text{gm}}$ ) and do not have a solid-solid transition. The remaining even n-paraffins (even number of carbon atoms) have a transition temperature within 4°K of the freezing point, with the same level of total energy (fusion + transition) available.

Table 3-2 lists the even n-paraffins found to be commercially available; no odd n-paraffins were found to be available. These materials are difficult to isolate from neighboring members of the homologous series; note, for example, the purities obtained by Eastman (Table 3-2).

### Thermophysical Properties

The thermophysical properties, not available in the literature, of the four n-paraffins required for analytical evaluation and system design were the solid densities of all four materials and the thermal conductivity of eicosane. The properties used in the thermal analysis and package design are presented in Figures 3-2 and 3-3.

Solid densities of selected materials. - The solid densities were determined experimentally, and the average values are presented in Figure 3-2. The liquid densities of these materials were also checked experimentally, good correlation being obtained with the values in the literature. The solid density of these paraffins ( $C_{14}H_{30}$ ,  $C_{16}H_{34}$ ,  $C_{18}H_{38}$ ,  $C_{20}H_{42}$ ) appears to be erratic near the melt point, as if crystal packing variations were taking place. The data presented in Figure 3-2 are sufficiently accurate for package design; a more detailed discussion is presented in Reference 1.

Thermal conductivity. - The thermal conductivity of eicosane was estimated using two techniques, and the results are in good agreement (within 3%). The data for  $C_{14}H_{30}$  through  $C_{18}H_{38}$  were extrapolated to the 20-carbon-atom homologue, eicosane. A method presented in Reference 9 for estimating the liquid thermal conductivity of hydrocarbons was also used, (Reference 1). The average values used in the analysis are presented in Figure 3-3.

### Liquefaction and Recrystallization

The melt points of the four paraffins were checked using melting point capillary tubes immersed in a constant-temperature bath. The observed variation of the melt point of the four paraffins was less than 1°K. Observed differences between the solidification point and the melt point were also less than 1°K, indicating absence of any significant supercooling effects in this bulk form. Tests on materials obtained on different dates indicate that the melt point can vary 3°K between batches.

Supercooling of a fusible material used for passive temperature control could result in a failure of the temperature-controlled device. Therefore, excessive supercooling or

erratic supercooling is justification for not using the fusible material as a heat sink. A general analytical and experimental study on supercooling was performed, and the selected fusible materials were used for experimentation. The selected materials are difficult to supercool in the bulk form, but can be supercooled when pure fractions are isolated, as demonstrated by the use of aqueous suspensions. The effects of gravity on the liquefaction-solidification process were also investigated. This study is discussed in Section 8.

### Melt Point Control

The melting points of the available paraffins cover a wide temperature range, 280-343°K, with melt point increments between homologues on the order of 6-15°K (Table 3-2). The experimental results of the system improvement models, discussed in Section 7, indicate that temperature control can be performed with a temperature rise, or variation, on the order of 5-10°K for 80% of the liquefaction period. Therefore, control and selection of the fusible material melt point within a few degrees become of practical significance.

A solution and phase equilibria study was performed with octadecane plus eicosane, and eicosane plus octacosane. The maximum freezing point depression does not appear to be greatly below the lower melting component as with eutectic mixtures of other material systems. A solution of paraffin may be useful when thermal control is desired over a given temperature range. This study is discussed in Section 9.

TABLE 3-1

FUSIBLE MATERIALS WITH A HEAT OF FUSION GREATER THAN 80 BTU/LB (3.1 WATT-MIN/gm)  
LISTED IN ORDER OF INCREASING MELT TEMPERATURE, FROM 40 TO 150°F (4.4 TO 65°C)

NO.	MATERIAL-FORMULA	MELT PT. °F/°C	HEAT OF FUSION		REF.
			BTU/LB	WATT-MIN/gm	
1.	Tetradecane $C_{14}H_{30}$	42/5.6	98/3.8		4
2.	Formic Acid $HCOOH$	46/7.8	106/4.1		5
3.	Pentadecane $C_{15}H_{32}$	50/10	89/3.5		6
4.	Myristic Acid Ethyl Ester $CH_3(CH_2)_{12}COOC_2H_5$	51/11	80/3.1		2
5.	Acetic Acid $CH_3CO_2H$	52/17	80/3.1		5
6.	Hexadecane $C_{16}H_{34}$	64/18	102/4.0		4
7.	Lithium Chloride Ethanolate $LiCl \cdot 4C_2H_6O$	69/21	80/3.1		2
8.	n-Heptadecane $C_{17}H_{36}$	71/22	92/3.6		6
9.	d-Lactic Acid $CH_3CHOHCOOH$	79/26	80/3.1		2
10.	Octadecane $C_{18}H_{38}$	82/28	105/4.1		7
11.	13-Methyl Pentacosane $C_{26}H_{54}$	84/29	84/3.3		2
12.	Methyl Palmitate $C_{17}H_{34}O_2$	84/29	88/3.4		2
13.	Nonadecane $C_{19}H_{40}$	90/32	95/3.7		6
14.	2-Dimethyl-n-docosane $C_{24}H_{50}$	95/35	85/3.3		7
15.	Eicosane $C_{20}H_{42}$	98/37	106/4.1		4
16.	1-Tetradecanol $CH_3(CH_2)_{12}CH_2OH$	100/38	99/3.8		2
17.	Camphenilone $C_9H_{14}O$	102/39	88/3.4		2
18.	Caprylone $(CH_3(CH_2)_6)_2CO$	104/40	111/4.3		2
19.	Docosyl Promide $C_{22}H_{45}BR$	104/40	87/3.4		2

TABLE 3-1 (Continued)

FUSIBLE MATERIALS WITH A HEAT OF FUSION GREATER THAN 80 BTU/LB (3.1 WATT-MIN/gm)  
LISTED IN ORDER OF INCREASING MELT TEMPERATURE, FROM 40 TO 150°F (4.4 TO 65°C)

NO.	MATERIAL-FORMULA	MELT PT. °F/°C	HEAT OF FUSION		REF.
			BTU/LB	WATT-MIN/gm	
20.	Heneicosane $C_{21}H_{44}$	105/41	92/3.6		6
21.	7-Heptadecanone $C_{17}H_{34}O$	105/41	86/3.3		2
22.	1-Cyclohexyloctadecane $C_{24}H_{48}$	106/41	94/3.6		2
23.	4-Heptadecanone $C_{17}H_{34}O$	106/41	85/3.3		2
24.	8-Heptadecanone $C_{17}H_{34}O$	107/42	87/3.4		5
25.	Cyanamide $CH_2N_2$	111/44	90/3.5		8
26.	Docosane $C_{22}H_{46}$	112/44	107/4.1		6
27.	Methyl Eicosanate $C_{21}H_{42}O_2$	113/45	98/3.8		2
28.	Tricosane $C_{23}H_{48}$	117/47	100/3.9		6
29.	3-Heptadecanone $C_{17}H_{34}O$	118/48	93/3.6		2
30.	2-Heptadecanone $C_{17}H_{34}O$	119/48	93/3.6		2
31.	Camphene $C_{10}H_{16}$	122/50	103/4.0		8
32.	9-Heptadecanone $C_{17}H_{34}O$	123/51	91/3.5		2
33.	Tetracosane $C_{24}H_{50}$	124/51	109/4.2		6
34.	Elaidic Acid $C_{18}H_{34}O_2$	124/51	94/3.6		8
35.	Methyl Behenate $C_{24}H_{46}O_2$	126/52	100/3.9		2
36.	Pentacosane $C_{25}H_{52}$	129/54	102/4.0		6
37.	Ethyl Lignocerate $C_{26}H_{52}O_2$	129/54	93/3.6		2

TABLE 3-1 (Continued)

FUSIBLE MATERIALS WITH A HEAT OF FUSION GREATER THAN 80 BTU/LB (3.1 WATT-MIN/gm)  
LISTED IN ORDER OF INCREASING MELT TEMPERATURE, FROM 40 TO 150°F (4.4 TO 65°C)

NO.	MATERIAL-FORMULA	MELT PT. °F/°C	HEAT OF FUSION BTU/LB WATT-MIN/gm	REF.
38.	Hypo Phosphoric Acid $H_4P_2O_6$	131/55	92/3.6	2
39.	n-Hexacosane $C_{26}H_{54}$	133/56	110/4.3	6
40.	Trimyristin $(C_{13}H_{27}COO)_3C_3H_3$	91/33 135/57	87/3.4 91/3.5	2
41.	Myristic Acid $C_{13}H_{27}COOH$	135/57	86/3.3	2
42.	Heptacosane $C_{27}H_{56}$	138/59	101/3.9	6
43.	Ethyl Cerotate $C_{28}H_{56}O_2$	140/60	96/3.7	2
44.	Octacosane $C_{28}H_{58}$	142/61	109/4.2	6
45.	Nonacosane $C_{29}H_{60}$	147/64	103/4.0	6
46.	Stearic Acid $C_{17}H_{35}CO_2H$	148/64	86/3.3	5
47.	Triacontane $C_{30}H_{62}$	150/65	108/4.2	6

TABLE 3.2

## NORMAL PARAFFINS

C<sub>14</sub>H<sub>30</sub> TO C<sub>40</sub>H<sub>82</sub>

## WITH AN EVEN NUMBER OF CARBON ATOMS

Compound	Formula	Freezing Point - °C (In Air at 1 Atm.)	Material Can Be Supplied	Availability	Melt Pt. Variation and Purity	Approx. Cost/Kg.
n-Tetradecane	CH <sub>3</sub> (CH <sub>2</sub> ) <sub>12</sub> CH <sub>3</sub>	5.6	Yes	In Stock	2-4°C (5.5-7°C) 92.3%	\$19.00
n-Hexadecane	CH <sub>3</sub> (CH <sub>2</sub> ) <sub>14</sub> CH <sub>3</sub>	16.7	Yes	"	17-18°C (17.5-18.5°C) 97.3%	\$18.50
n-Octadecane	CH <sub>3</sub> (CH <sub>2</sub> ) <sub>16</sub> CH <sub>3</sub>	27.8	Yes	"	27-28.5°C (28-28.5°C) 99+%	\$18.50
n-Eicosane	CH <sub>3</sub> (CH <sub>2</sub> ) <sub>18</sub> CH <sub>3</sub>	36.7	Yes	"	35.5-37.5°C (35-36°C) 97%	\$158.25
n-Docosane	CH <sub>3</sub> (CH <sub>2</sub> ) <sub>20</sub> CH <sub>3</sub>	44.4	No	?		
n-Tetracosane	CH <sub>3</sub> (CH <sub>2</sub> ) <sub>22</sub> CH <sub>3</sub>	51.1	Yes	In Stock	48-50°C (48-50°C) 96%	\$318.50

Note: (1) The listed freezing points are from Selected Values of Physical and Thermodynamic Properties of Hydrocarbons and Related Compounds, American Petroleum Institute Research Project 44, Carnegie Press, Pittsburgh, Pennsylvania, 1953.

(2) The reason why the specific unavailable compounds could not be supplied was not stated. A review of the available data indicates a shortage of raw material from which these compounds could be economically processed.

(3) Information courtesy of Eastman Organic Chemicals - 14 December, 1965.

Top melt pt. - Eastman specifications, actual melt point will not fall below this value.

( ) melt pt. - Eastman's last batch

% - purity last batch (analyzed by gas chromatography), a guide to practical purification limitation.

TABLE 3-2 (Cont.)

## NORMAL PARAFFINS

C<sub>14</sub>H<sub>30</sub> TO C<sub>40</sub>H<sub>82</sub>

## WITH AN EVEN NUMBER OF CARBON ATOMS

Compound	Formula	Freezing Point - °C (In Air at 1 Atm.)	Material Can Be Supplied	Availability	Melt Pt. (3) Variation and Purity	Approx. Cost/ Kg.
n-Hexacosane	CH <sub>3</sub> (CH <sub>2</sub> ) <sub>24</sub> CH <sub>3</sub>	56.7	Yes	In Stock	56-58°C (56-57.5°C) 90%	\$985.00
n-Octacosane	CH <sub>3</sub> (CH <sub>2</sub> ) <sub>26</sub> CH <sub>3</sub>	61.7	Yes	" "	59-61°C (61-62.5°C) 96%	\$330.00
n-Triacontane	CH <sub>3</sub> (CH <sub>2</sub> ) <sub>28</sub> CH <sub>3</sub>	65.5	No	?		
n-Dotriacontane	CH <sub>3</sub> (CH <sub>2</sub> ) <sub>30</sub> CH <sub>3</sub>	69.4	Yes	In Stock	69-70°C (69-70°C) 96%	\$339.00
n-Tetatriacontane	CH <sub>3</sub> (CH <sub>2</sub> ) <sub>32</sub> CH <sub>3</sub>	73.3	No	?		
n-Hexatriacontane	CH <sub>3</sub> (CH <sub>2</sub> ) <sub>34</sub> CH <sub>3</sub>	76.1	No	?		
n-Octatriacontane	CH <sub>3</sub> (CH <sub>2</sub> ) <sub>36</sub> CH <sub>3</sub>	78.9	No	?		
n-Tetracontane	CH <sub>3</sub> (CH <sub>2</sub> ) <sub>38</sub> CH <sub>3</sub>	81.7	No	?		

Note:

Only the paraffins with 14, 16, 18, 20, 24, 26, 28, and 32 carbon atoms have been found to be commercially available.

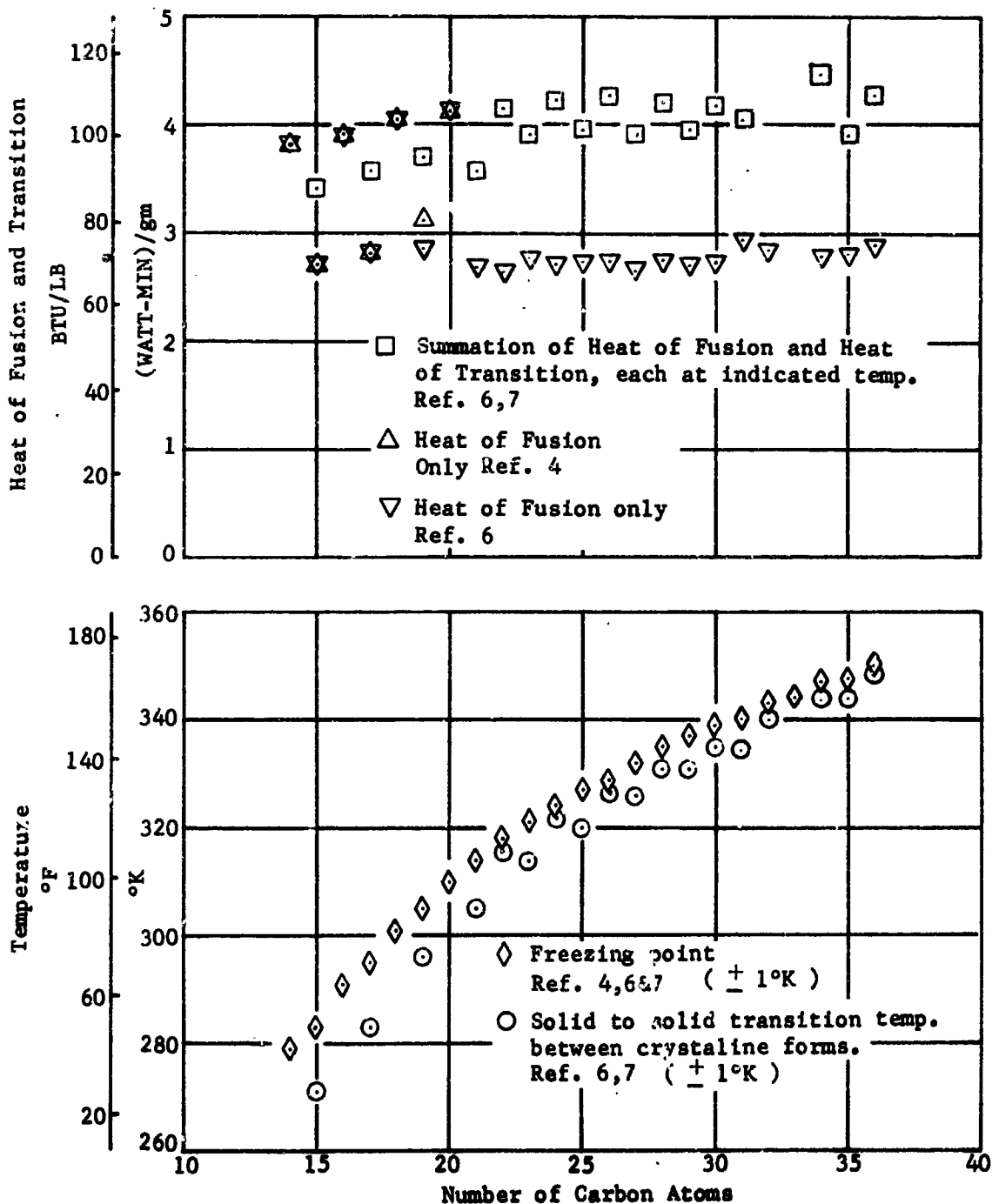


FIGURE 3-1 ENERGY AND TEMPERATURE FOR SOLID-LIQUID PHASE CHANGE AND SOLID-SOLID TRANSITION OF n-PARAFFINS, FROM C<sub>14</sub> TO C<sub>36</sub>

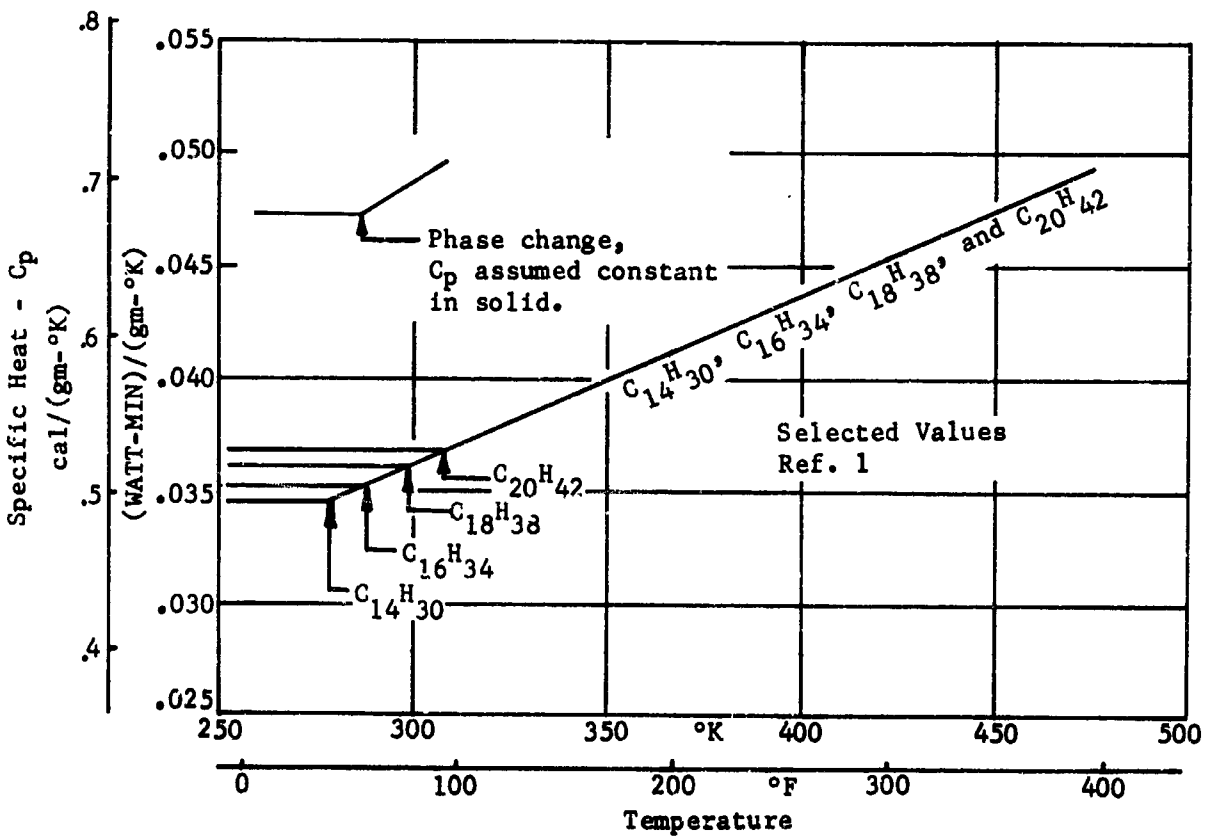
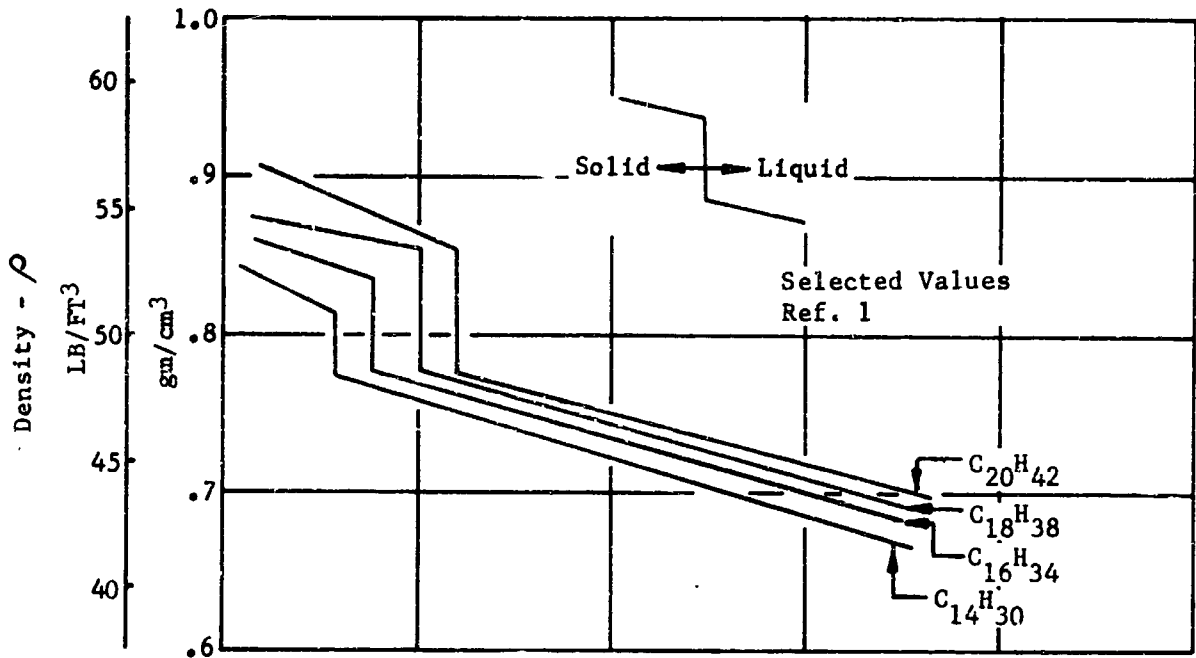


FIGURE 3-2 DENSITY AND SPECIFIC HEAT OF SELECTED n-PARAFFINS

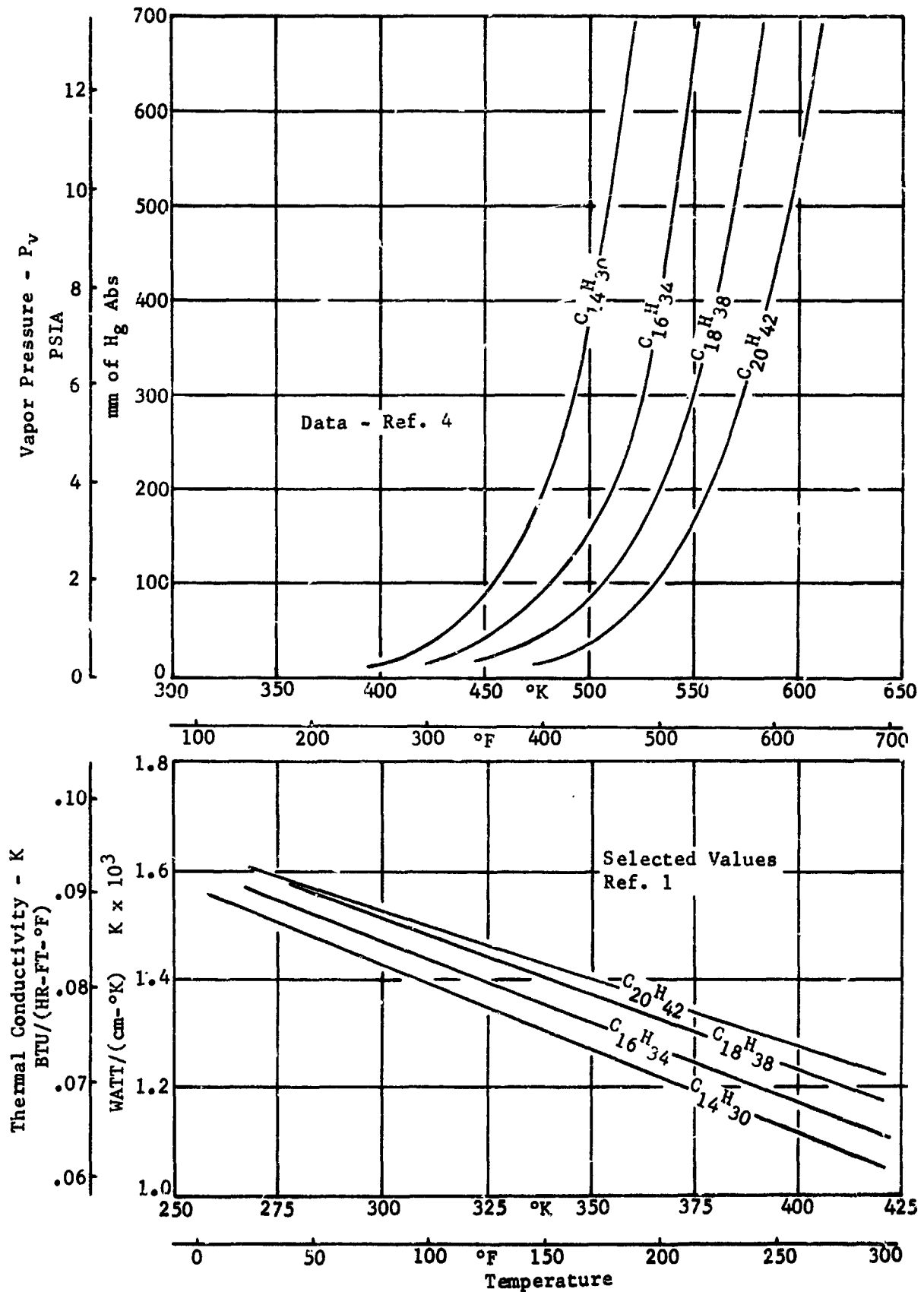


FIGURE 3-3 VAPOR PRESSURE AND THERMAL CONDUCTIVITY OF SELECTED n-PARAFFINS

**BLANK PAGE**

## SECTION 4

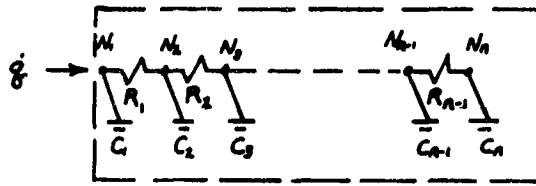
### SYSTEM PERFORMANCE ANALYTICAL TECHNIQUES

The performance analysis of the two selected methods of temperature control using fusible materials (Figure 2-1) was conducted on an IBM 7090 digital computer. A modified SHARE Thermal Network Analysis Program (Reference 10) was used. This program produces a temperature history for a physical system which has, through the concept of lumped parameters, been expressed as a finite difference electrical analog of the heat transfer problem. The physical parameters are represented by a thermal resistance-thermal capacitance network, with the capability of heat input at any of the discrete "nodes" in the network. A solution for the temperature at all nodes is calculated at the end of each of a series of finite time steps.

When any node has phase transition capability, program control is transferred to the Latent Heat Subroutine after the temperatures of all the nodes in the network have been calculated. This subroutine recalculates the node energy balance and temperature, if the node is in phase transition. The subroutine was modified from the SHARE Program (Reference 10), which did not allow for sensible temperature rise at the calculation time interval when a node passed through the transition phase. The SHARE routine was also modified so that the partial heat of transition was accounted for with a change of direction in phase transition.

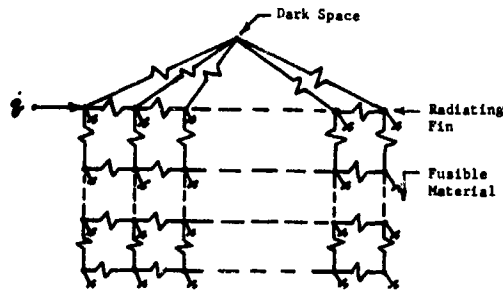
The program input-output control was changed to better suit the particular problems. A subroutine was added that calculates and prints instantaneous heat flux to any node at the print interval. These changes to the Thermal Network Analysis computer program are discussed in more detail in Reference 1.

The electrical analog networks for the one-dimensional adiabatic system and the radiating fin with attached fusible material are presented in Figure 4-1. The node size and spacing were kept continuous where possible to facilitate computer program usage. The nodes at the material boundary and heating points were reduced in size by one-half to define a " $\pi$ " network (Reference 10). This approach more closely predicts the boundary temperature by better representing the actual differential equations than is the case in a continuous network. The input parameters, thermal resistance and capacitance, were varied as a function of temperature for this analysis. Since the analysis is representing space conditions (zero g), zero convection is assumed in the molten fusible material.

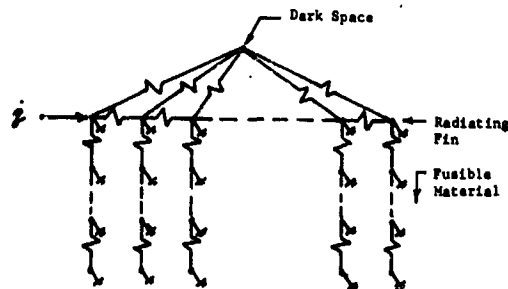


Electrical Analog  
 $\dot{q}$  = Heat Input To Node 1  
 $N$  = Nodes of Constant Temperature at Any Time Increment  
 $C$  = Node Thermal Capacity  
 $C_2 = C_3 = C_n, C_1 = C_n/2.0$   
 $R$  = Thermal Resistance  
 $R_1 = R_2 = R_n$

FIGURE 4-1a Analytical Model (1-D) Adiabatic System



Correct Electrical Analog



$\dot{q}$  = Heat Input To Node 1  
 $N$  = Nodes of Constant Temperature at Any Time Increment  
 $C$  = Node Thermal Capacity  
 $R$  = Thermal Resistance

Simplified Electrical Analog  
Used in Final Analysis

FIGURE 4-1b Analytical Model (2-D) System Of Radiating Fin With Attached Fusible Material

FIGURE 4-1 ANALYTICAL MODELS FOR THE SELECTED TEMPERATURE CONTROL SYSTEMS

## SECTION 5

### ONE-DIMENSIONAL ADIABATIC SYSTEM

A thermal analysis of a fusible material with the simple, one-dimensional adiabatic system concept presented in Figure 2-1 will define the performance capabilities and limitations of the material when it is used as a heat sink. The usefulness of a fusible material as a heat sink is also dependent on other properties, such as its capability to be handled, packaged, and resolidified.

The performance of a fusible material/heat sink system can be increased by various design techniques once the system's shortcomings are identified and the magnitude of the required improvements determined. Therefore, the initial analytical effect of this study was to predict the performance of the four selected fusible materials with the simple adiabatic system. Experimental models were then built and tested to verify the analytical results.

The performance of the selected fusible materials and a simple adiabatic system is limited by the insulating effect of the molten liquid layer. The performance of these fusible materials can be greatly increased in an improved adiabatic system, as described in Section .

#### Thermal Analysis

A transient thermal analysis of the adiabatic system (Figure 2-1), represented by the electrical analog network (Figure 4-1), was performed for the four selected fusible materials. The thermal conductance and capacitance are temperature-dependent and were calculated from the thermophysical properties in Figures 3-2 and 3-3. The additional input parameters are latent heat, melt temperature, heating rate, node size, and initial conditions. The latent heat and melt temperature are presented in Figure 3-2. This analysis was performed for a one-square-foot cross section of fusible material (semi-infinite slab), with five constant heat input rates at node 1 (Figure 4-1a), and with no heat exchange at the other boundaries. The selected node thickness was .016667 in. (.042334 cm) for node 1, and .033333 in. (.08466 cm) for the remaining nodes.

This node size was selected for the final analysis after a sensitivity analysis was performed to obtain good temperature stability (a smooth increase in the temperature of the melted material) and a steady progression of melt thickness. There is a trade-off between program stability versus computer time. The analysis became unstable when the ratio of

latent heat to heat rate  $H_L/\dot{q}$  ( $\frac{\text{Btu/node}}{\text{Btu/hour}}$ ) increased above .1. This ratio varied from approximately .015 to .075 for the heating rates and materials used in the analysis. For program stability, the computation was started with the first node  $1^\circ\text{F}$  below melt point and the following node temperatures decreasing by  $.1^\circ\text{F}$  per node.

The temperature of interest is a node 1 (Figure 4-1a). This point represents the boundary between the heat source and the fusible material and hereafter will be defined as the cold plate.

### Analytical Results

The analytical results for the cold plate temperature rise and the melt layer thickness as a function of time and constant power input are presented in Figure 5-1. Note that the temperature rise increases rapidly with an increase in input power rate. This rapid temperature rise above the melt point is caused by the insulating effect of the low-conductivity molten layer, since the fusion process is at constant temperature. This insulating effect limits the use of the simple adiabatic-paraffin system to low power rates, depending on the desired temperature control period and the temperature rise that can be tolerated.

The performance of the four n-paraffins is essentially equivalent, especially at lower levels of total input energy (i. e.,  $1500 \text{ watt-min/ft}^2$  at  $50 \text{ watts/ft}^2$  for 30 minutes to  $250 \text{ watts/ft}^2$  for 6 minutes), as shown in Figure 5-1. The lower performance capability of the n-paraffins with fewer carbon atoms ( $\text{C}_{14}\text{H}_{30}$  and  $\text{C}_{16}\text{H}_{34}$ ) is more distinct at greater total energy levels, especially at the higher flux densities ( $250 \text{ watts/ft}^2$  for 20 minutes, Figure 5-1). The variation in performance of the selected n-paraffin (cold plate temperature rise) is not significant when compared with the total temperature rise at the cold plate.

Because of the similar properties and thermal performance of these even n-paraffins, any techniques developed to improve their performance as heat sink materials should apply equally to the homologous series.

### Parametric Analysis

The computation techniques used in the analysis of the one-dimensional adiabatic model result in computer program instabilities at rates of heat flow slightly below  $50 \text{ watts/ft}^2$ . A parametric analysis, assuming constant thermophysical properties for the molten fusible material, was performed. For the heat rates below  $50 \text{ watts/ft}^2$  the melt layer temperature does not increase significantly above the melt point for a considerable period of heat addition. Therefore, the assumption of constant fluid properties for the melt will not result in a significant error.

The parametric results are presented in Figure 5-2. The temperature parameter ( $T^*$ ) can be used to calculate the temperature change across the liquid melt layer, and the melt

thickness parameter ( $\Delta X^*$ ) provides the thickness of the liquid layer as a function of time. These data were correlated with the computer results and fitted with the equations presented in Figure 5-2. The equations can be used to calculate the performance parameters, cold plate temperature rise, and melt layer thickness directly. The accuracy of these results will decrease with increasing power rate and increasing total energy input. No attempt was made to define limitations of this parametric approach.

### Verification Experiment

An experimental model was built and tested to verify the analytical results. The boundary conditions assumed for the analytical model were simulated as accurately as possible. An attempt was made to calculate out the dissimilar effects so that the analytical and experimental results could be compared directly.

The fusible material must be thermally isolated from external heat sinks and maintained in good thermal contact with the heat source (i. e. , cold plate) while the material expands and contracts as a function of temperature. The cold plate is placed above the fusible material to eliminate convection currents caused by density variation (temperature difference) and earth gravity. Octadecane was the selected test material because of the high purity available (Table 3-2), and because its melt point is slightly above room temperature.

Experimental model. - The first attempts at packaging used a silicone rubber boot to contain the fusible material in good contact with the cold plate and to allow for expansion and contraction with temperature variation. A moldable elastomeric container was initially selected over a metallic bellows to develop packaging techniques that could be applied to various shapes. Problems were encountered, however, with leakage and tearing of the boots. By the time a model was developed to satisfactorily contain the fusible material, the thermal mass was excessive for reliable thermal experimentation.

A stainless steel bellows model (Figures 5-3 and 5-4) was constructed and tested to simulate the adiabatic system. The bellows model was calibrated for spring rate. The model was filled with octadecane at 105 °F (314 °K) to 12 psig, resulting in a bellows expansion ratio at 14%. With the octadecane solidified, the bellows is still 6% expanded, exerting a pressure of 5-6 psig on the fusible material.

The three-foot-diameter vacuum chamber shown in Figure 5-5 was used for all the system performance testing. The chamber has an internal shroud for liquid nitrogen cooling. Since the vacuum chamber was only used to thermally isolate the adiabatic models, the chamber walls were kept at room temperature.

Ten test runs were made with the metallic bellows model (Figure 5-4) for verification of the one-dimensional adiabatic system. The tests were conducted in a vacuum of  $10^{-5}$  torr, with the model insulated in 30 layers of aluminized mylar. The model was suspended by thin cords to reduce heat leaks.

Experimental results. - The cold plate temperature histories obtained by test and by analysis are presented for comparison in Figure 5-6. The test results indicate somewhat better performance than the analysis, i. e., less cold plate temperature rise as a function of heat rate and time. For these data curves, electrical heat inputs have been corrected by subtracting the heat losses to the environment and the heat required to raise the package and heater temperature. Thus, a corrected heat input rate to the fusible material was obtained.

The complete model temperature history for Test Run 6 is presented in Figure 5-7. Note that the temperatures at thermocouples 6 and 8 indicate that liquefaction (melt point = 300°K) has occurred. The power histogram is shown in Figure 5-8. The heat stored by the container and heater was determined to be less than 15% of the total heat input. The heat loss to the external environment and through the electrical leads was calculated to be only a few percent. The same test conditions were used for Runs 5 and 6. A comparison of the cold plate temperature rise is shown in Figure 5-9. The test results were in good agreement with the analysis for a 10-minute period. At this time, the test results deviated, demonstrating better performance than the analytical results.

A comparison of the thickness of the melted fusible material obtained by test and analysis is presented in Figure 5-10. The data from thermocouple 6 are in good agreement with the analytical results. Heat transfer in the stainless steel bellows will not significantly change the time of melting because of the long heat path in the bellows (Figure 5-3). The thermal resistance of the bellows is greater than that of the fusible material from the cold plate to the location of thermocouple 6. The distance of thermocouple 8 from the cold plate cannot be accurately determined because the top and bottom plates warped when they were silver-soldered and also buckled slightly under pressurization. This distance is approximately  $.47 \pm .05$  in. ( $1.19 \pm .1$  cm), (Figures 5-3 and 5-10).<sup>1</sup>

#### Correlation of Analytical and Experimental Results

The majority of the total energy absorbed by this system is accomplished by phase change. A small percentage of the total energy is used to raise the temperature of the molten fusible material. The good correlation for melt depth (total energy) indicates that the heat transfer parameters should be questioned. Some temperature lag is induced by the package even though the heat stored therein has been calculated out of the results. The nominal bellows cross sectional area used in data comparison and the fin effect of the stainless steel bellows can also induce a small error that is difficult to correct. Another questionable parameter is the thermal conductivity. The test results would indicate a higher conductivity than that used in the analysis.

The findings of Thomas and Westwater (Reference 11) reveal an interesting area effect when working with the same material system, octadecane. They report on a microscopic study of the solid-liquid interface during melting and freezing. The interface was populated

with microscopic bumps and valleys which increased in height with an increase in heat flux. In the analytical model, the solid-liquid interface is a semi-infinite plane. The increase in surface area at the melt interface, caused by surface roughness, would result in better cold plate temperature performance, as predicted by the test results.

Fusible Material			Melt Pt.
I.D.	Name	Formula	°K
A	Tetradecane	C <sub>14</sub> H <sub>30</sub>	278
B	Hexadecane	C <sub>16</sub> H <sub>34</sub>	289
C	Oct. decane	C <sub>18</sub> H <sub>38</sub>	300
D	Eicosane	C <sub>20</sub> H <sub>42</sub>	310

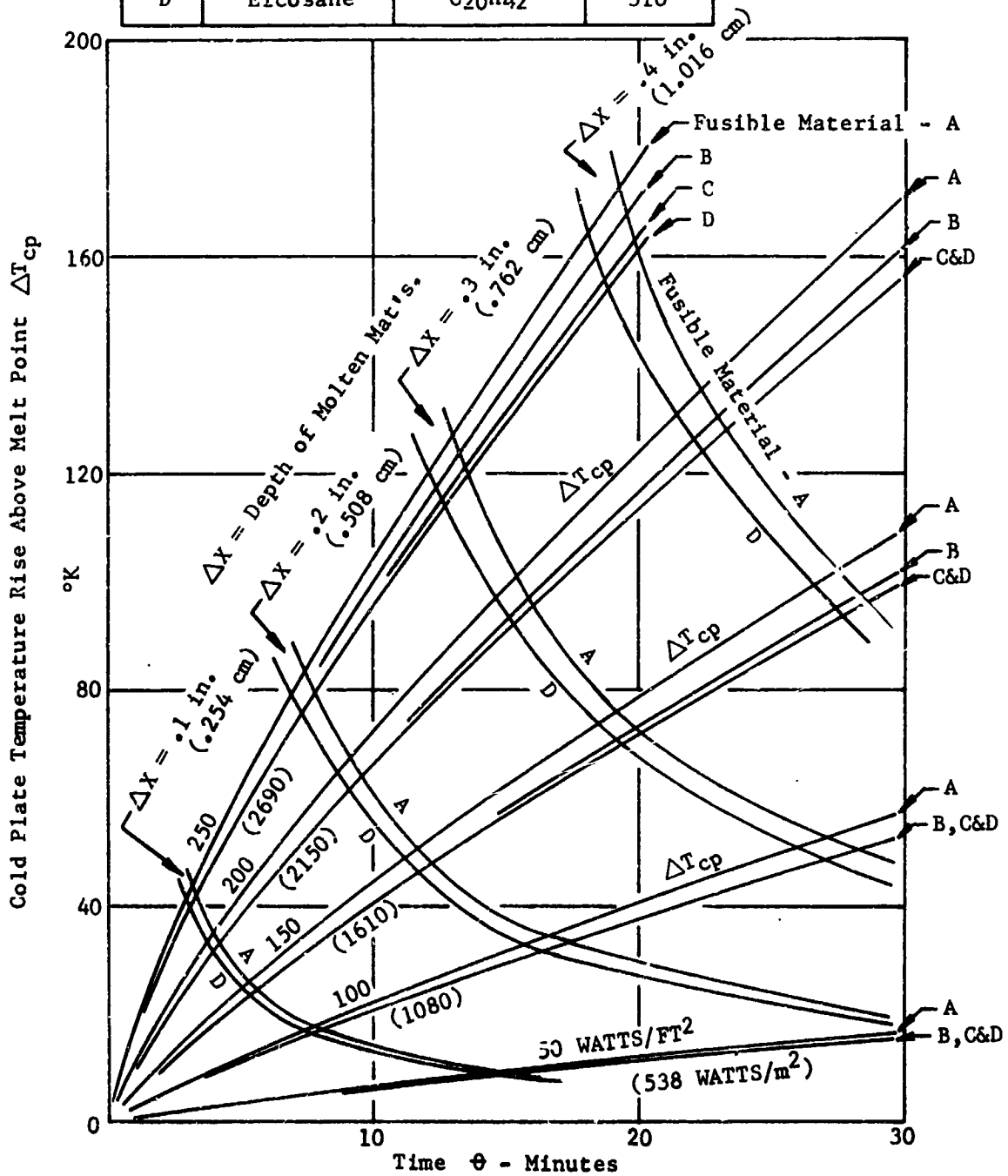


FIGURE 5-1 SIMPLE AND ONE DIMENSIONAL ADIABATIC SYSTEM PERFORMANCE WITH FOUR n-PARAFFINS AS FUSIBLE MATERIALS

Assumptions:

1. Constant Heat Input
2. Material Properties Constant & at Melt Point
3. Slab at Time Zero is at  $T_{Melt}$
4. Zero Heat Conducted Through Solid
5. Zero Convection

Symbols:

- H = Heat of Fusion - BTU/Lb  
 $\rho$  = Density - Lb/Ft<sup>3</sup>  
 $C_p$  = Specific Heat - BTU/Lb-°F  
 $a$  = Thermal Diffusivity - Ft<sup>2</sup>/Hr  
 $q/A$  = Heat Rate Per Unit Area - BTU/HR-Ft<sup>2</sup>  
 $k$  = Thermal Conductivity - BTU/HR-Ft-°F  
 $\theta$  = Time - Hrs.  
 $\Delta X$  = Melt Thickness - Ft.  
 $T_{Cp}$  = Temperature at liquid Face - °F (Cold Plate)  
 $T_{Melt}$  = Melt Temperature - °F (Temperature at Liquid-Solid Interface)
- $$T^* = (T_{Cp} - T_{Melt}) / \left( \frac{H}{C_p} \right)$$
- $$\Delta X^* = \left[ \left( \frac{q/A}{k} \right) \frac{C_p}{H} \right] \Delta X$$

Fitted Equations:

$$T_{Cp} - T_{Melt} = .745 \left[ (q/A)^2 \theta \cdot \frac{1}{k \rho H^{.944} C_p^{.056}} \right]^{.947}$$

$$\Delta X = .837 \left[ (q/A)^{.927} \theta \cdot \frac{(k/C_p)^{.073}}{\rho H^{.927}} \right]^{.931}$$

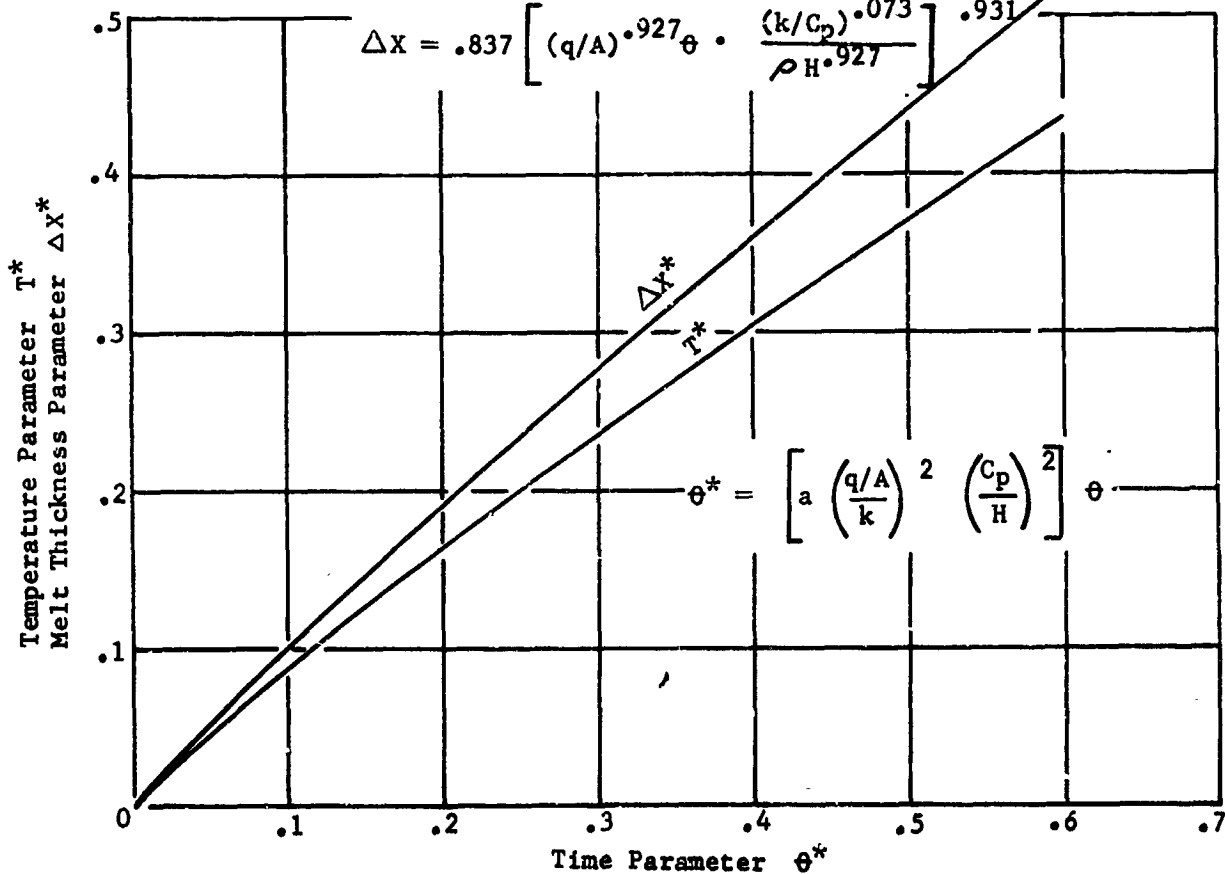


FIGURE 5-2 TEMPERATURE AND MELT THICKNESS PARAMETERS VERSUS TIME PARAMETER FOR MELTING OF SEMI-INFINITE SLABS



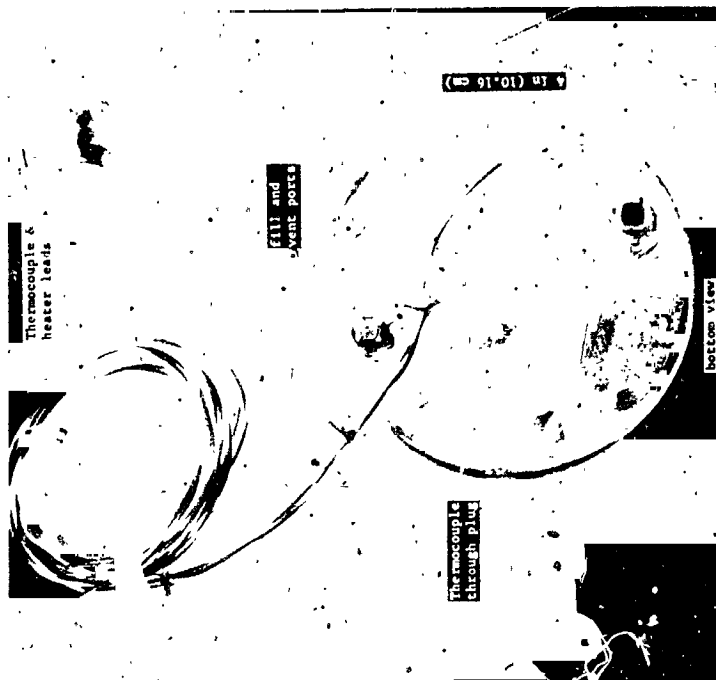
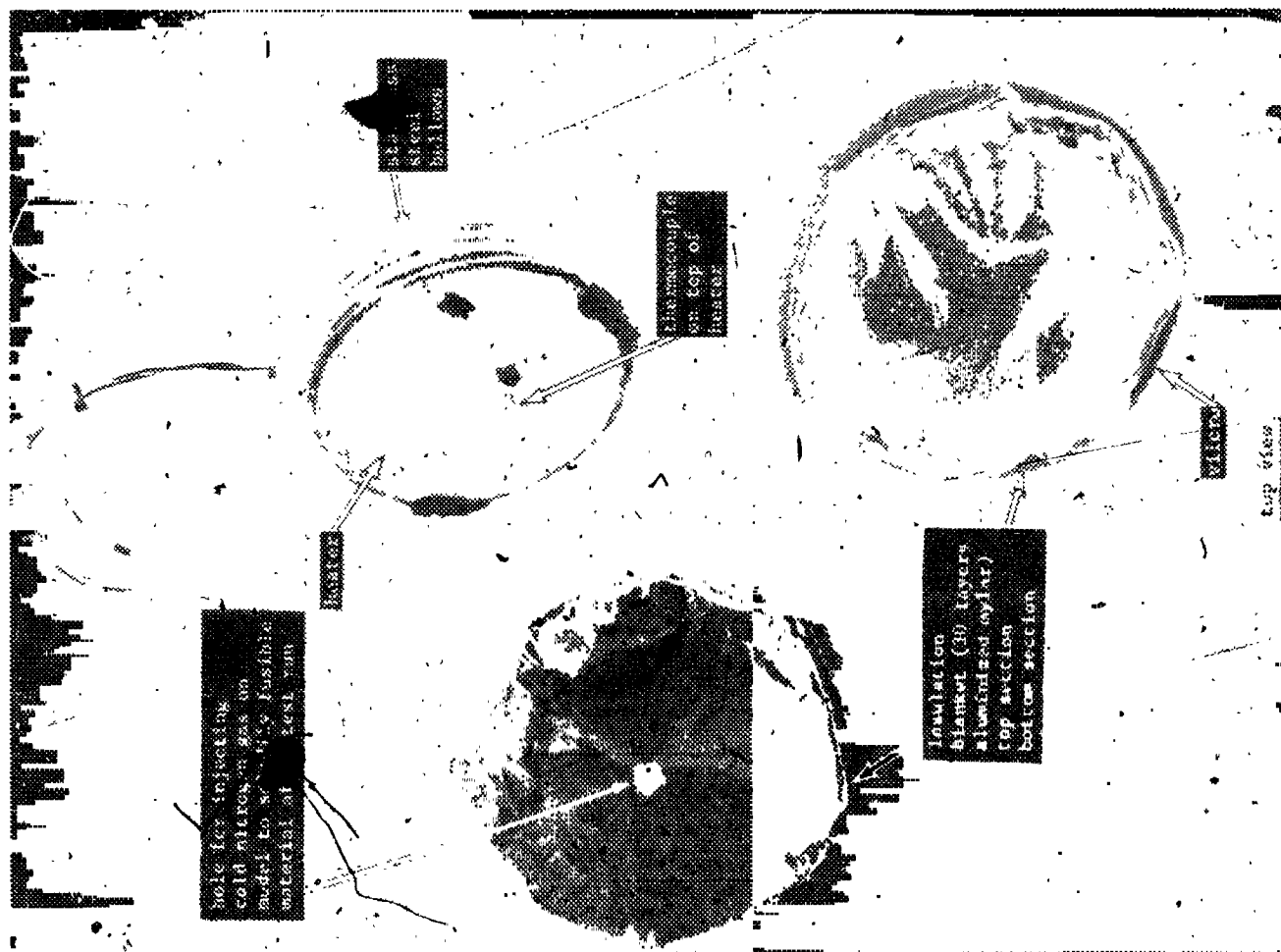


FIGURE 5-4 ASSEMBLED SIMPLE ADIABATIC TEST MODEL

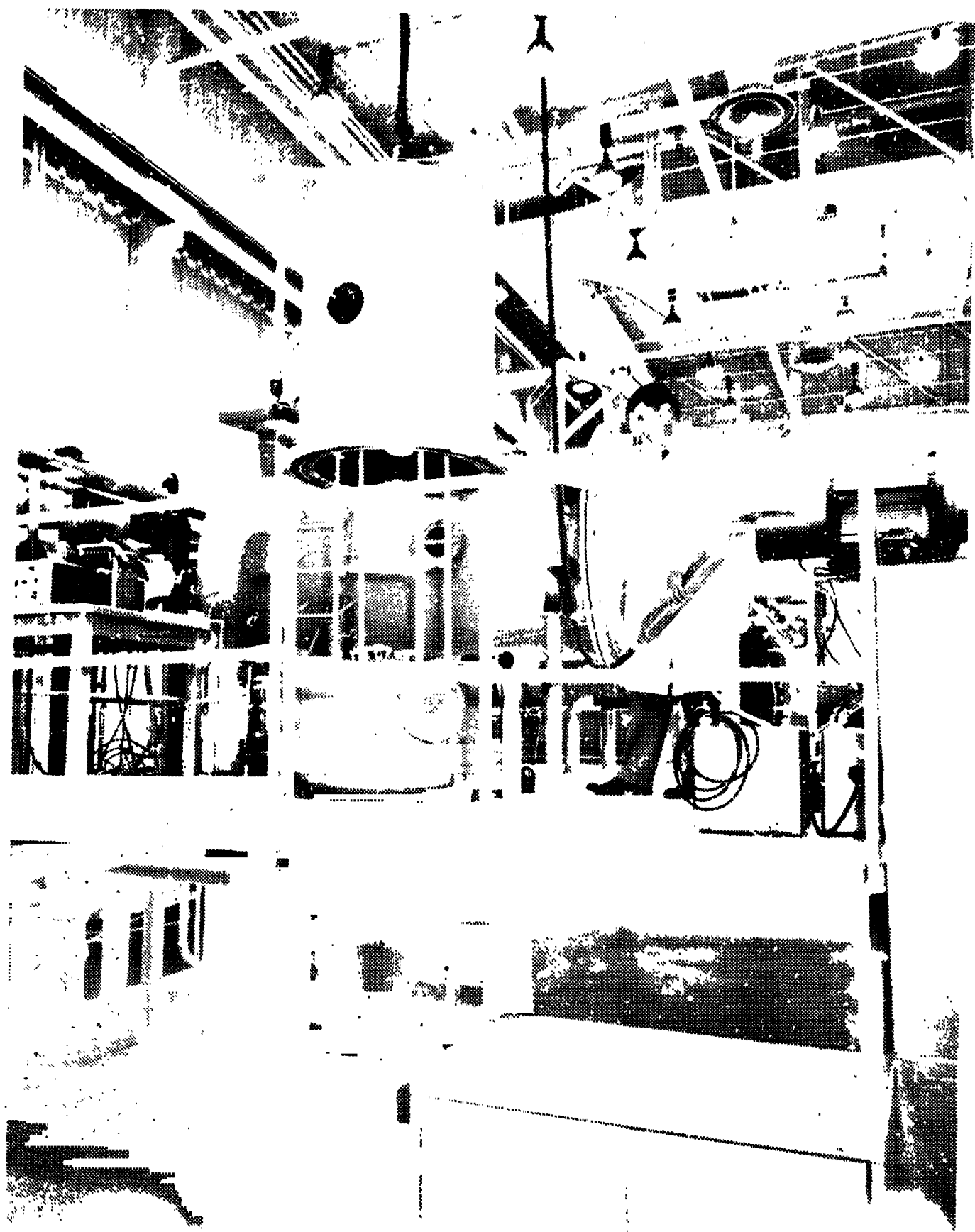


FIGURE 5-5 THREE FOOT VACUUM CHAMBER FACILITY

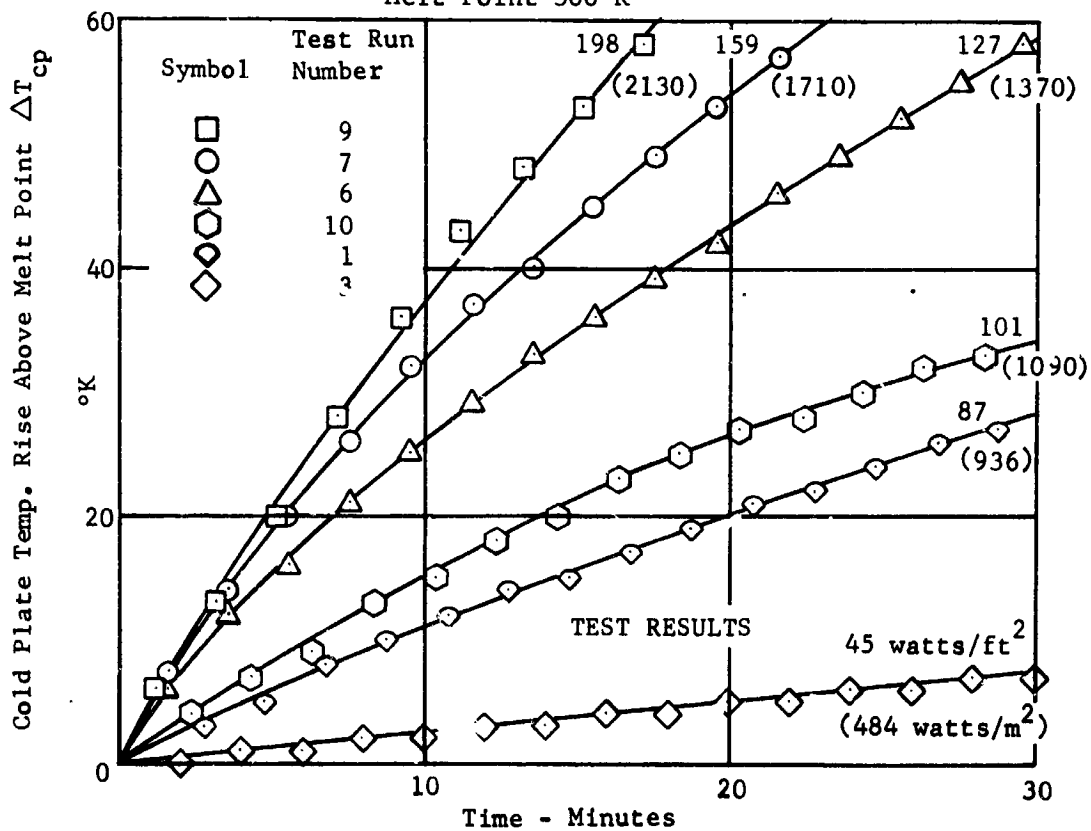
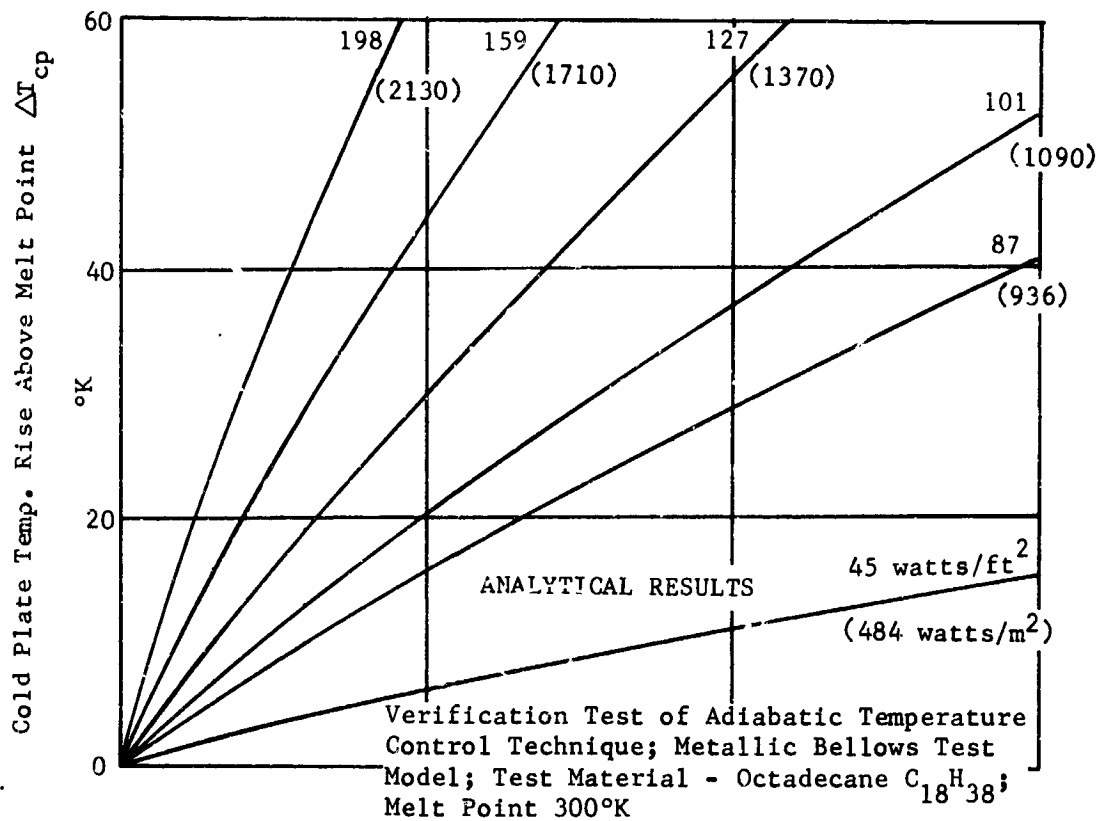


FIGURE 5-6 COMPARISON OF ANALYTICAL AND TEST RESULTS - SIMPLE ADIABATIC MODEL

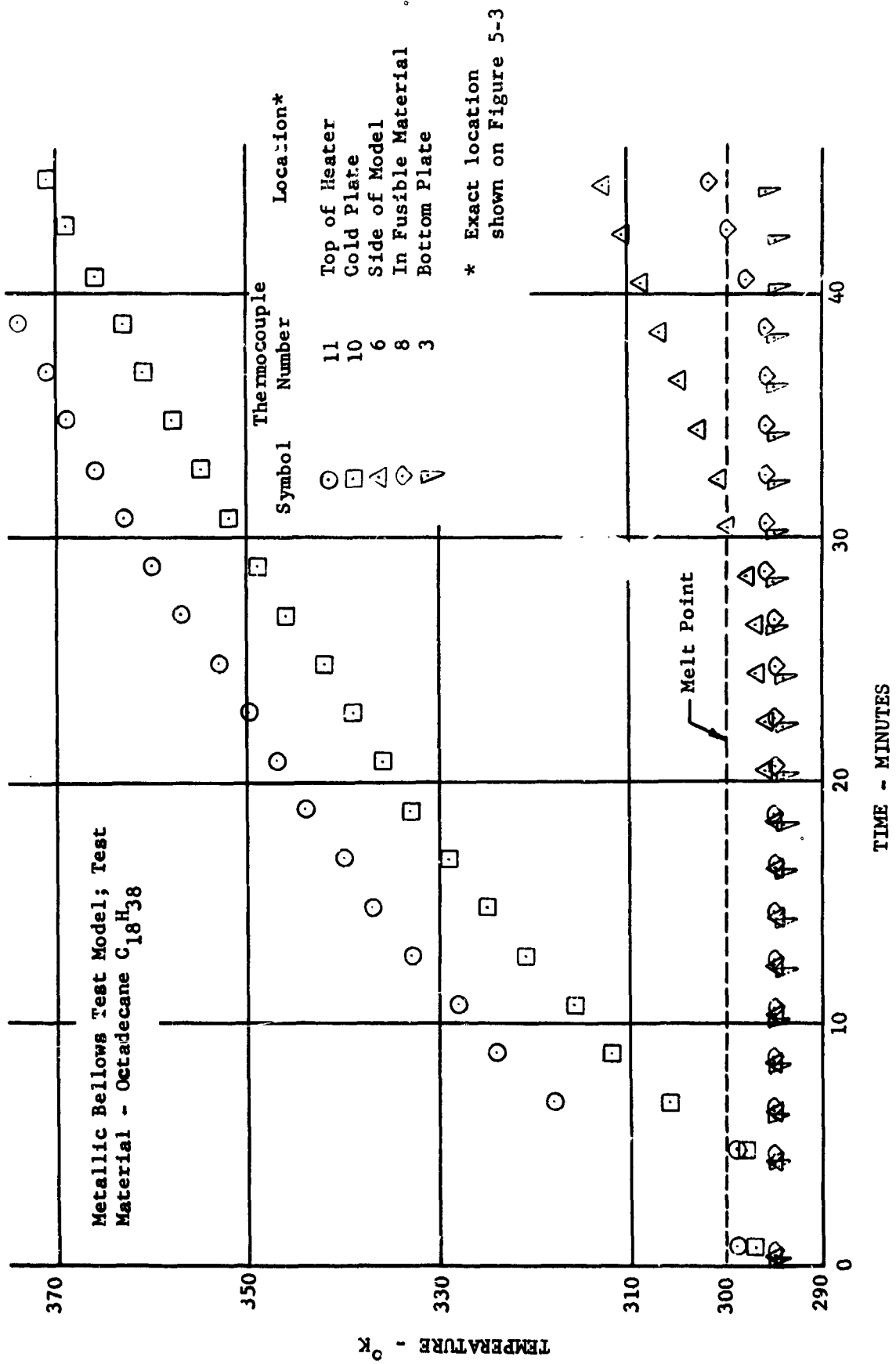


FIGURE 5-7 TEMPERATURE HISTORY OF METALLIC BELLOWS TEST MODEL FOR TEST RUN NO. 6

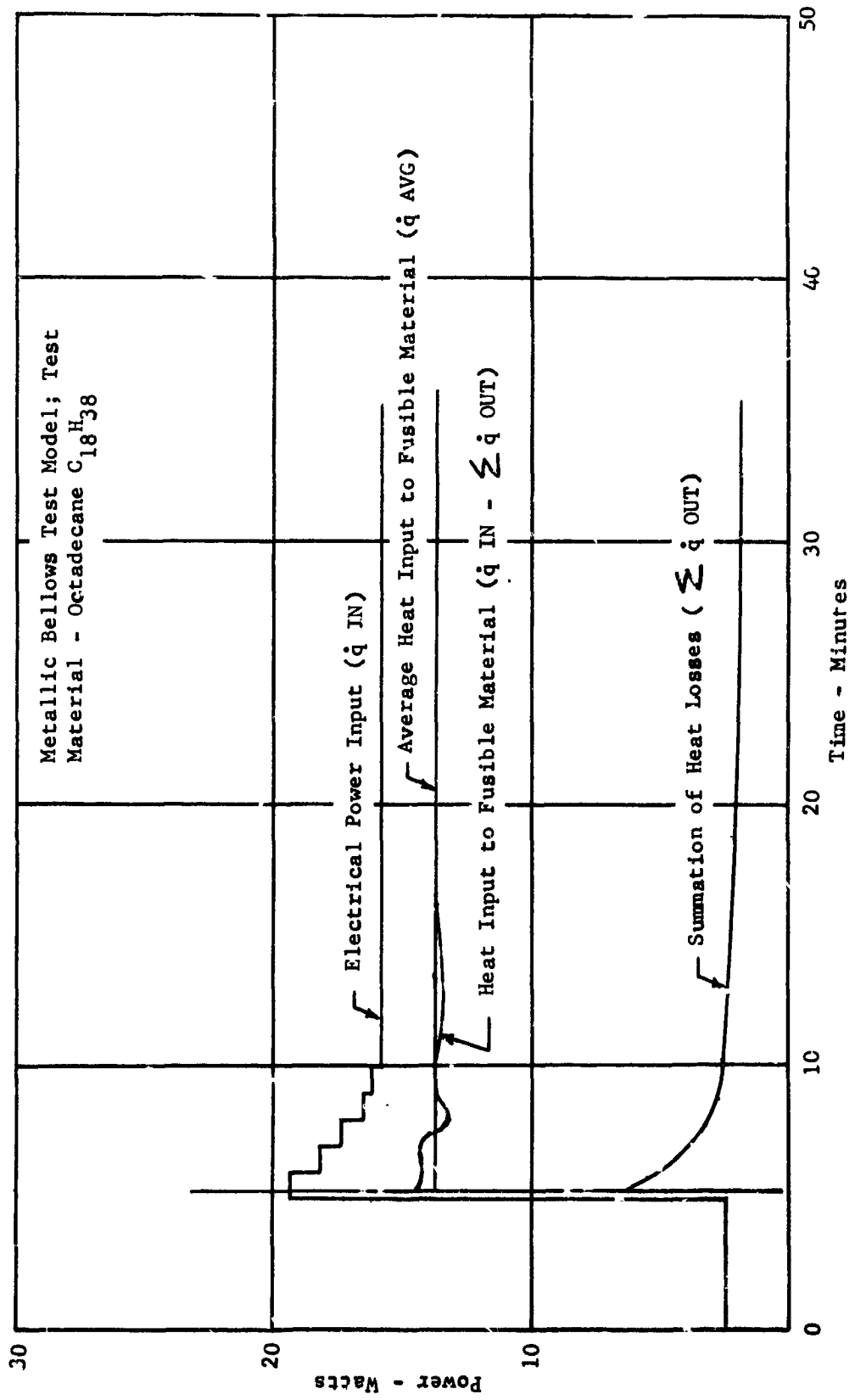


FIGURE 5-8 POWER HISTOGRAM FOR TEST RUN NO. 6 - SIMPLE ADIABATIC BELLOWS MODEL

Verification Test of Adiabatic  
 Temperature Control Technique;  
 Metallic Bellows Test Model; Test  
 Material - Octadecane  $C_{18}H_{38}$ ;  
 Test Run Nos. 5 and 6

— Analytical Results (Heat Rate = 127 Watts/Ft<sup>2</sup>, 1370 Watts/m<sup>2</sup>)  
 ○ Test Run No. 5 Results (Heat Rate = 127 Watts/Ft<sup>2</sup>, 1370 Watts/m<sup>2</sup>)  
 □ Test Run No. 6 Results (Heat Rate = 126 Watts/Ft<sup>2</sup>, 1360 Watts/m<sup>2</sup>)

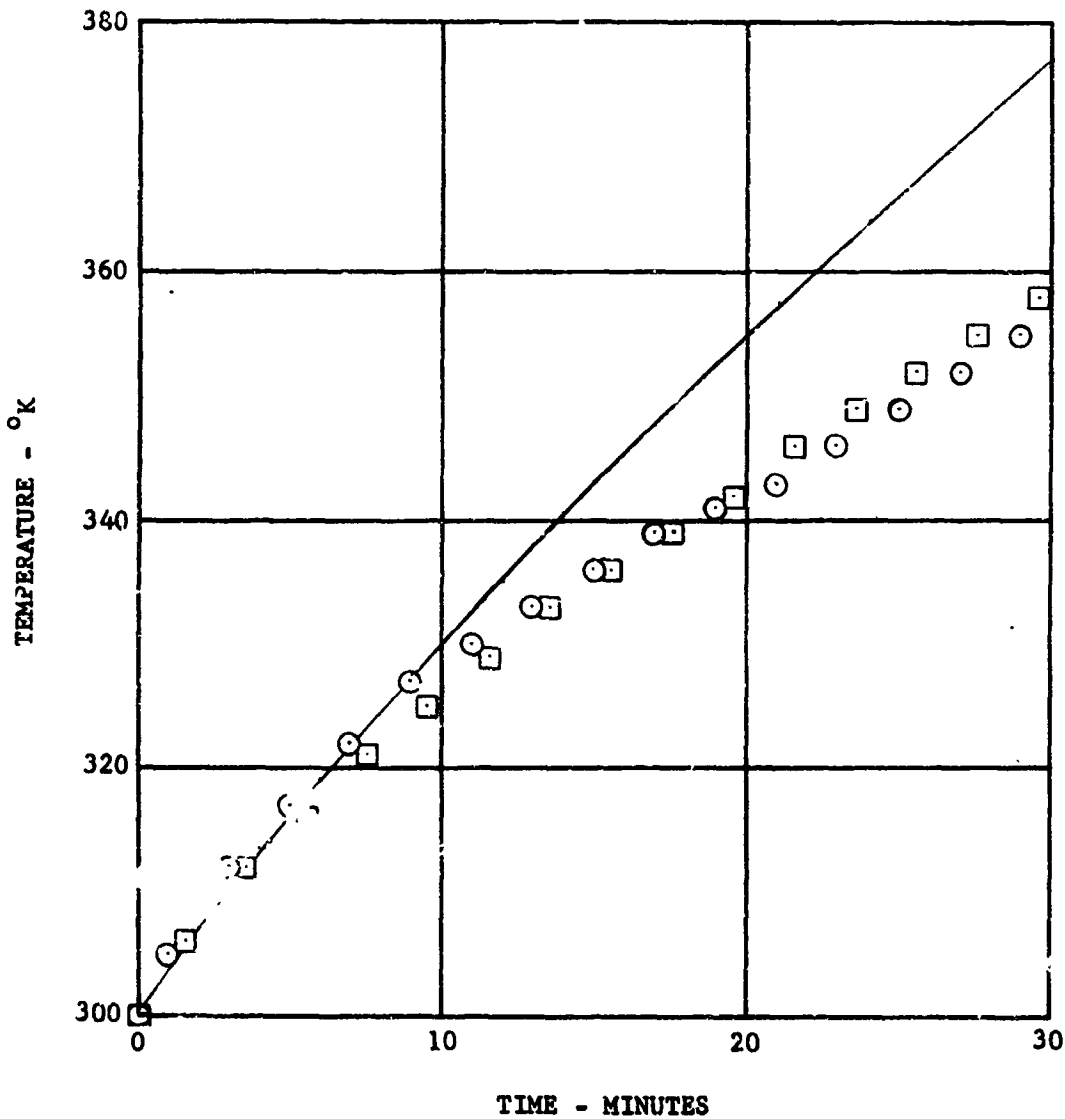


FIGURE 5-9 COMPARISON OF TEST RUNS WITH EQUAL POWER INPUT -  
 GOLD PLATE TEMPERATURE HISTORY

Time - where fusible material temperature passed 300° K

- ⊙ Thermocouple No. 6 (location - midpoint at bellows)  
 $\Delta X = .35$  in. (solid octadecane)  
 $\Delta X = .38$  in. (liquid octadecane @ approx. 310° K)
- ⊠ Thermocouple No. 8 (location - in fusible material)  
 $\Delta X = .40 \pm .05$  (unpressurized model)  
 $\Delta X = .47 \pm .05$  (solid and/or liquid octadecane)

⊞ End of test run (Thermocouple No. 8 less than 300° K)

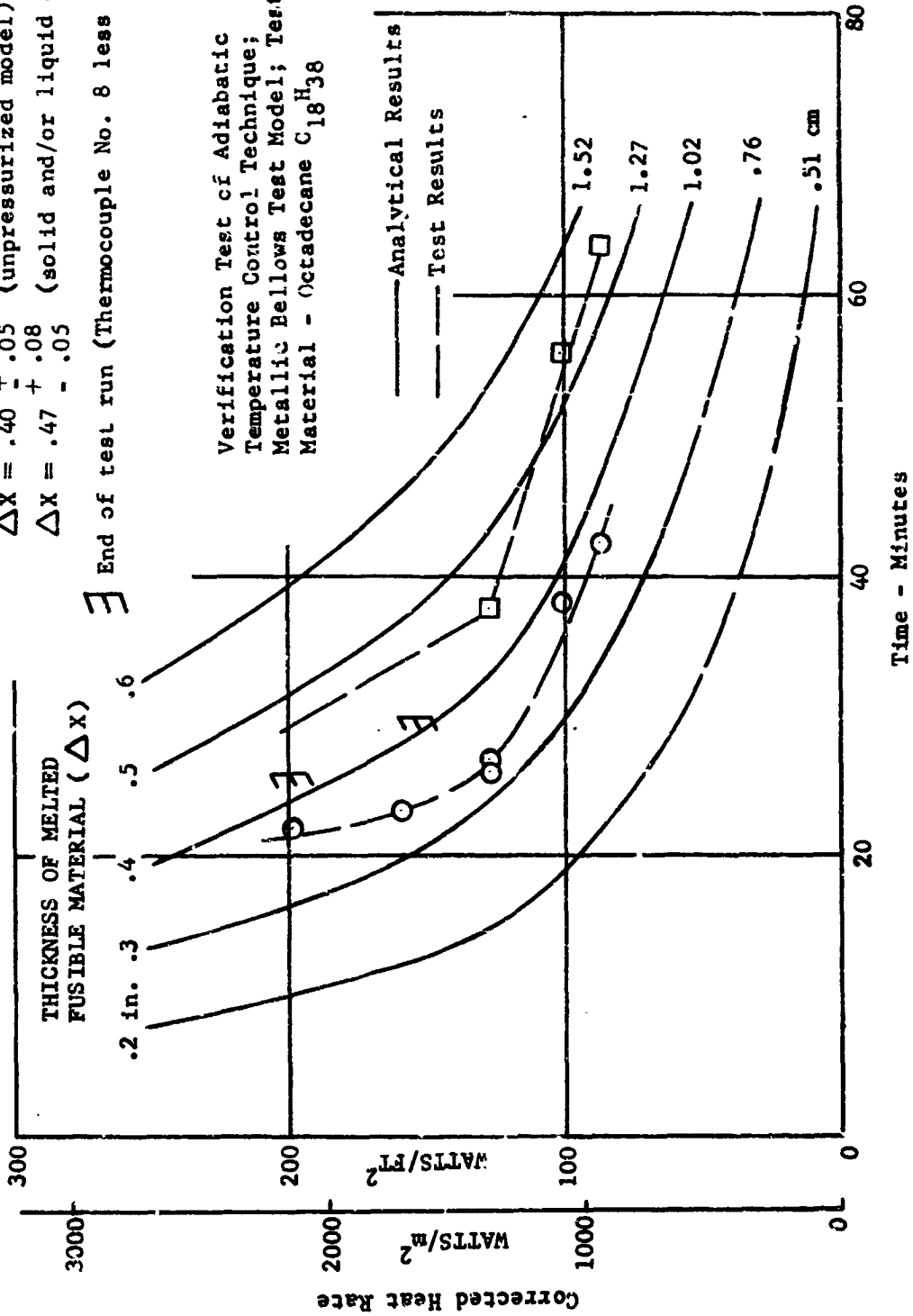


FIGURE 5-10 COMPARISON OF ANALYTICAL AND TEST RESULTS - THICKNESS OF MELTED FUSIBLE MATERIAL

**BLANK PAGE**

## SECTION 6

### RADIATING FIN WITH ATTACHED FUSIBLE MATERIAL

This study was conducted to determine the feasibility of increasing the thermal mass or inertia of a space radiator by attaching fusible materials. The fusible material would be attached to a radiating fin (Figure 2-1) and absorb heat by melting at high power levels. This would retard the temperature rise at the fin root. The fusible material would resolidify at low power densities by continued thermal radiation to space. In this manner, the fusible material would reduce the temperature excursion and allow the radiator to be sized for a nominal power level instead of the maximum power density.

#### Fin Selection Analysis

The first step of this study was to select a typical fin size for the transient analysis. The fin analysis could not be generalized because of the temperature decay along the fin length, which is a function of temperature level, fin material, fin length, and fin thickness. An optimum fin thickness study was performed for various fin lengths using the procedure presented in Reference 12. The theoretical optimum weight thickness is marginal in structural requirements for a spacecraft's exterior skin with electronic gear directly mounted to it; therefore, .05 in. (.13 cm) was selected as the minimum fin thickness for this study.

The fin material is aluminum with a surface coating having an infrared emissivity of .90. The radiating fin steady-state temperature distribution was calculated using an analytical method developed by J.W. Tatom (Reference 13), and it was checked by the transient computer program of Reference 10, which was allowed to reach steady state. The sink was deep space with an assumed temperature of zero degrees Rankine. The results were in good agreement, and the procedure of Reference 13 was used to calculate fin temperature distribution for various fin lengths with root temperatures equal to the melt point of octadecane.

For the selected fin thickness, .05 in. (.13 cm) the rate of temperature decay increased with fin length to approximately 4.8 in. (12 cm) where it became essentially linear (Reference 1). Since the addition of fusible material to the thermal radiating fin is useful only where the fin temperature is above the melt point for most of the duty cycle, a fin length of 4 in. (10 cm) was selected as a practical maximum for the stated melt temperature and fin thickness. The transient analysis was performed for this fin length.

## Radiating Fin Performance Analysis

The final transient analysis of the radiating fin with and without attached fusible material was performed with the simplified electrical analog network (Figure 4-1). The selected size of an aluminum fin node was .4 in. along the fin, .05 in. thick, and 1 ft wide. The fusible material node size was the same length and width, but only .025 in. thick. The conductances between fusible material nodes along the fin were neglected to conserve computer time. This had little effect on the analytical results due to the ratio of thermal resistances of aluminum and fusible material, which is still two orders of magnitude when assuming a 0.5 in. layer of fusible material.

Analytical results. - The fin root temperature history for three heating rates — 25, 50, and 66 watts/ft of fin root (82, 164, and 216 watts/m) for radiating fins of equal thickness with and without attached fusible material — is shown in Figure 6-1. The fusible material greatly retards the fin temperature rise. The fin root temperature rise and decay for the 50 watts/ft (164 watts/m) heating rate with a zero heat input during cooling is shown in Figure 6-2 for three heating periods (5, 10, and 15 minutes). Once the fin root heat input is stopped, the fin root temperature drops very sharply. With no heat pulse, the temperature decay along the fin disappears and the temperature along the fin becomes a constant (independent of length), dropping very rapidly to the fusible material freezing point (300°K). The period between the time when the root temperature,  $T_R$ , becomes 300°K until it intersects the line of solidification loci (Figure 6-2) is the time required to solidify all the fusible material melted during the heat pulse. The melt profiles for these conditions are also presented in Figure 6-2. For weight effectiveness, the melt profile is the most efficient fusible material package outline. Note that, because of the temperature decay along the fin, the melt profile is also a function of fin geometry and effectiveness.

### Experimental Verification

The melt line for the 10-minute heat pulse at 50 watts/ft (164 watts/m) (Figure 6-2) was selected for the experimental model. The selected fusible material profile is linear, being .20 in. (.51 cm) deep at the fin root and .05 in. (.13 cm) at the fin tip. The fusible material is contained in a convoluted aluminum package, with a .016 in. (.041 cm) wall, welded to the .05 in. (.13 cm) aluminum fin (Figure 6-3). The fin is extended 2 in. (5.1 cm) past the fin root to provide for a heater attachment. The fin and package were made from 6061-SO aluminum, which was heat-treated to T4 after welding. This technique provided a satisfactory spring rate in the package to maintain the fusible material in good thermal contact with the fin. A nichrome wire and laminated fiberglass heater was bonded on the fin extension. The package was filled so that the octadecane was at 1.5-2 psig, with the material in the solid state. The fill and vent nipples (Figures 6-3 and 6-4) were then removed, and the vents were sealed with epoxy and small plates.

An equal weight solid aluminum fin. - A solid aluminum fin (6061-T4) was made having the same length and width as the radiating fin described above. This solid aluminum fin was equal in weight to the radiating fin with package and fusible material (Figure 6-5). The resultant fin thickness is .108 in. (.274 cm). This solid aluminum equal weight fin used in the comparative tests will show better performance than the .05 in. (.13 cm) thick fin used in the analytical comparison. The performance comparison for equal weight fins is more realistic, since performance per unit weight is a primary consideration in selecting spacecraft subsystems. After manufacture, the solid aluminum fin was 5% lighter than the one with fusible material. This percentage of weight difference can be neglected when considering the overall performance of the radiating fins.

Experimental installation. - The two fins were instrumented with 40-gage thermocouples and 28-gage heater leads to minimize heat losses. The radiating surfaces were painted with CAT-A-LAC black at the same time to minimize different coating properties. Insulating gloves with 15 layers of aluminized mylar were fitted to the test models to allow thermal radiation from only the top surface of the fin (Figure 6-6). The assemblies were installed and tested in a cold wall vacuum chamber (Figure 6-7). Note that the insulating gloves interfered with the cold wall view factor only at the top edge of the heater and that the only other obstructions are thermocouple leads.

Experimental results. - The models were tested with the vacuum chamber pressure level in the  $10^{-5}$  torr range and the cold wall temperature at less than 80°K. No fusible material leakage was observed after four days of continuous exposure to this low pressure and approximately 25 liquefaction-solidification cycles (Figure 6-8).

The steady-state power input required to maintain the fin root at 81°F (300°K), the melt point of octadecane, was  $2.0 \pm .5$  watts/model. The analytical value for a .05 in. (.13 cm) thick fin is 12.2 watts/ft of fin root (40 watts/m) or 2.1 watts/model. This steady-state condition was not determined more accurately because of its secondary importance and because of the long time period required to reach a steady-state condition.

The transient tests were run at three input power levels, 25, 50, and 75 watts/ft of fin root (82, 164 and 246 watts/m). The fin root temperature history is presented in Figures 6-9, 6-10, and 6-11 for the three power levels. The reduction of the fin root temperature excursion by the attached fusible material is well demonstrated for the three power levels. Notice the effect of the different heating and cooling periods at the three power levels for the two models. The last cooling period for each heat pulse level demonstrates the capability of resolidifying the fusible material at a reduced power level.

The corrected power input to the fin root is also shown in Figures 6-9, 6-10, and 6-11. The power input to the heater was changed in step functions. The difference between the power to the heater and the average corrected power is the energy required to raise the heater and the fin root extension temperature and the energy lost through the heater leads and insulation.

The fin temperature distribution at selected time intervals for the three power levels is shown in Figures 6-12 through 6-17. When the fin tip temperature rises sharply above the melt point ( $300^{\circ}\text{K}$ ), the fusible material is assumed to be completely melted. For the fourth heat pulse at 50 watts/ft (164 watts/m), Figure 6-15, the fusible material is melted between 8 and 14 minutes. The fusible material is resolidified for the same case after a total time period of 34-54 minutes and a cooling period at 2.9 watts/ft (9.5 watts/m).

Seven temperatures are read along the fin length in 35 seconds, and five of these are plotted as if they were instantaneous. Therefore, the actual temperature decay along the fin is slightly greater than that shown during the heat pulses. The measured lateral temperature gradient at the fin root and tip was less than  $3^{\circ}\text{F}$  for all runs, with a nominal value of 0 to  $1^{\circ}\text{F}$ . The fin with attached fusible material performed better (i. e., exhibited less temperature rise) for all the test heat pulses than the equal weight solid aluminum fin.

### Correlation of Analytical and Experimental Results

The fin with attached fusible material was designed for a 10 minute, 50 watts/ft of fin root (164 watts/m) heat pulse, i. e., complete liquefaction of the fusible material for this period and power rate. The test results indicate somewhat better performance than the analysis. The required cooling period to obtain complete solidification also appears less than that predicted by analysis. Some performance improvement was expected due to the aluminum package; this was not considered in the analysis. A comparison of the analytical and experimental fin root temperature histories for the fin with attached fusible material is presented in Figure 6-18. The lower temperature rise for the test model reflects the influence of the aluminum package.

A computer analysis was rerun for the solid aluminum fin, .108 in. (.274 cm) thick. A comparison of the analytical and test results for this model is presented in Figure 6-19. The fin root temperature increases more rapidly for the analytical model. An analysis of these results indicates that up to 10% of the input power was not accounted for in reducing the test data.

Aluminum Fin Geometry

Length	4 in.(10.2 cm)
Width	12 in.(30.5 cm)
Thickness	.05 in.(.13cm)
$\epsilon_{IR}$	.90

Radiation from one side only.

----- Fin Only  
 \_\_\_\_\_ Fin & Octadecane

Radiation Sink (Space) = 0°K

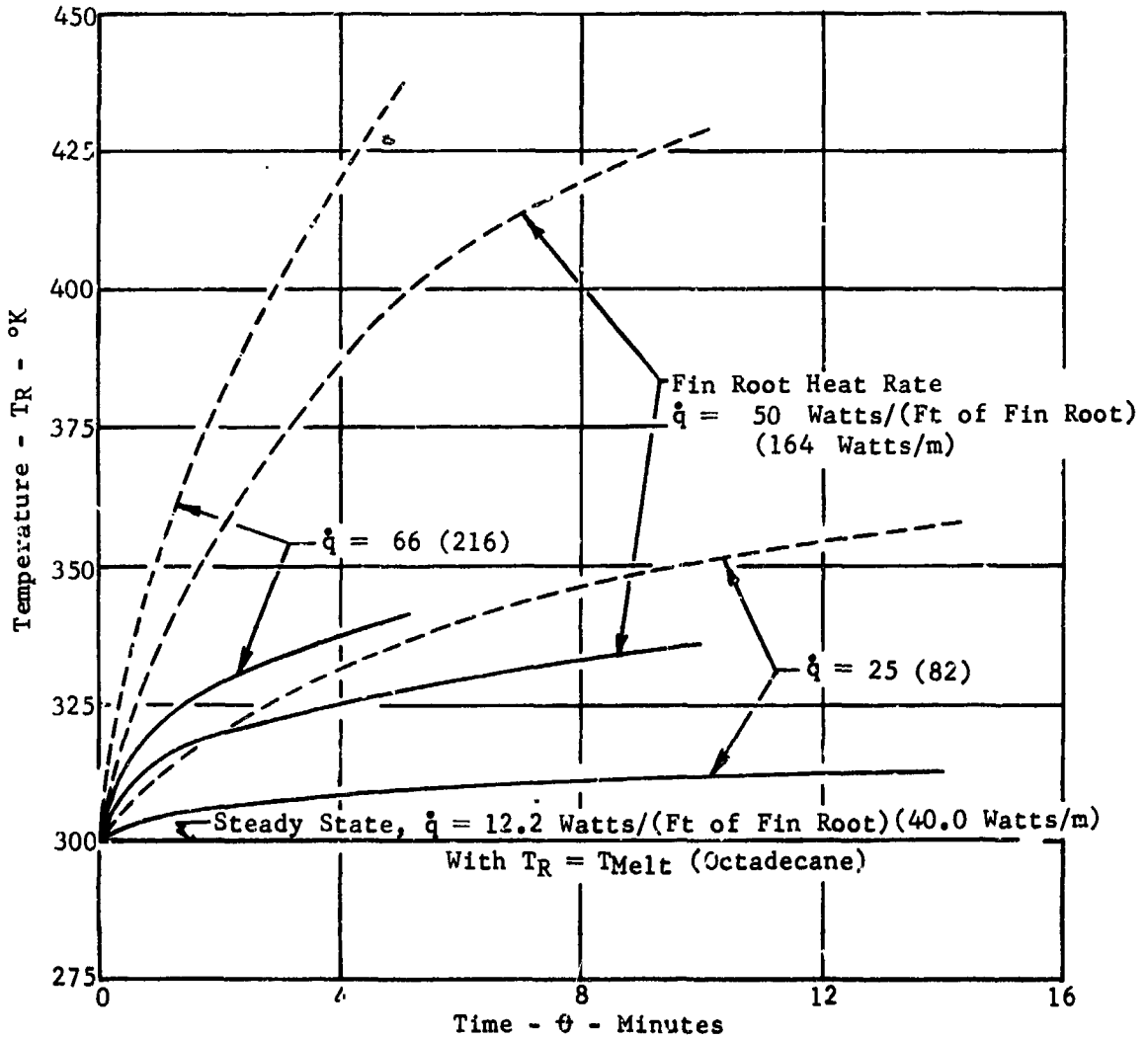
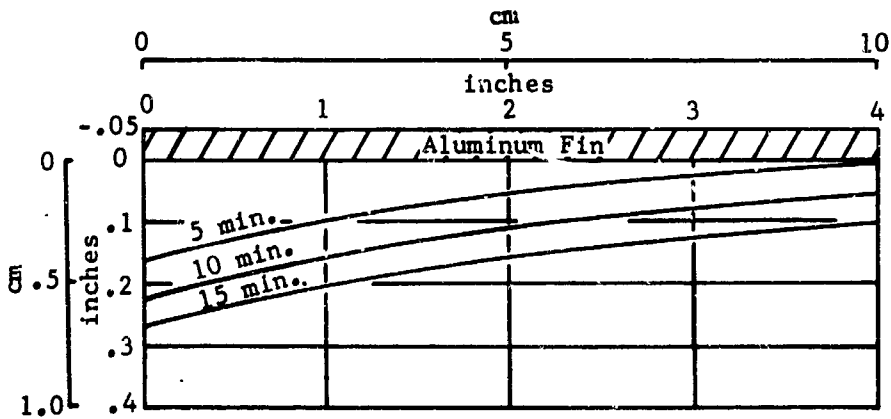


FIGURE 6-1 ROOT TEMPERATURE HISTORY OF A RADIATING FIN WITH AND WITHOUT ATTACHED FUSIBLE MATERIAL



MELT LAYER HISTORY OF FUSIBLE MATERIAL ATTACHED TO A RADIATING FIN AT 50 WATTS/FT (164 WATTS/m)

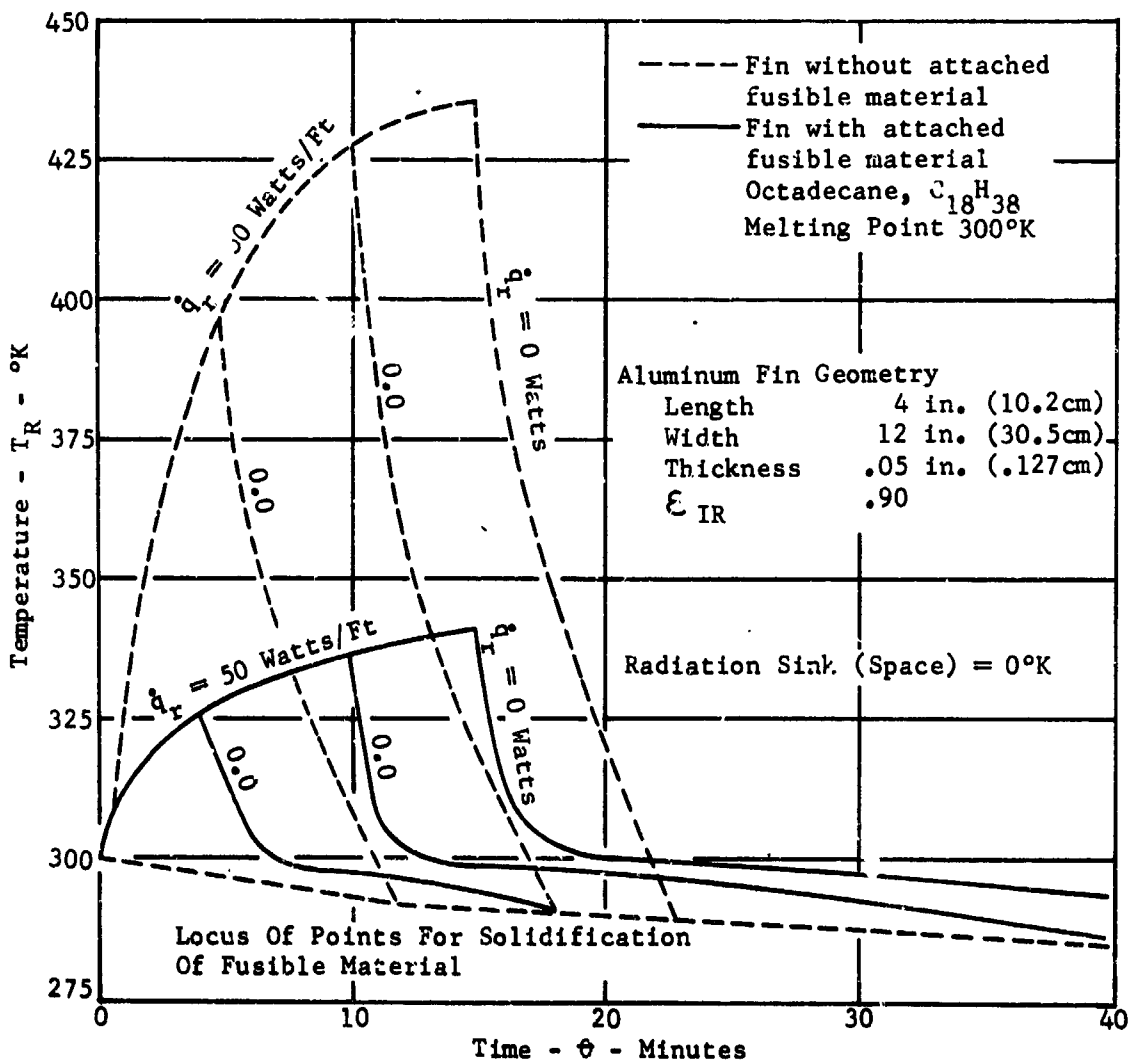


FIGURE 6-2 ROOT TEMPERATURE HISTORY OF A RADIATING FIN WITH AND WITHOUT ATTACHED FUSIBLE MATERIAL AT 50 WATTS/(FOOT OF FIN ROOT) (164 WATTS/m)



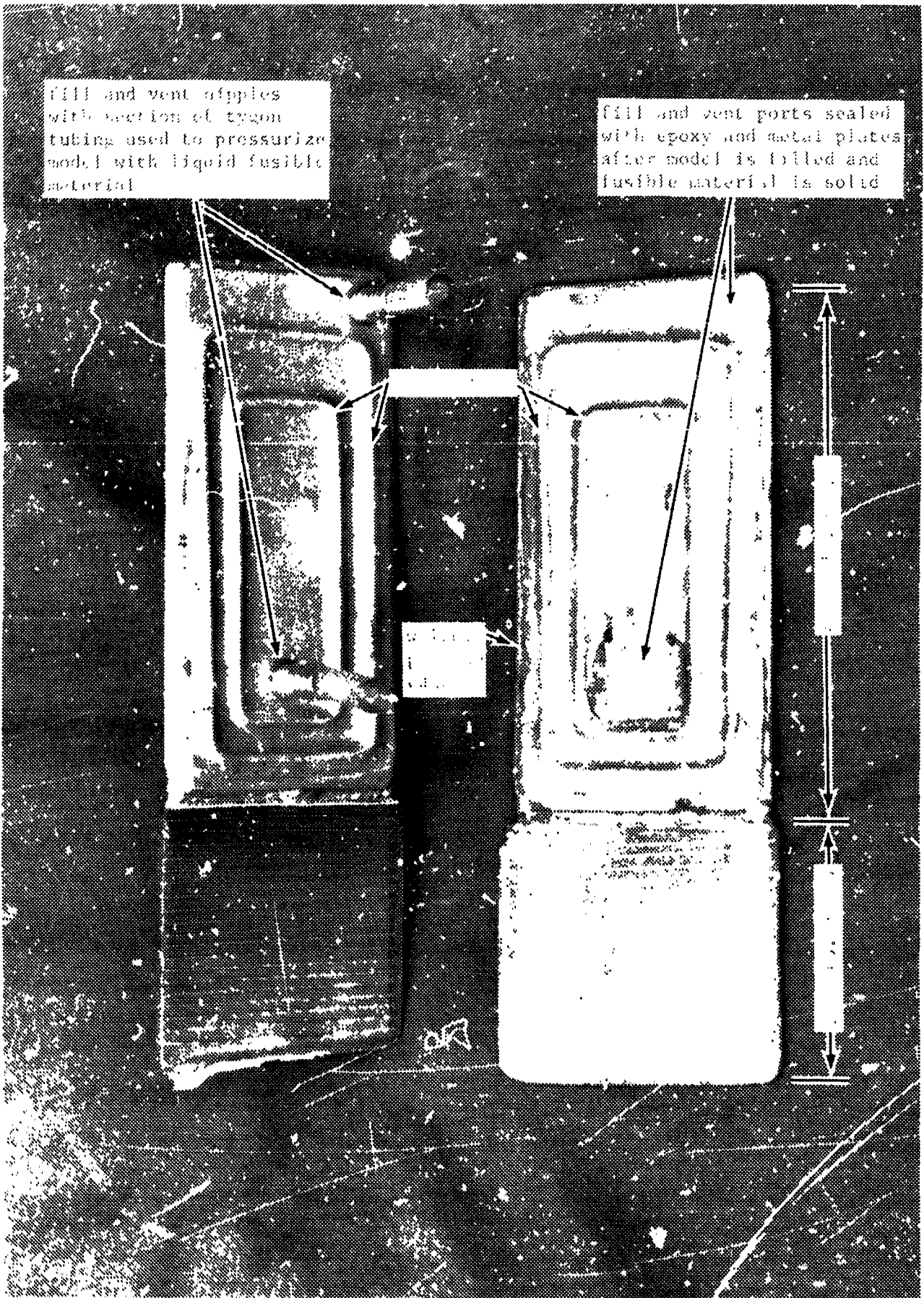
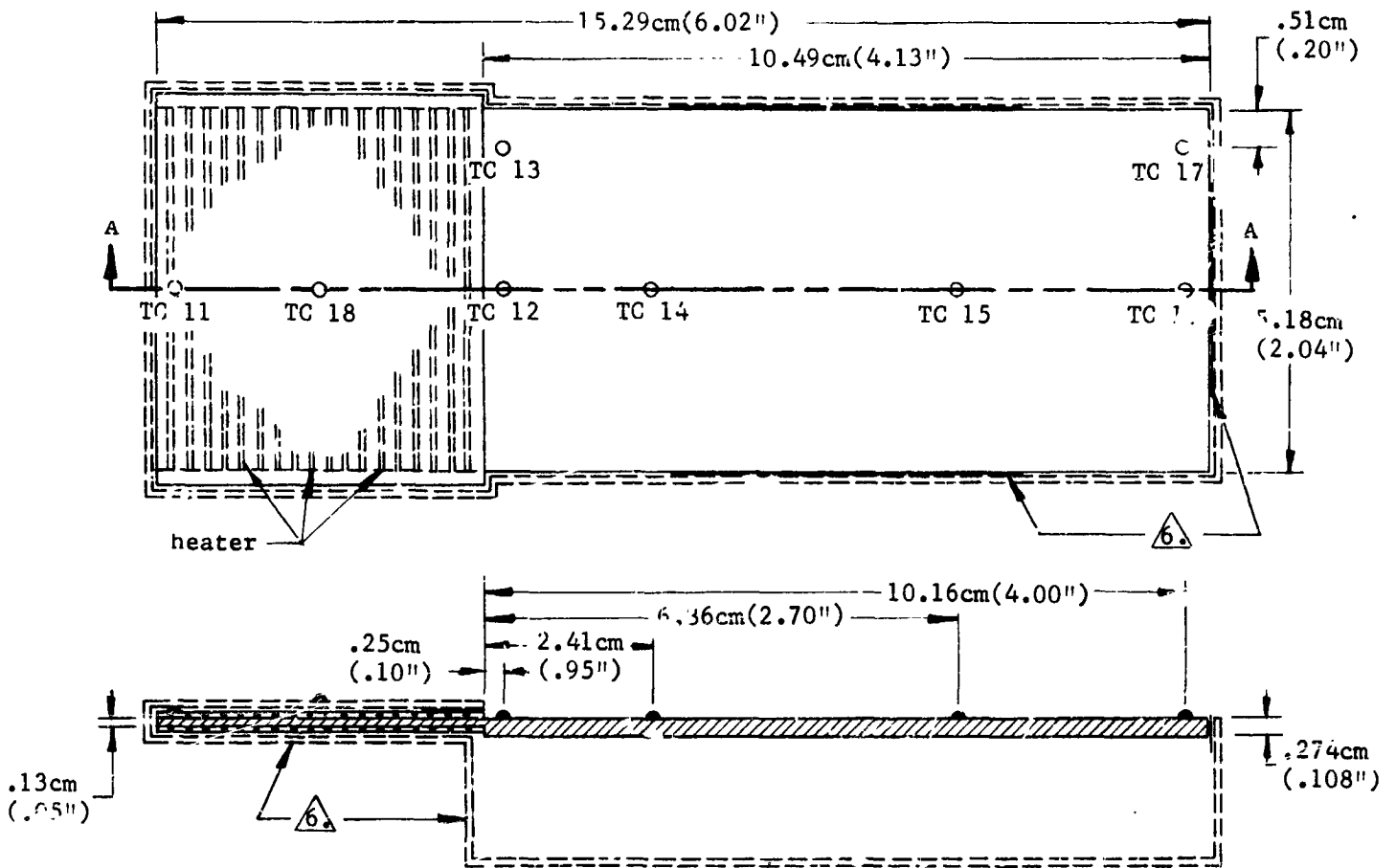


FIGURE 6-4 RADIATING FIN WITH ATTACHED FUSIBLE MATERIAL - FILL & VENT PORTS BEFORE AND AFTER FILLING



SECTION A-A

Notes:

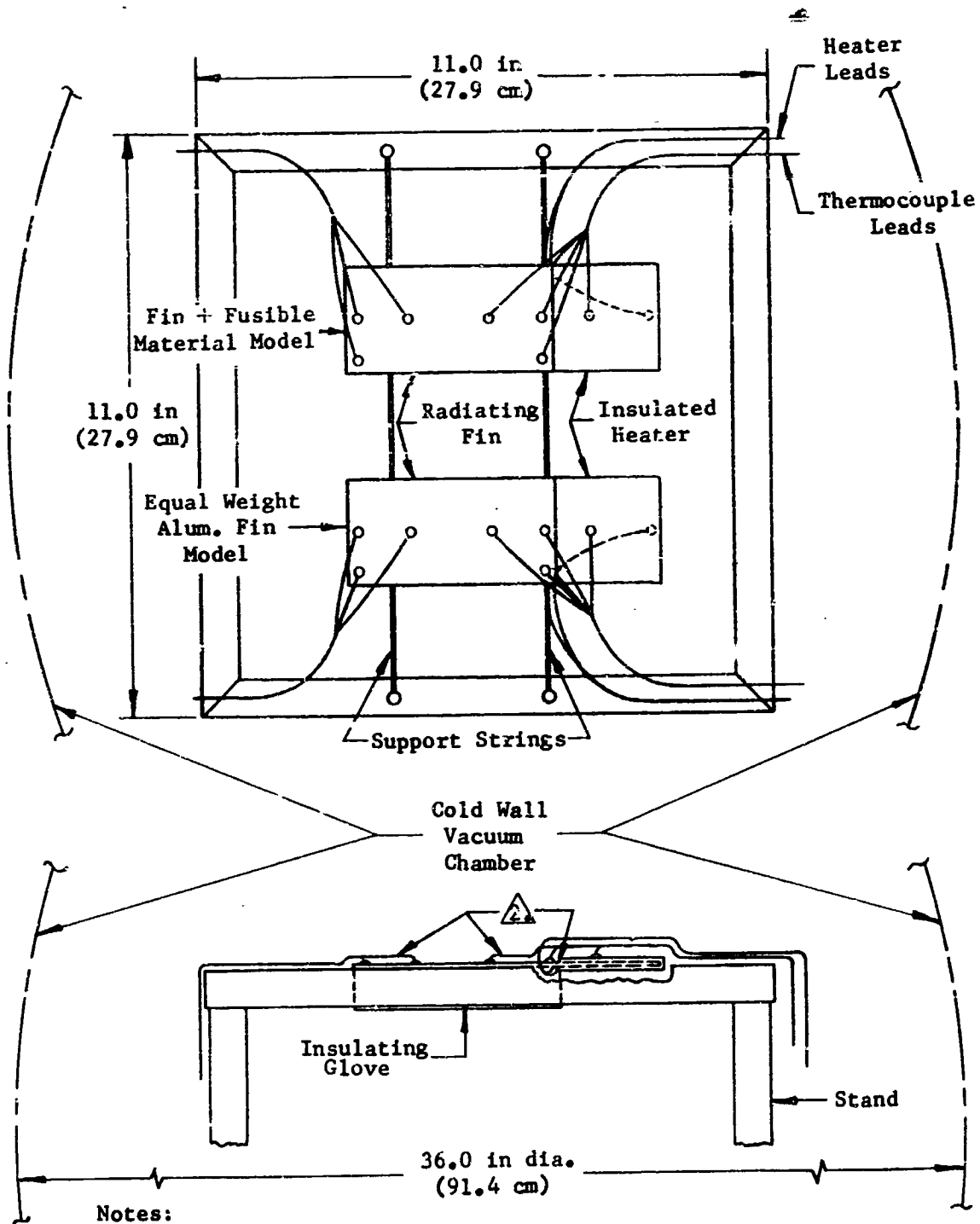
1. Material - fin machined from 6061 T-4 aluminum.
2. Fin surface coating CAT-A-LAC black, 2-4 mils, infrared hemispherical emissivity .88
3. Electric heater - nichrome wire and laminated fiberglass, epoxy filled, 35 ohms.
4. Thermocouples (TC) -chromel constantan.
  - a. TC 11 - bonded on top of heater and under insulating glove.
  - b. TC 18 - bonded on top of insulating glove.
5. Leads - heater - first 12.0 in. 28 gage, remainder 22 gage.  
 thermocouples - first 12.0 in. 40 gage, remainder 30 gage.
6. Insulating glove - 15 layers aluminized mylar, attached to model four(4) places with double backed tape.
7. Weights:
 

Fin	39.10 gm
Fin Extension	8.56 gm
Heater	6.00 gm

FIGURE 6.5 SOLID ALUMINUM RADIATING FIN TEST MODEL.



FIGURE 6-6 RADIATING FIN TEST MODEL INSTALLED IN INSULATING GLOVE



Notes:

1. Radiating surfaces are in the same plane.
2. Items interfering with total hemispherical view of cold wall from radiating surface(s):
  - a. 40 gage thermocouple leads.
  - b. Top edge of insulating glove.

FIGURE 6-7 INSTALLATION FOR TWO(2) RADIATING FIN MODELS

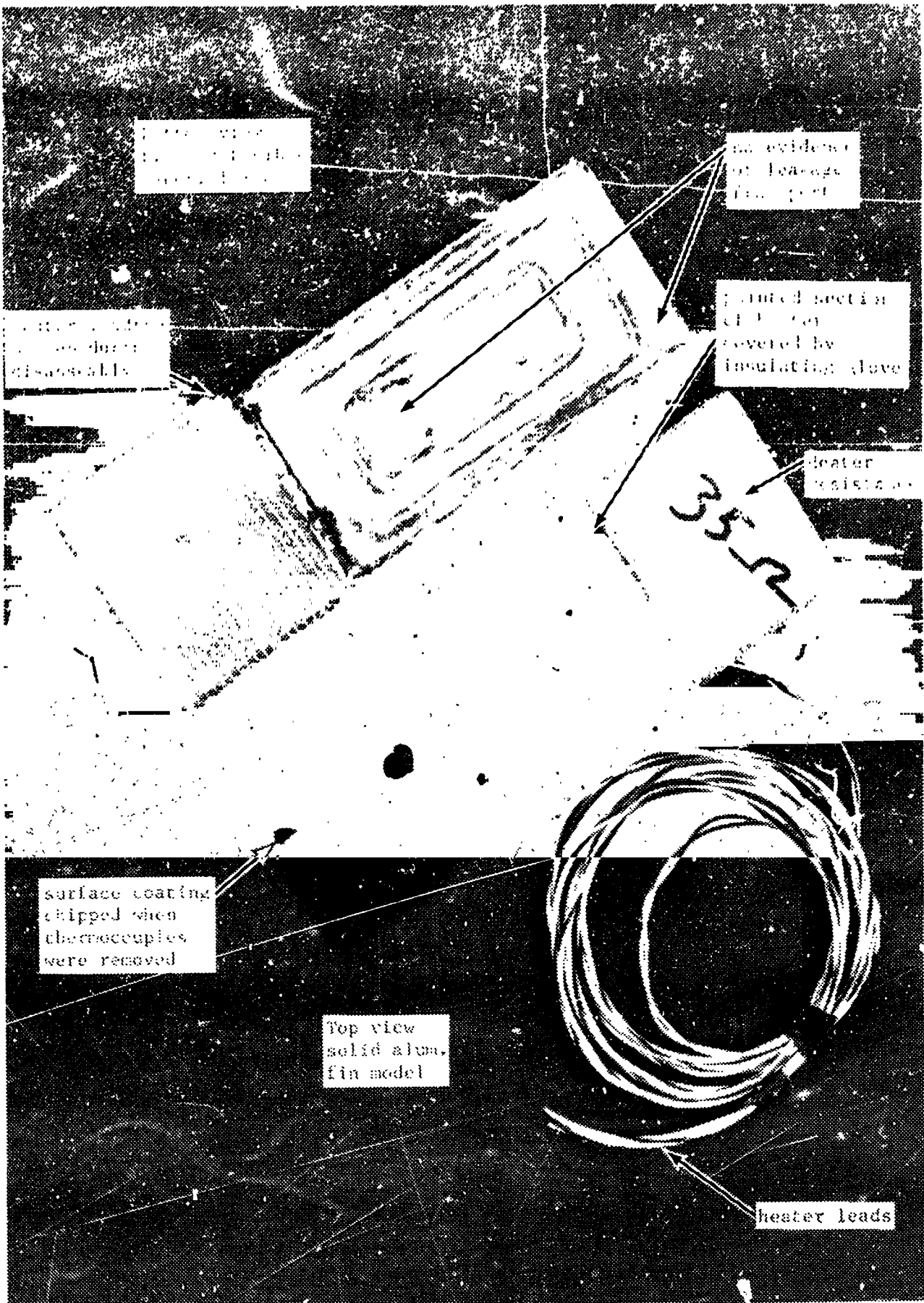


FIGURE 6-8 RADIATING FIN MODELS AFTER TEST

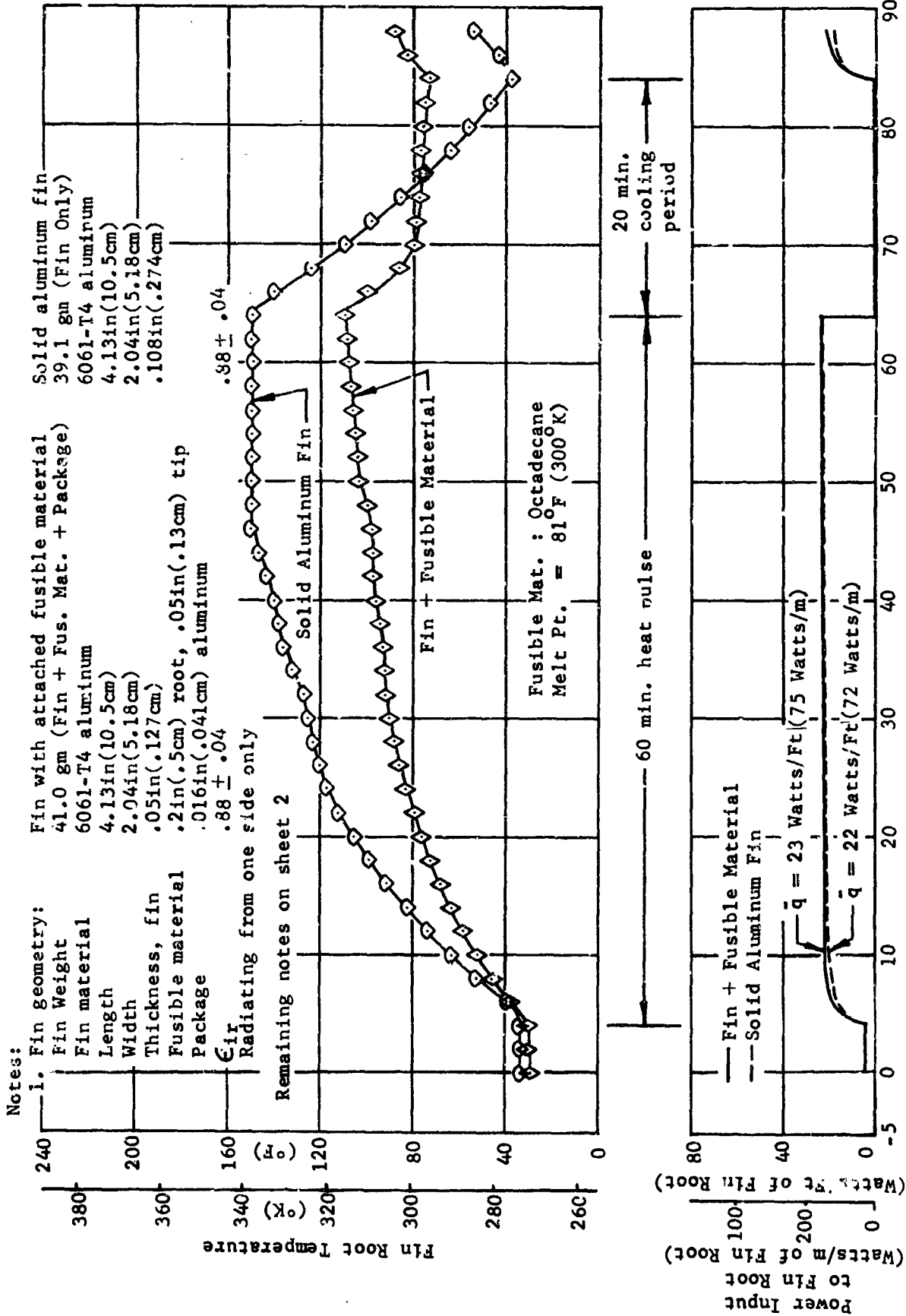


FIGURE 6-9 RESULTANT FIN ROOT TEMPERATURE HISTORY FOR TWO EQUAL WEIGHT RADIATING FINS (ONE WITH ATTACHED FUSIBLE MATERIAL, ONE OF SOLID ALUMINUM) ENERGIZED BY HEAT PULSES OF 25 WATTS/FT OF FIN ROOT WITH VARIOUS COOLING PERIODS (RUN 2)



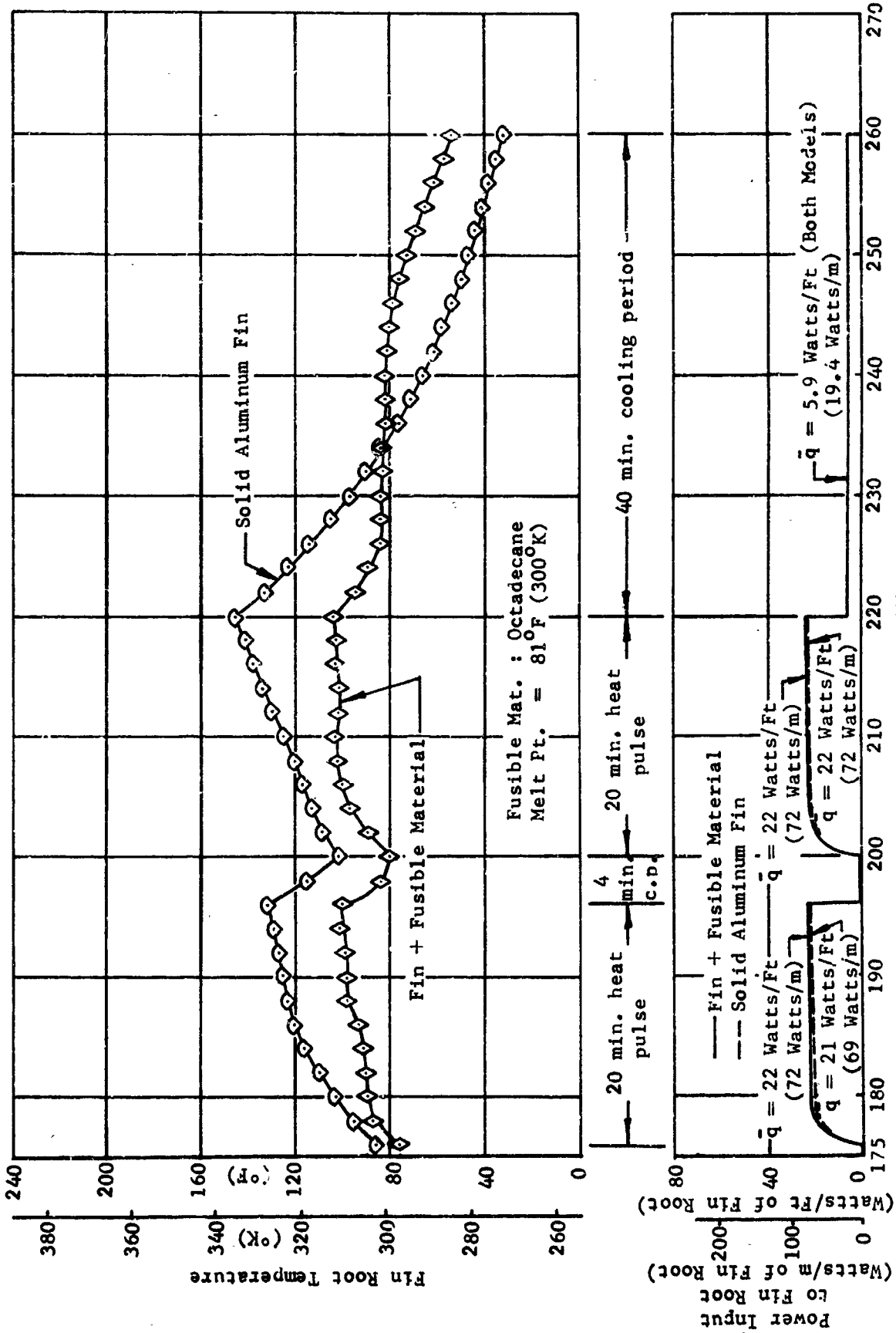


FIGURE 6-9 (CONTINUED)

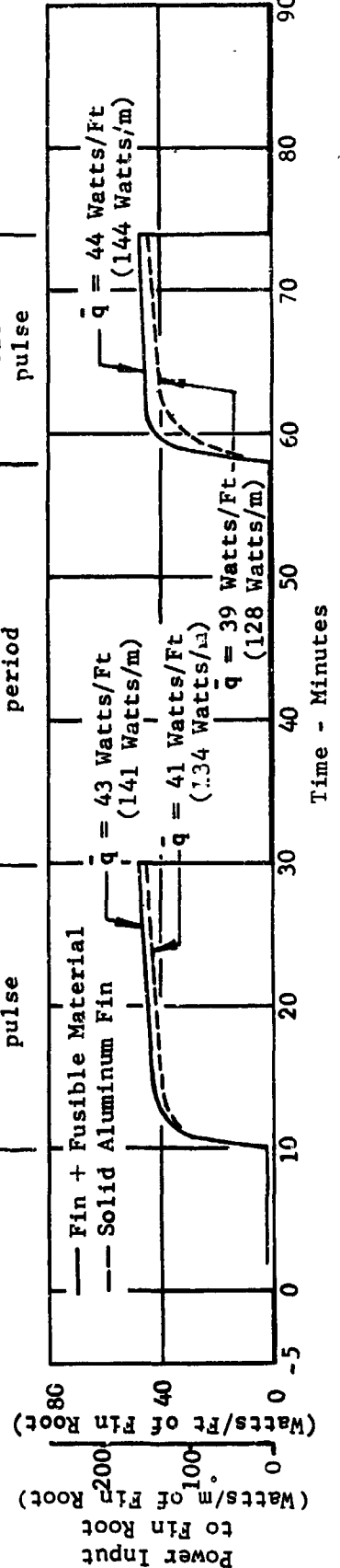
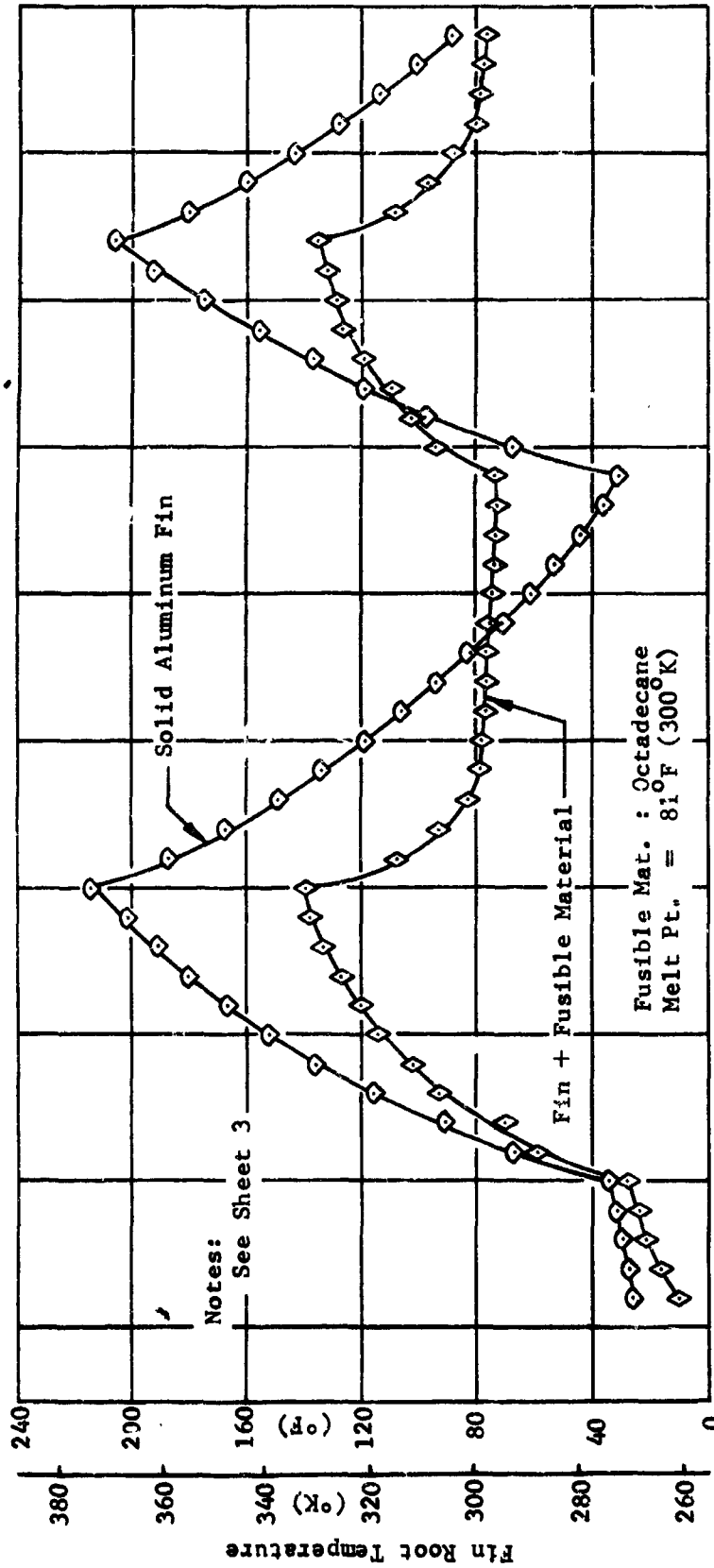


FIGURE 6-10 RESULTANT FIN ROOT TEMPERATURE HISTORY FOR TWO EQUAL WEIGHT RADIATING FINS (ONE WITH ATTACHED FUSIBLE MATERIAL, ONE OF SOLID ALUMINUM) ENERGIZED BY HEAT PULSES OF 50 WATTS/FT OF FIN ROOT WITH VARIOUS COOLING PERIODS (RUN 3) Sheet 1 of 3

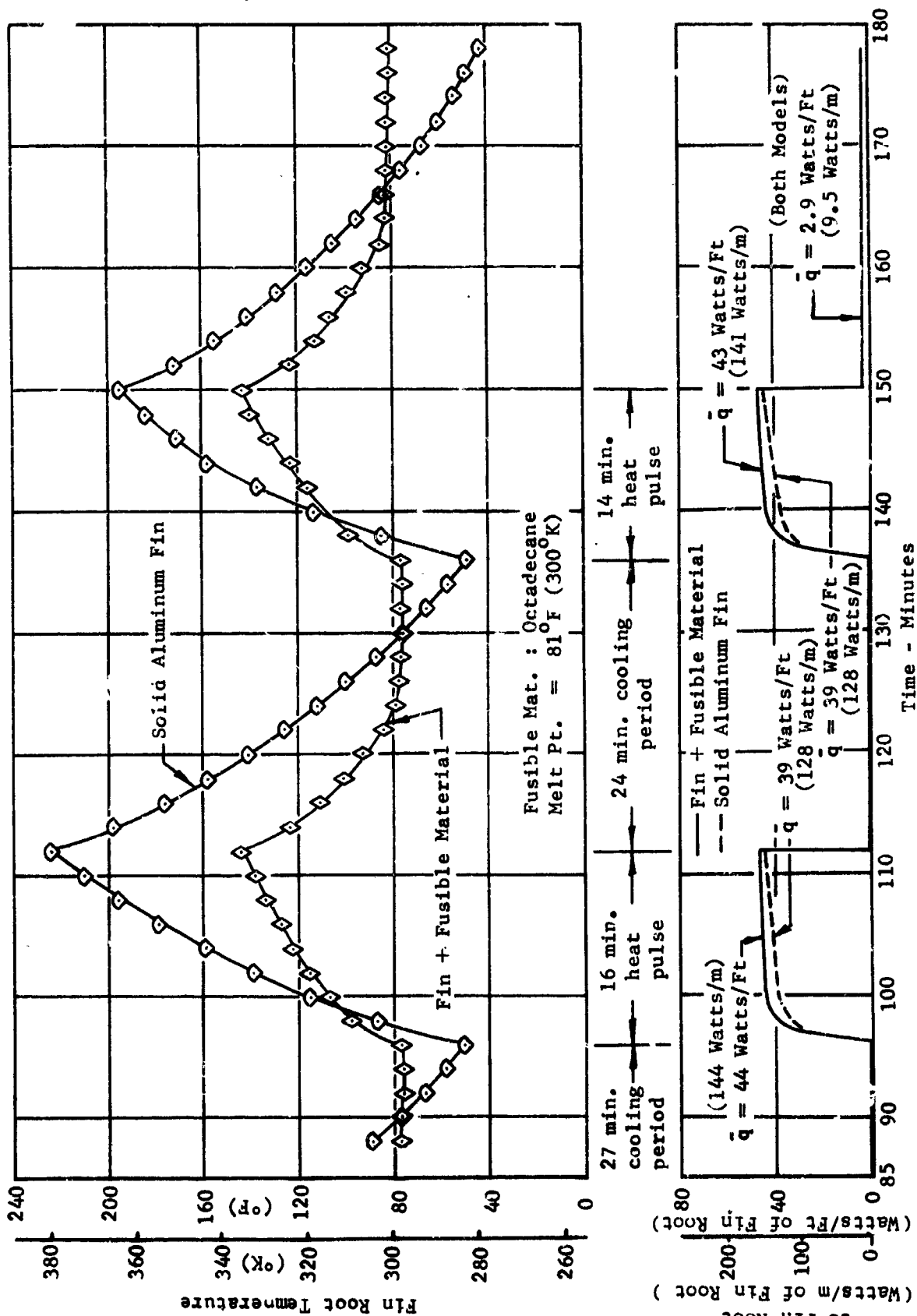


FIGURE 6-10 (CONTINUED)

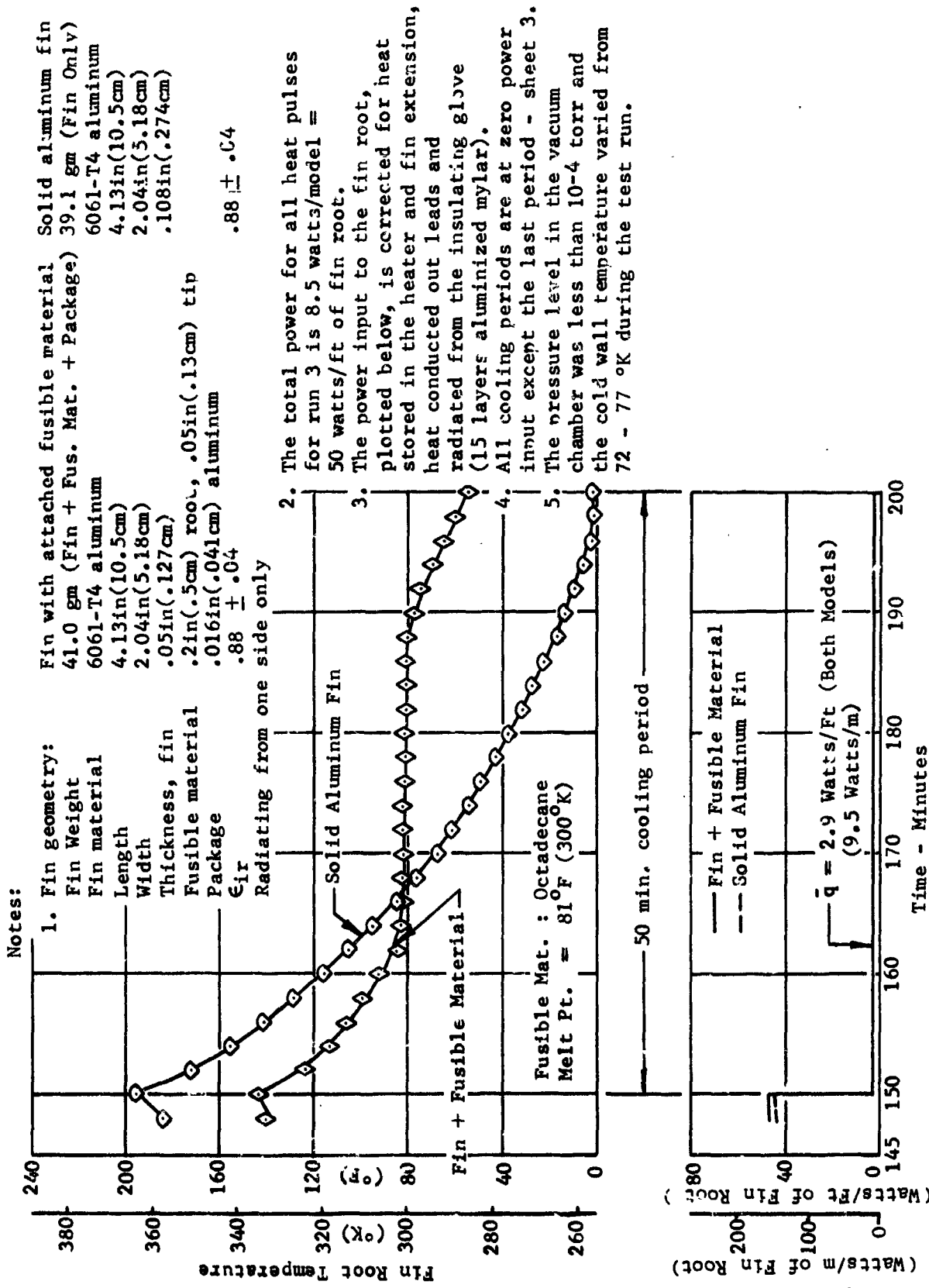


FIGURE 6-10 (CONTINUED)

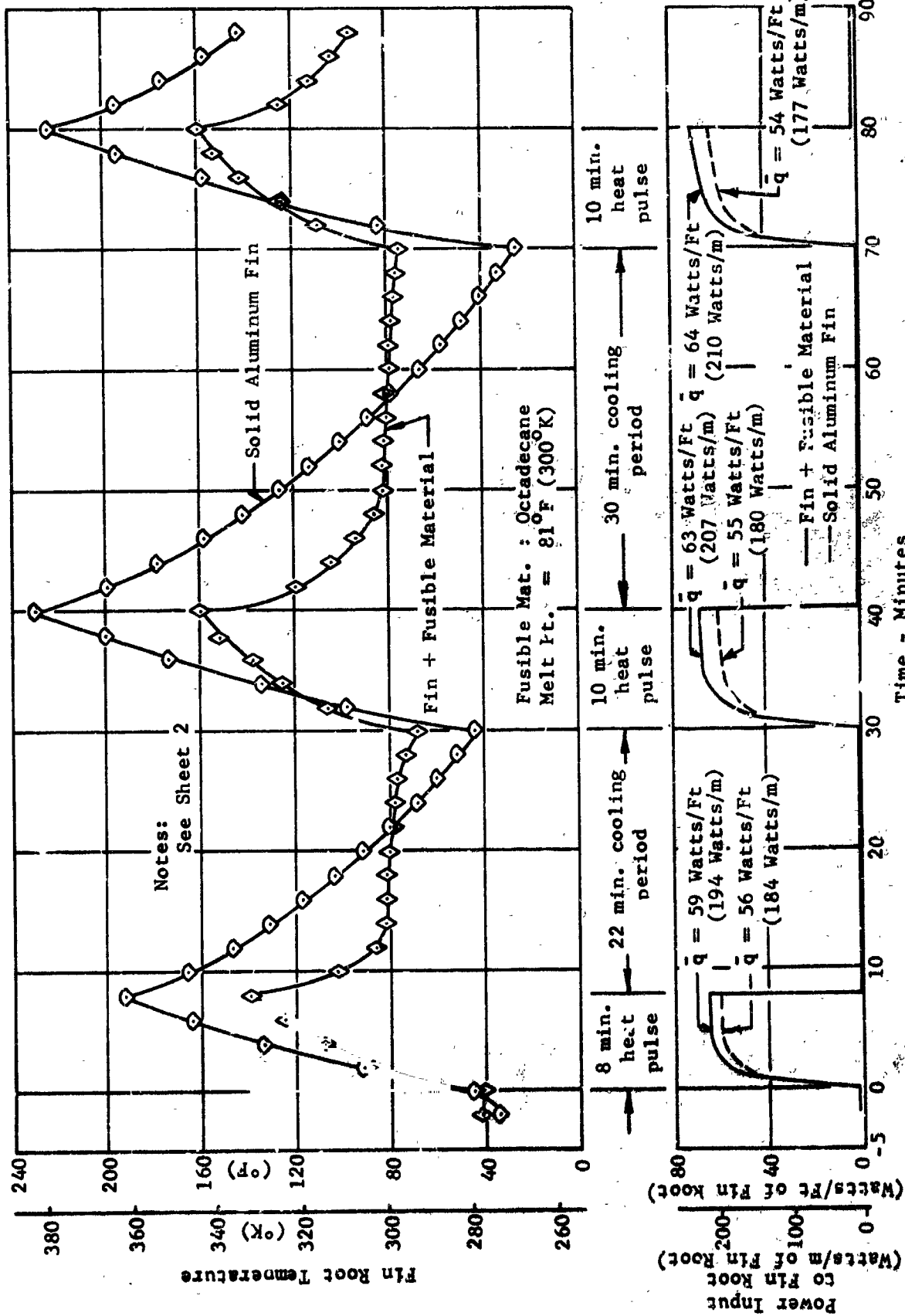


FIGURE 6-11 RESULANT FIN ROOT TEMPERATURE HISTORY FOR TWO EQUAL WEIGHT RADIATING FINS (ONE WITH ATTACHED FUSIBLE MATERIAL, ONE OF SOLID ALUMINUM) ENERGIZED BY HEAT PULSES OF 75 WATTS/FT OF FIN ROOT WITH VARIOUS COOLING PERIODS (RUN 4)

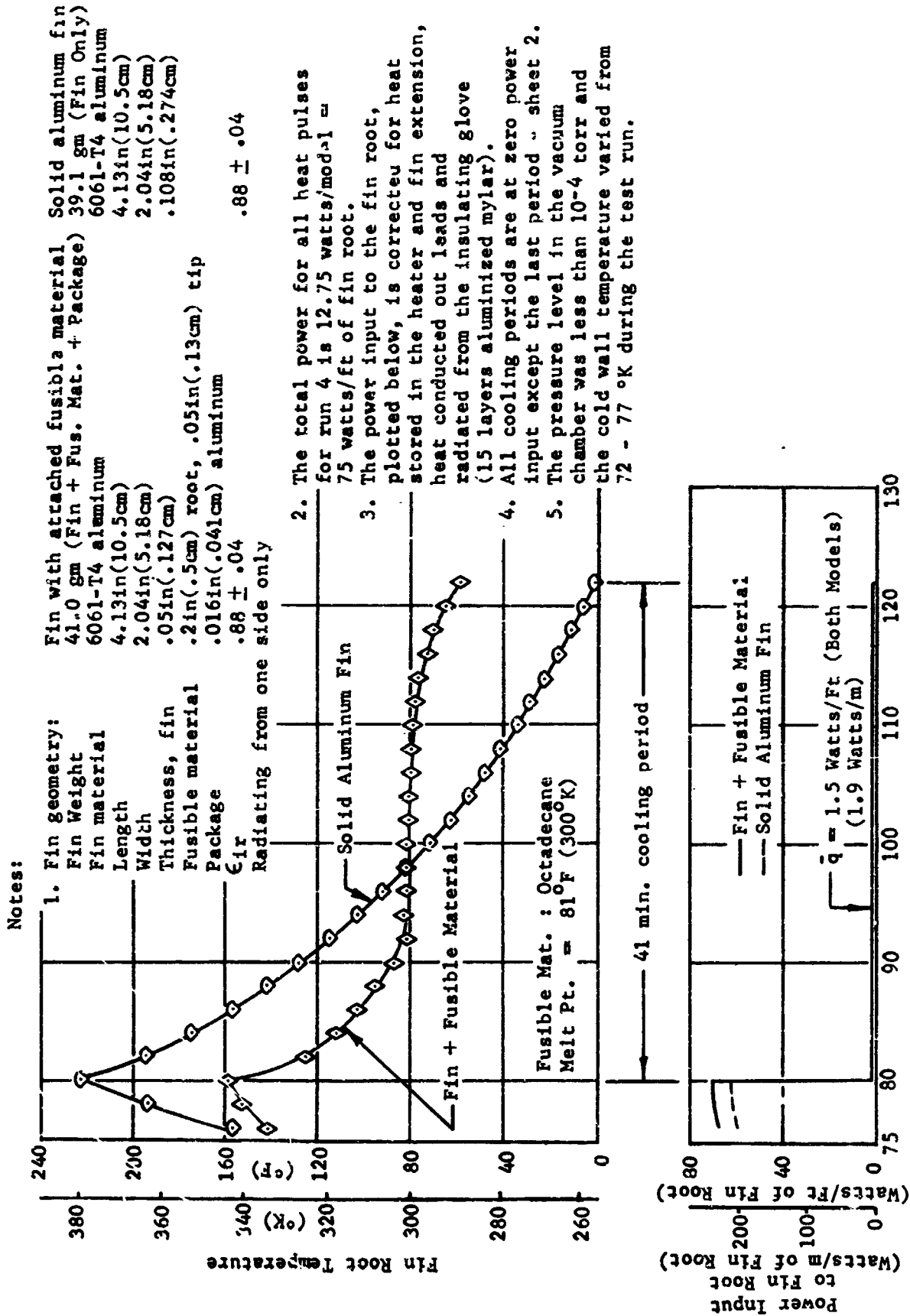
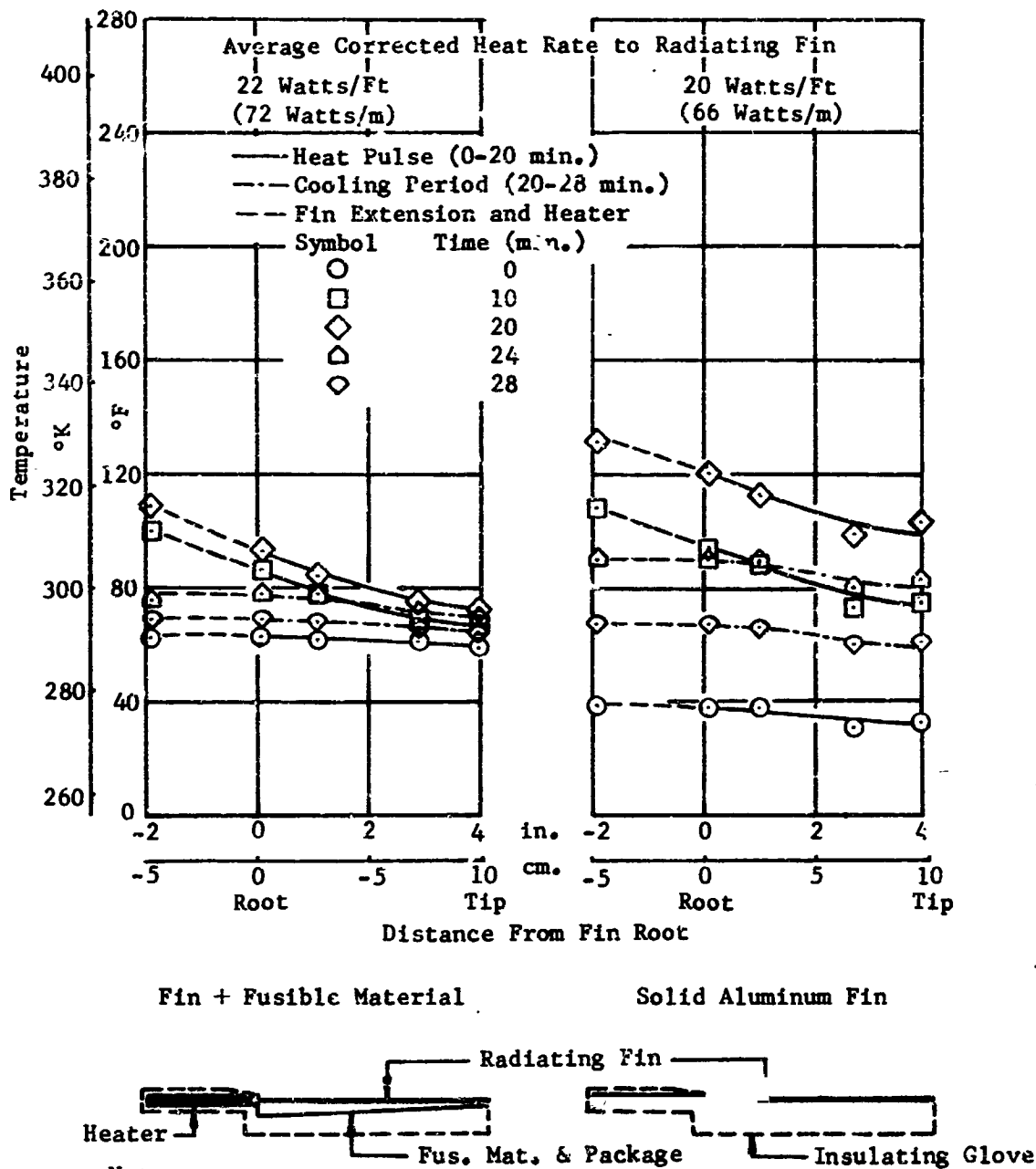


FIGURE 6-11 (CONTINUED)

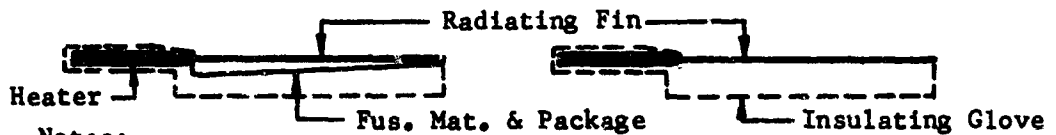
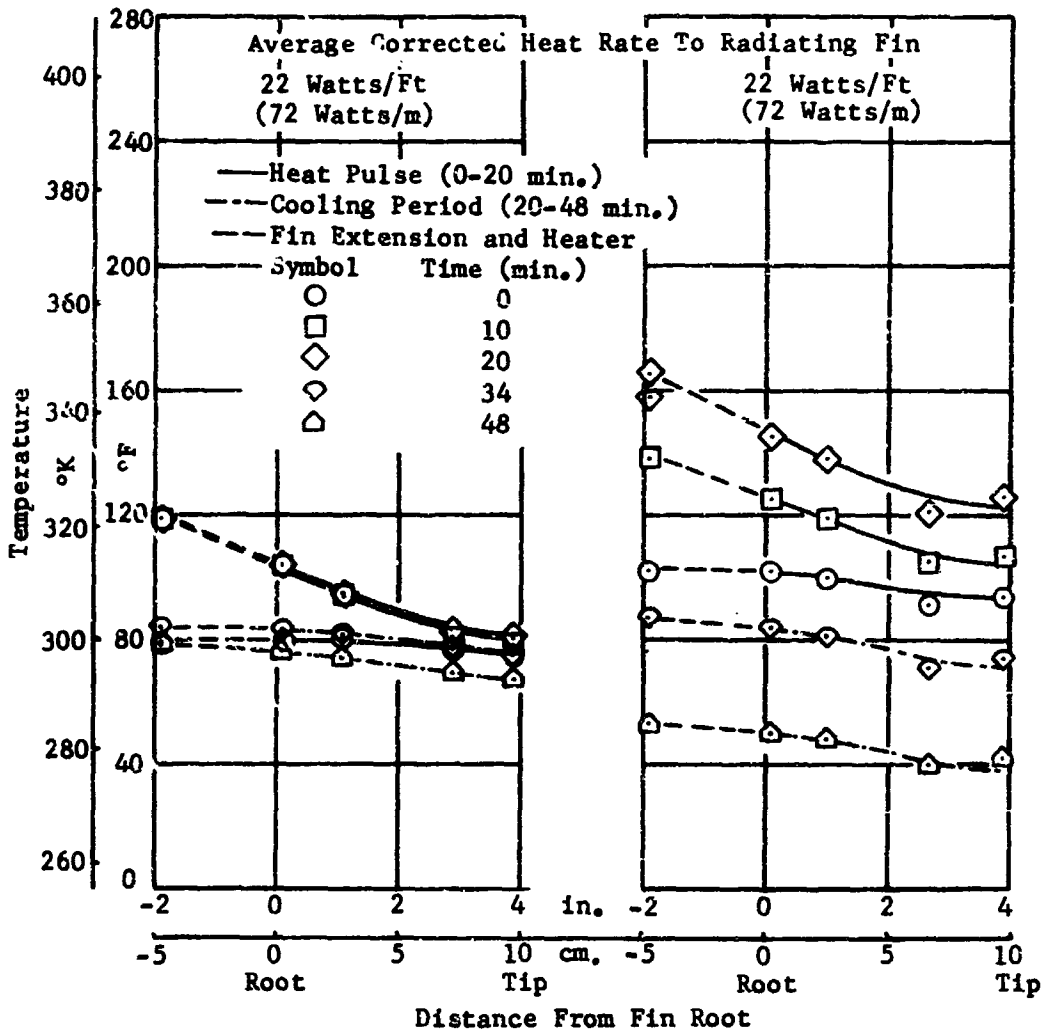
Time - Minutes



**Notes:**

- Fusible Material: Octadecane, Melting Point  $\approx 81^\circ\text{F}$  ( $300^\circ\text{K}$ )
- Insulating Glove: 15 Layers Aluminized Mylar
- Vacuum Chamber Pressure: less than  $10^{-4}$  Torr
- Cold Wall Temperature:  $72 - 77^\circ\text{K}$
- Thermocouple at  $-1.9$  in. is bonded on top of heater (inside insulating glove)

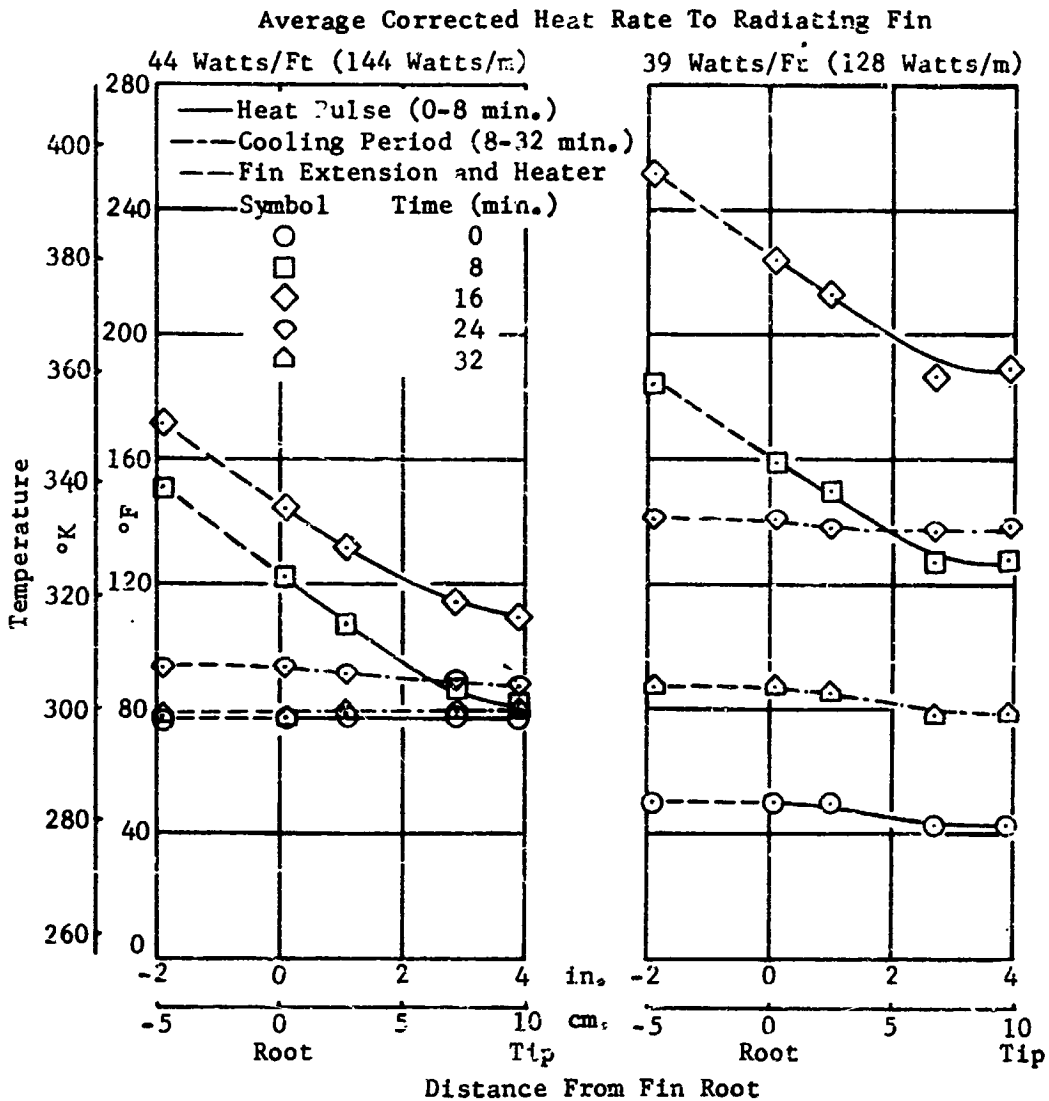
**FIGURE 6-12 TEMPERATURE DISTRIBUTION FOR TWO EQUAL WEIGHT RADIATING FINS (ONE WITH ATTACHED FUSIBLE MATERIAL, ONE OF SOLID ALUMINUM) FOR A 25 WATTS/FT OF FIN ROOT HEAT PULSE AND A ZERO WATT COOLING PERIOD (RUN 2, 3RD HEAT PULSE)**



**Notes:**

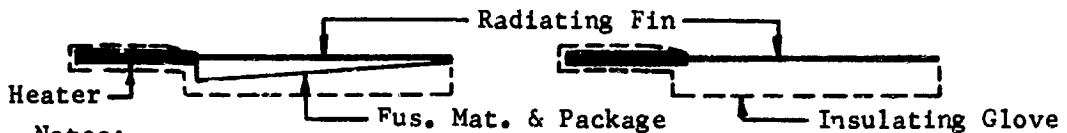
- Fusible Material: Octadecane, Melting Point = 81 °F (300 °K)
- Insulating Glove: 15 Layers Aluminized Mylar
- Vacuum Chamber Pressure: less than 10<sup>-4</sup> Torr
- Cold Wall Temperature: 72 - 77 °K
- Thermocouple at -1.9 in. is bonded on top of heater (inside insulating glove)

**FIGURE 6-13 TEMPERATURE DISTRIBUTION FOR TWO EQUAL WEIGHT RADIATING FINS (ONE WITH ATTACHED FUSIBLE MATERIAL, ONE OF SOLID ALUMINUM) FOR A 25 WATTS/FT OF FIN ROOT HEAT PULSE AND A 5.9 WATTS/FT COOLING PERIOD (RUN 2, 6TH HEAT PULSE)**



Fin + Fusible Material

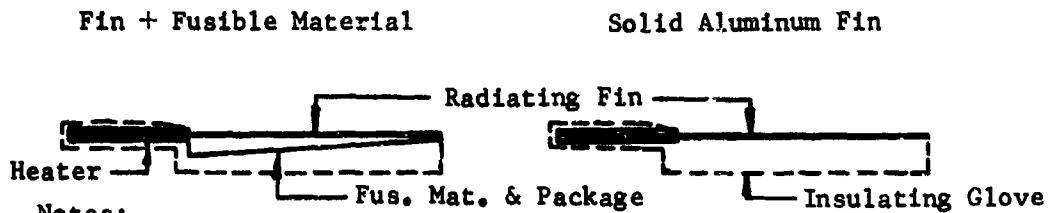
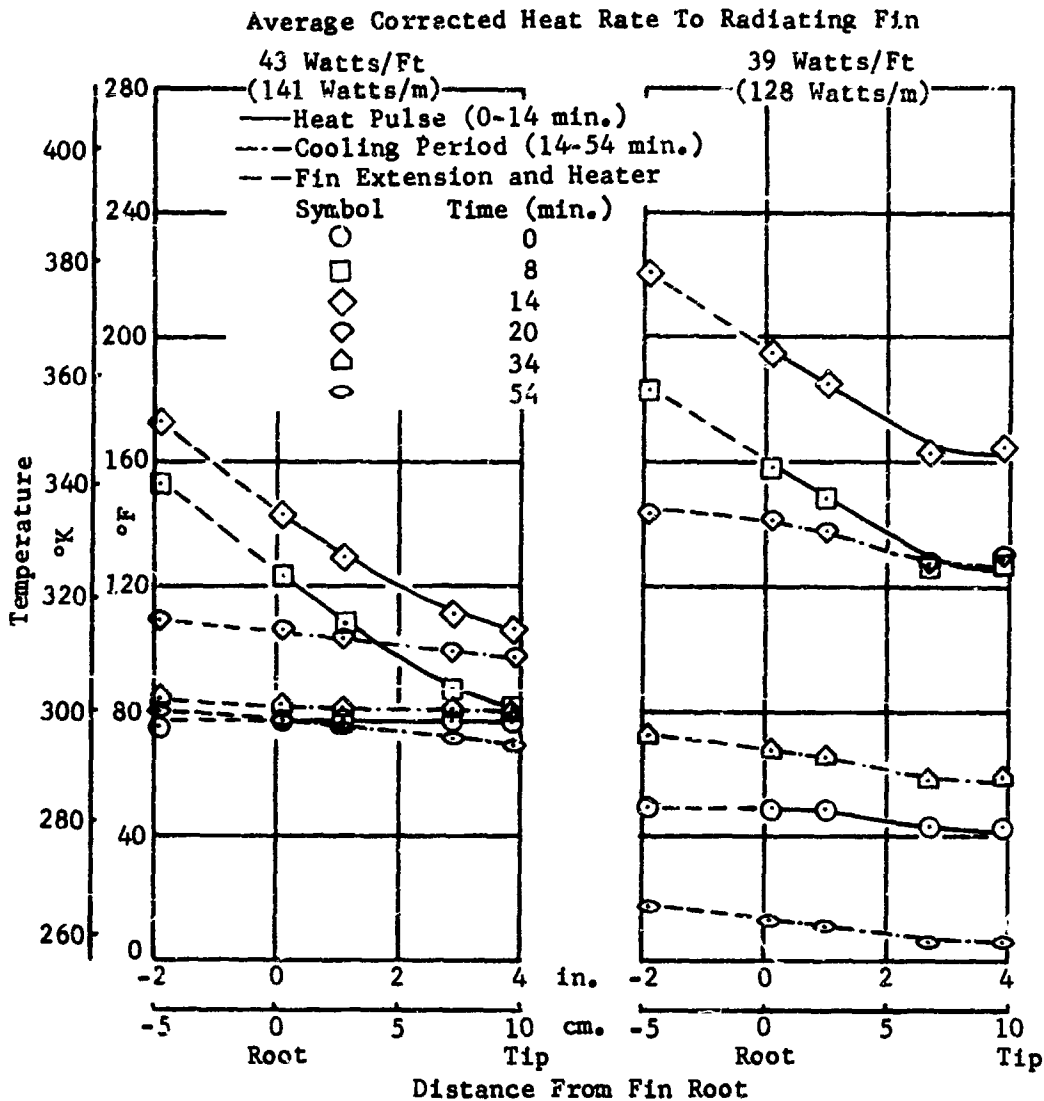
Solid Aluminum Fin



Notes:

- Fusible Material: Octadecane, Melting Point = 81°F (300°K)
- Insulating Glove: 15 Layers Aluminized Mylar
- Vacuum Chamber Pressure: less than  $10^{-4}$  Torr
- Cold Wall Temperature: 72 - 77 °K
- Thermocouple at -1.9in. is bonded on top of heater (inside insulating glove)

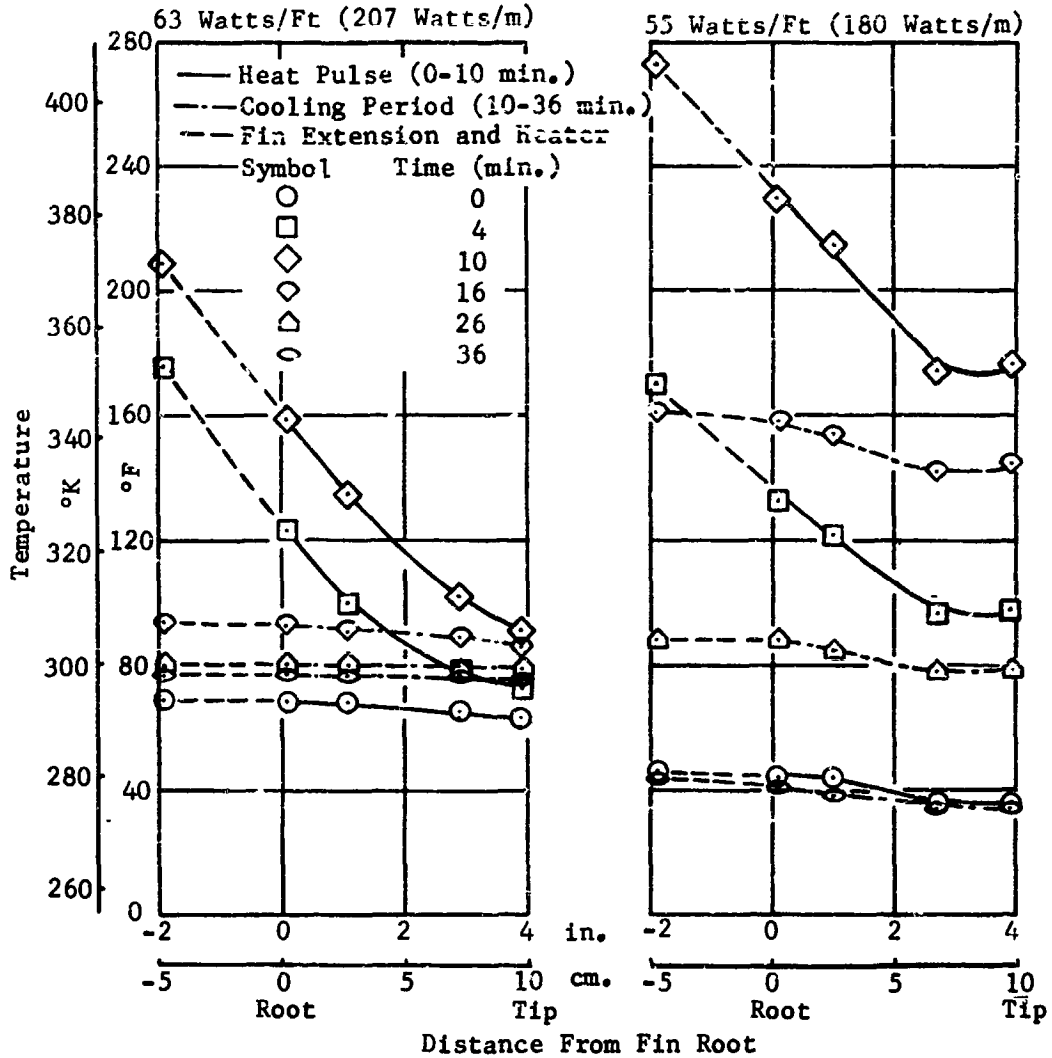
FIGURE 6-14 TEMPERATURE DISTRIBUTION FOR TWO EQUAL WEIGHT RADIATING FINS (ONE WITH ATTACHED FUSIBLE MATERIAL, ONE OF SOLID ALUMINUM) FOR A 50 WATTS/FT OF FIN ROOT HEAT PULSE AND A ZERO WATT COOLING PERIOD (RUN 3, 3RD HEAT PULSE)



Notes:  
 Fusible Material: Octadecane, Melting Point = 81 °F (300 °K)  
 Insulating Glove: 15 Layers Aluminized Mylar  
 Vacuum Chamber Pressure: less than 10<sup>-4</sup> Torr  
 Cold Wall Temperature: 72 - 77 °K  
 Thermocouple at -1.9 in. is bonded on top of heater  
 (inside insulating glove)

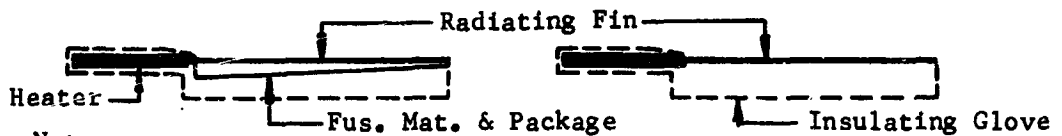
FIGURE 6-15 TEMPERATURE DISTRIBUTION FOR TWO EQUAL WEIGHT RADIATING FINS (ONE WITH ATTACHED FUSIBLE MATERIAL, ONE OF SOLID ALUMINUM) FOR A 50 WATTS/FT OF FIN ROOT HEAT PULSE AND A 2.9 WATTS/FT COOLING PERIOD ( RUN 3, 4TH HEAT PULSE)

Average Corrected Heat Rate To Radiating Fin



Fin + Fusible Material

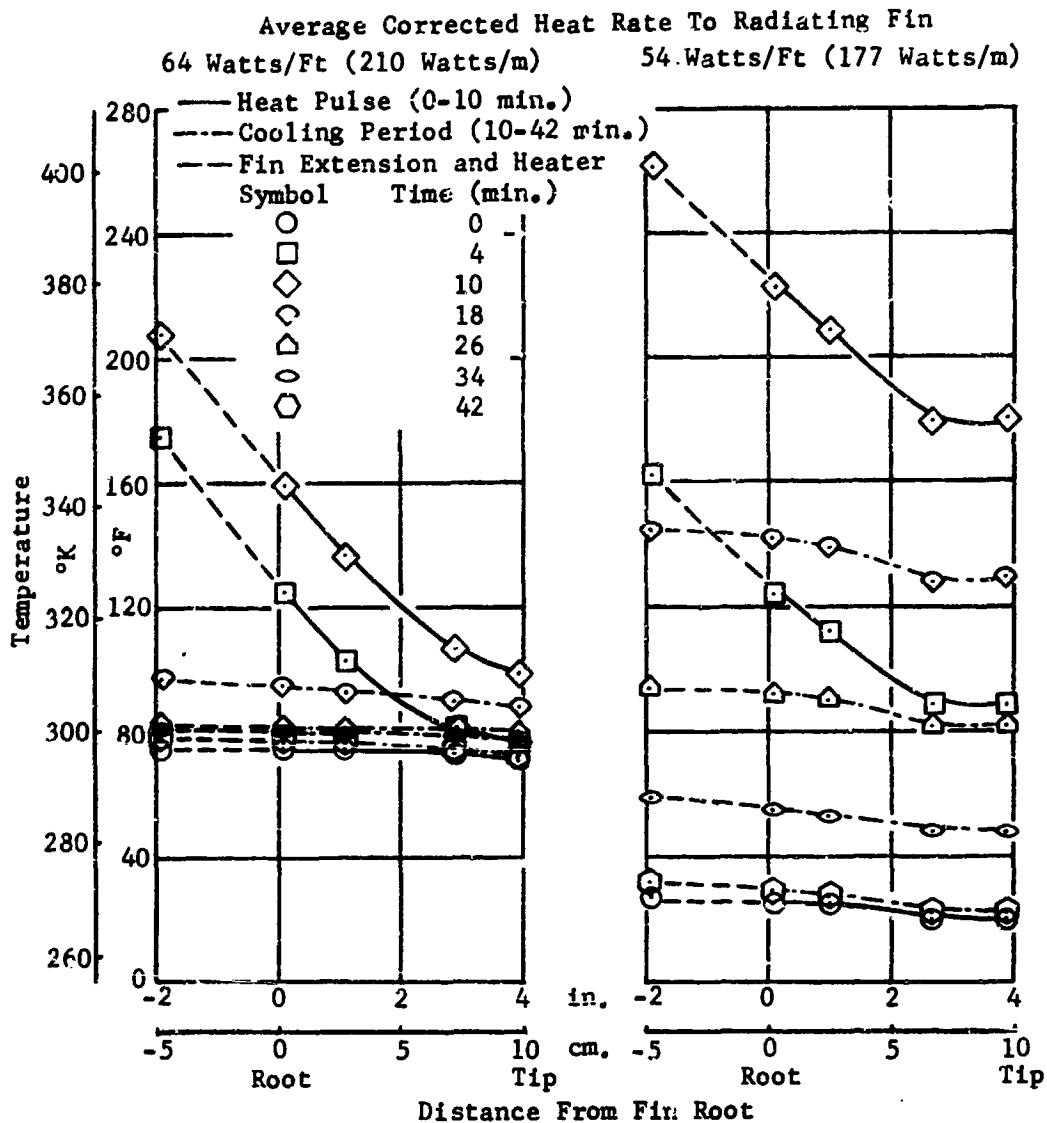
Solid Aluminum Fin



Notes:

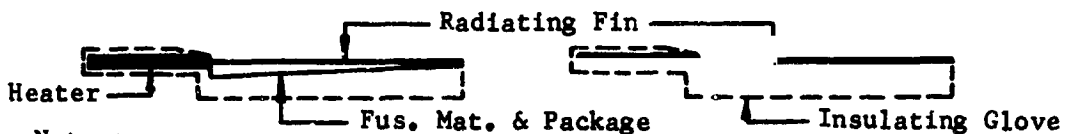
- Fusible Material: Octadecane, Melting Point = 81 °F (300 °K)
- Insulating Glove: 15 Layers Aluminized Mylar
- Vacuum Chamber Pressure: less than  $10^{-4}$  Torr
- Cold Wall Temperature: 72 - 77 °K
- Thermocouple at -1.9 in. is bonded on top of heater (inside insulating glove)

FIGURE 6-16 TEMPERATURE DISTRIBUTION FOR TWO EQUAL WEIGHT RADIATING FINS (ONE WITH ATTACHED FUSIBLE MATERIAL, ONE OF SOLID ALUMINUM) FOR A 75 WATTS/FT OF FIN ROOT HEAT PULSE AND A ZERO WATT COOLING PERIOD (RUN 4, 2ND HEAT PULSE)



Fin + Fusible Material

Solid Aluminum Fin



Notes:

- Fusible Material: Octadecane, Melting Point = 81 °F (300 °K)
- Insulating Glove: 15 Layers Aluminized Mylar
- Vacuum Chamber Pressure: less than  $10^{-4}$  Torr
- Cold Wall Temperature: 72 - 77 °K
- Thermocouple at -1.9 in. is bonded on top of heater (inside insulating glove)

FIGURE 6-17 TEMPERATURE DISTRIBUTION FOR TWO EQUAL WEIGHT RADIATING FINS (ONE WITH ATTACHED FUSIBLE MATERIAL, ONE OF SOLID ALUMINUM) FOR A 75 WATTS/FT OF FIN ROOT HEAT PULSE AND A 1.5 WATTS/FT COOLING PERIOD (RUN 4, 3rd HEAT PULSE)

Analytical Model

Aluminum Fin Geometry  
 Length 4in. (10.2cm)  
 Width 12in. (30.5cm)  
 Thickness .05in. (.13cm)  
 Package None  
 $\epsilon_{IR}$  .90  
 K Aluminum 120 BTU/HR-FT-°R  
 (2.08 WATT/cm-°K)  
 Radiation sink 0°K

Experimental Model

Aluminum Fin Geometry  
 Length 4.13in (10.49cm)  
 Width 2.04in (5.18cm)  
 Thickness .05in (.13cm)  
 Package .016in (.40cm)  
 (see model design)  
 $\epsilon_{IR}$  .88 ± .04  
 K Aluminum 90 ± 10 BTU/HR-FT-°R  
 (1.56 ± .17 WATTS/cm-°K)  
 Radiation Sink ≤ 72-77 °K

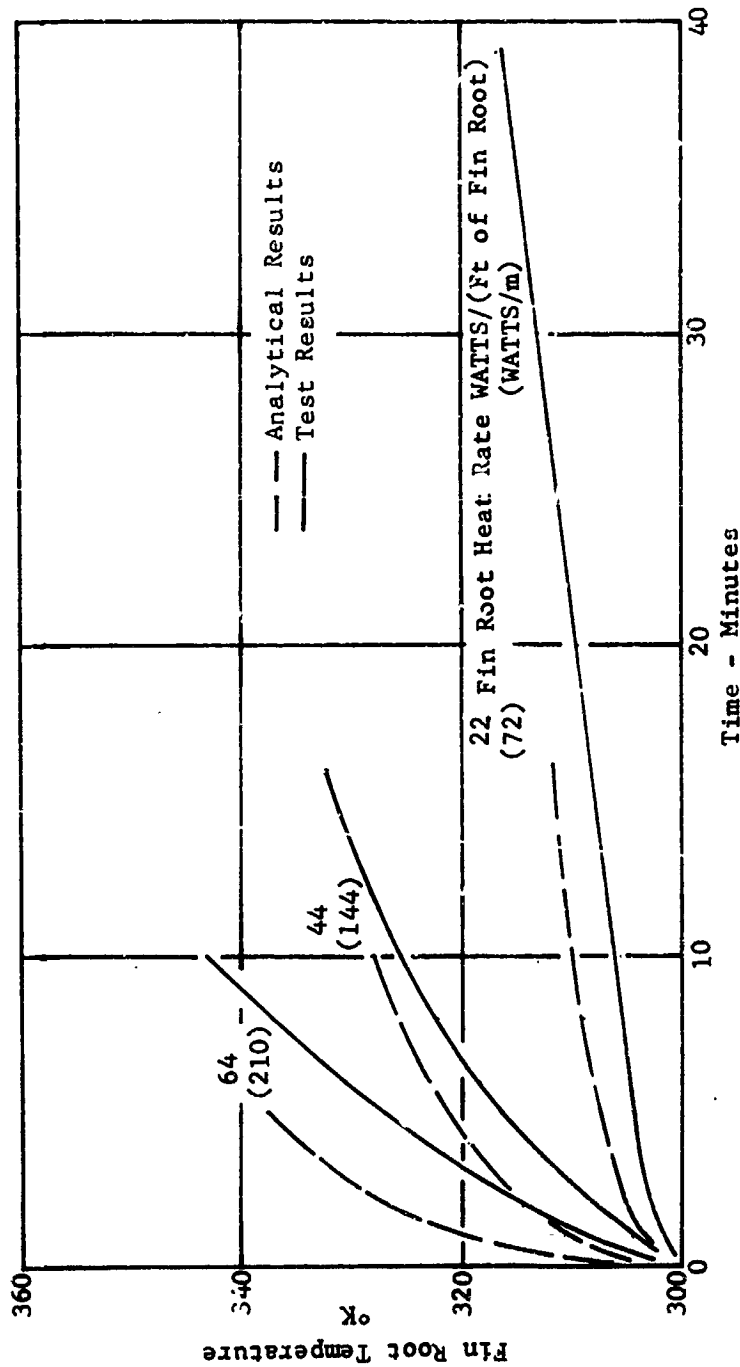


FIGURE 6-18 COMPARISON OF ANALYTICAL AND EXPERIMENTAL RESULTS FOR RADIATING FIN WITH ATTACHED FUSIBLE MATERIAL

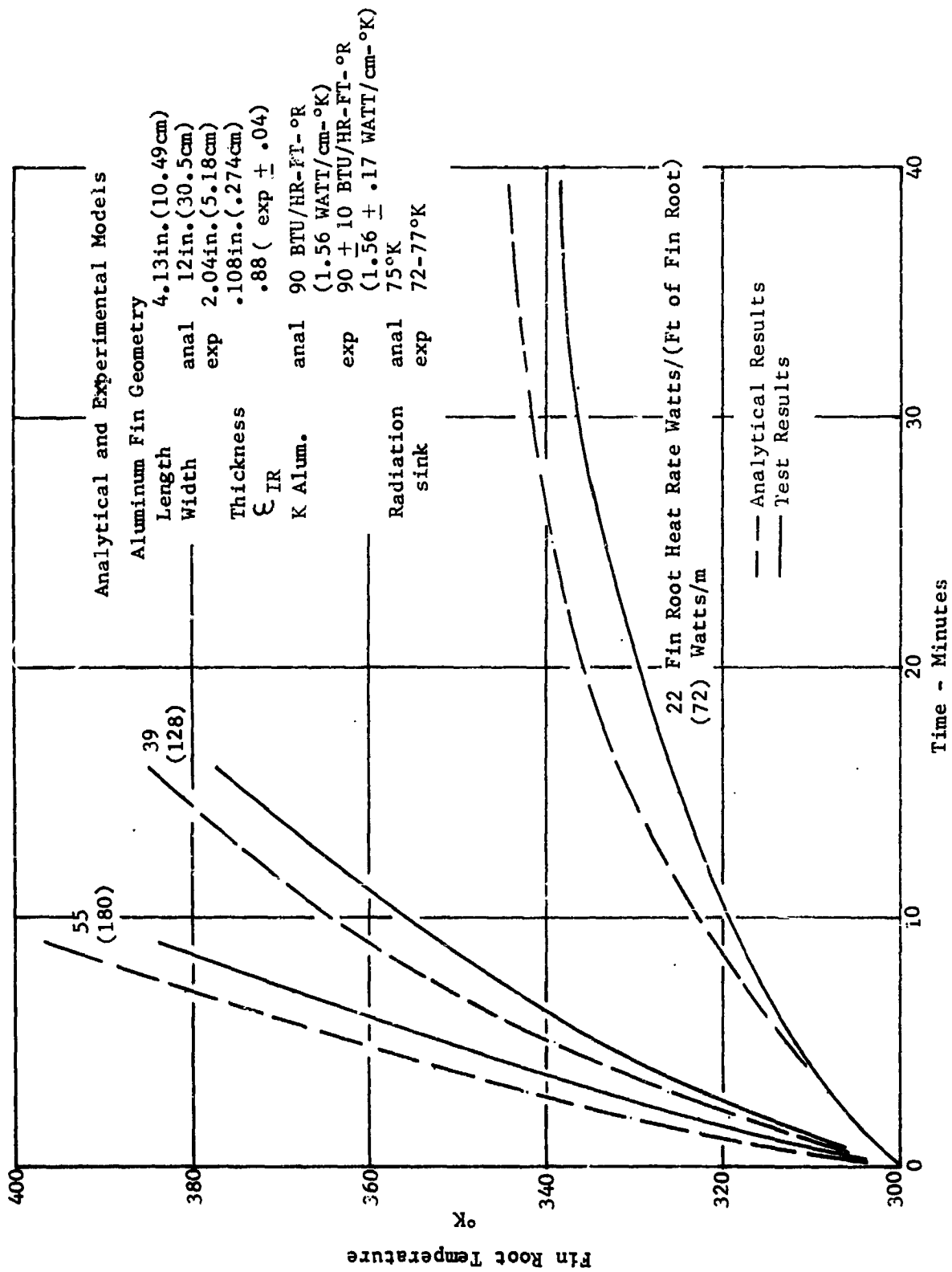


FIGURE 6-17 COMPARISON OF ANALYTICAL AND EXPERIMENTAL RESULTS FOR EQUAL WEIGHT, SOLID ALUMINUM RADIATING FIN

## SECTION 7

### SYSTEM PERFORMANCE IMPROVEMENT

The thermal analysis and experimental verification studies demonstrated the feasibility of using fusible materials for thermal control. These studies also emphasized the following two major shortcomings of the materials and systems used:

1. The poor thermal diffusivity of the paraffins limits the useful heat flux rate (power density) that can be absorbed with a tolerable temperature rise at the heat source, and/or it limits the fusible materials to thin slabs and the system to low total energy levels.
2. Maintaining the fusible material in good thermal contact with the heat source requires a pressurized container capable of expanding and contracting to allow for volume changes.

A system improvement study, conducted to overcome these shortcomings, resulted in the development of rigid packages with metallic filler materials that greatly improved the thermal diffusivity of the system at reasonable weight penalties. The improved packaging techniques and increased thermal diffusivity were verified experimentally using the adiabatic system and the four selected fusible materials: tetradecane, hexadecane, octadecane, and eicosane.

The metallic filler materials used were aluminum wool, aluminum foam, copper foam (Figure 7-1), and aluminum honeycomb (Figure 7-2). The best results were obtained with aluminum honeycomb. Honeycomb offers distinct advantages over the other filler materials. It provides a more effective heat transfer fin that can be selected in various fin (honeycomb sheet) thicknesses. Also, the fin spacing can be set at any desired position between zero (unexpanded honeycomb Hobe) and the fully open cell position.

The test results indicate that the fin spacing was the parameter controlling performance for the package depth and fusible materials tested. The selected packaging concept can limit the cold plate temperature rise to  $10^{\circ}\text{K}$  using n-paraffins as fusible materials, power densities up to  $500 \text{ watts/ft}^2$  ( $5,400 \text{ watts/m}^2$ ), and a total power input level of  $3000 \text{ watt-min/ft}^2$  ( $32,000 \text{ watt-min/m}^2$ ). The packaging weight penalty is less than the fusible material weight (50-85%) for this total energy level, which represents a 0.5 in. (1.27 cm) package depth.

The rigid package consists of thin aluminum skins with a rigid metallic filler material core, which carries the structural loads and increases the thermal diffusivity. The package

is filled with liquid fusible material at a high temperature and then sealed. When the fusible material solidifies, a partial void volume is formed. This void volume is filled with fusible material vapor and air at reduced pressures. There are no excessive loads imposed on the package until the fusible material fill temperature is exceeded. With the whole package above the fill temperature, the package would burst and leak due to the incompressibility of the liquid fusible material. Designing the heat sink with an adequate margin of safety will result in a reliable temperature control package.

The thermal analysis, package development, and performance testing that resulted in the improved design are discussed in the following subsections.

#### Aluminum Wool Filler Materials

Metallic wool was considered as a filler material for two reasons. First, the wool can retain the fusible material in good thermal contact with the cold plate by capillary action; this capillary action, in turn, allows a lightweight, unpressurized package. Second, the metallic wool improves the thermal diffusivity of the fusible material-wool matrix.

Two performance test models were built and tested with aluminum wool fillers for improved thermal diffusivity (Figures 7-3 and 7-4). The volume of compressed aluminum wool used in the two models was 10 and 18% of bulk volume. The models were only partly filled with octadecane at 140° F (333° K) and then sealed. The void volume with the fusible material solid is estimated at 20 to 23% of the total volume for the two models. The aluminum wool was attached to the cold plate by being pressed in a thin layer of epoxy. The side walls on the 18% aluminum wool model consisted of one layer of epoxy-impregnated glass cloth, with the package surface plates being separated by four posts (Figure 7-4). The side walls on the 10% aluminum wool model were 0.016 in. aluminum sheet. The models are shown with thermocouples installed in Figure 7-5.

As shown in Figure 7-6, the 10% aluminum wool model showed some improvement in performance (cold plate temperature rise as a function of corrected heat rate and time), but significantly less improvement than that indicated by the preliminary analysis at the aluminum concentration used. The performance of the 18% wool model (Figure 7-7) was essentially the same as that of the pressurized, stainless steel bellows model.

The marginal gain in performance with the addition of aluminum wool is probably due to the long heat path in the wool and the contact resistance between fibers. The better performance of the 10% wool model can be attributed to the aluminum side walls, which act as an effective heat transfer fin. While the aluminum wool models did not show marked improvement in system performance, they did verify the new packaging technique, i. e., the unpressurized rigid package concept.

## Metallic Foam Filler Materials

Metallic foams have capillary retention properties similar to those of compressed wool, providing the cell size is small. Since the cells are interconnected, the heat transfer capabilities should be greatly increased. After a material availability survey, three open cell metallic foams were found that warranted further investigation. All three foams are manufactured by Emerson and Cuming, Inc. One foam is aluminum with a density of 0.9 gm/cc, which is one-third that of solid aluminum. The other foams are copper with a density of 0.5 gm/cc; these foams have 10 and 30 cells/in. (Figure 7-1).

A preliminary weight analysis indicated that filling the package void volume with 20-25% aluminum would reduce the heat of fusion per total weight by a factor of two. This reduction in total energy was selected as a practical maximum for increasing the thermal diffusivity of the n-paraffins by dense filler materials. The copper foams are within this selected weight requirement, but the aluminum is too dense. Because the foams can be machined, it was assumed that the aluminum foam could be drilled or slotted to obtain a lower density. A performance analysis of octadecane with aluminum foam at various densities was performed to select a test configuration.

### Simplified Analysis of a Foam-Octadecane System

An analysis was performed using an Emerson and Cuming, Inc., open cell aluminum foam, Eccofoam MC-AO, with octadecane as the fusible material. This foam has a reported conductivity of 12.5 Btu/hr ft<sup>2</sup>F (10% that of solid aluminum). The foam was assumed to be slotted or drilled to lower densities in the analysis. A simplified form of the parametric analysis (see Section 5) was assumed for the analytical model. Zero lateral thermal resistance was assumed, making the results optimistic. The results are presented in Figure 7-8, which shows cold plate temperature rise and melt thickness as a function of heat rate, time, and percent aluminum. The thermophysical properties used in the analysis are shown in Figure 7-9. This analysis, though simplified and optimistic, indicated that significant performance improvement can be obtained by increasing the thermal diffusivity.

A weight analysis was performed using reasonable package wall thicknesses and adhesive weights (Figure 7-10). Package weight can also be optimized by this packaging technique if a stainless steel bellows is required for the simple adiabatic model (Figure 7-10). The optimum filler material concentration is on the order of 5-10% aluminum, considering both cold plate temperature performance and minimum weight. It did not appear feasible to reduce the aluminum foam to this density, and since the analysis is known to be optimistic, a test density of 15-20% solid aluminum was selected for the aluminum foam.

### Metallic Honeycomb Filler Materials

Initially, the available honeycomb cell sizes appeared too large to be useful for improving the thermal diffusivity of fusible material packages. Once it was determined that honey-

comb could be used reliably with even sheet spacing and with the cells partly open, a honeycomb package design was selected for further study.

The package has a 10-20% void volume for fusible material expansion. A wool or foam matrix will provide an even distribution of the fusible material except under high g loading. This reduces the heat path length from the cold plate to the fusible material. In the honeycomb design, the fusible material will be at the bottom of the cell under one g conditions, creating a longer heat path from the cold plate, which is located at the top of the model. At zero g, the fusible material should adhere to the cell walls with the void in the center. This is due to the high wetting capabilities of the paraffin-aluminum material system.

Honeycomb design analysis. - A fin effectiveness study indicated that a fin thickness on the order of 0.001-0.003 in. (0.0025-0.0076 cm), with fin spacings of less than 0.07 in. (0.18 cm), is required for optimum performance for a 0.5 in. (1.27 cm) package depth. Adapting a weight optimizing technique for parallel fins and a convective system (Reference 14) to the honeycomb geometry and a static fusible material (molten octadecane at 311°K) resulted in the optimum weight performance presented in Figure 7-11. Note that the abscissa (% aluminum) for Figure 7-11 is the same as for Figure 7-8, but in the case of honeycomb is represented by fin edge area over total surface area. The performance presented in Figures 7-8 and 7-10 can be used as an approximation for the honeycomb system, as well as for the foam system.

The lower the aluminum concentration in this analytical model, the more optimistic are the results. Considering this, test models were designed with aluminum filler material concentrations of 5-20%. To limit the number of variables, only one package depth (honeycomb fin length) was tested; this depth was 0.5 in. (1.27 cm).

#### Model Design and Fabrication

It was planned to test the three previously mentioned foams and aluminum honeycomb at four core densities, with two additional honeycomb models being tested at one density. Three honeycomb models at one density were selected to define the effects of fin (honeycomb) geometry. Octadecane was selected as the test fusible material. The final system improvement model design is shown in Figure 7-12.

The aluminum foam previously studied was not used because of the poor structural continuity revealed while the foam was being machined. Two copper foam models (5% copper) were built with cell sizes of 10 and 30 cells/in. The 30 cell/in. model failed when it was pressure-tested at 16 psig (Figure 7-13). The 10 cell/in. copper foam model and 12 honeycomb models were tested. The honeycomb sheet thicknesses used were 0.0012, 0.0019, and 0.0024 in. (0.0030, 0.0048, and 0.0061 cm), with the sheet spacing (honeycomb cell opening) varying from 0.019 to 0.072 in. (0.048 to 0.18 cm). The honeycomb geometries tested are shown in Figure 7-14.

The honeycomb Hobe (unexpanded honeycomb) was obtained from Hexcel Products, Inc. It consisted of 3003 aluminum sheet with a three-eighth-inch cell size. The cataloged nominal sheet thicknesses for the honeycomb tested are 0.001, 0.0015, and 0.0020 in. (0.0025, 0.0038, and 0.0051 cm) The variation from actual sheet thickness is due to density requirements in specifications that must be met by the manufacturer. The actual nominal sheet thicknesses define the package weight and performance parameters and are used throughout this report.

Two 1/16-in. holes were drilled through each honeycomb cell (Figure 7-12) to accommodate the filling of the fusible material. Prior to filling, the fusible material and the model were stabilized at 64-66°K above the melt point. The model was then evacuated and filled with the fusible material by vacuum filling. The model was sealed by shutoff valves and cooled in such a position that frozen material plugged the inlet and outlet ports. The valves were then removed and the ports capped.

Leakage and bond performance. - Three epoxies were used to bond the filler materials to the surface plates. A high-conductivity, silver-filled epoxy (56C) and a thin-sheet structural epoxy (FM-1000), Figure 7-12, were used on the first two models (-11 and -45) to determine the effect of the bond on heat transfer. The thermal performance of these two models; which were similar except for the adhesive, was essentially equivalent; therefore, the use of the heavy, silver-filled epoxy was discontinued. Apparently the honeycomb is forced through the epoxy during the cure process, forming a metal-to-metal contact. The first models built with FM-1000 did not bubble-leak when pressurized with helium to 30 psig, but high trace leakage was detected with a helium sniffer. Some poor curing results were also observed with the FM-1000. Bubble leakage was detected for two models (-7 Mod 1 and -9 Mod 1) at the flange (Figure 7-12). These models were patched with epoxy and fiberglass prior to performance testing. The remaining models were built with 3M Company adhesive AF-300. The thermal performance of this adhesive was equivalent to FM-1000; no helium leakage was detected to 30 psig. The adhesive used for each model is noted on the test results.

Model identification. - Twelve additional models were built after the performance tests on Models -11 and -45. The first group was designated Mod 1 and the second group Mod 2. The complete title (Dash No., Mod No.) must be used to identify a model because the honeycomb geometry was varied for equivalent dash numbers. The last two models built (-19 Mod 1 and Mod 2) deviate considerably from the optimum weight effectiveness line shown in Figure 7-14 ( $t = 0.0019$  in.,  $2x = 0.072$  in.). These models were built at a low density with the honeycomb stock available at the time of manufacture.

The only foam model (-1 Mod 1) that was performance tested contained copper foam (10 cells/in.). Two honeycomb models (-11 Mod 1, -15 Mod 1) were tested with two fusible materials (octadecane and eicosane). The models were evaluated at high temperature and flushed with carbon tetrachloride for cleaning. The first test material used was octadecane. The total number of configurations tested (model + fusible material) was 15. A minimum of two

models were tested with each of the four selected fusible materials: tetradecane, hexadecane, octadecane, and eicosane.

### Experimental Evaluation of System Improvement Models

The system improvement models were insulated in 20 layers of aluminized Mylar and tested in a vacuum chamber maintained in the  $10^{-5}$  torr range. A model with thermocouples installed and ready for testing is shown in Figure 7-15. Two models were tested at the same time; the test installation is shown in Figure 7-16. Note the Tygon tube manifold on the top of each model. The fusible material was solidified after each test run by discharging cold nitrogen gas onto the models. When the fusible material was solidified, the chamber was re-evacuated and another test run made. The Tygon tube is a poor thermal conductor, and the net energy that can be stored or transferred by the Tygon manifold was calculated to be less than two percent of the total energy available in the test model.

The model temperature level was stabilized a few degrees below the melt point of the fusible material. The test was started with a three-step power input to obtain a constant power input to the model. The first two steps were 10 and 5% above the continuous load and lasted for one minute. The majority of the initial excess power is absorbed by the heater. Test runs were made for most models at six power levels, with one rerun being made for one half the models. The power levels used were 10, 15, 20, 30, 40, and 50 watts/model, resulting in corrected power levels of approximately 105, 157, 210, 315, 420, and 525 watts/ft<sup>2</sup>. The heat stored in the heater and lost to the environment was subtracted from the input power, and this power history was averaged as a function of time to obtain the corrected power input to the package. Note that the highest power level tested for the simple adiabatic model was approximately 200 watts/ft<sup>2</sup>.

Initial models with honeycomb filler materials. - As previously mentioned, Models -11 and -45 were built and tested to determine the effect of the bond between the core and surface plates on thermal performance. The models were built as similar as possible except for the adhesive used to bond the aforementioned joint (Figure 7-12). The selected honeycomb sheet thickness for the models was 0.0019 in. (0.0048 cm) with a nominal maximum fin spacing of 0.032 in. (0.081 cm). The test fusible material was octadecane. The test results for these models (cold plate temperature rise and corrected power input as a function of time) are presented in Figures 7-17 through 7-23.

Both models displayed good thermal performances. The cold plate temperature remained relatively constant after the initial increase at less than 10°K above the melt point for the majority of the liquefaction period. The cold plate temperature started rising rapidly just prior to complete liquefaction. Note that the temperature at the bottom of the package is above the melt point for the majority of the test period (Figures 7-17 through 7-23). Therefore, melting is being accomplished at all metal surfaces.

A good indication of complete liquefaction is the sharp increase in temperature at the bottom of the package. This is demonstrated by the results shown in Figures 7-17 through 7-23. A comparison of these results with the total energy available (Figure 7-24) shows good correlation for both models. The correlation is better for Model -45, as indicated by the comparison of cold plate temperature at the corresponding  $\theta_t$  and power input. Figure 7-24 also shows that over half the temperature rise occurs during the last 20 percent of the liquefaction period and that the temperature rise is only on the order of 5°K for the first 80%. In addition, the results indicate that this temperature control technique is useful for heat pulses at the 500 watts/ft<sup>2</sup> level for short time periods. Figure 7-25 is a graphic comparison of the performance improvement obtained with the system improvement adiabatic test model.

Additional test models. - The test results for the additional models are presented in Figures 7-26 through 7-38. The pertinent data defining the fusible material tested and the model configuration are noted in each figure. The time period ( $\theta_{eff}$ ) noted in these figures identifies the time at which the cold plate temperature started rising rapidly. The time ( $\theta_T$ ) identifies the total liquefaction period as indicated by the sharp temperature rise at the bottom of the package.  $\theta_{eff}$  varied from 75 to 95 percent of  $\theta_T$  for all test models.

The best cold plate temperature rise performance is on the order of 10°K at  $\theta_T$ , 5°K at  $\theta_{eff}$  with an input power of 500 watts/ft<sup>2</sup> (5400 watts/m<sup>2</sup>). Note the varying cold plate temperature rise as a function of fin (honeycomb sheet) spacing. The total energy absorbed for each test run is the product of  $\theta_T$  and the corrected average power listed in each figure. The actual package weight and weight per unit area are also noted in each figure.

### Correlation of Test Results

The repeatability of results for tests rerun on the same model is quite good, as illustrated by the results presented in Table 7-1. As previously mentioned, reruns were made for half the models. The product of the complete liquefaction period ( $\theta_T$ ) and the average corrected power input ( $\bar{q}$ ) is the total energy absorbed by the package and fusible material for a particular run. The cold plate temperature is rising rapidly at  $\theta_T$ , resulting in more scatter of cold plate temperature performance than total energy for these rerun conditions.

There is considerably more variation in the total energy per test for the final test models and fusible materials than for the initial test models (-11 Mod 1, -45), as shown in Figure 7-24. The total energy varied from 2530 watt-min/ft<sup>2</sup> (+13%) for Model -9 Mod 2 (hexadecane) to 3330 watt-min/ft<sup>2</sup> (+8%) for Model -19 Mod 1 (octadecane). Some variation is due to the quantity and purity of the fusible material, some to the variation in model temperature rise (mass x specific heat x  $\Delta T$ ), and some, undoubtedly, to test accuracy. Therefore, the test results were correlated and smoothed for each test model before the data were analyzed to determine the effect of the honeycomb configuration.

The correlation of the test results is presented in Figures 7-39 through 7-50, with each figure representing one model and test fusible material. The effective temperature control periods in these figures correspond to the break in cold plate temperature from the test results shown in Figures 7-27 through 7-38. No attempt was made to correlate the results for the copper foam model (Figure 7-26) with the honeycomb data.

#### Analysis of Test Results

A preliminary analysis of the correlated test results indicated that the controlling parameter for minimizing cold plate temperature was the honeycomb sheet spacing. Various models with different fusible materials and honeycomb sheet thicknesses, but equal sheet spacing, had equivalent performance. This indicated that the optimum honeycomb geometry presented in Figures 7-11 and 7-14 was pessimistic and that the tested fin length, 0.5 in. (1.27 cm), has an optimum thickness of less than 0.0012 in. (0.0030 cm).

The performance parameters selected for comparison were cold plate temperature rise per unit time ( $\Delta T_{cp}/\theta$ ) and input power density ( $\bar{q}$ ). These results are presented in Figure 7-51 as a function of fin (honeycomb sheet) spacing and independent of fin (honeycomb sheet) thickness. The results for the honeycomb test models are also presented independent of the test fusible material.

Good correlation was obtained at the lower power densities, 100-300 watts/ft<sup>2</sup> (1075-3230 watts/m<sup>2</sup>), and at the effective temperature control period ( $\theta_{eff}$ ). There is more scatter in the results at the higher power densities and at the complete liquefaction period ( $\theta_T$ ). The two points at a 0.04 in. (0.10 cm) fin spacing show good correlation and represent Models -7 Mod 1 and -13 Mod 1 with fin thicknesses of 0.0012 and 0.0024 in. (0.0030 and 0.0061 cm).

#### Summary of Experimental Results

The analysis of the test results for the honeycomb models and n-paraffin fusible materials tested resulted in the adiabatic system performance presented in Figure 7-52. This performance is obtainable for any fusible material with equivalent thermophysical properties. The controlling material properties are thermal conductivity, density, and heat of fusion. The controlling packaging parameters are fin spacing and length. The optimum fin thickness is less than 0.012 in. (0.030 cm) at a fin spacing of less than 0.04 in. (0.10 cm). The optimum fin thickness is less than 0.0019 in. (0.0048 cm) at a fin spacing of 0.07 in. (0.18 cm) for the aforementioned fin length.

The difference between the effective temperature control period and the complete liquefaction period can be reduced, probably to less than 5%. The model design shown in Figure 7-12 allowed a void space between the core edge and package edge. This void space resulted from the double radii used to form the surface plates. Also note the chambered corner of the core. For all test cases, the thermocouple at the corner of the package bottom determined

the complete liquefaction period. The bottom thermocouple at the package center indicated that the temperature at this location followed the cold temperature more closely. This suggests that the edge effect which causes the difference between  $\theta_{\text{eff}}$  and  $\theta_T$  could be greatly reduced by reducing the aforementioned void volume.

A package weight of 55 to 85% of the fusible material weight is practical for the package depth and total energy level of the test models. The package weight penalty will depend on the tolerable temperature rise and the power density.

#### Comparison of Test Results and Simplified Analytical Model

A comparison was made of the parameters controlling the improved adiabatic system performance for the simplified analytical model, using aluminum foam to improve thermal diffusivity and using an aluminum honeycomb filler material in the test model. The selected honeycomb sheet thickness was 0.0012 in. (0.0030 cm), which is the most effective test fin thickness. The fusible material is octadecane. The controlling parameter (as presented in the simplified analysis) is the effective thermal conductivity at a given aluminum concentration. The equation for cold plate temperature rise from the parametric analysis (Figure 5-2) was used to calculate the effective conductivity from the test results (Figure 7-52).

The results are presented in Figure 7-53. The cold plate temperature rise of the analytical model is a result of the assumed conductivity, while the effective conductivity for the test model is a result of the test performance and the assumed analytical model. Note the good correlation for melt thickness present in Figure 7-53. The increase in effective conductivity for the test results above that of pure octadecane ( $A_f/A_S = 0$ ) is greater than an order of magnitude.

The influence of induced convection currents caused by the material density temperature dependence and by earth gravity is difficult to estimate. The lightest liquid fusible material is at the top next to the heat source, but the fusible material is molten at all metal boundaries. Therefore, the dense solid core will fall toward the package bottom, causing a forced convection effect. The small cell size 0.5 in. (1.27 cm) high by 0.02-0.07 in. (0.051-0.18 cm) wide—and the low temperature potential 5-10°K will greatly restrict convection effects. This transient problem with irregular-moving boundaries and discontinuities (assuming the solid fusible material does fall) would be difficult to solve by any analytical technique.

The effects of convection are probably much less than the influence of the reduced fin spacing, as demonstrated in Figure 7-53. The effective conductivity is greatly increased as the cell size and temperature potential are reduced, both factors reducing the potential for convection.

TABLE 7-1  
 REPEATABILITY OF TEST RESULTS (COMPARISON OF  
 RESULTS FOR TESTS REPEATED ON THE SAME MODEL)

MODEL		TEST FUSIBLE MATERIAL	RESULTS OF INITIAL TEST RUN			RESULTS OF REPEATED TEST RUN		
DASH NO.	MOD NO.		$\theta_T$	$\Delta T_{cp}$	$\bar{q}$	$\theta_T$	$\Delta T_{cp}$	$\bar{q}$
-9	1	Octadecane	25.3	5.5	103	*25.4	4.2	105
-13	1	Octadecane	15.1	13.0	211	*15.1	13.1	211
-15	1	Octadecane	*14.1	9.3	210	13.9	6.2	212
-7	2	Tetradecane	*23.4	5.5	106	23.5	6.3	107
-9	2	Hexadecane	*22.3	6.1	106	21.1	6.1	107
		Hexadecane	*11.9	9.0	211	11.3	8.3	211
-11	1	Eicosane	20.2	6.0	106	*21.0	5.2	105
-15	1	Eicosane	*21.5	6.2	105	20.0	3.7	106

Notes:

\* = Selected data for presentation and correlation.

$\theta_T$  = Complete liquefaction period determined by break in temperature at bottom of package. (Minutes)

$\Delta T_{cp}$  = Cold plate temperature rise at  $\theta_T$ . ( $^{\circ}K$ )

$\bar{q}$  = Average corrected power input (Watts/Ft<sup>2</sup>)

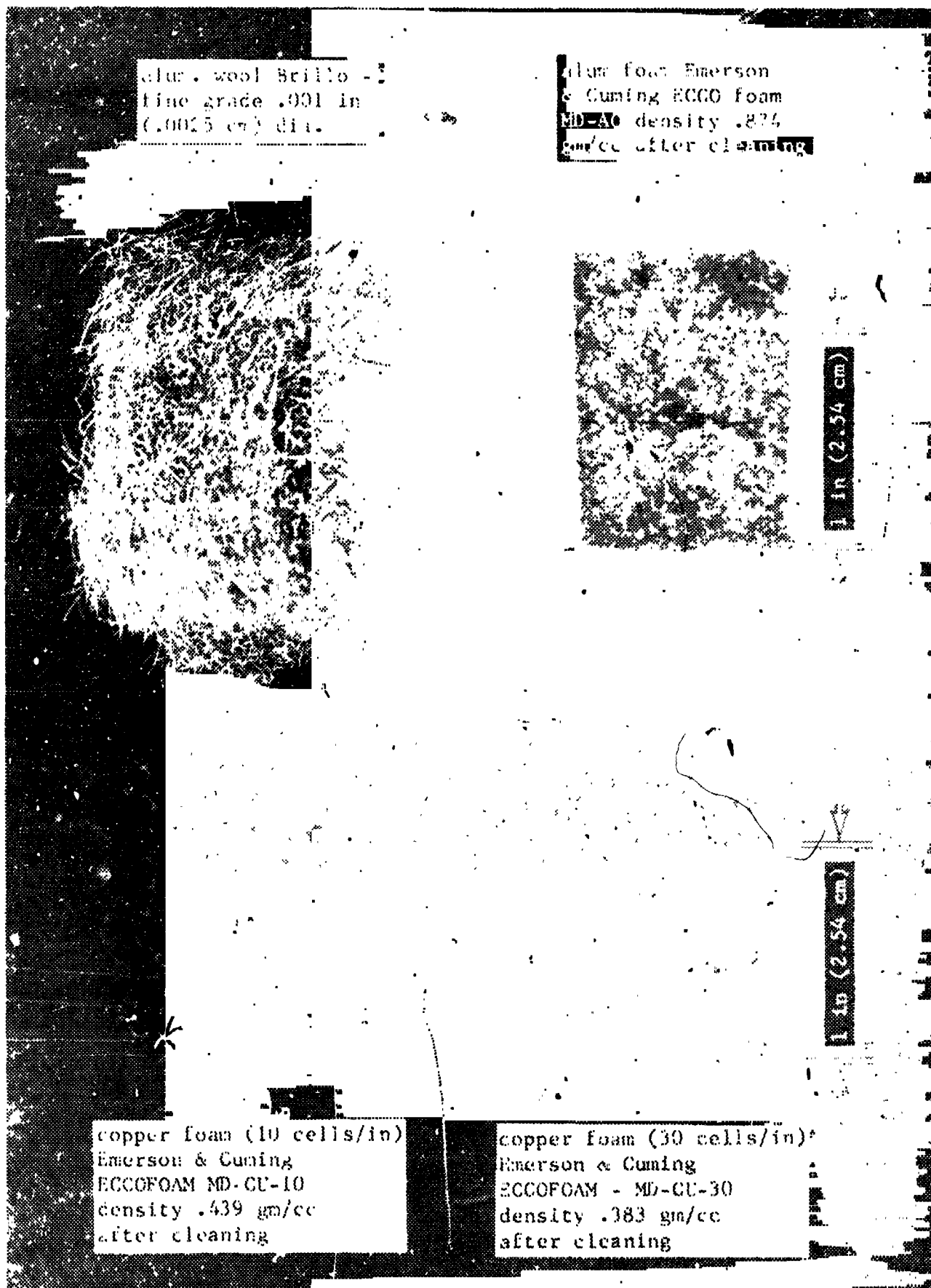


FIGURE 7-1 METALLIC WOOL & FOAM FILLER MATERIALS INVESTIGATED TO IMPROVE THERMAL DIFFUSIVITY

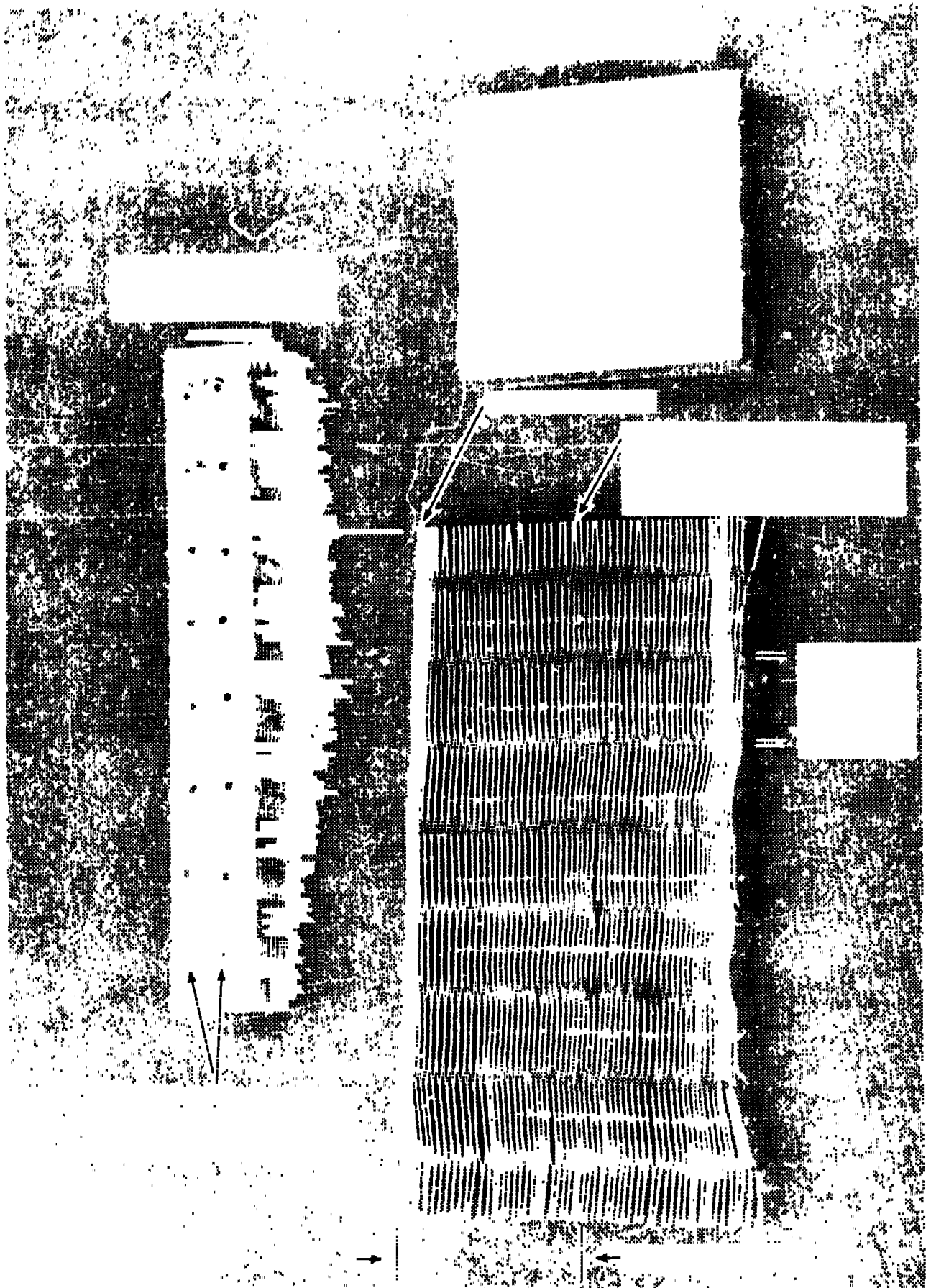
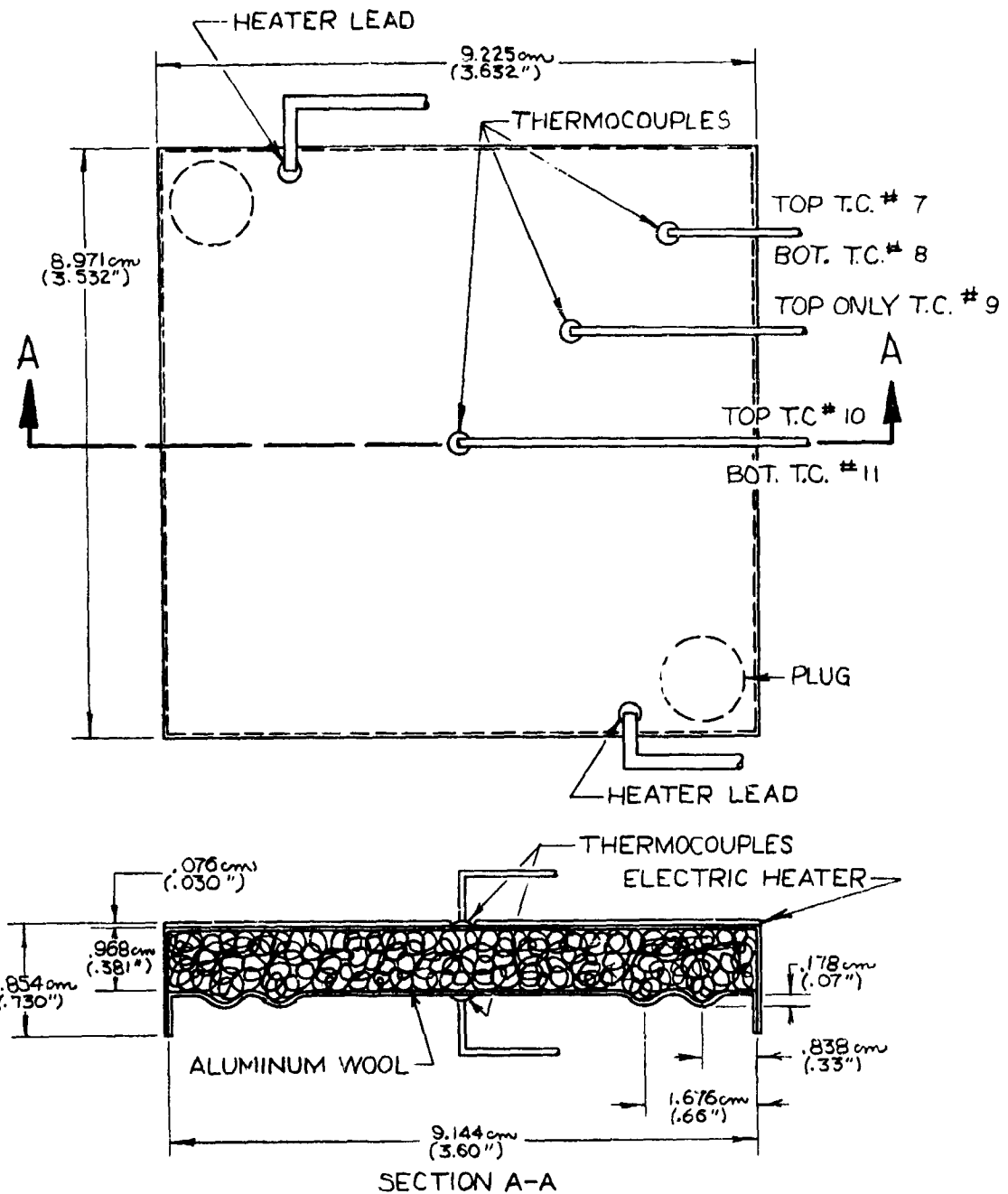


FIGURE 7-2 ALUMINUM HONEYCOMB FILLER MATERIALS USED TO IMPROVE THERMAL DIFFUSIVITY



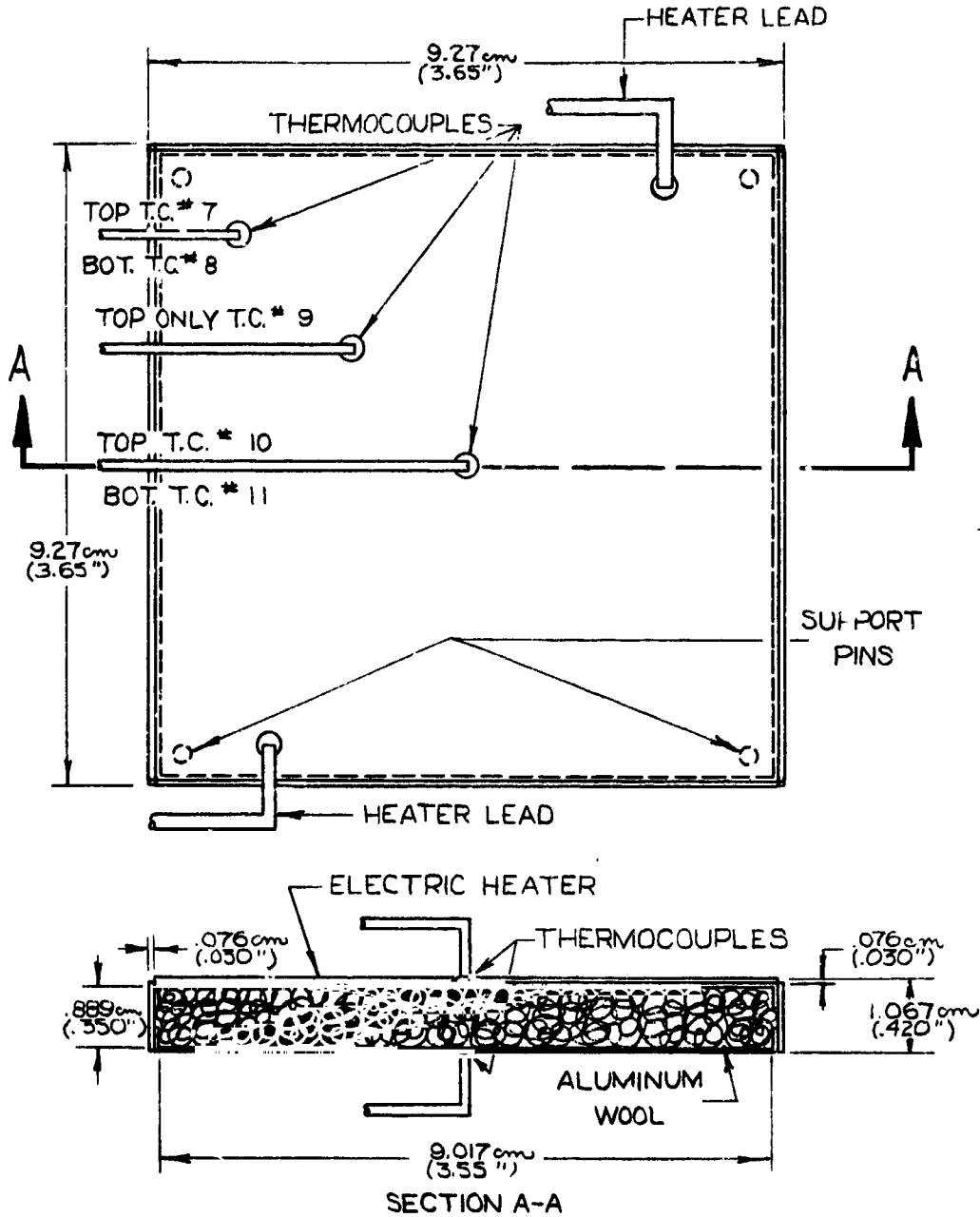
NOTES:

1. Materials:

- a. All surfaces .041cm(.016") aluminum.
- b. Aluminum wool Brillo wool fine grade dia. .0025cm.(.001") approx. Cavity filled 10.% by volume with aluminum wool.
- c. Fusible material tested - Octadecane  $C_{18}H_{38}$
- d. Electric heater - nichrome wire and laminated fiberglass, epoxy filled.
- e. Thermocouples - cromel constantan.

- 2. All bonds and seals are epoxy, including aluminum wool to top and bottom plate.

FIGURE 7-3 ADIABATIC TEST MODEL FILLED WITH 10.% ALUMINUM WOOL



NOTES:

1. Materials:

- a. Top and bottom plates .051cm(.020") aluminum.
- b. Sides fiberglass .076cm(.030") approx.
- c. Aluminum wool Brillo wool fine grade dia. .0025cm (.001") approx. Cavity filled 18% by volume with aluminum wool.
- d. Fusible material tested - Octadecane  $C_{18}H_{38}$
- e. Electric heater - nichrome wire and laminated fiberglass, epoxy filled.
- f. Thermocouples - cromel constantan.

2. All bonds and seals are epoxy, including aluminum wool to top and bottom plate.

FIGURE 7-4 ADIABATIC TEST MODEL FILLED WITH 18% ALUMINUM WOOL

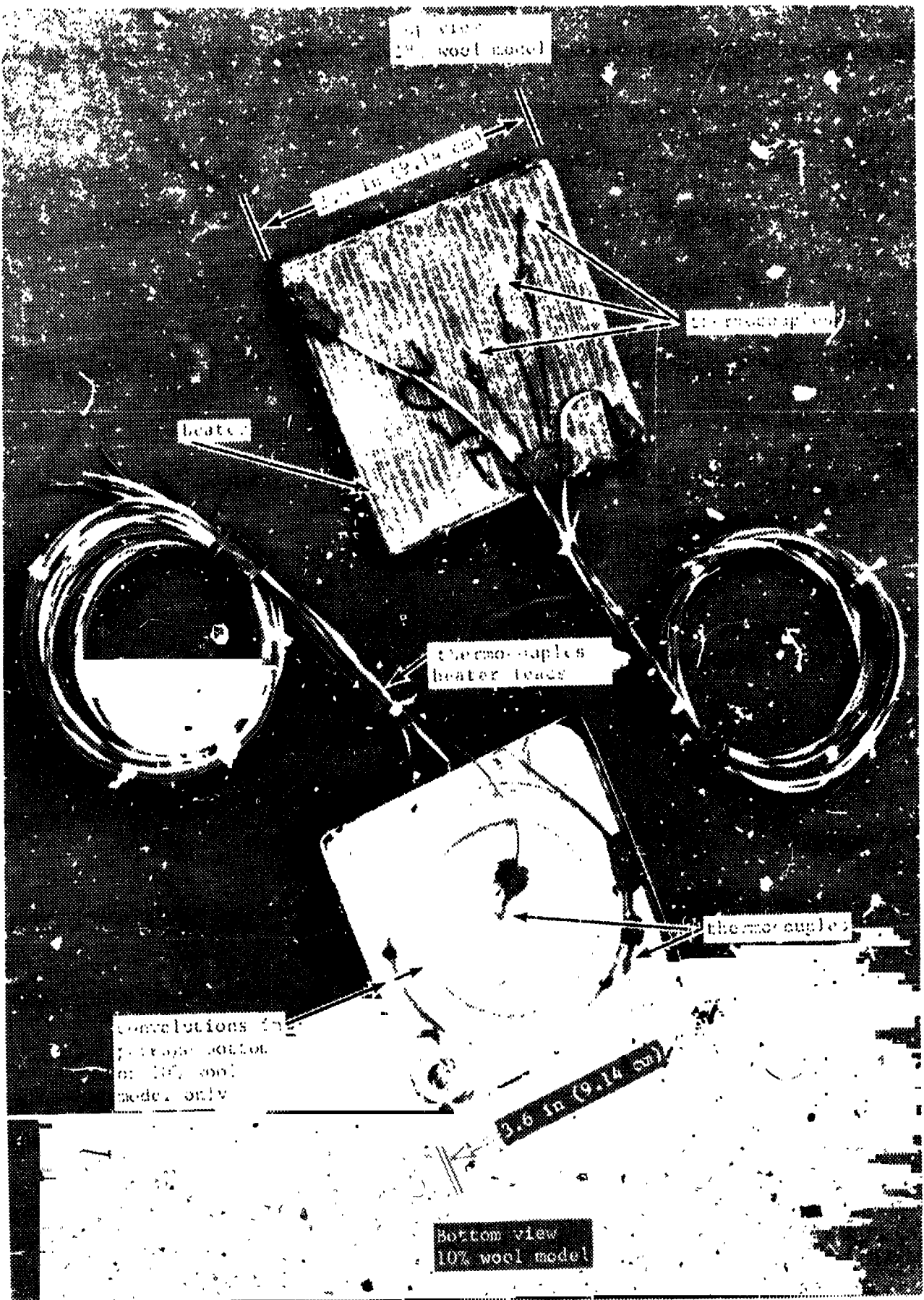
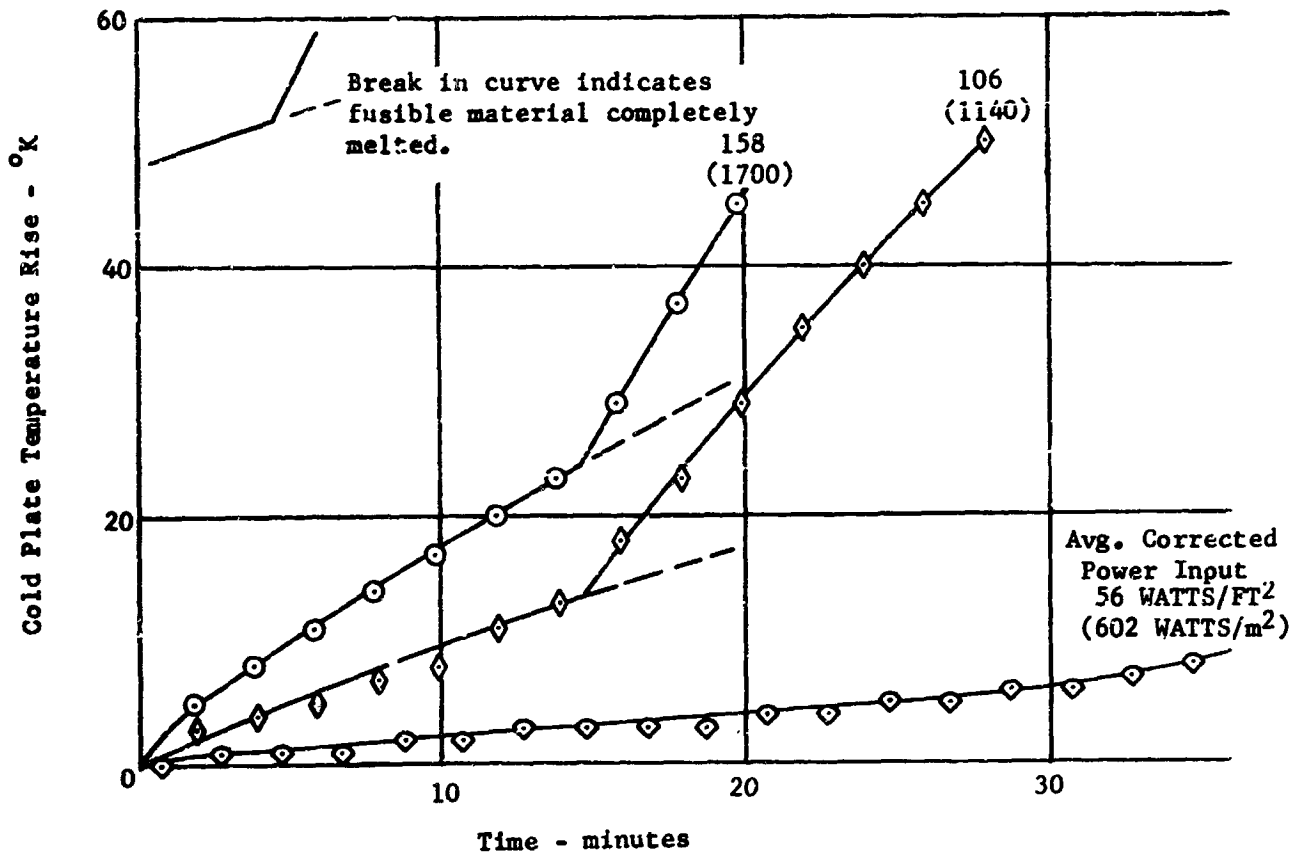


FIGURE 7-5 ALUMINUM WOOL MODELS

10% cavity by volume filled with aluminum wool, dia. .0025cm(.001"). Aluminum sides .041cm(.016"). Fusible material - Octadecane. Void volume with solid fusible material 21%.

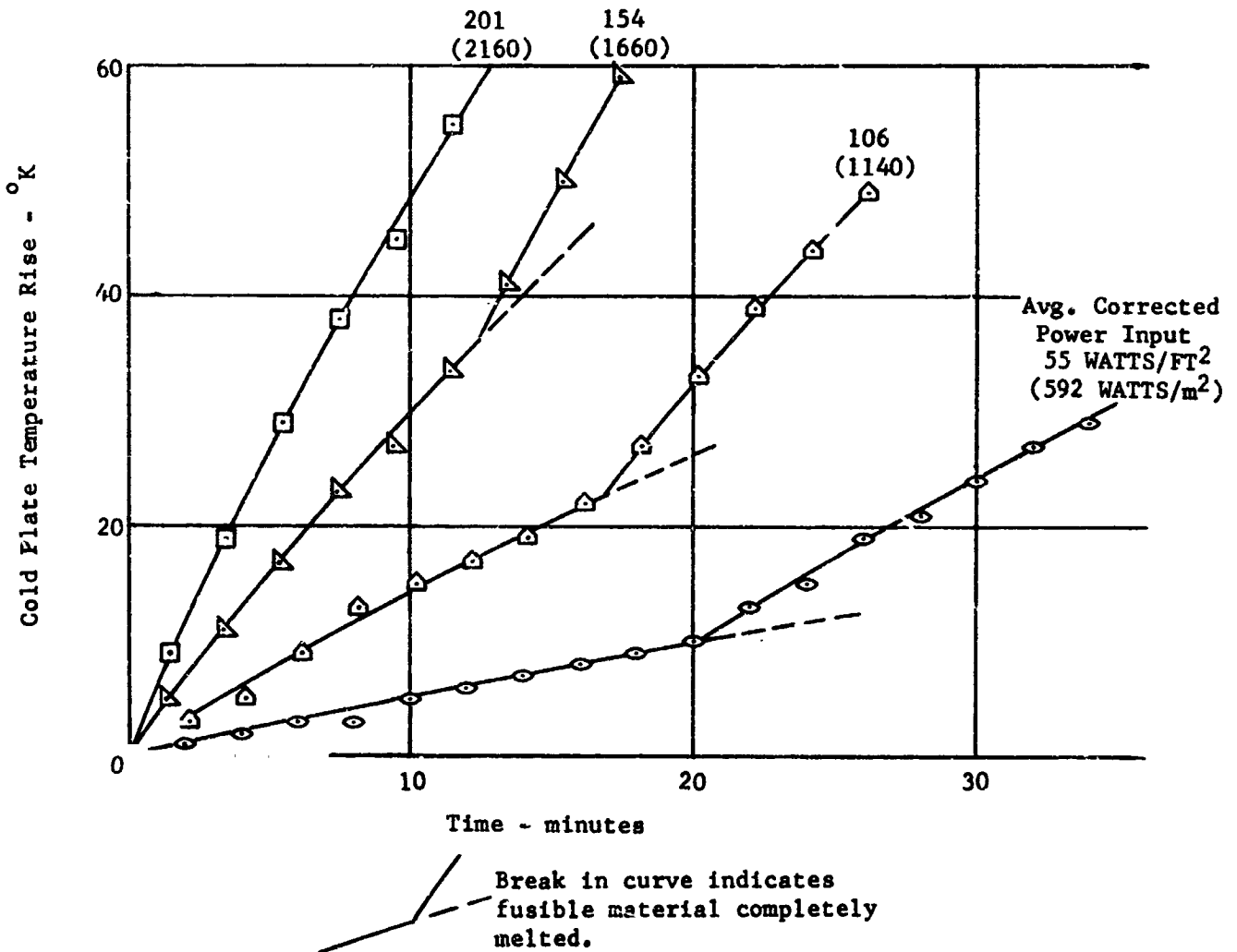


Notes:

1. Time 0 taken when cold plate temperature exceeded 300 °K (melting point of Octadecane).
2. Measured deviation of cold plate temperature less than 2 °K from the thermocouple shown.

FIGURE 7-6 TEST RESULTS OF ADIABATIC MODEL FILLED WITH 10% BY VOLUME ALUMINUM WOOL

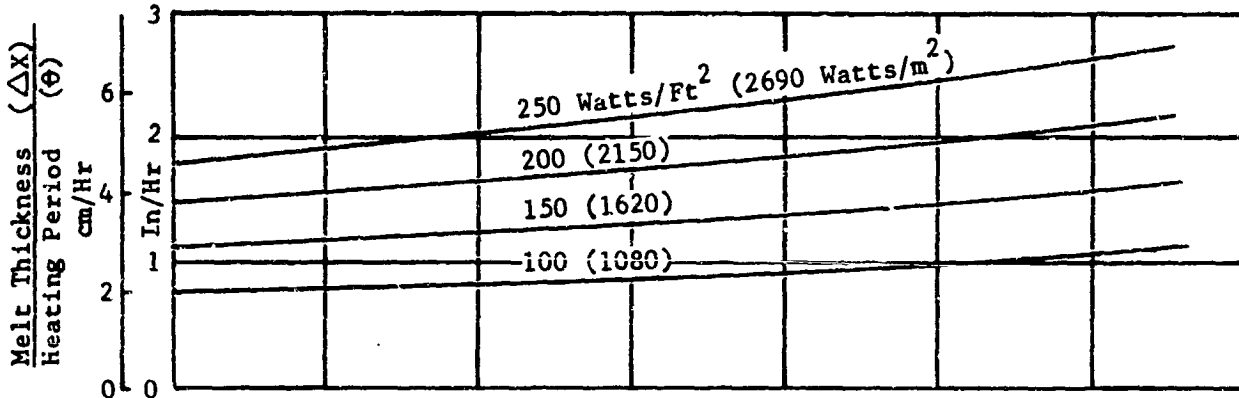
18% cavity by volume filled with aluminum wool, dia. .0025cm(.001"). Fiberglass sides .076cm(.030") approx. Fusible material - Octadecane. Void volume with solid fusible material 23%.



Notes:

1. Time 0 taken when cold plate temperature exceeded 300 °K (melting point of Octadecane).
2. Measured deviation of cold plate temperature less than 2 °K from the thermocouple shown.

FIGURE 7-7 TEST RESULTS OF ADIABATIC MODEL FILLED WITH 18% BY VOLUME ALUMINUM WOOL



**Assumptions:**

1. One-dimensional system
2. Fusible Material - Octadecane
3. Time Parameter =  $\theta^* = .5 = \theta a \left( \frac{q/A}{k} \right)^2 \left( \frac{C_p}{H} \right)^2$
4.  $\frac{\Delta T}{\theta} = .744 (q/A)^2 / \rho k H$
5.  $\frac{\Delta X}{\theta} = .866 (q/A) / \rho H$
6. Thermal Resistance (R)
  - a. Cold plate to solid fusible material - parallel resistance for aluminum and octadecane
  - b. Thermal resistance parallel to cold plate is zero
  - c. Aluminum foam  
Emerson & Cuming, Inc.  
ECCOFOAM MD-AO  
Thermal Conductivity (K)  
K = 12.5 BTU/FT<sup>2</sup>°F HR  
@ 33% by Volume

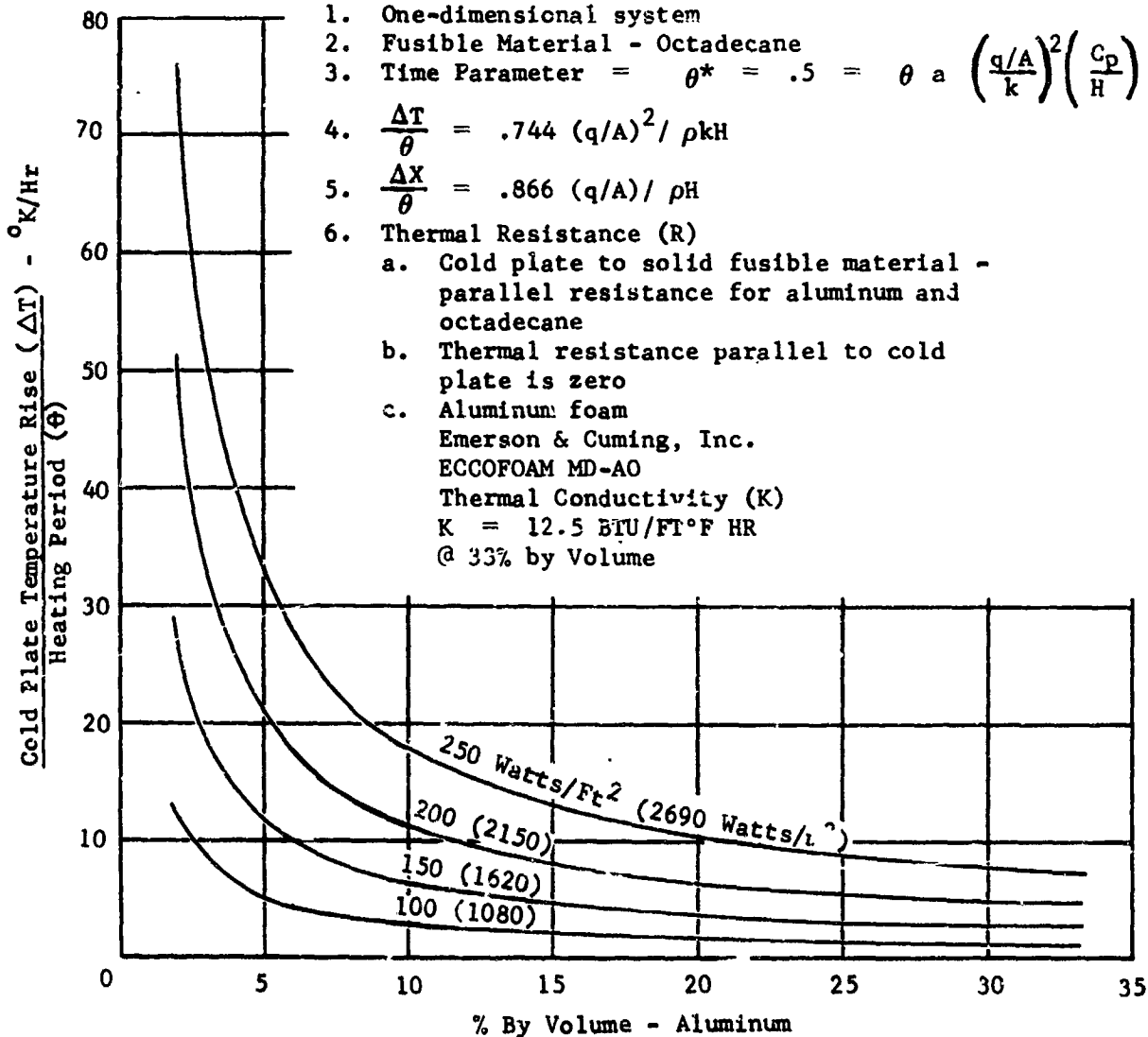


FIGURE 7-8 - IMPROVEMENT OF ADIABATIC SYSTEM PERFORMANCE; SIMPLIFIED ONE-DIMENSIONAL ANALYTICAL MODEL; ALUMINUM FOAM AND FUSIBLE MATERIAL WITH INFINITE CROSS CONDUCTION

$\bar{H}$  1 BTU/LB = 0.0388 watt min/gm  
 $\rho$  1 LB/Ft<sup>3</sup> = 0.0160 gm/cc  
 $\bar{C}_p$  1 BTU/HR FT °F = 0.0173 watt min/cm °K  
 $\bar{K}$  1 BTU/LB °F = 0.0698 watt min/gm °K

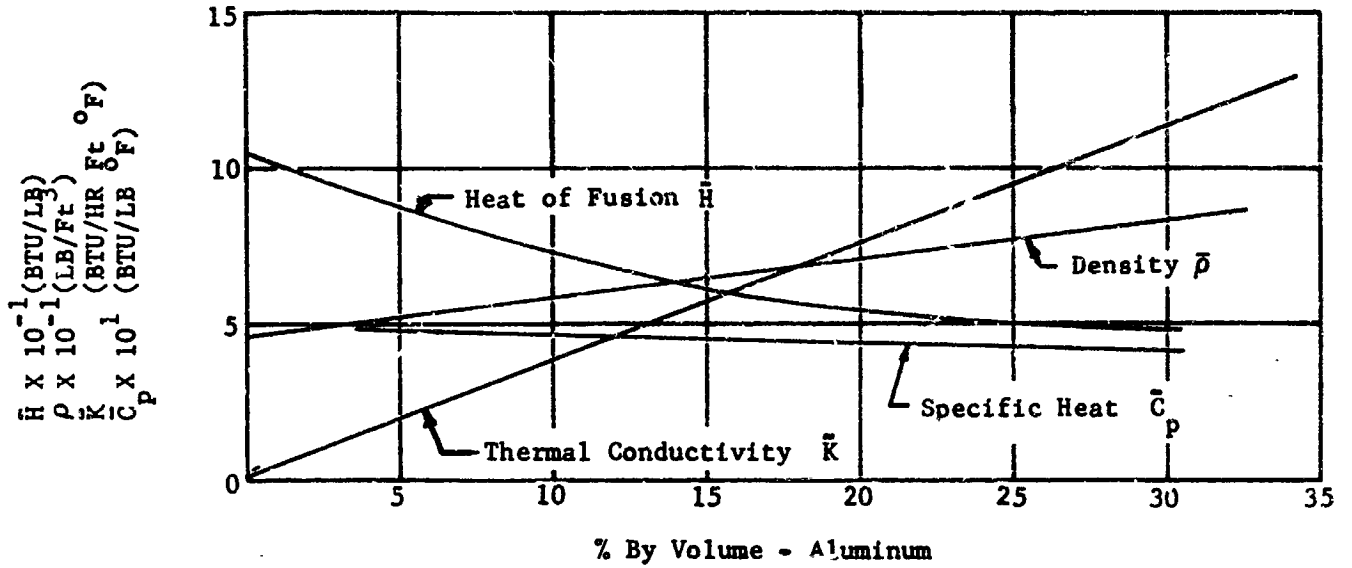


FIGURE 7-9 THERMOPHYSICAL PROPERTIES USED FOR THE IMPROVED - ADIABATIC - SYSTEM ANALYSIS INCORPORATING ALUMINUM FOAM

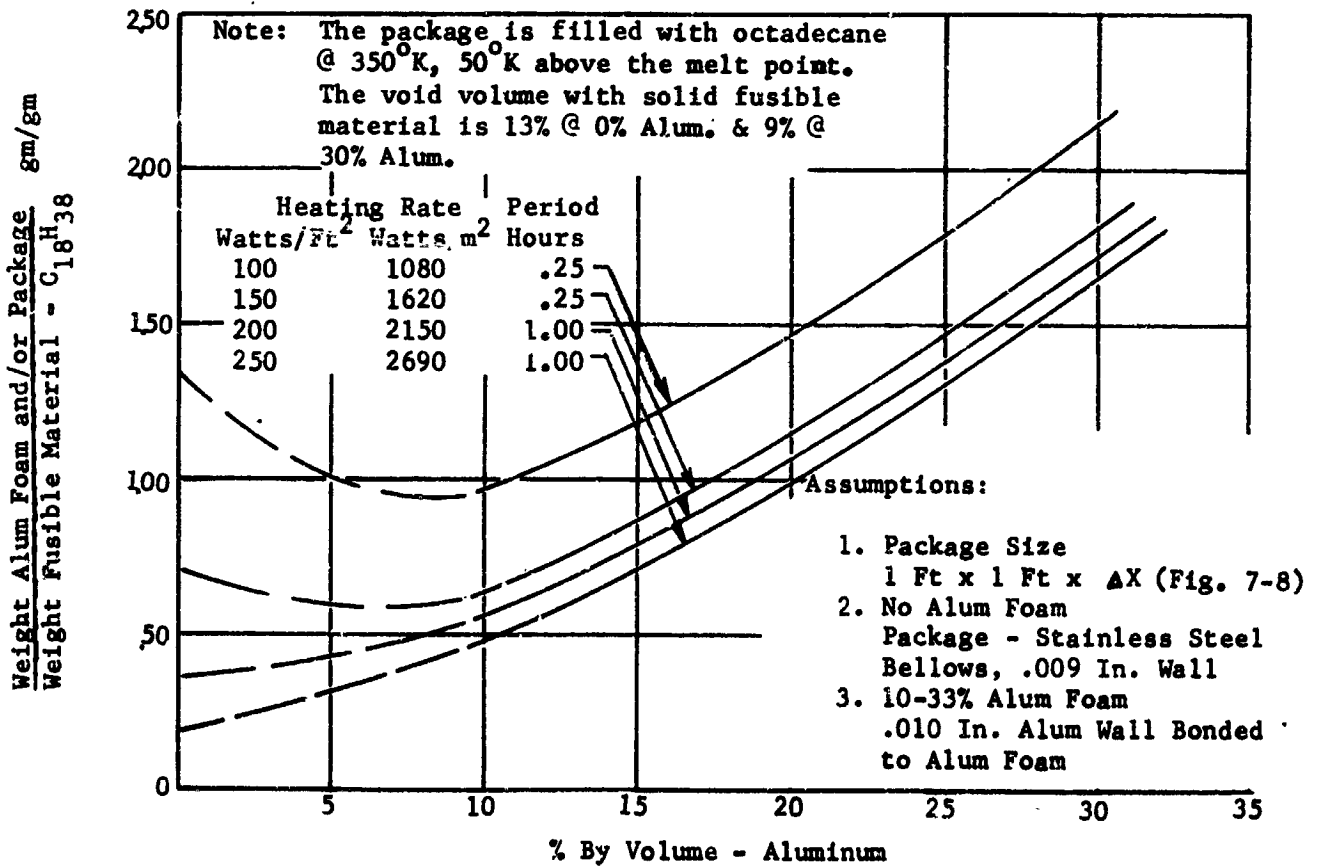


FIGURE 7-10 WEIGHT ESTIMATE FOR IMPROVED ADIABATIC SYSTEM INCORPORATING ALUMINUM FOAM & HONEYCOMB FILLER MATERIALS

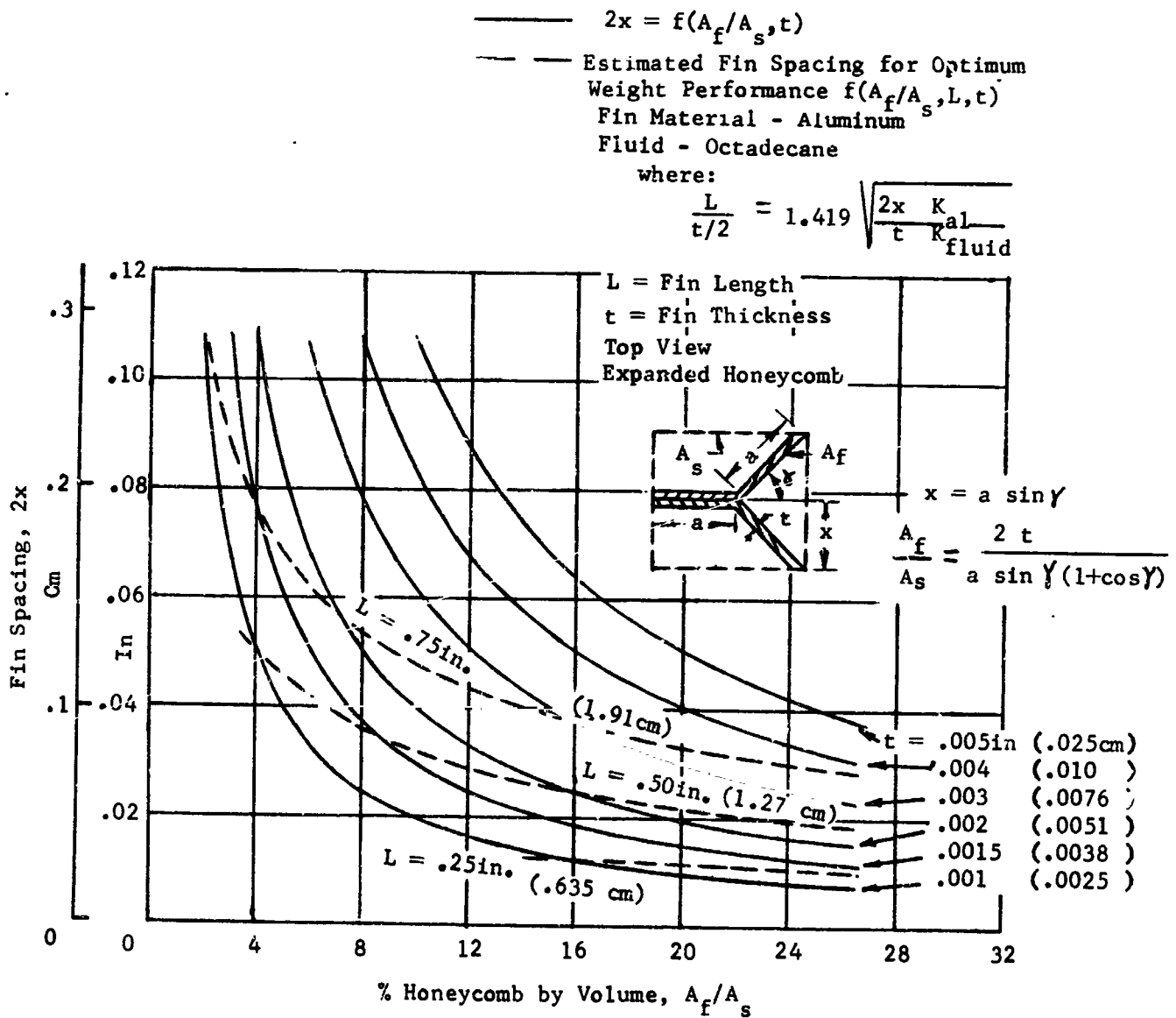
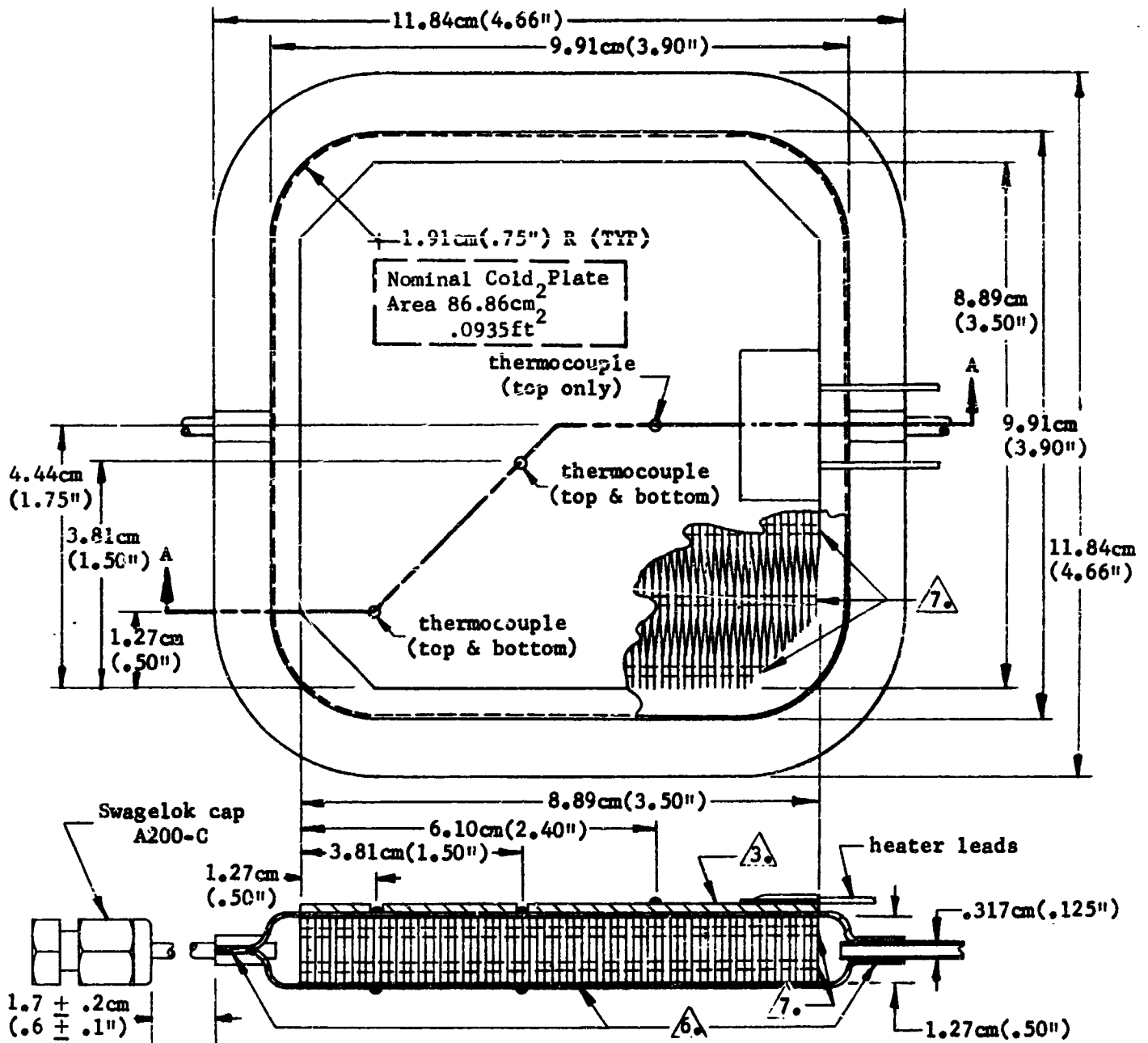


FIGURE 7-11 FIN SPACING FOR REGULAR HEXAGONAL HONEYCOMB AND ESTIMATED FIN SPACING FOR OPTIMUM WEIGHT PERFORMANCE



Notes:

SECTION A-A

1. Top and bottom sections - formed pans, .025cm(.010") 6061-0 aluminum.
2. Filler materials (core) - open cell copper foam and aluminum honeycomb with various sheet thicknesses and sheet spacings.
3. Electric heater - nichrome wire (150 ohms) and laminated glass cloth, silicone rubber filled, .15cm(.06") thick. 26 gage leads first 12.0 in. remainder 22 gage.
4. Thermocouples - chromel constantan (30 gage).
5. Fusible material tested - Octadecane,  $C_{18}H_{38}$ , melting point  $81^{\circ}F$  ( $300^{\circ}K$ ). Models filled and capped at  $200^{\circ}F$  ( $367^{\circ}K$ ). A low pressure void volume is formed when the fusible material solidifies.
6. Adhesives: a. Flange and tube bond (all models)  
American Cyanamid Co., Plastics and Resins Division,  
Bloomingdale Dept., FM-1000 .05-.06 lbs/ft<sup>2</sup>  
b. Core to top and bottom pans  
Model -45 Emerson & Cumming 56C (silver filled epoxy)  
remaining models (-1,-3,-7,-11,-13,-15,-19) FM-1000 or 3M Co. A7-300
7. All honeycomb cells are opened by two .157cm(.062") drill holes for filling.

FIGURE 7-12 ADIABATIC TEST MODELS (DWG. NO. 126-00100) WITH METALLIC FOAM AND HONEYCOMB FILLER MATERIALS

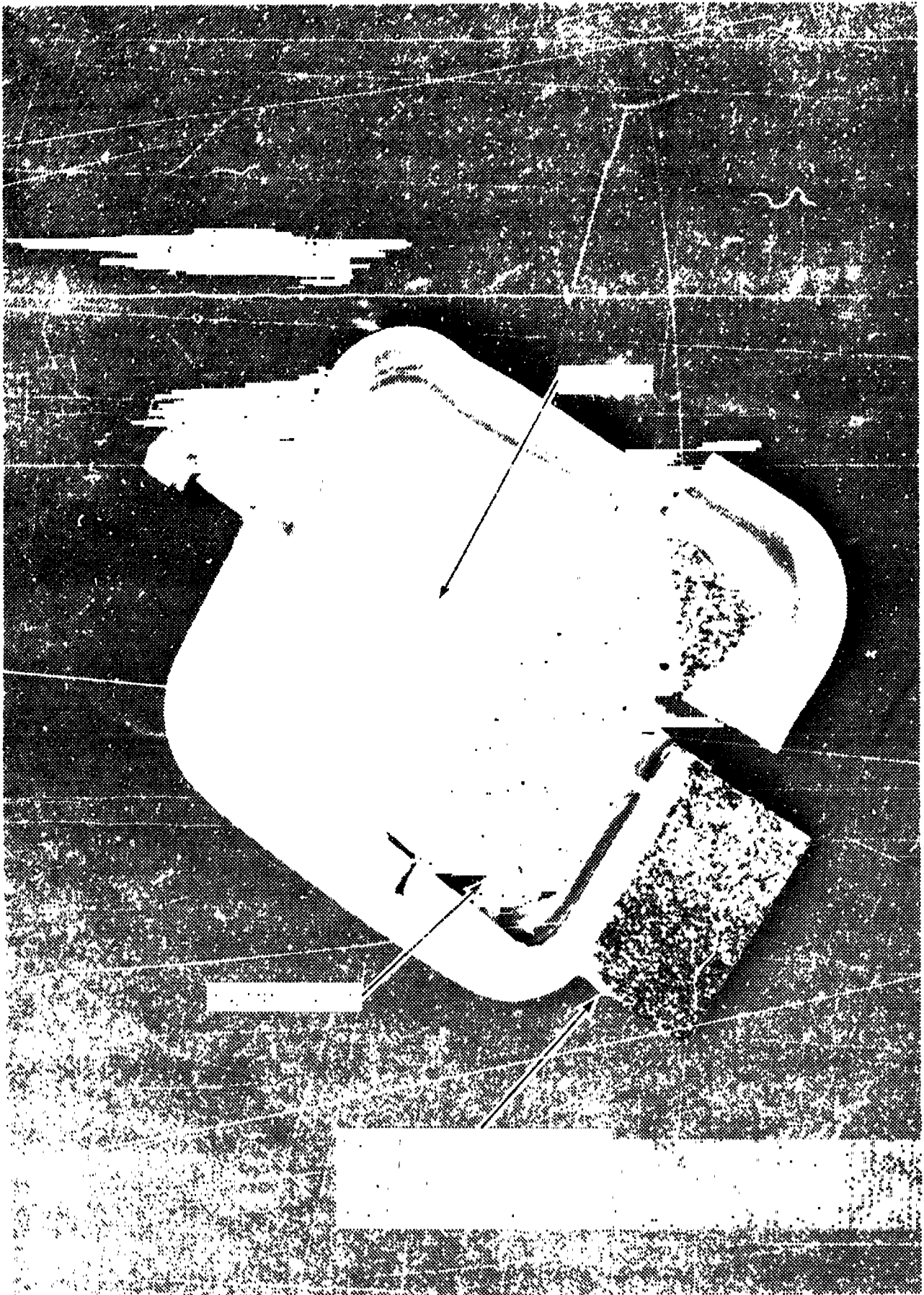


FIGURE 7-13 RUPTURED COPPER FOAM (30 CELLS/IN) MODEL

Nominal Fin Spacing For Test Models Tested With The Noted Fusible Materials:

- Tetradecane
- Hexadecane
- Octadecane
- ◇ Eicocene

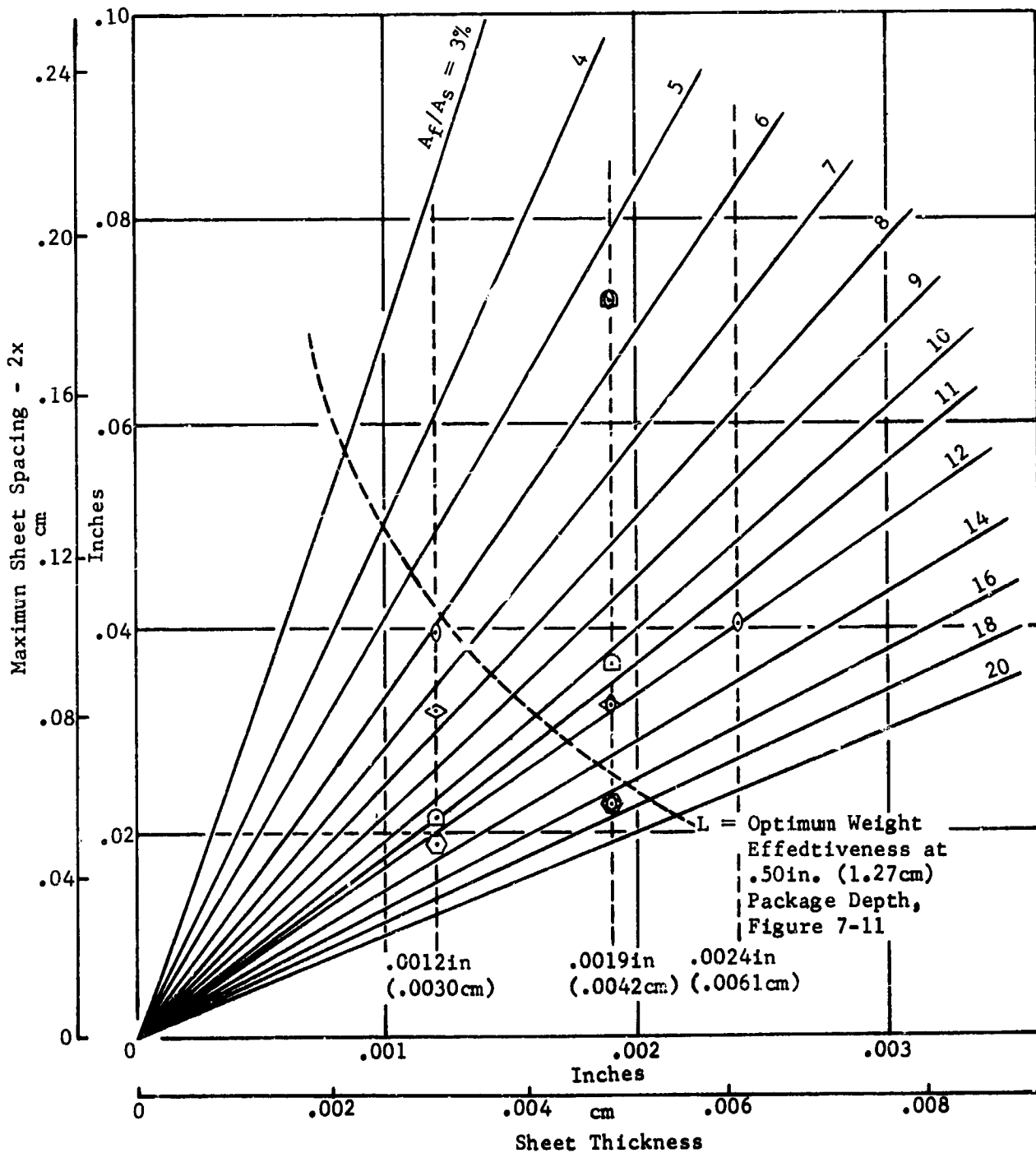


FIGURE 7-14 NOMINAL HONEYCOMB SHEET THICKNESS AND SPACING OF THE SYSTEM IMPROVEMENT - ADIABATIC TEST MODELS

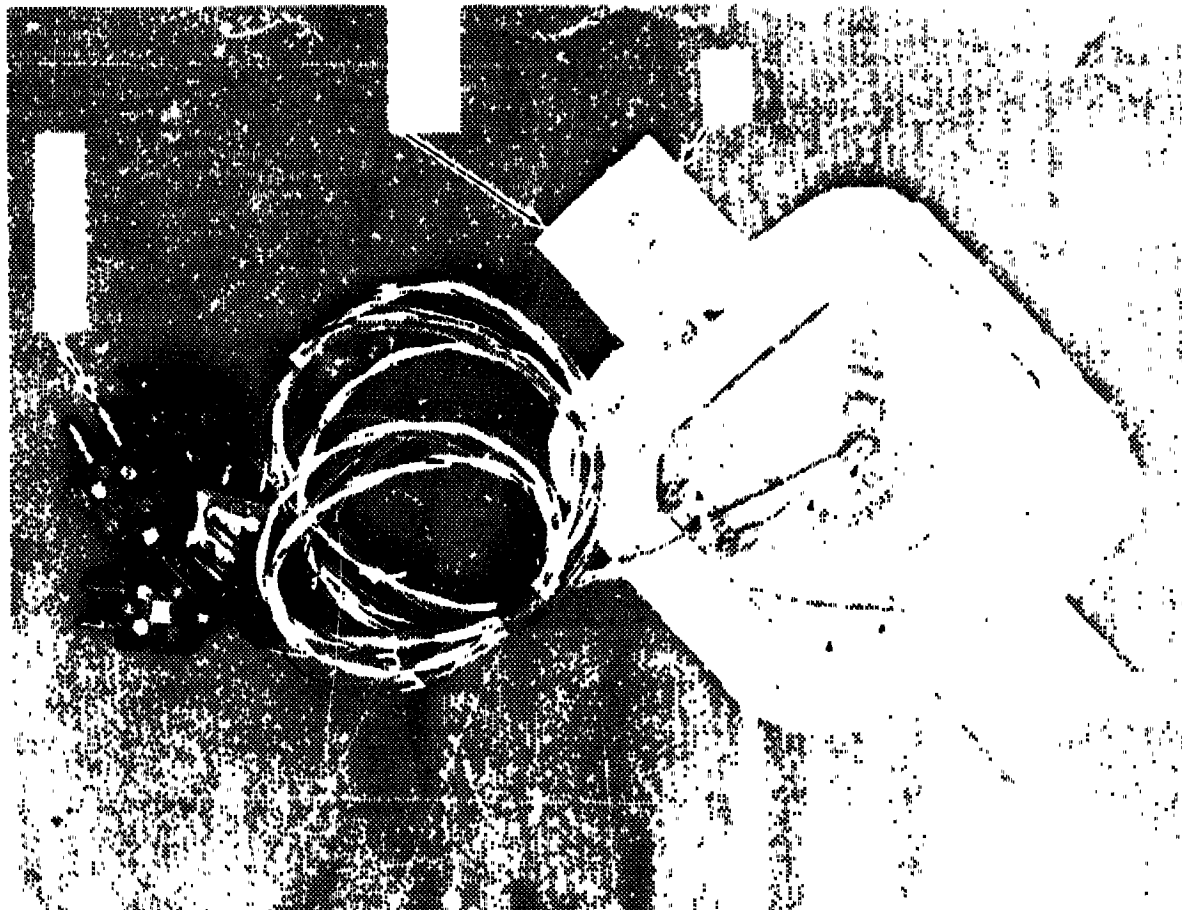
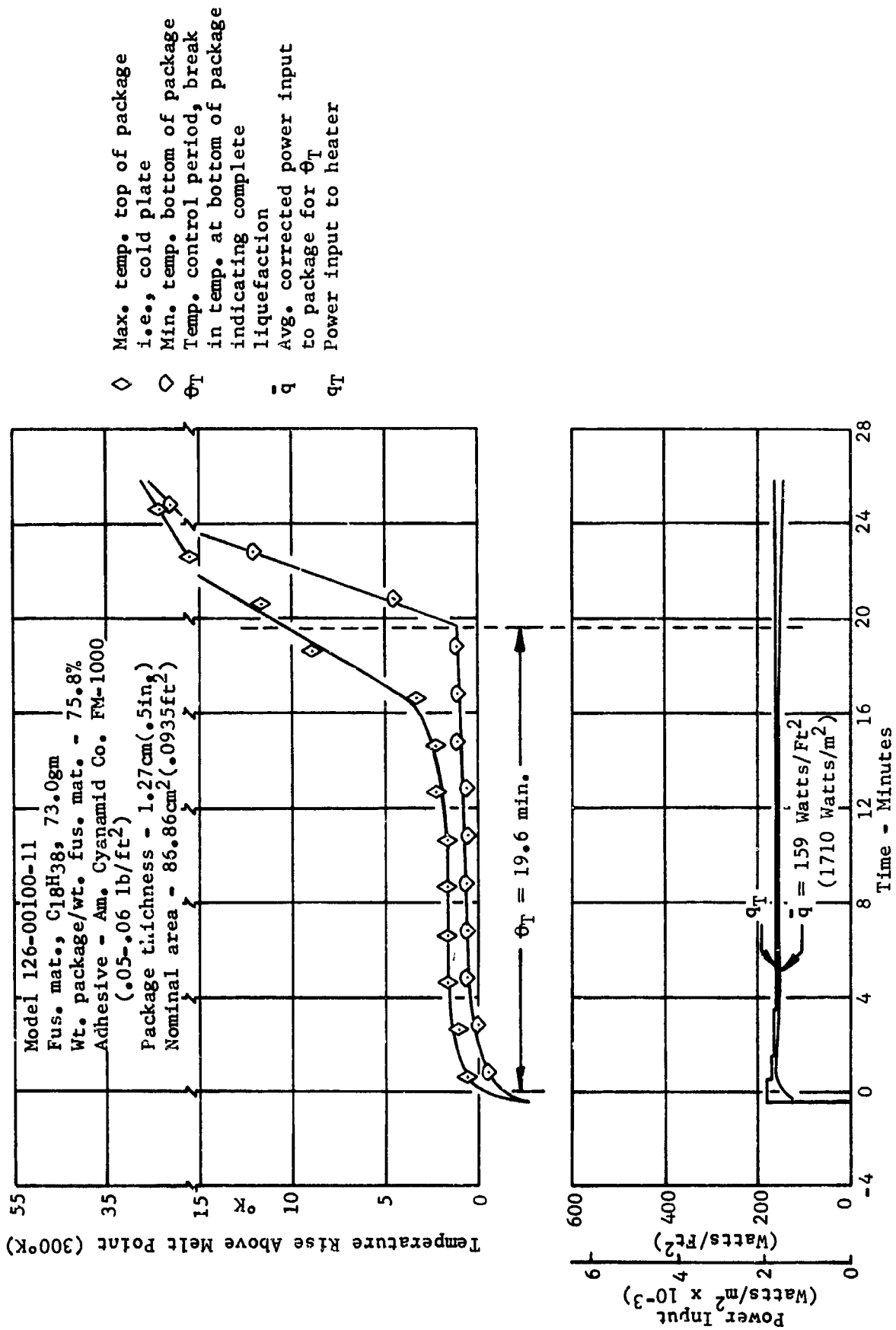


FIGURE 7-15 A SYSTEM IMPROVEMENT - ADIABATIC - MODEL READY FOR TEST



FIGURE 7-16 INSTALLATION OF SYSTEM IMPROVEMENT - ADIABATIC - MODEL IN VACUUM CHAMBER



- ◇ Max. temp. top of package i.e., cold plate
- ◇ Min. temp. bottom of package
- ◇  $\theta_T$  Temp. control period, break in temp. at bottom of package indicating complete liquefaction
- $\bar{q}$  Avg. corrected power input to package for  $\theta_T$
- $q_T$  Power input to heater

FIGURE 7-17 TEST RESULTS, RUN 1, FOR AN ADIABATIC TEST MODEL WITH A STRUCTURAL ADHESIVE. FUSIBLE MATERIAL IS OCTADECANE WITH ALUMINUM HONEYCOMB FILLER MATERIAL ( $t = .0048\text{CM}, .0019\text{IN.}$ ), 10.8% OF TOTAL VOID VOLUME.

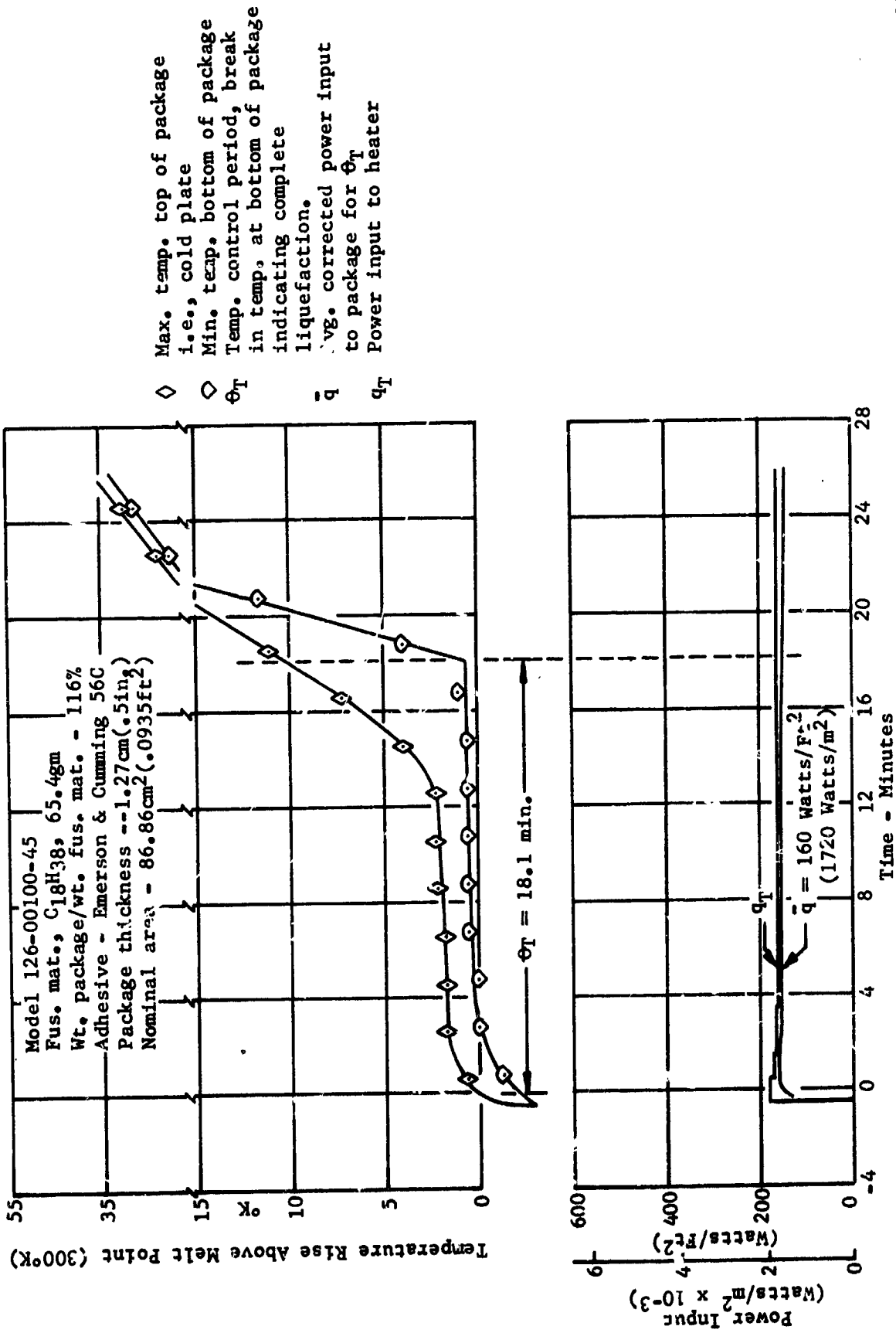


FIGURE 7-18 TEST RESULTS, RUN 1, FOR AN ADIABATIC TEST MODEL WITH A HIGH CONDUCTIVITY ADHESIVE. FUSIBLE MATERIAL IS OCTADECANE WITH ALUMINUM HONEYCOMB FILLER MATERIAL (t = .0048CM,.0019IN.), 10.8% OF TOTAL VOID VOLUME.

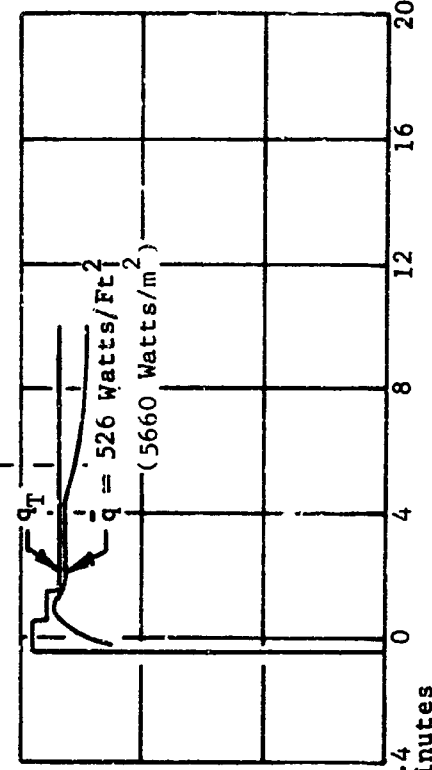
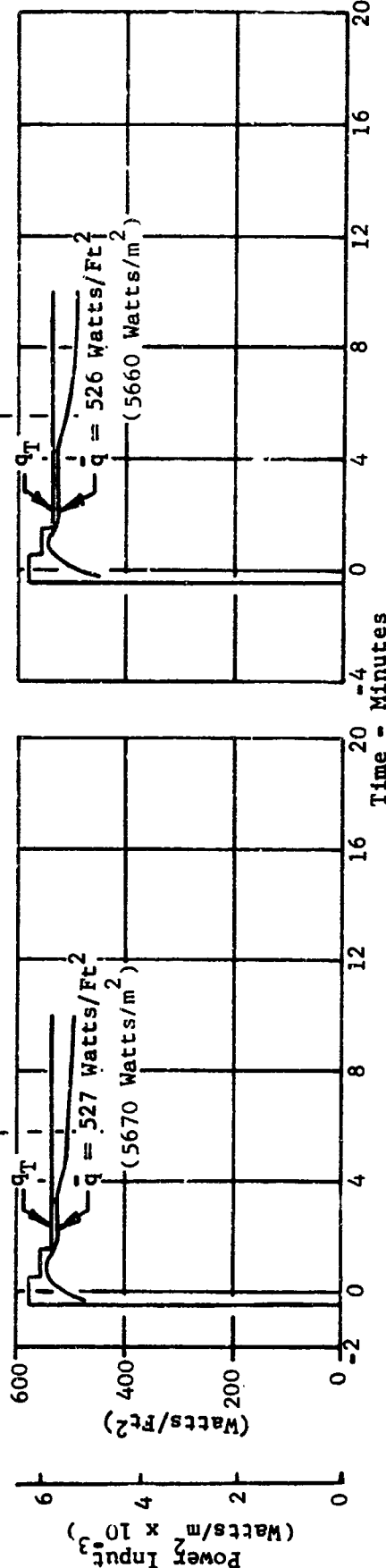
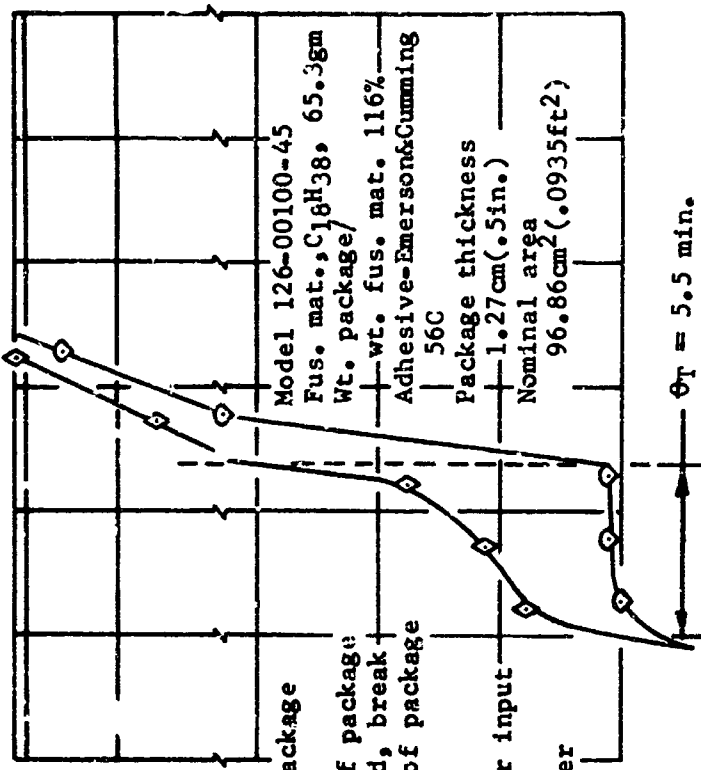
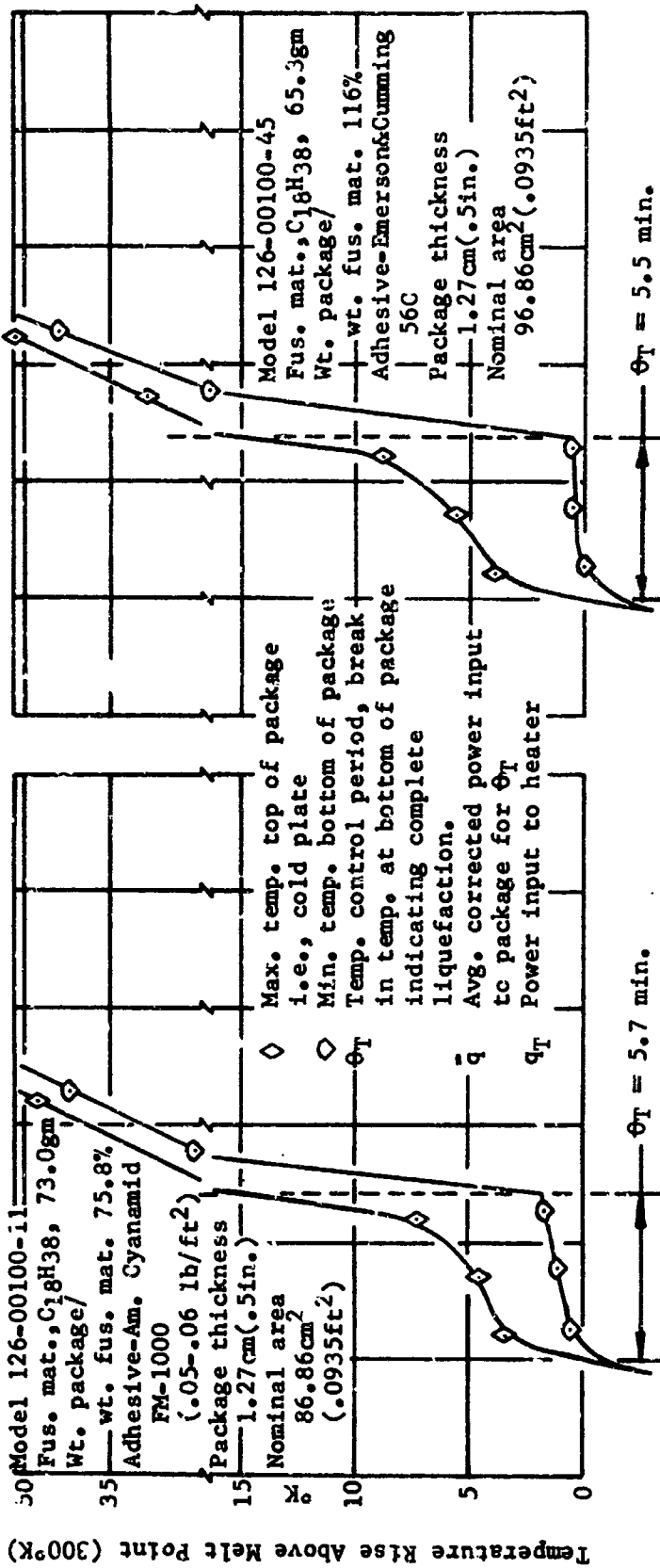


FIGURE 7-19 TEST RESULTS, RUN 2, FOR TWO ADIABATIC TEST MODELS WITH DIFFERENT ADHESIVES. FUSIBLE MATERIAL IS OCTADECANE WITH ALUMINUM HONEYCOMB FILLER MATERIAL ( $t = .0048$  in.,  $.0019$  in.), 10.8% OF TOTAL VOID VOLUME.

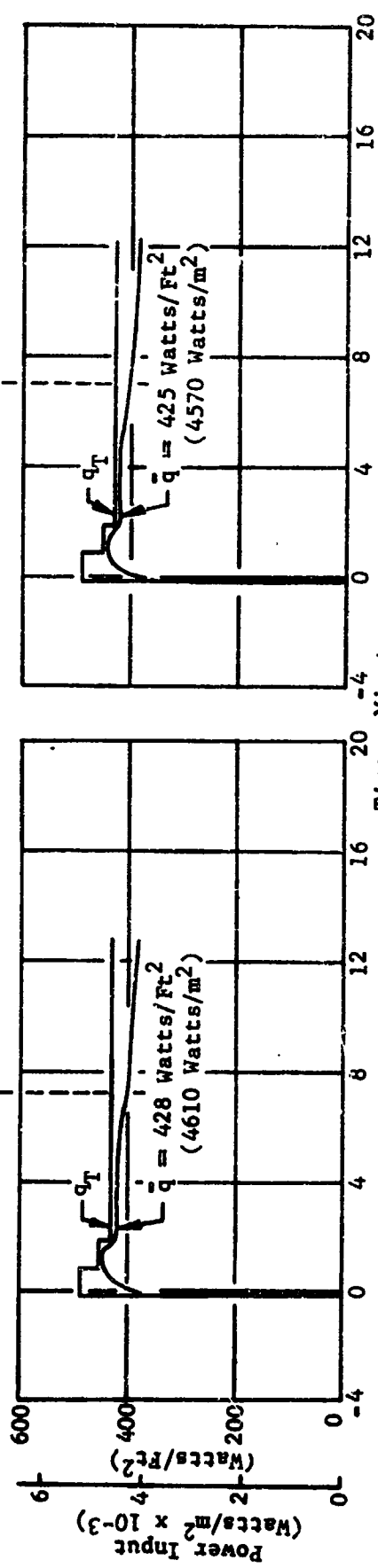
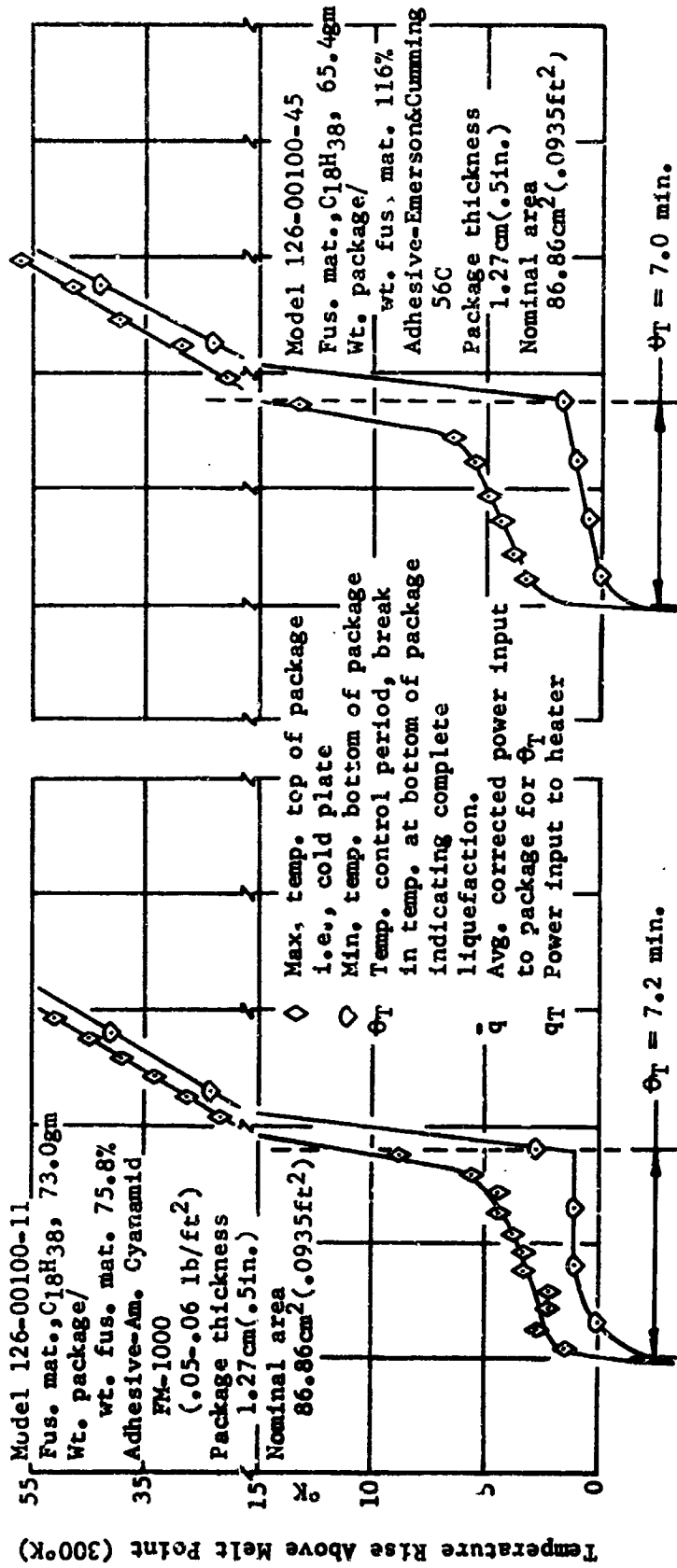


FIGURE 7-20 TEST RESULTS, RUN 3, FOR TWO ADIABATIC TEST MODELS WITH DIFFERENT ADHESIVES. FUSIBLE MATERIAL IS OCTADECANE WITH ALUMINUM HONEYCOMB FILLER MATERIAL ( $t = .0048$ CM,  $.0019$ IN.), 10.8% OF TOTAL VOID VOLUME.

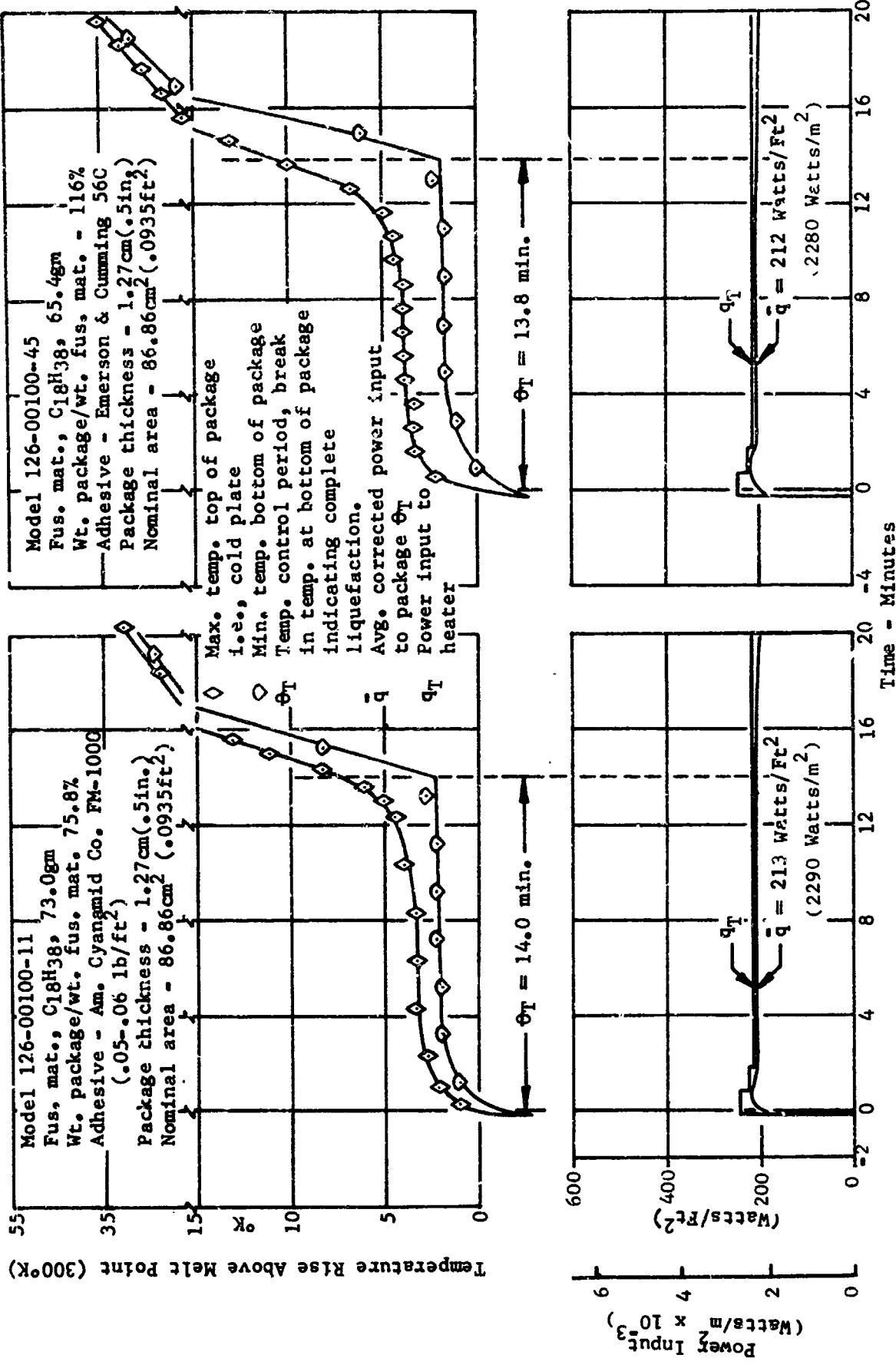
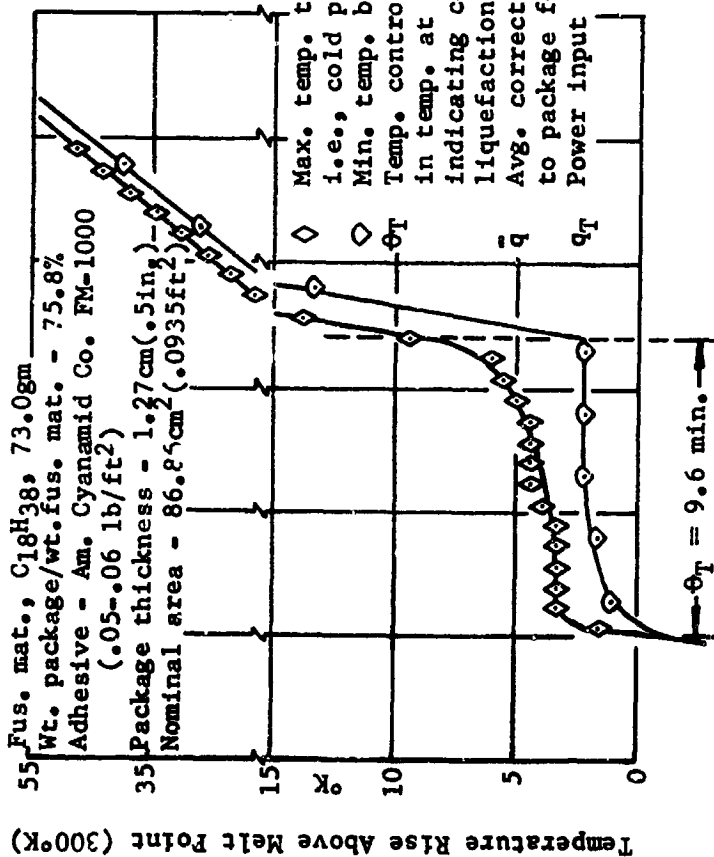


FIGURE 7-21 TEST RESULTS, RUN 4, FOR TWO ADIABATIC TEST MODELS WITH DIFFERENT ADHESIVES. FUSIBLE MATERIAL IS OCTADECANE WITH ALUMINUM HONEYCOMB FILLER MATERIAL (FM-0048CM, 0019IN.), 10.8% OF TOTAL VOID VOLUME.

Model 126-00100-11

Fus. mat., C18H38, 73.0gm  
 Wt. package/wt.fus. mat. - 75.8%  
 Adhesive - Am. Cyanamid Co. FM-1000  
 (.05-.06 lb/ft<sup>2</sup>)  
 Package thickness - 1.27cm(.5in.)  
 Nominal area - 86.84cm<sup>2</sup>(.0935ft<sup>2</sup>)



Max. temp. top of package  
 i.e., cold plate  
 Min. temp. bottom of package  
 Temp. control period, break  
 in temp. at bottom of package  
 indicating complete  
 liquefaction.  
 Avg. corrected power input  
 to package for  $\theta_T$   
 Power input to heater

Model 126-00100-45

Fus. mat., C18H38, 65.4gm  
 Wt. package/wt. fus. mat. - 116%  
 Adhesive - Emerson & Cumming 56C  
 Package thickness - 1.27cm(.5in.)  
 Nominal area - 86.86cm<sup>2</sup>(.0935ft<sup>2</sup>)

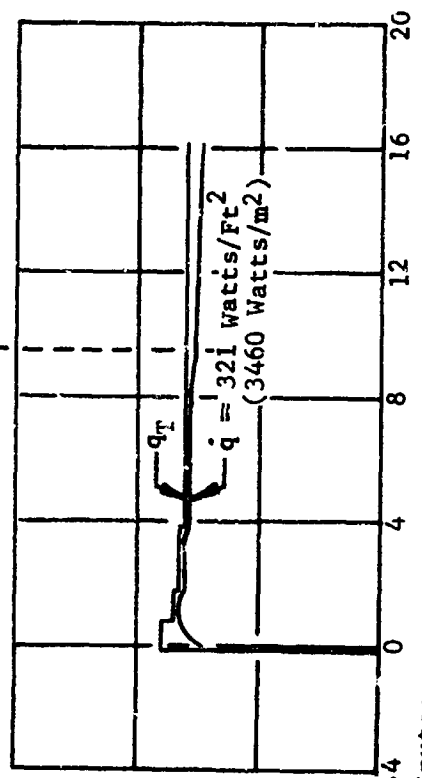
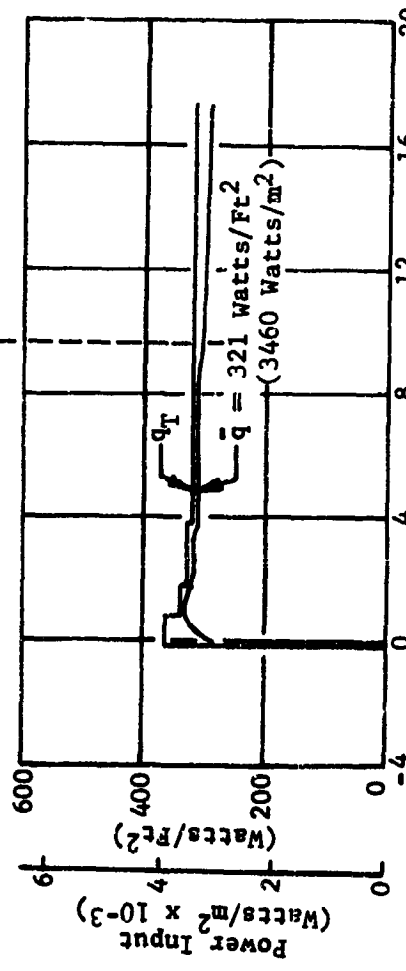
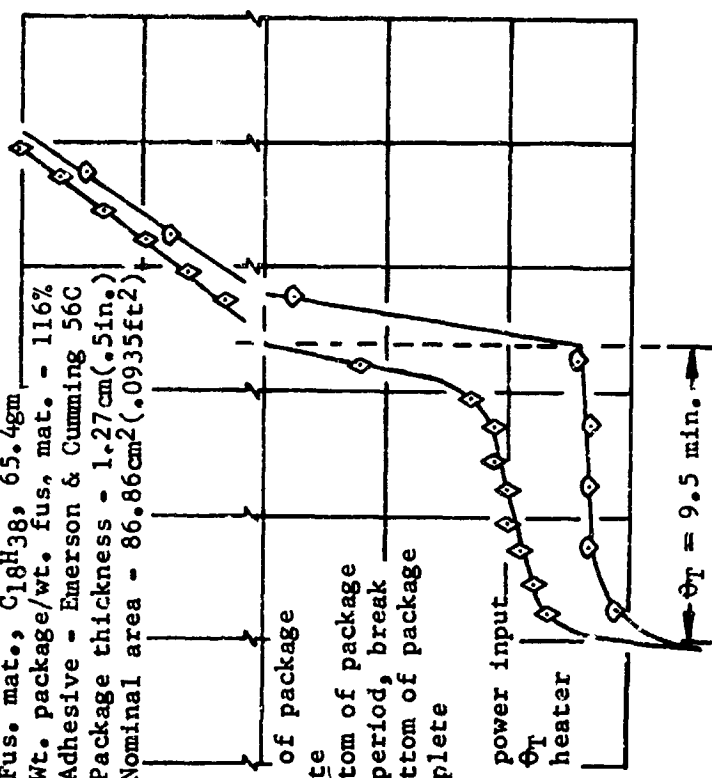


FIGURE 7-22 TEST RESULTS, RUN 5, FOR TWO ADIABATIC TEST MODELS WITH DIFFERENT ADHESIVES. FUSIBLE MATERIAL IS OCTADECANE WITH ALUMINUM HONEYCOMB FILLER MATERIAL ( $t = .0048 \text{ CM}$ ,  $.0019 \text{ IN.}$ ), 10.8% OF TOTAL VOID VOLUME.

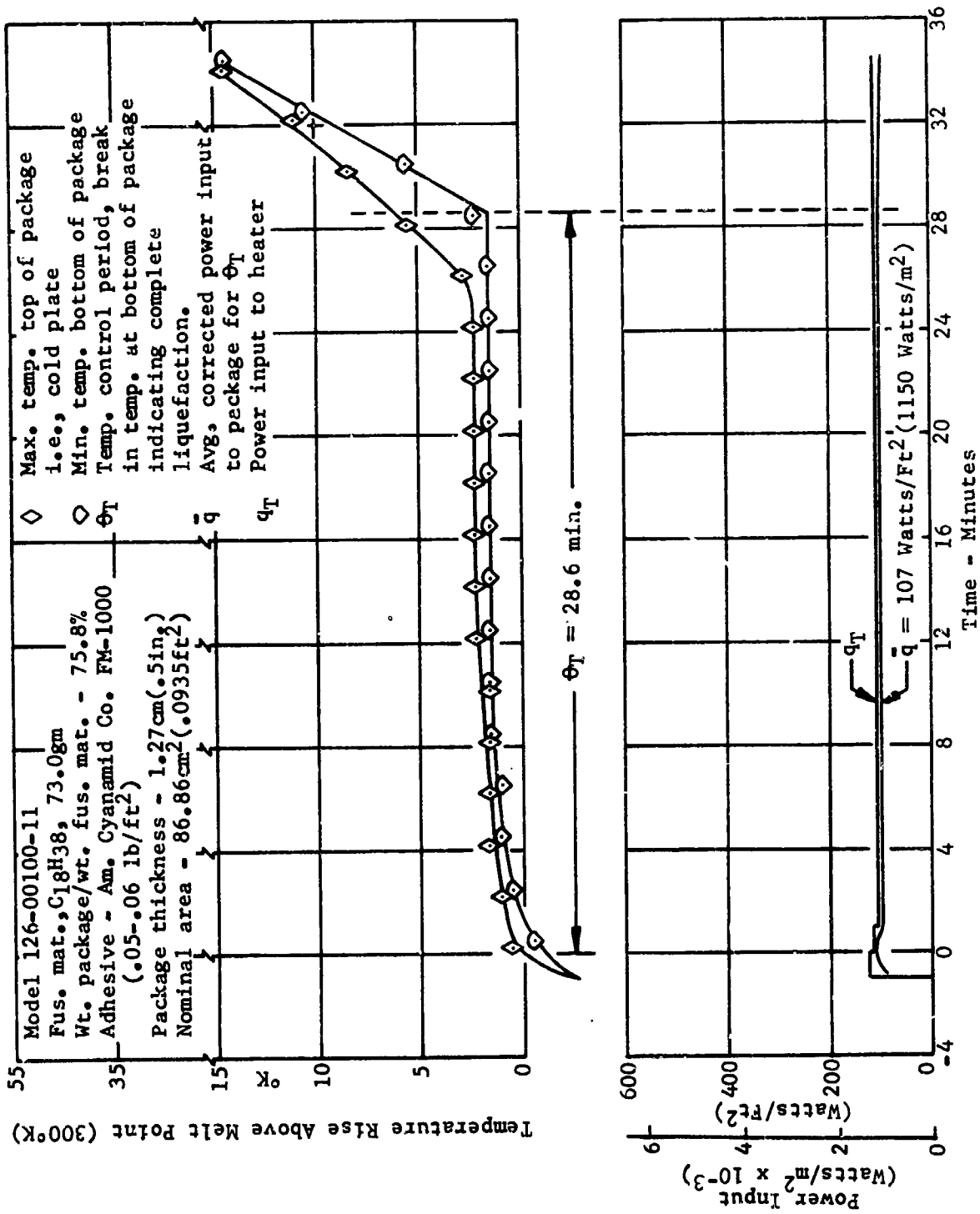
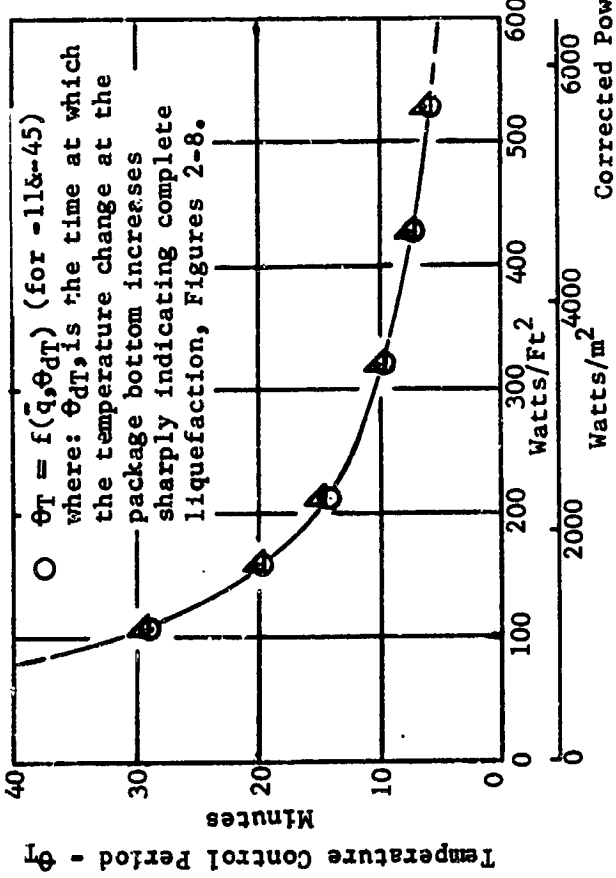
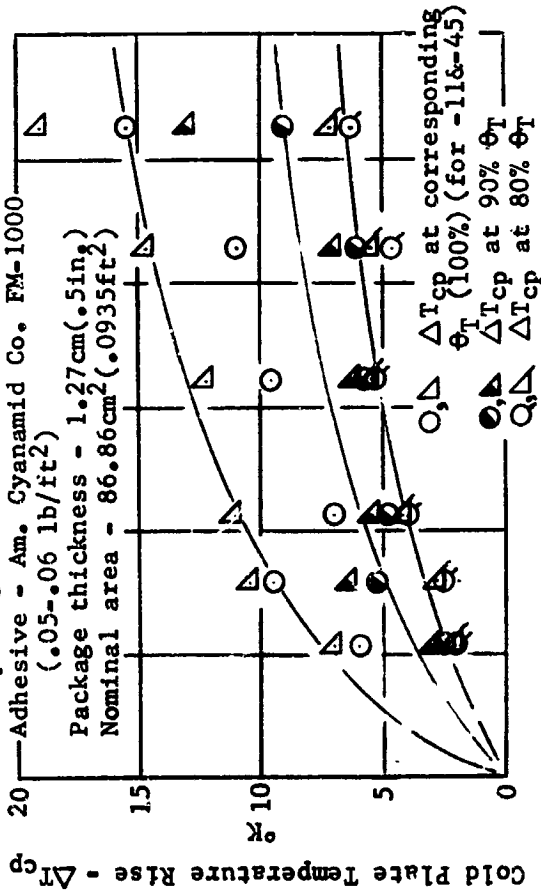


FIGURE 7-23 TEST RESULTS, RUN 6, FOR AN ADIABATIC TEST MODEL WITH A STRUCTURAL ADHESIVE. FUSIBLE MATERIAL IS OCTADECANE WITH ALUMINUM HONEYCOMB FILLER MATERIAL ( $t = .0048$ CM,  $.0019$ IN.), 10.8% OF TOTAL VOID VOLUME.

Model 126-00100-11

Fus. mat., C18H38, 73.0gm  
 Wt. package/wt. fus. mat. - 75.8%  
 Adhesive - Am. Cyanamid Co. FM-1000  
 (.05-.06 lb/ft<sup>2</sup>)  
 Package thickness - 1.27cm(.5in.)  
 Nominal area - 86.86cm<sup>2</sup>(.0935ft<sup>2</sup>)



Model 126-00100-45

Fus. mat., C18H38, 65.4gm  
 Wt. package/wt. fus. mat. - 116%  
 Adhesive - Emerson & Cumming 56C  
 Package thickness - 1.27cm(.5in.)  
 Nominal area - 86.86cm<sup>2</sup>(.0935ft<sup>2</sup>)

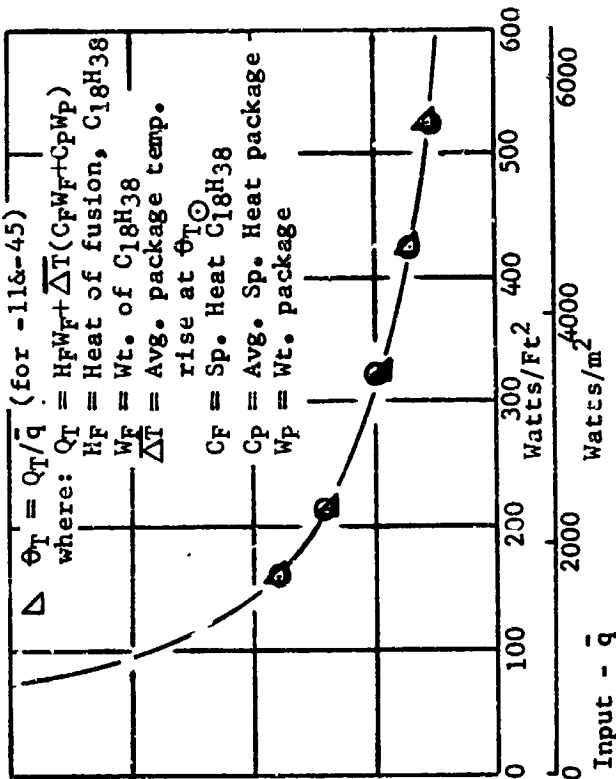
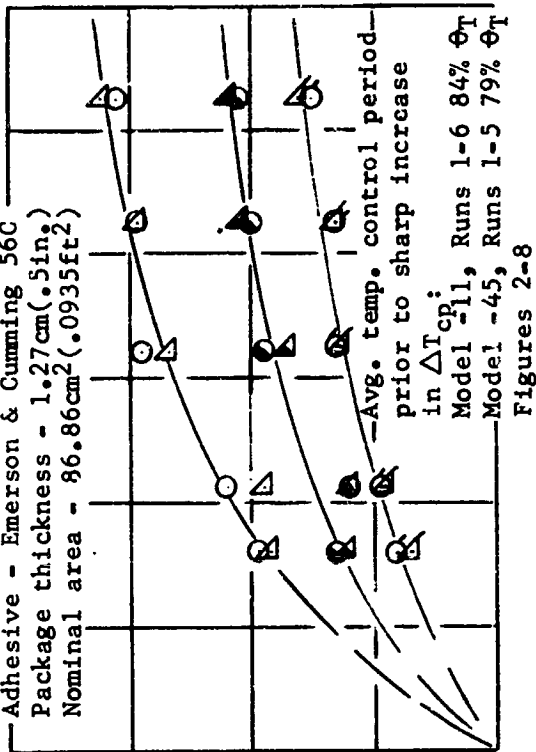


FIGURE 7-24 CORRELATION OF TEST RESULTS FOR TWO SYSTEM IMPROVEMENT - ADIABATIC - TEST MODELS WITH DIFFERENT ADHESIVES. FUSIBLE MATERIAL - OCTADECANE, FILLER MATERIAL - ALUMINUM HONEYCOMB (t = .0048cm, .0019in.), 10.8% OF TOTAL VOID VOLUME.

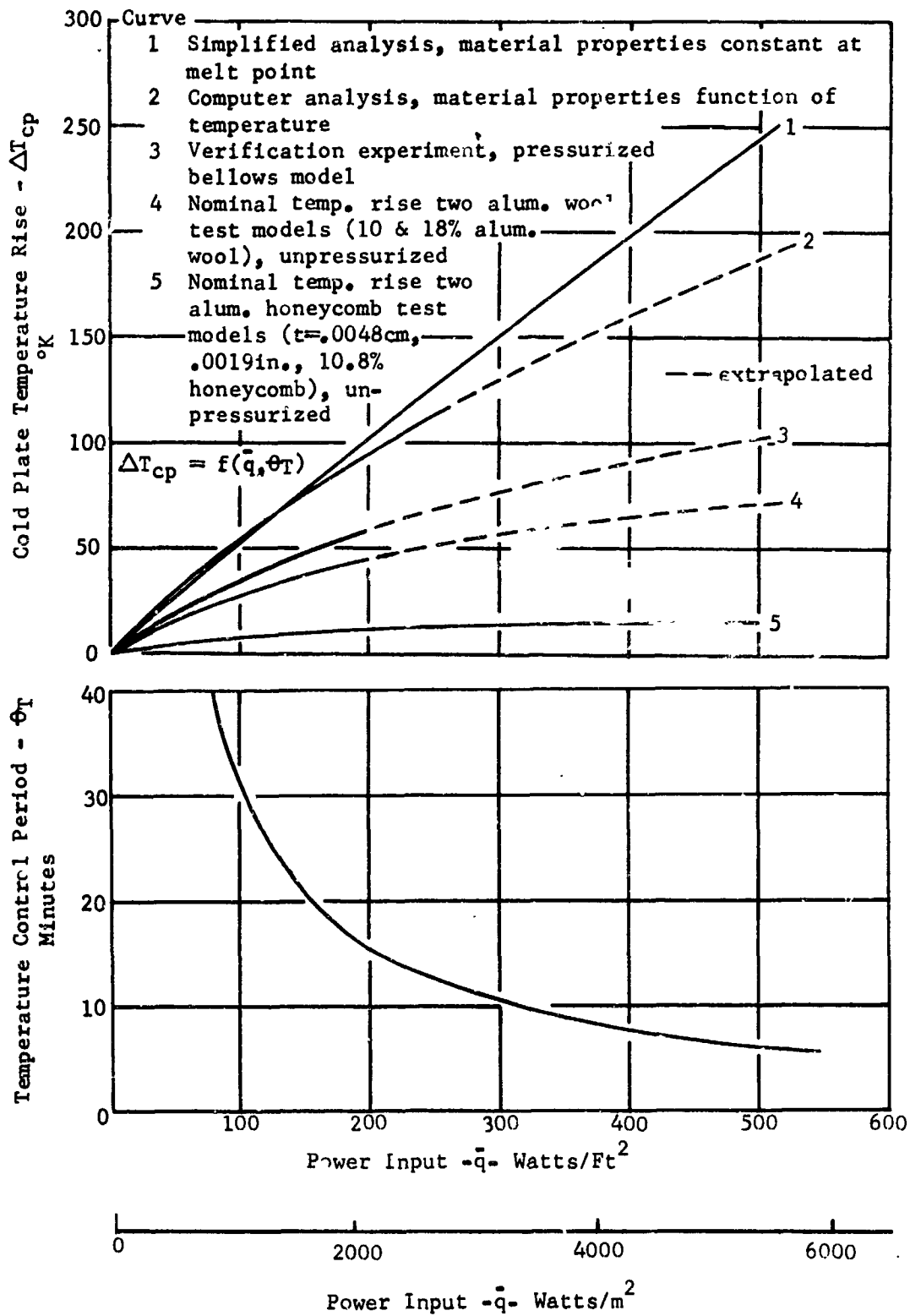


FIGURE 7-25 PERFORMANCE COMPARISON FOR VARIOUS ANALYTICAL AND TEST ADIABATIC MODELS WITH AN EQUAL TOTAL ENERGY INPUT. FUSIBLE MATERIAL IS OCTADECANE

SYMBOL	AVG CORRECTED POWER INPUT		$\theta_T$
	WATTS/F <sup>-2</sup>	WATTS/M <sup>2</sup>	MIN
□	105	1130	32.4
△			
◻	211	2270	15.5
◇	315	3390	9.8
◊	420	4520	8.0
◀	521	5610	5.9

MODEL 1, MOD 1  
 COPPER FOAM FILLER MAT'S.  
 4.8% TOTAL VOID VOL.  
 OPEN CELL  
 10 CELLS/IN (25.4 CELLS/CM)  
 PACKAGE THICKNESS .5 IN (1.27 CM)  
 WT. FUS. MAT. 79.4 GM  
 WT. PACKAGE/WT. FUS. MAT. 86.7%  
 NOMINAL COLD PLATE AREA .0935 FT<sup>2</sup> (86.86 CM<sup>2</sup>)  
 TOTAL W I / AREA 3.50 LB / FT<sup>2</sup> (17.1 KG / M<sup>2</sup>)  
 ADHESIVE AM. CYANAMID COMPANY FM-1000

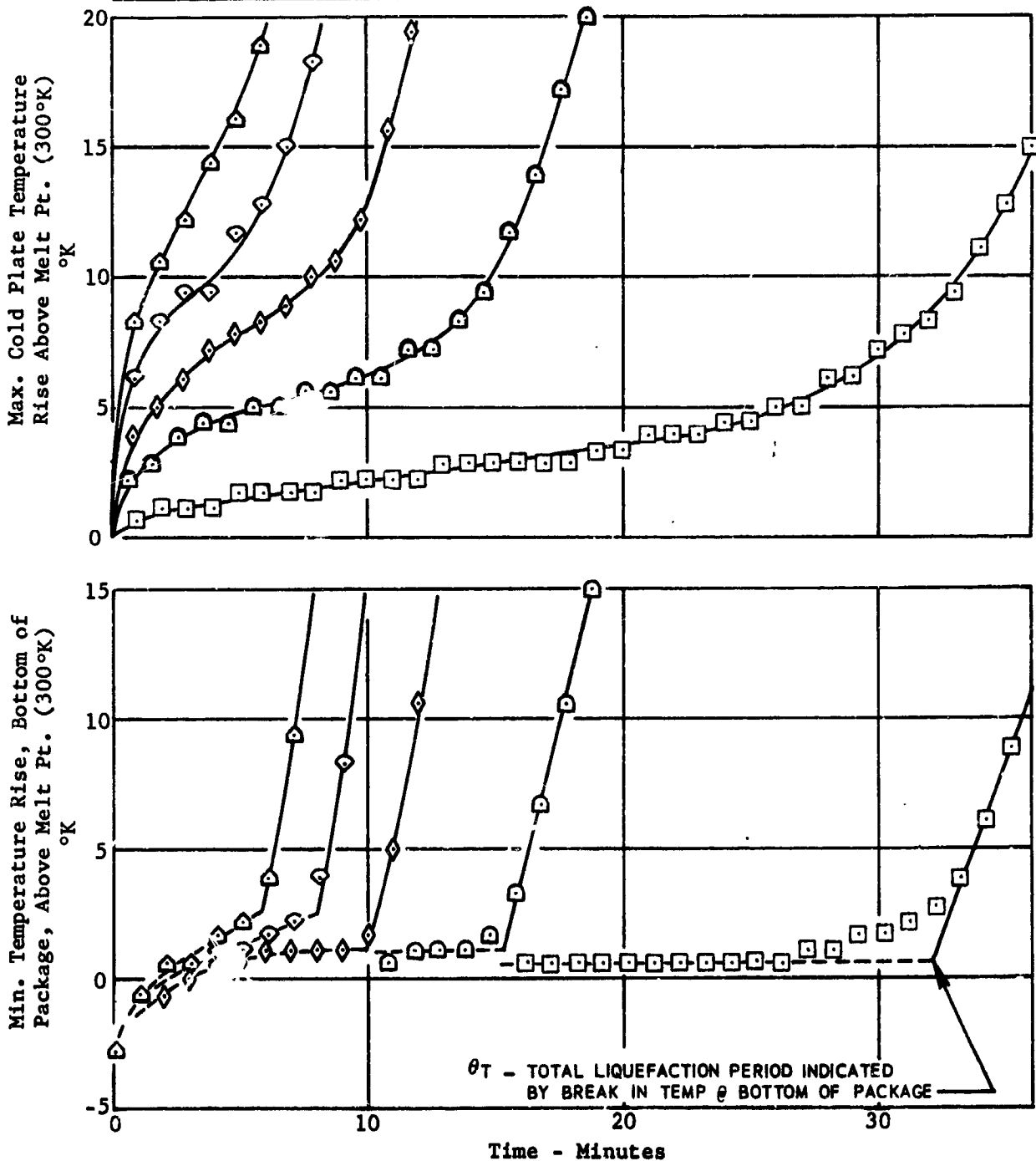


FIGURE 7-26 SYSTEM IMPROVEMENT ADIABATIC TEST RESULTS, FUSIBLE MATERIAL - OCTADECANE, MODEL 126-00100-1, MOD 1

SYMBOL	AVG CORRECTED POWER INPUT		$\theta_T$	$\theta_{EFF}$
	WATTS/FT <sup>2</sup>	WATTS/M <sup>2</sup>	MIN	MIN
□	106	1140	30.0	26.4
△	158	1700	21.1	17.8
◻	211	2270	16.1	13.0
◇	315	10.6	8.5	
◊	418	4500	8.3	7.2
◕	522	5620	6.1	5.1

MODEL 7, MOD 1  
 ALUM. HONEYCOMB FILLER MAT'S.  
 5.5% TOTAL VOID VOL.  
 SHEET THICKNESS .0012 IN (.0030 CM)  
 NOMINAL MAX SHEET SPACING .040 IN (.102 CM)  
 PACKAGE THICKNESS .5 IN (1.27 CM)  
 WT. FUS. MAT. 76.8 GM  
 WT. PACKAGE/WT. FUS. MA 55.7%  
 NOMINAL COLD PLATE AREA .0935 FT<sup>2</sup> (86.86 CM<sup>2</sup>)  
 TOTAL WT/AREA 2.82 LB/FT<sup>2</sup> (13.8 KG/M<sup>2</sup>)  
 ADHESIVE AM. CYANAMID COMPANY FM-1000

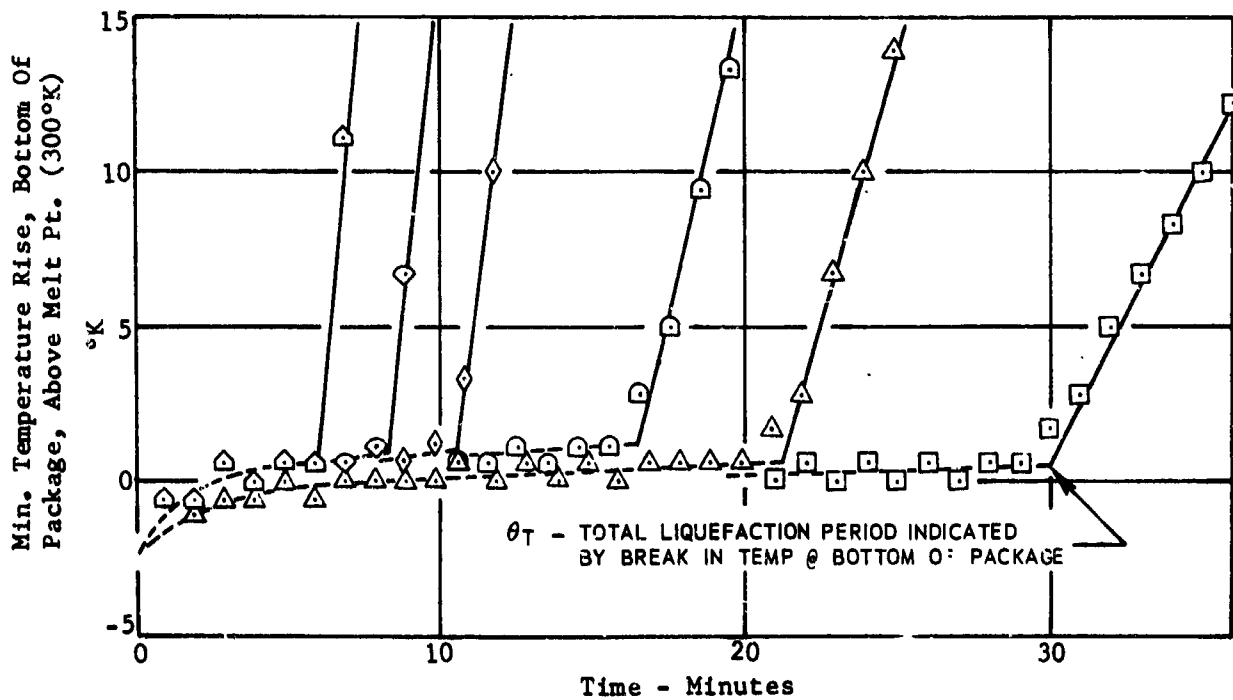
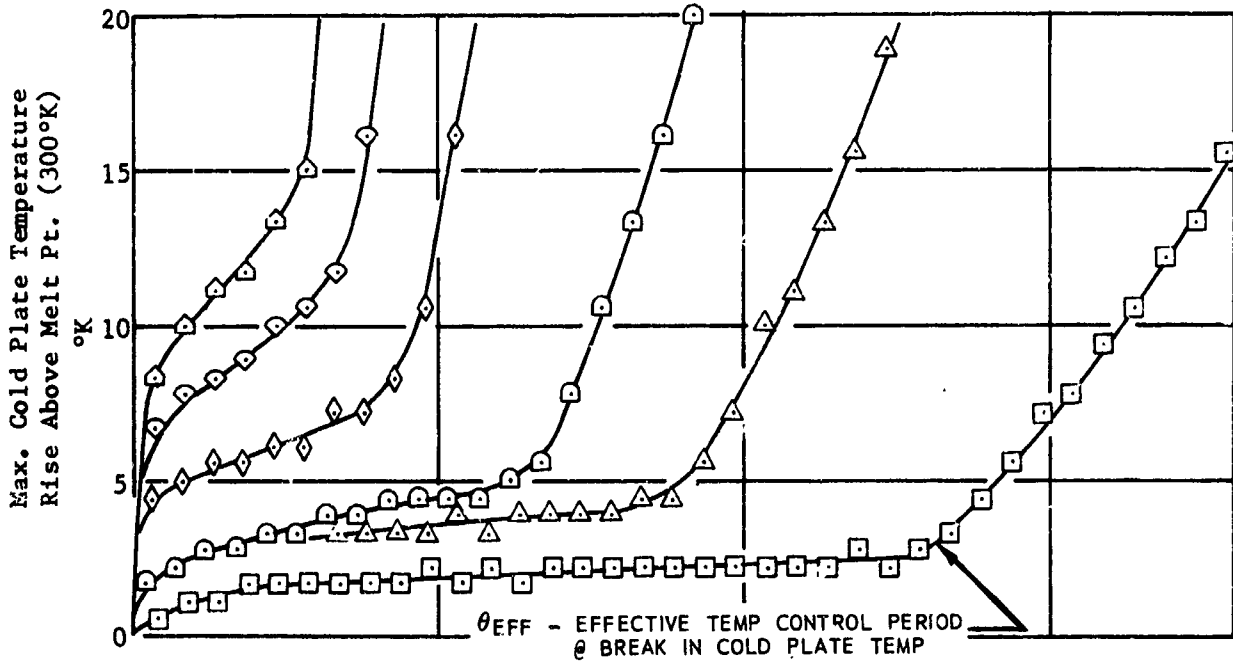


FIGURE 7-27 SYSTEM IMPROVEMENT ADIABATIC TEST RESULTS, FUSIBLE MATERIAL - OCTADECANE, MODEL 126-00100-7, MOD 1

SYMBOL	AVG CORRECTED POWER INPUT		$\theta_T$	$\theta_{EFF}$
	WATTS/FT <sup>2</sup>	WATTS/M <sup>2</sup>	MIN	MIN
□	105	1130	25.4	23.0
△	158	1700	16.7	15.0
◻	211	2270	13.1	11.5
◇	314	3380	8.7	7.8
◊	419	4510	6.7	6.2
◈	518	5580	5.7	5.0

MODEL 9, MOD 1  
 ALUM. HONEYCOMB FILLER MAT. S.  
 10.5% TOTAL VOID VOL.  
 SHEET THICKNESS .0012 IN (.0030 CM)  
 NOMINAL MAX. SHEET SPACING .020 IN (.051 CM)  
 PACKAGE THICKNESS .5 IN (1.27 CM)  
 WT. FUS. MAT. 69.0 GM  
 WT. PACKAGE/WT. FUS. MAT. 83.7%  
 NOMINAL COLD PLATE AREA .0935 FT<sup>2</sup> (86.86 CM<sup>2</sup>)  
 TOTAL WT/AREA 2.99 LB/FT<sup>2</sup> (14.6 KG/M<sup>2</sup>)  
 ADHESIVE AM. CYANAMID COMPANY FM-1000

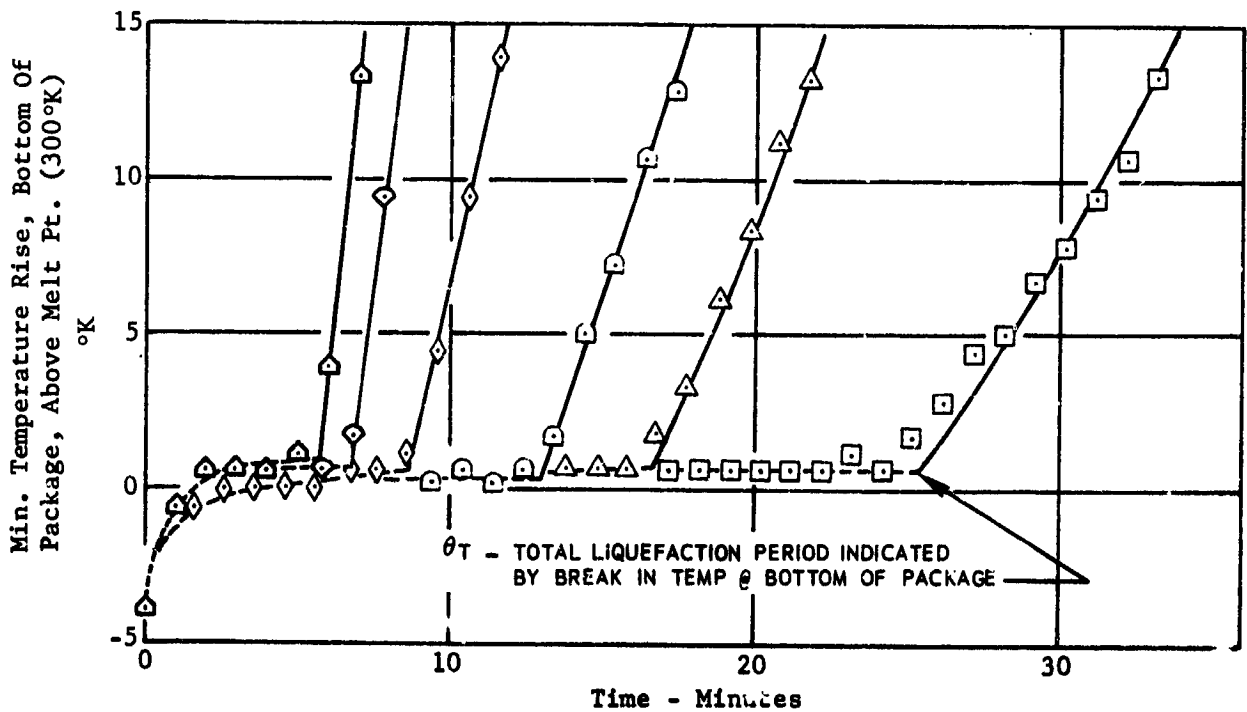
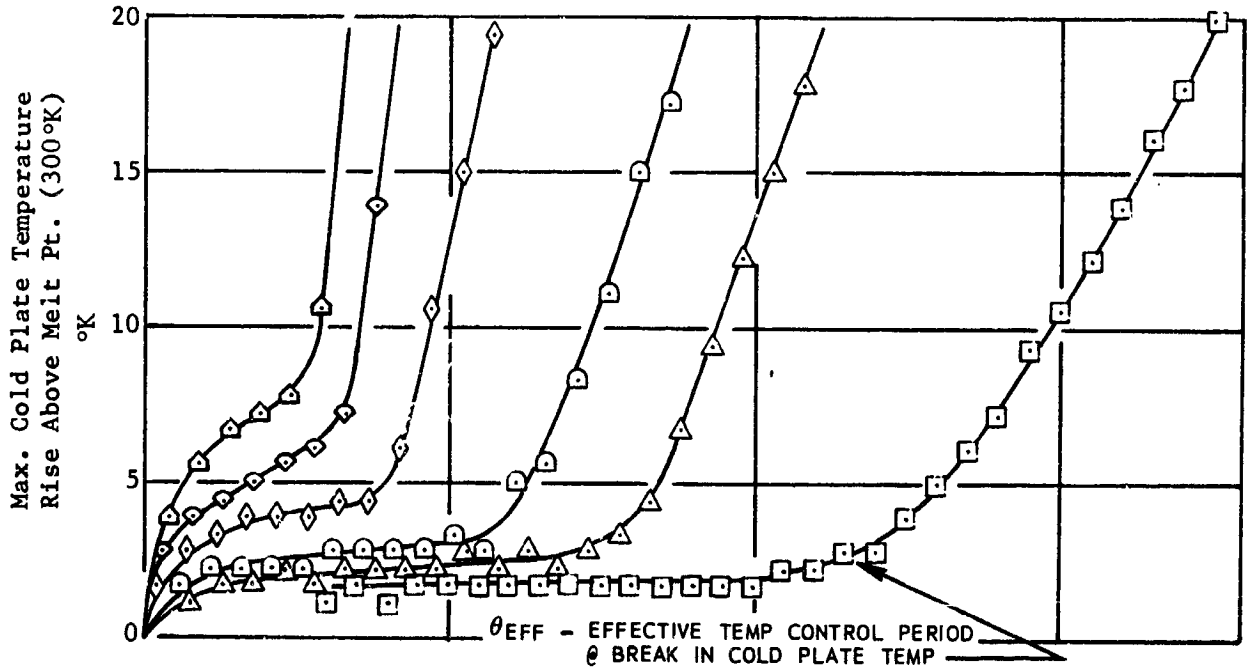


FIGURE 7-28 SYSTEM IMPROVEMENT ADIABATIC TEST RESULTS, FUSIBLE MATERIAL - OCTADECANE, MODEL 126-00100-9, MOD 1

SYMBOL	AVG CORRECTED POWER INPUT		$\theta_T$	$\theta_{EFF}$
	WATTS/FT <sup>2</sup>	WATTS/M <sup>2</sup>	MIN	MIN
□	106	1140	29.4	25.5
△	158	1700	19.4	16.5
○	211	2270	15.1	12.5
◇	315	9.8	7.5	
◊	416	4480	7.6	6.6
◕	515	5540	5.9	5.2

MODEL 13, MCD 1  
 ALUM. HONEYCOMB FILLER MAT'S  
 10.8% TOTAL VOID VOL.  
 SHEET THICKNESS .0024 IN (.0061 CM)  
 NOMINAL MAX. SHEET SPACING .041 IN (.104 CM)  
 PACKAGE THICKNESS .5 IN (1.27 CM)  
 WT. FUS. MAT. 75.1 GM  
 WT. PACKAGE/WT. FUS. MAT. 78.2%  
 NOMINAL COLD PLATE AREA .09352 (86.86 CM<sup>2</sup>)  
 TOTAL WT/AREA 3.16 LB/FT<sup>2</sup> (15.4 KG/M<sup>2</sup>)  
 ADHESIVE AM. CYANAMID COMPANY FM-1000

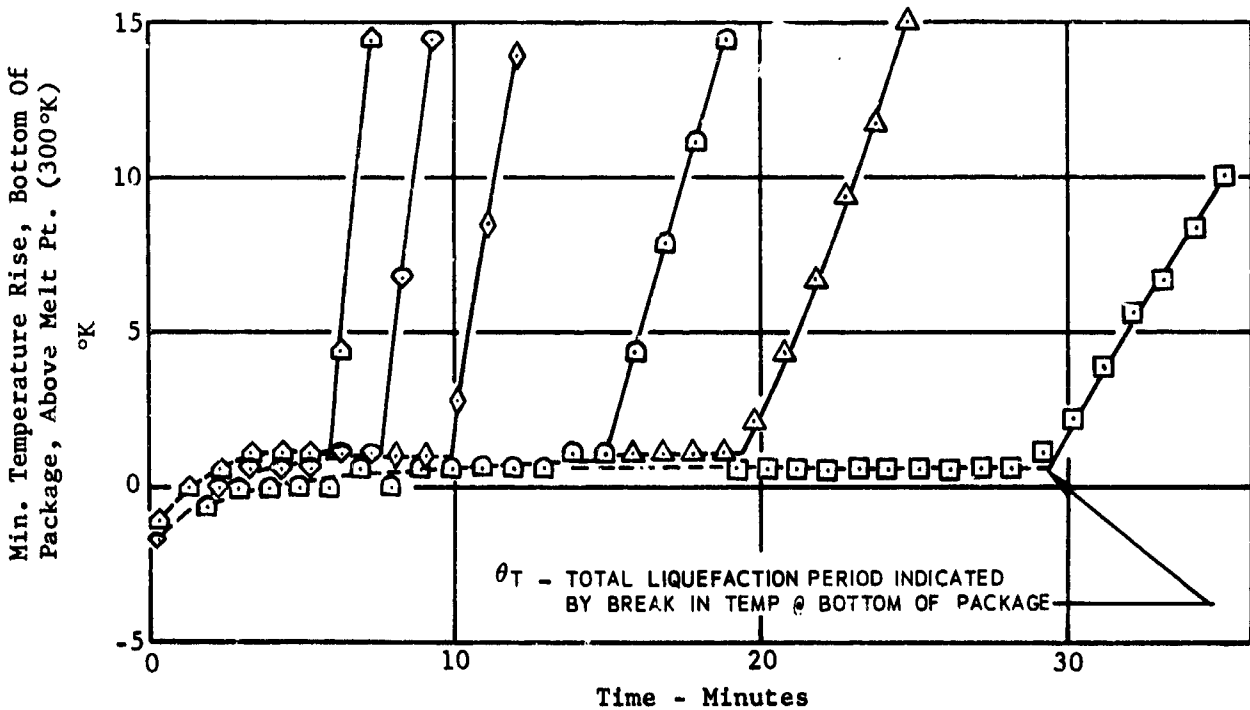
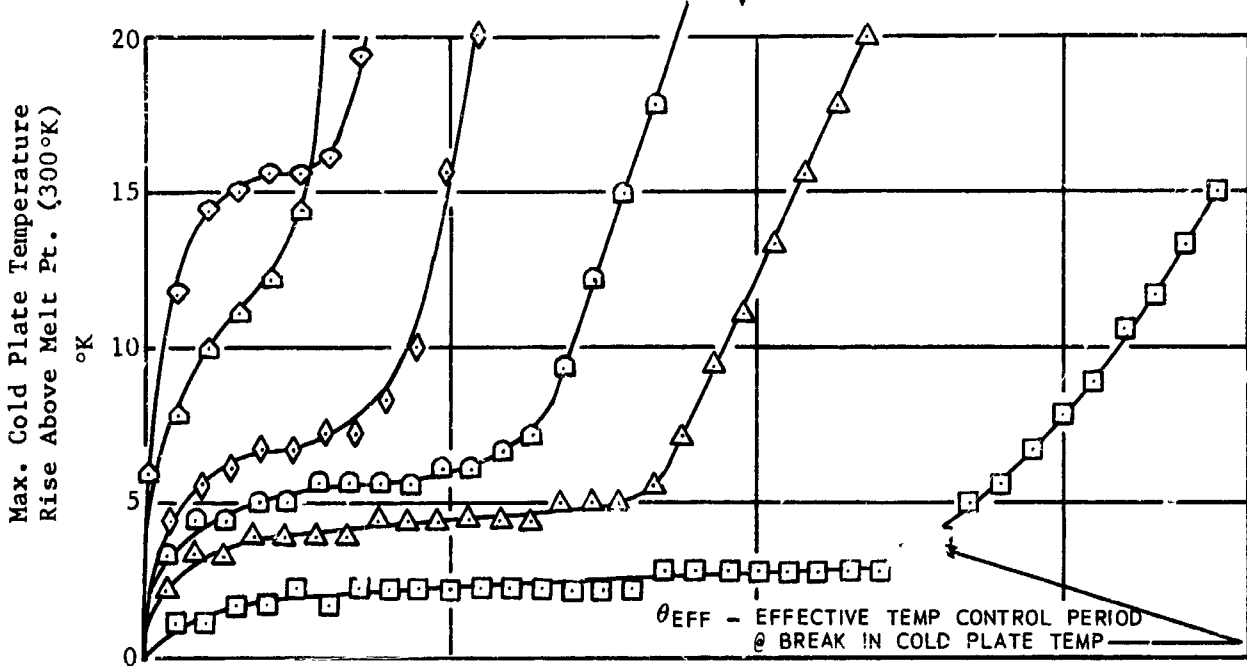


FIGURE 7-29 SYSTEM IMPROVEMENT ADIABATIC TEST RESULTS, FUSIBLE MATERIAL - OCTADECANE, MODEL 126-00100-13, MOD 1

SYMBOL	AVG CORRECTED POWER INPUT		$\theta_T$	$\theta_{EFF}$
	WATTS/FT <sup>2</sup>	WATTS/M <sup>2</sup>	MIN	MIN
□	106	1140	27.3	25.5
△	159	1710	18.3	17.4
◻	210	2260	14.1	11.6
◇	315	3390	9.9	8.2
◊	421	4530	7.6	6.7
△	523	5630	6.0	5.2

MODEL 15, MOD 1  
 ALUM. HONEYCOMB FILLER MAT'S  
 15.7% TOTAL VOID VOL.  
 SHEET THICKNESS .0019 IN (.0048 CM)  
 NOMINAL MAX. SHEET SPACING .023 IN (.058 CM)  
 PACKAGE THICKNESS .5 IN (1.27 CM)  
 WT. FUS. MAT. 71.1 GM  
 WT. PACKAGE/WT. FUS. MAT. 102.4%  
 NOMINAL COLD PLATE AREA .0935 FT<sup>2</sup> (86.86 CM<sup>2</sup>)  
 TOTAL WT/AREA 3.39 LB/FT<sup>2</sup> (16.6 KG/M<sup>2</sup>)  
 ADHESIVE AM. CYANAMID COMPANY FM-1000

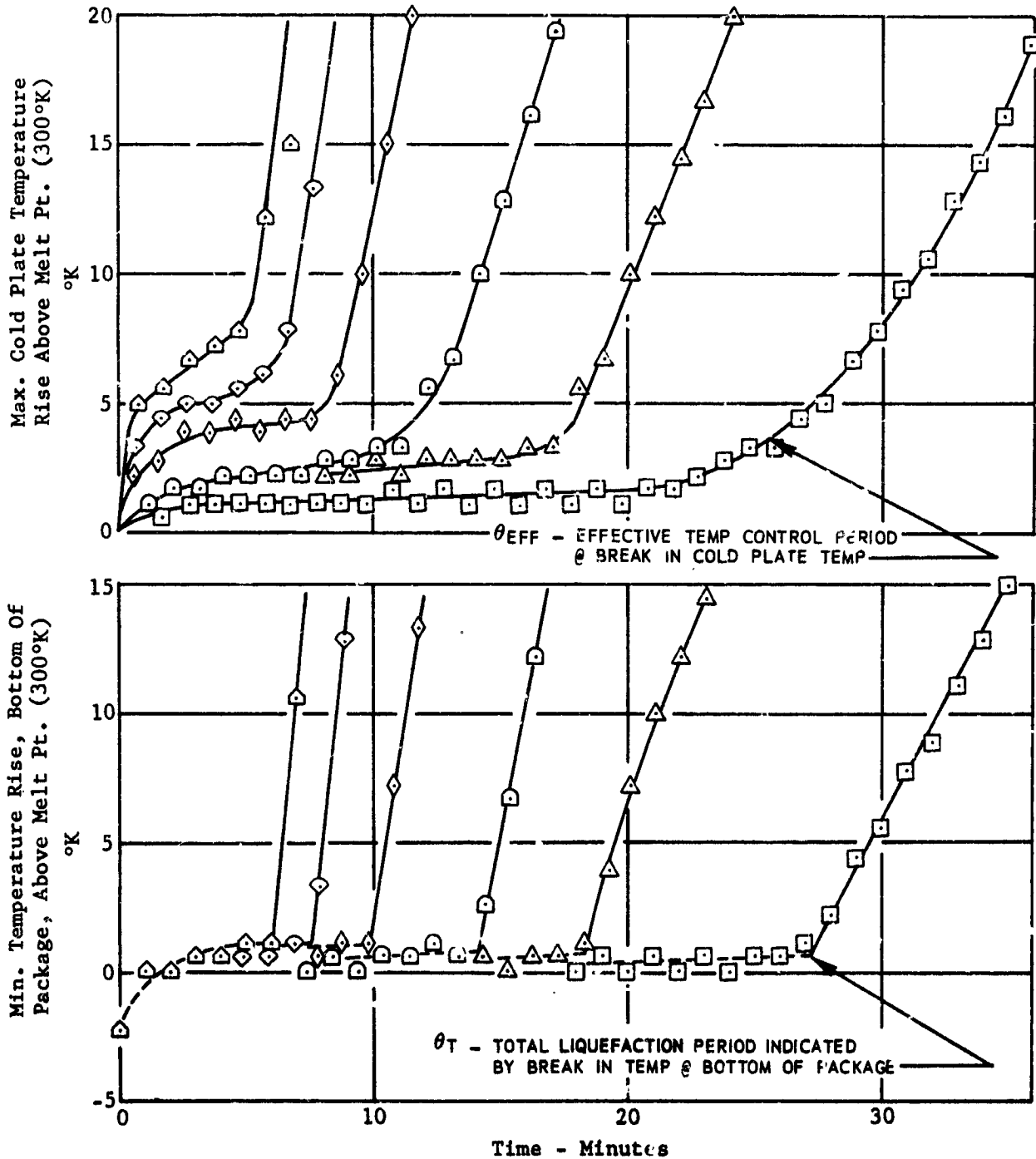


FIGURE 7-30 SYSTEM IMPROVEMENT ADIABATIC TEST RESULTS, FUSIBLE MATERIAL - OCTADECANE, MODEL 126-00100-15, MOD 1

MODEL 19, MOD 1  
 ALUM. HONEYCOMB FILLER MAT'S  
 4.9% TOTAL VOIL. VOL.  
 SHEET THICKNESS .0012 IN (.0030 CM)  
 NOMINAL MAX. SHEET SPACING .072 IN (.183 CM)  
 PACKAGE THICKNESS .5 IN (1.27 CM)  
 WT. FUS. MAT. 77.2 GM  
 WT. PACKAGE/WT. FUS. MAT. 54.7%  
 NOMINAL COLD PLATE AREA .0935 FT<sup>2</sup> (8.86 CM<sup>2</sup>)  
 TOTAL WT/AREA 2.82 LB/FT<sup>2</sup> (13.7 KG/M<sup>2</sup>)  
 ADHESIVE 3 M COMPANY AF-300

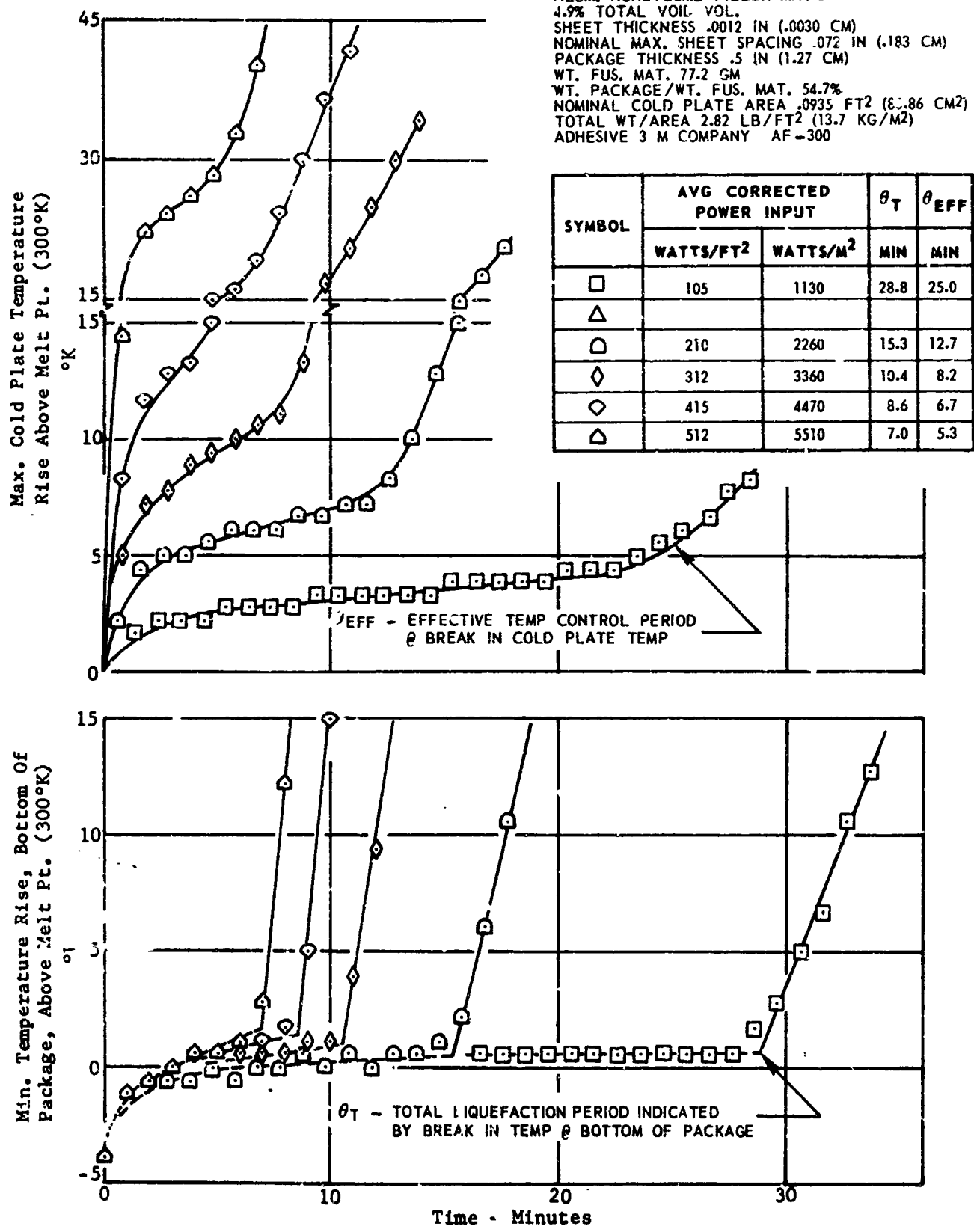


FIGURE 7-31 SYSTEM IMPROVEMENT ADIABATIC TEST RESULTS, FUSIBLE MATERIAL - OCTADECANE, MODEL 126-00100-19, MOD 1

SYMBOL	AVG CORRECTED POWER INPUT		$\theta_T$	$\theta_{EFF}$
	WATTS/FT <sup>2</sup>	WATTS/M <sup>2</sup>	MIN	MIN
□	106	1140	23.4	22.0
△	159	1710	16.0	14.5
◻	212	2280	12.3	10.8
◇	317	3410	8.3	7.4
◊	421	4530	6.8	6.1
△	522	5620	5.4	4.9

MODEL 7, MOD 2  
 ALUM. HONEYCOMB FILLER MAT'S.  
 9.4% TOTAL VOID VOL.  
 SHEET THICKNESS .0012 IN (.0030 CM)  
 NOMINAL MAX. SHEET SPACING .036 IN (.091 CM)  
 PACKAGE THICKNESS .5 IN (1.27 CM)  
 WT. FUS. MAT. 74.0 GM  
 WT. PACKAGE/WT. FUS. MAT 32.6%  
 NOMINAL COLD PLATE AREA .0935 FT<sup>2</sup> (86.86 CM<sup>2</sup>)  
 TOTAL WT/AREA 2.66 LB/FT<sup>2</sup> (13.0 KG/M<sup>2</sup>)  
 ADHESIVE 3 M CO. AF-300

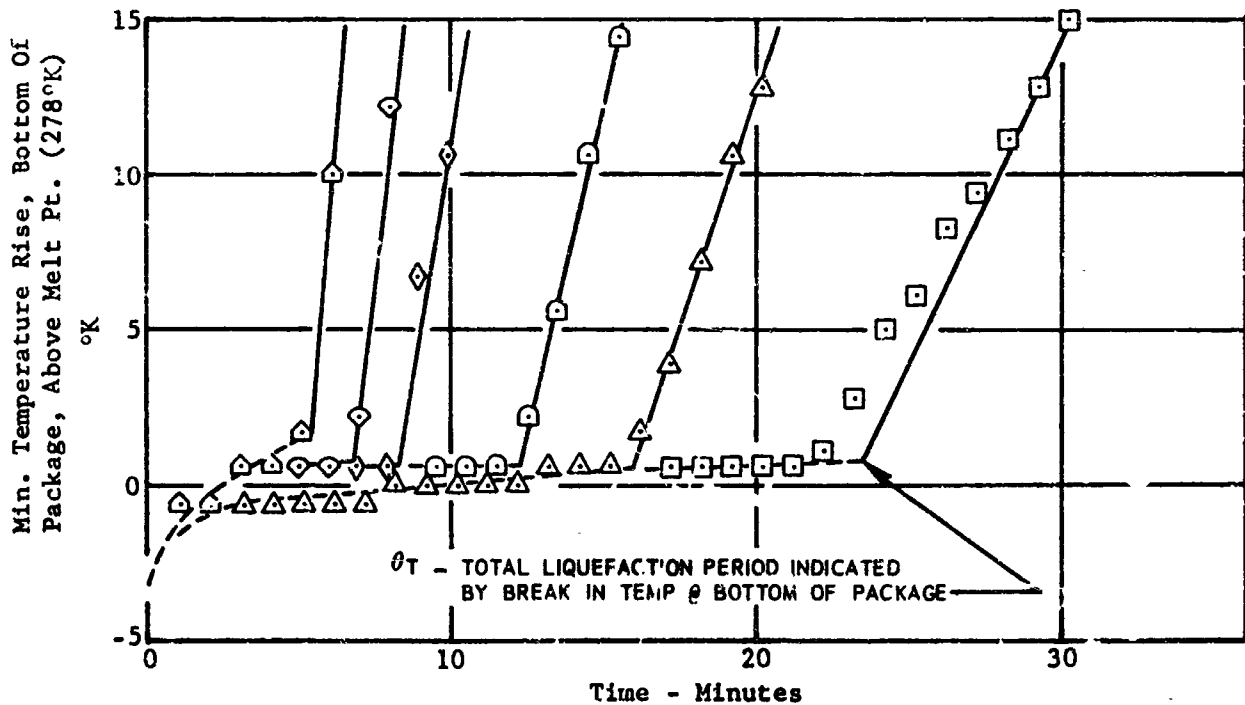
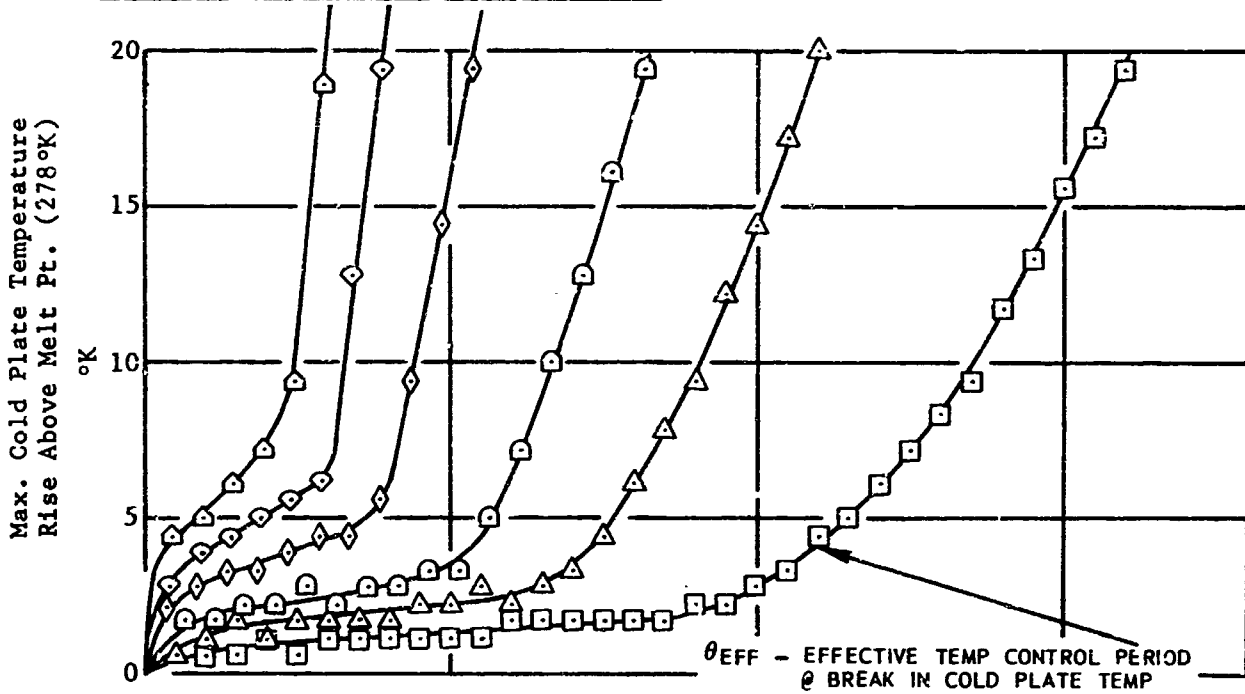


FIGURE 7-32 SYSTEM IMPROVEMENT ADIABATIC TEST RESULTS, FUSIBLE MATERIAL - TETRADECANE, MODEL 126-00100-7, MOD 2

MODEL 19, MOD 2  
 1/16" HONEYCOMB FILLER MAT'S.  
 4.8% TOTAL VOID VOL.  
 SHEET THICKNESS .0012 IN (.0030 CM)  
 NOMINAL MAX. SHEET SPACING .072 IN (.183 CM)  
 PACKAGE THICKNESS .5 IN (1.27 CM)  
 WT. FUS. MAT. 75.8 GM  
 WT. PACKAGE/WT. FUS. MAT. 42.2%  
 NOMINAL COLD PLATE AREA .0935 FT<sup>2</sup> (86.86 CM<sup>2</sup>)  
 TOTAL WT/AREA 2.58 LB/FT<sup>2</sup> (12.6 KG/M<sup>2</sup>)  
 ADHESIVE 3 M COMPANY AF-300

SYMBOL	AVG CORRECTED POWER INPUT		$\theta_T$	$\theta_{EFF}$
	WATTS/FT <sup>2</sup>	WATTS/M <sup>2</sup>	MIN	MIN
□	106	1140	26.4	23.0
△	158	1700	19.2	16.5
○	211	2270	11.7	11.5
◇	315	3390	10.1	7.4
◊	420	4520	8.0	6.4
◓	523	5630	6.5	5.2

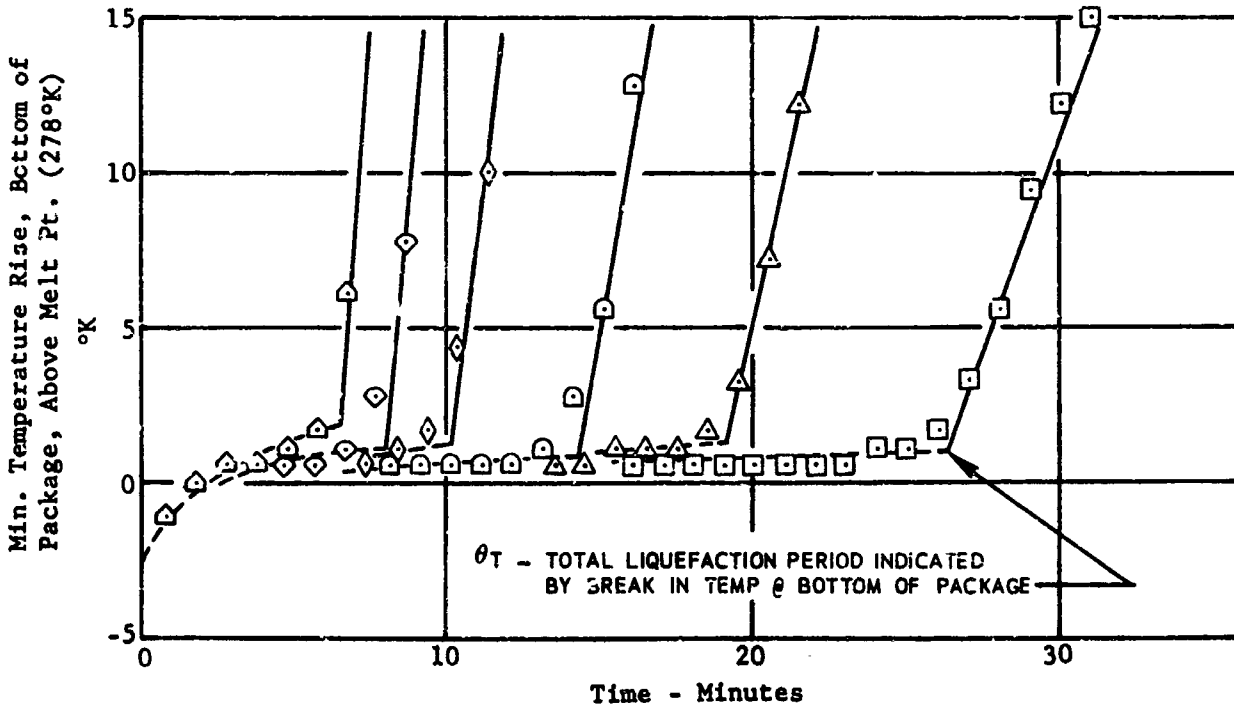
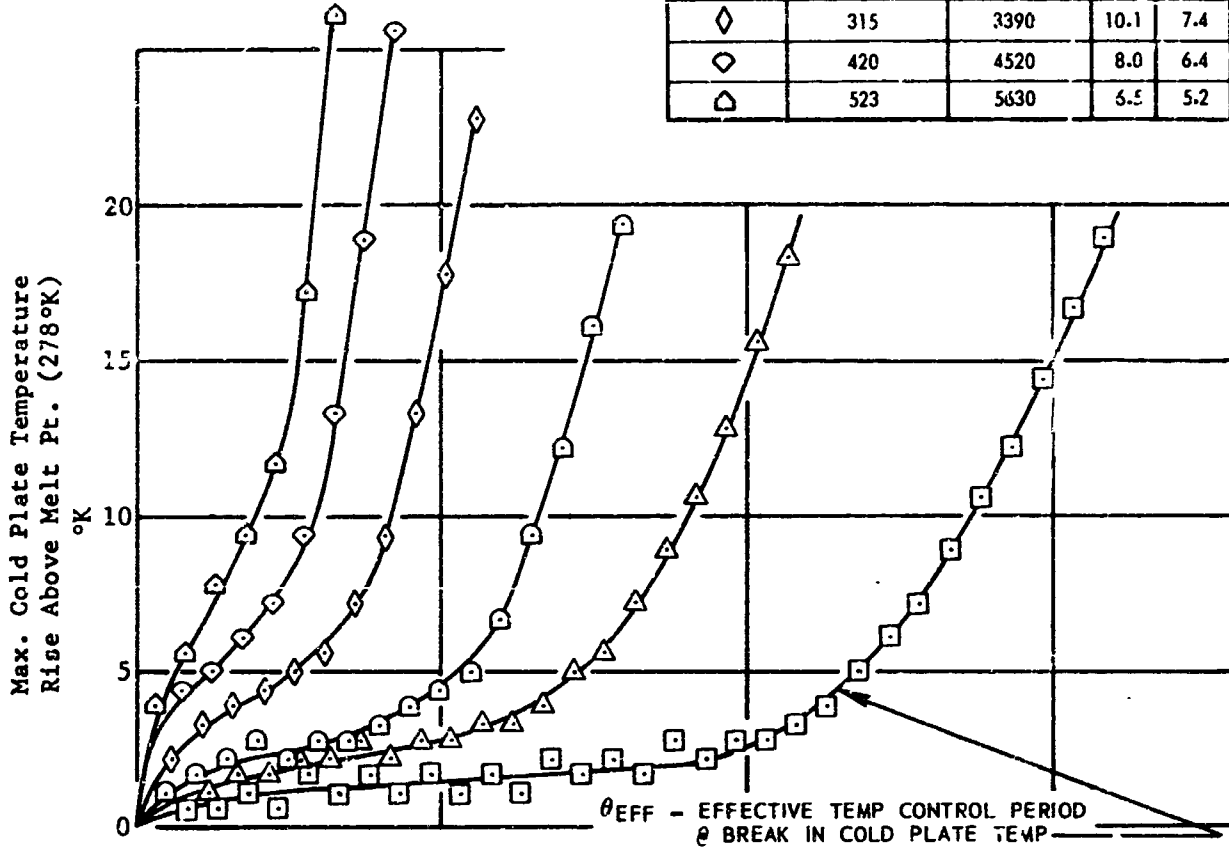


FIGURE 7-33 SYSTEM IMPROVEMENT ADIABATIC TEST RESULTS, FUSIBLE MATERIAL - TETRADECANE, MODEL 126-00100-19, MOD 2

SYMBOL	AVG CORRECTED POWER INPUT		$\theta_T$	$\theta_{EFF}$
	WATTS/FT <sup>2</sup>	WATTS/M <sup>2</sup>	MIN	MIN
□	106	1140	22.3	17.5
△	159	1710	14.0	11.7
◻	211	2270	11.9	9.5
◇	316	3400	8.1	6.5
○	420	4520	6.9	5.2
△	522	5620	5.0	3.9

MODEL 9, MOD 2  
 LUM. HONEYCOMB FILLER MAT'S.  
 11.4% TOTAL VOID VOL.  
 SHEET THICKNESS .0012 IN (.0030 CM)  
 NOMINAL MAX. SHEET SPACING .019 IN (.048 CM)  
 PACKAGE THICKNESS .5 IN (1.27 CM)  
 WT. FUS. MAT. 72.1 GM  
 WT. PACKAGE / WT. FUS. MAT 86.0%  
 NOMINAL COLD PLATE AREA .0935 FT<sup>2</sup> (86.86 CM<sup>2</sup>)  
 TOTAL WT / AREA 3.16 LB / FT<sup>2</sup> (15.4 KG / M<sup>2</sup>)  
 ADHESIVE 3 M COMPANY AF-300

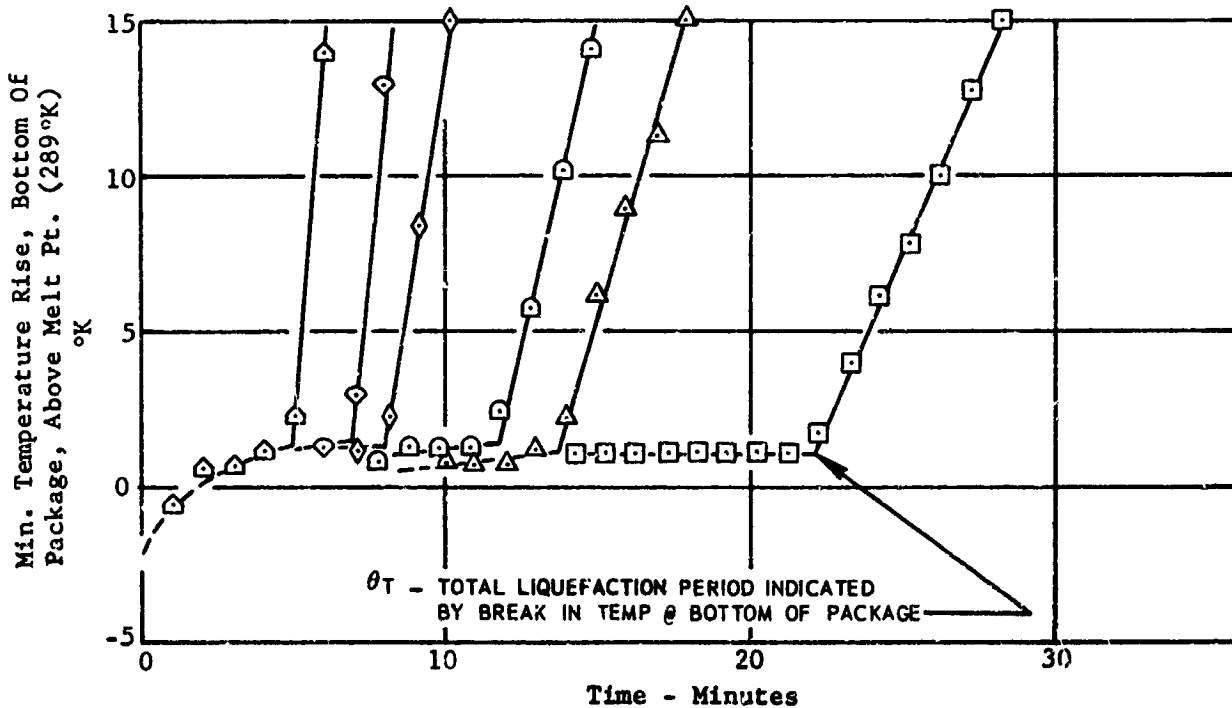
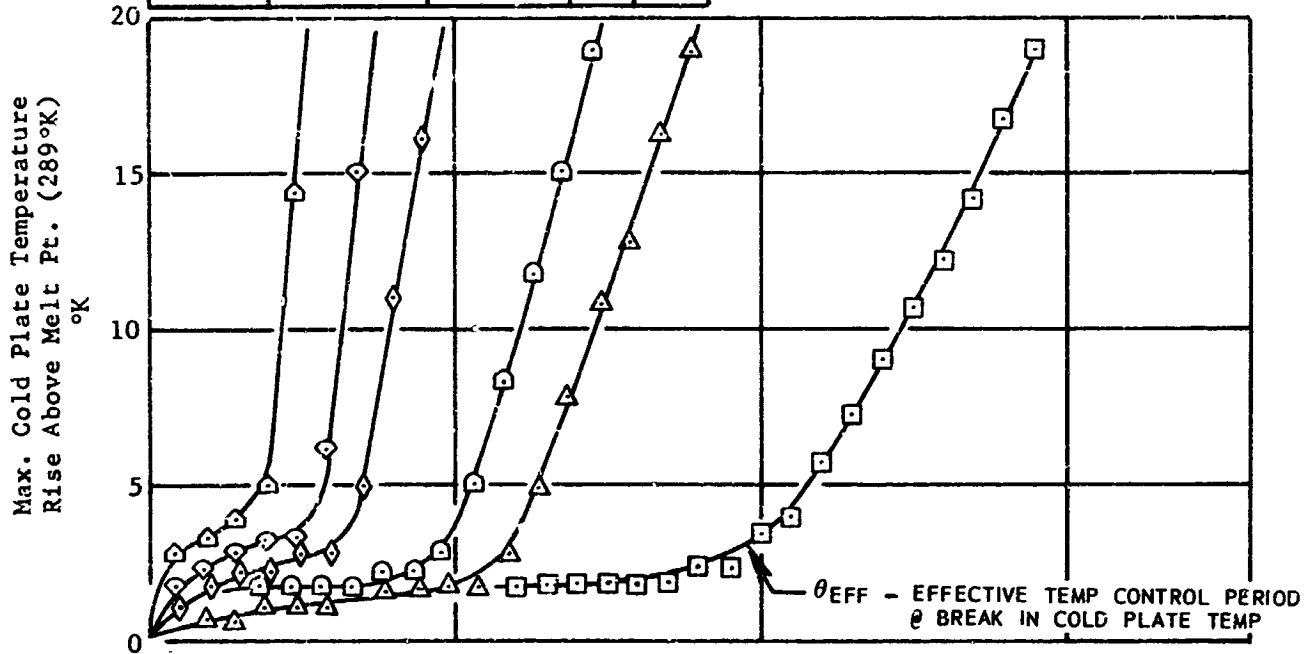


FIGURE 7-34 SYSTEM IMPROVEMENT ADIABATIC TEST RESULTS, FUSIBLE MATERIAL - HEXADECANE, MODEL 126-00100-9, MODEL 2

SYMBOL	AVG CORRECTED POWER INPUT		$\theta_T$	$\theta_{EFF}$
	WATTS/FT <sup>2</sup>	WATTS/M <sup>2</sup>	MIN	MIN
□	106	1140	22.4	19.1
△	158	1700	14.9	11.4
○	211	2270	12.2	9.6
◇	315	3390	8.1	6.5
◊	422	4540	6.3	4.8
△	526	5660	5.3	4.1

MODEL 15, MOD 2  
 ALUM. HONEYCOMB FILLER MAT'S.  
 15.8% TOTAL VOID VOL.  
 SHEET THICKNESS .0019 IN (.0048 CM)  
 NOMINAL MAX. SHEET SPACING .023 IN (.058 CM)  
 PACKAGE THICKNESS .5 IN (1.27 CM)  
 WT. FUS. MAT. 68.7 GM  
 WT. PACKAGE/WT. FUS. MAT. 108.5%  
 NOMINAL COLD PLATE AREA .0935 FT<sup>2</sup> (86.86 CM<sup>2</sup>)  
 TOTAL WT/AREA 3.38 LB/FT<sup>2</sup> (16.5 KG/M<sup>2</sup>)  
 ADHESIVE 3 M COMPANY AF-300

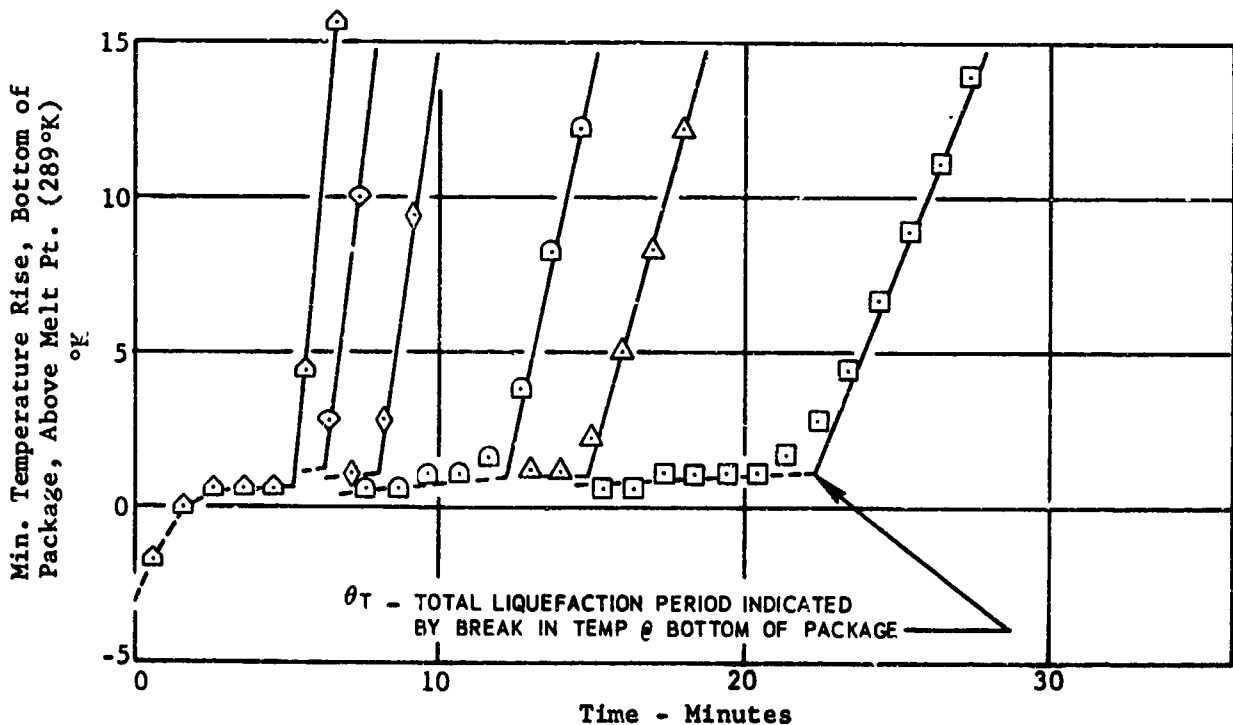
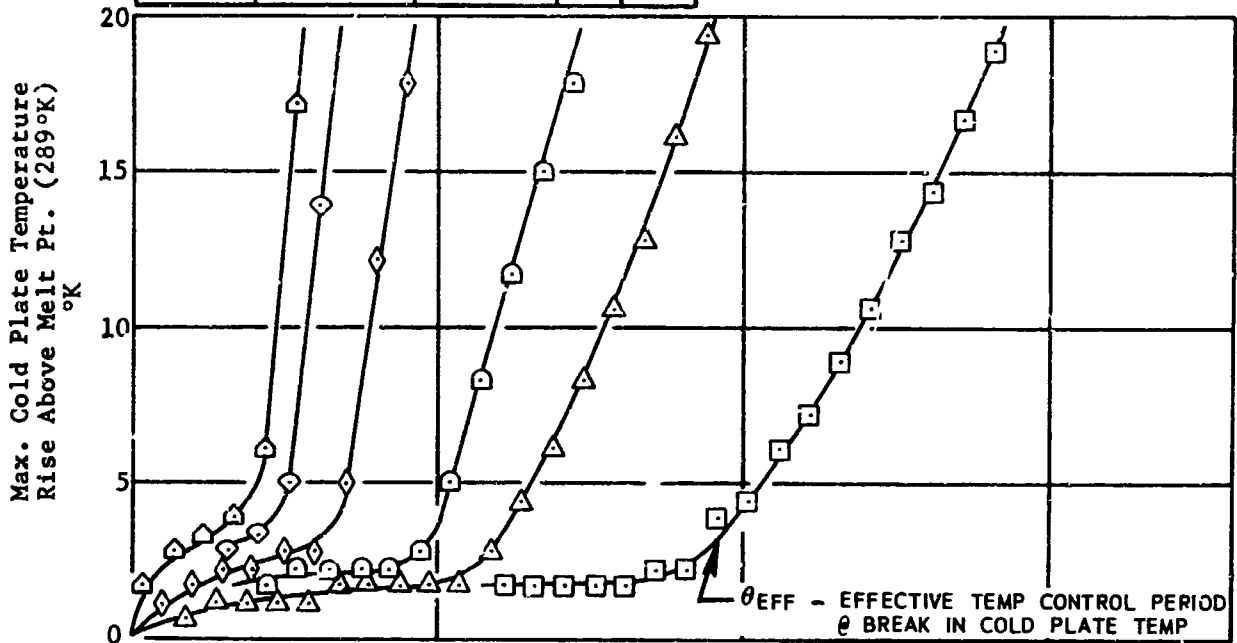


FIGURE 7-35 SYSTEM IMPROVEMENT ADIABATIC TEST RESULTS, FUSIBLE MATERIAL - HEXADECANE, MODEL 126-00100-15, MOD 2

SYMBOL	AVG CORRECTED POWER INPUT		$\theta_T$	$\theta_{EFF}$
	WATTS/FT <sup>2</sup>	WATTS/M <sup>2</sup>	MIN	MIN
□	105	1130	21.0	18.0
△	158	1700	15.3	12.9
◻	211	2270	11.7	9.6
◇	315	3390	8.0	6.4
◊	422	4540	6.5	5.3
△	524	5640	5.6	4.6

MODEL 11, MOD 1  
 ALUM. HONEYCOMB FILLER MAT'S.  
 10.8% TOTAL VOID VOL.  
 SHEET THICKNESS .0019 IN (.0048 CM)  
 NOMINAL MAX. SHEET SPACING .032 IN (.081 CM)  
 PACKAGE THICKNESS .5 IN (1.27 CM)  
 WT. FUS. MAT. 75.2 GM  
 WT. PACKAGE/WT. FUS. MAT. 73.6%  
 NOMINAL COLD PLATE AREA .0935 FT<sup>2</sup> (86.86 CM<sup>2</sup>)  
 TOTAL WT/AREA 3.08 LB/FT<sup>2</sup> (15.0 KG/M<sup>2</sup>)  
 ADHESIVE AM. CYANAMID COMPANY FM-1000

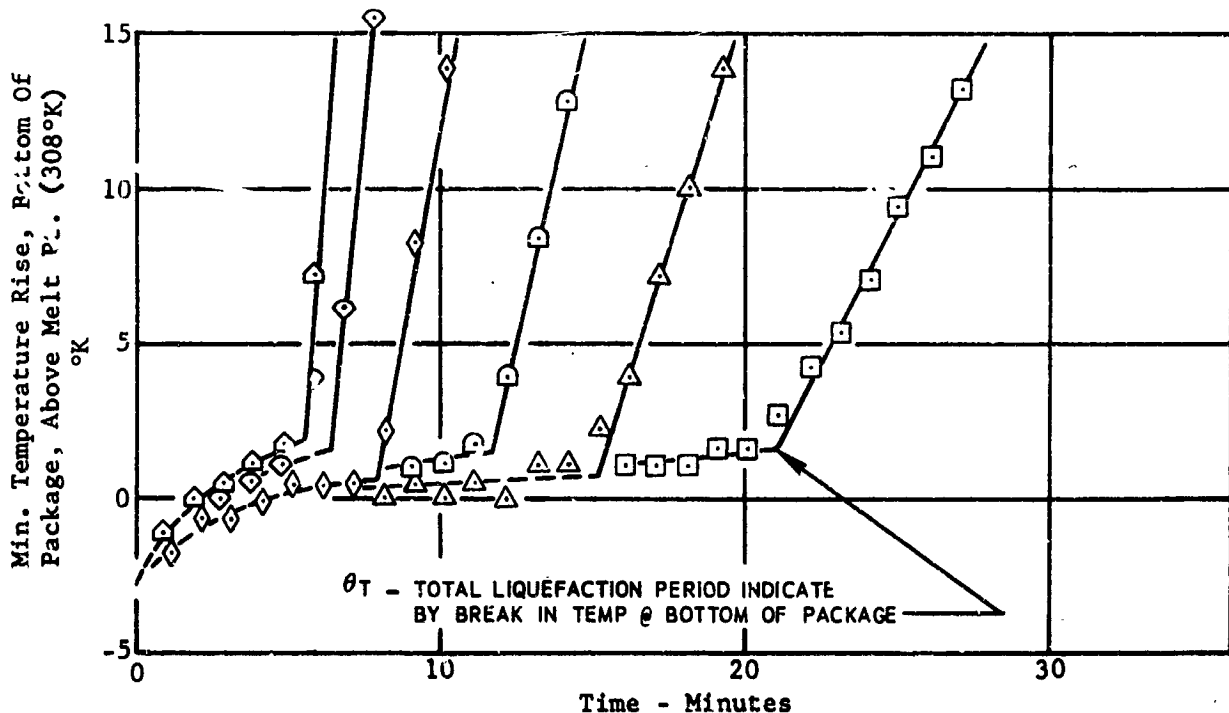
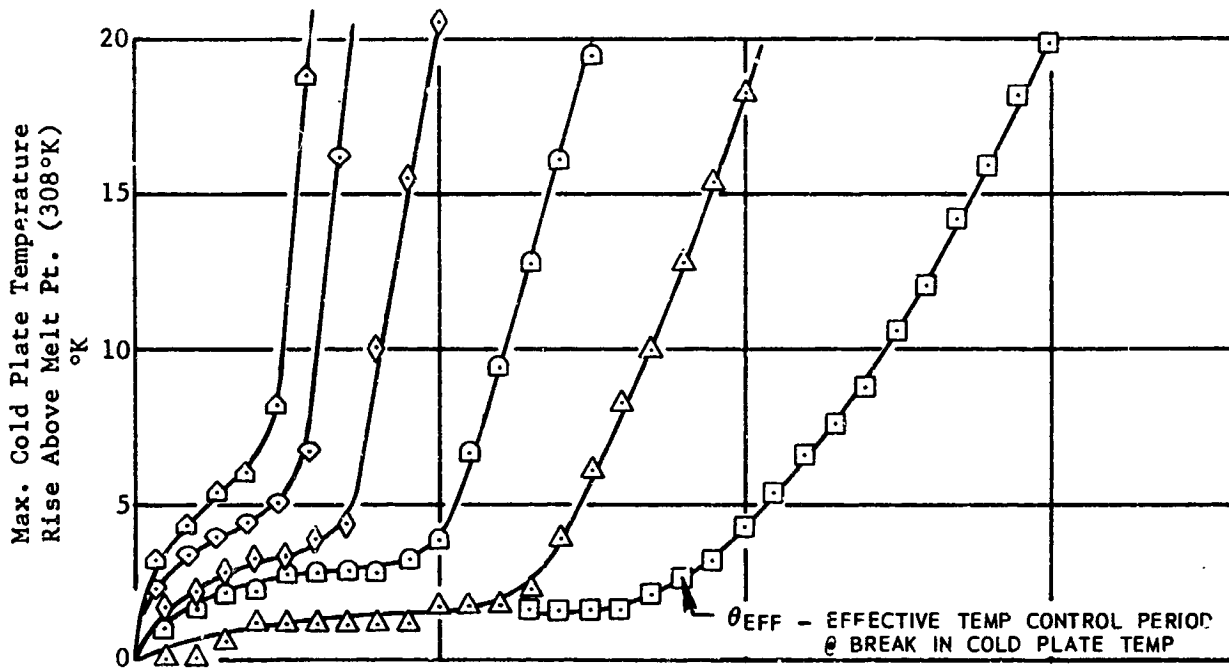


FIGURE 7-36 SYSTEM IMPROVEMENT ADIABATIC TEST RESULTS, FUSIBLE MATERIAL - EICOSANE, MODEL 126-00100-11, MOD 1

SYMBOL	AVG CORRECTED POWER INPUT		$\theta_T$	$\theta_{EFF}$
	WATTS/FT <sup>2</sup>	WATTS/M <sup>2</sup>	MIN	MIN
□	105	1130	20.5	18.5
△	157	1690	15.6	12.2
○	209	2250	11.6	8.7
◇	314	3380	8.8	6.9
◊	416	4480	7.0	5.5
△	516	5550	5.6	4.3

MODEL 11, MOD 2  
 ALUM. HONEYCOMB FILLER MAT'S  
 7.7% TOTAL VOID VOL.  
 SHEET THICKNESS .0019 IN (.0048 CM)  
 NOMINAL MAX. SHEET SPACING .028 IN (.071 CM)  
 PACKAGE THICKNESS .5 IN (1.27 CM)  
 WT. FUS. MAT. 74.6 GM  
 WT. PACKAGE / WT. FUS. MAT. 67.0%  
 NOMINAL COLD PLATE AREA .0935 FT<sup>2</sup> (86.86 CM<sup>2</sup>)  
 TOTAL WT / AREA 2.94 LB / FT<sup>2</sup> (14.3 KG / M<sup>2</sup>)  
 ADHESIVE 3 M COMPANY AF-300

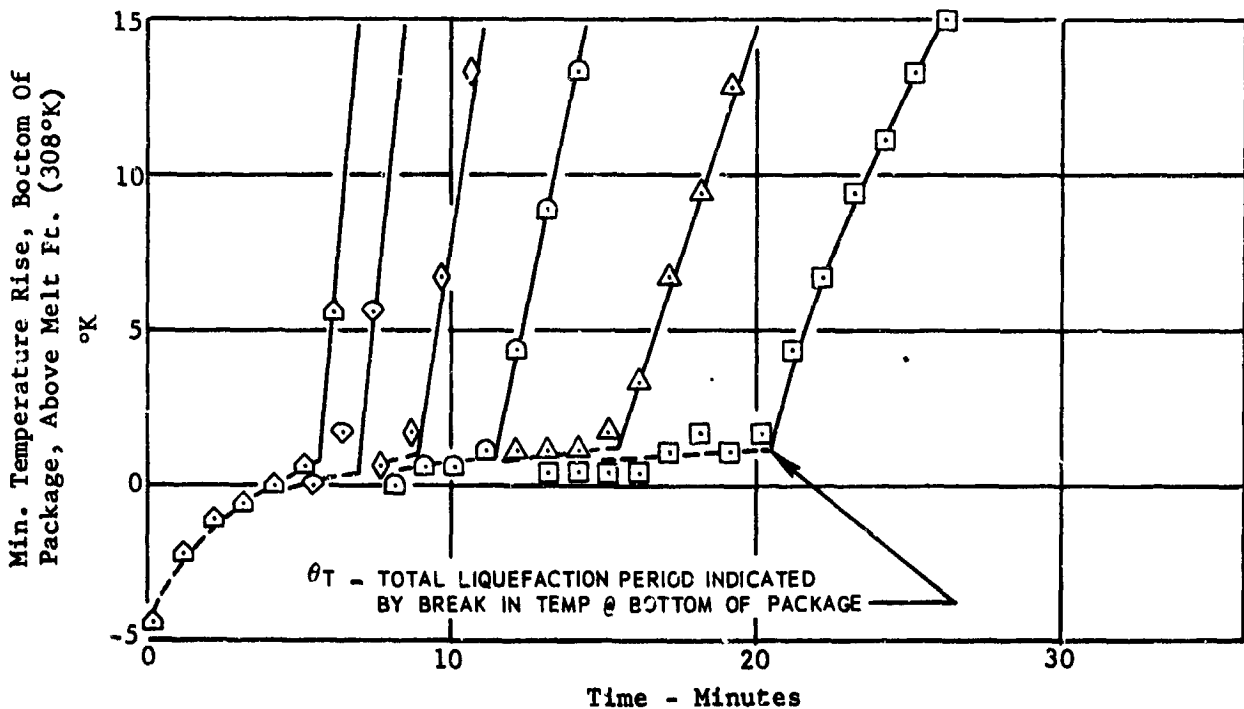
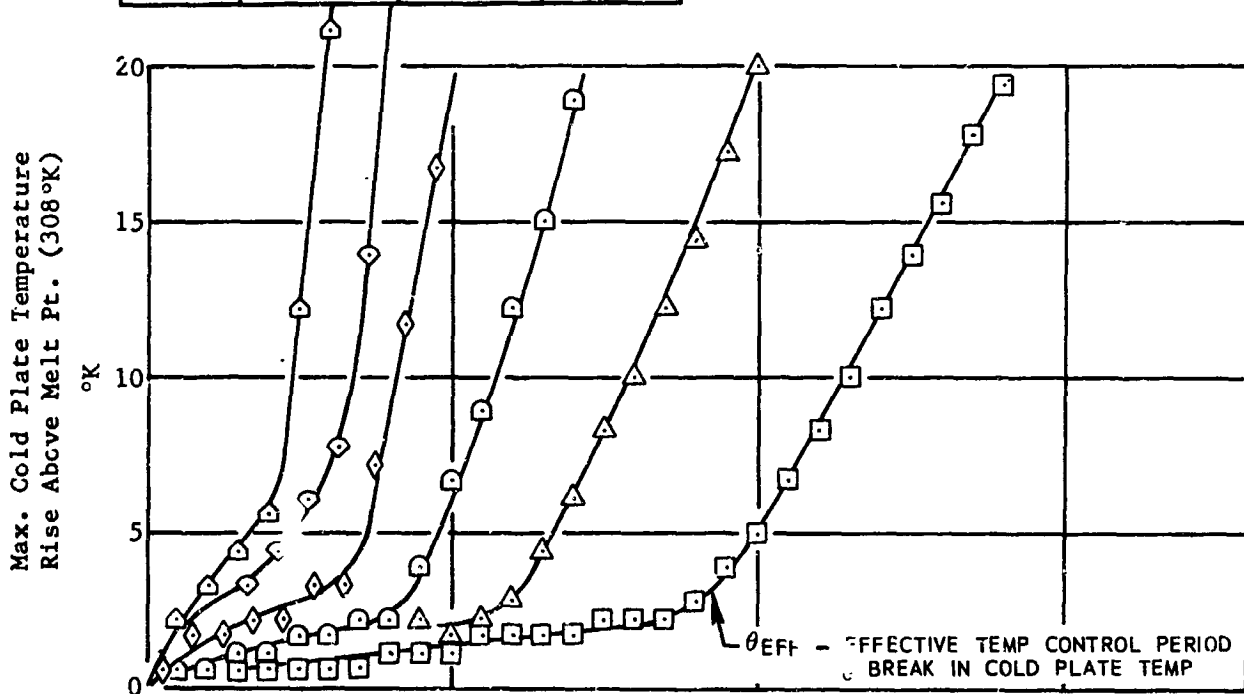


FIGURE 7-37 SYSTEM IMPROVEMENT ADIABATIC TEST RESULTS, FUSIBLE MATERIAL - EICOSANE, MODEL 126-00100-11, MOD 2

SYMBOL	AVG CORRECTED POWER INPUT		$\theta_T$	$\theta_{EFF}$
	WATTS/FT <sup>2</sup>	WATTS/M <sup>2</sup>	MIN	MIN
□	105	1130	21.5	19.2
△	158	1700	14.8	12.8
○	211	2270	12.8	10.5
◇	314	3380	8.8	7.3
◊	417	4490	7.5	5.8
◓	519	5590	5.7	4.7

MODEL 15, MOD 1  
 ALUM. HONEYCOMB FILLER MAT'S.  
 15.7% TOTAL VOID VOL.  
 SHEET THICKNESS .0019 IN (.0048 CM)  
 NOMINAL MAX. SHEET SPACING .023 IN (.058 CM)  
 PACKAGE THICKNESS .5 IN (1.27 CM)  
 WT. FUS. MAT. 72.0 GM  
 WT. PACKAGE / WT. FUS. MAT. 101.1%  
 NOMINAL COLD PLATE AREA .0935 FT<sup>2</sup> (86.86 CM<sup>2</sup>)  
 TOTAL WT / AREA 3.42 LB / FT<sup>2</sup> (16.7 KG / M<sup>2</sup>)  
 ADHESIVE AM. CYANAMID COMPANY FM-1000

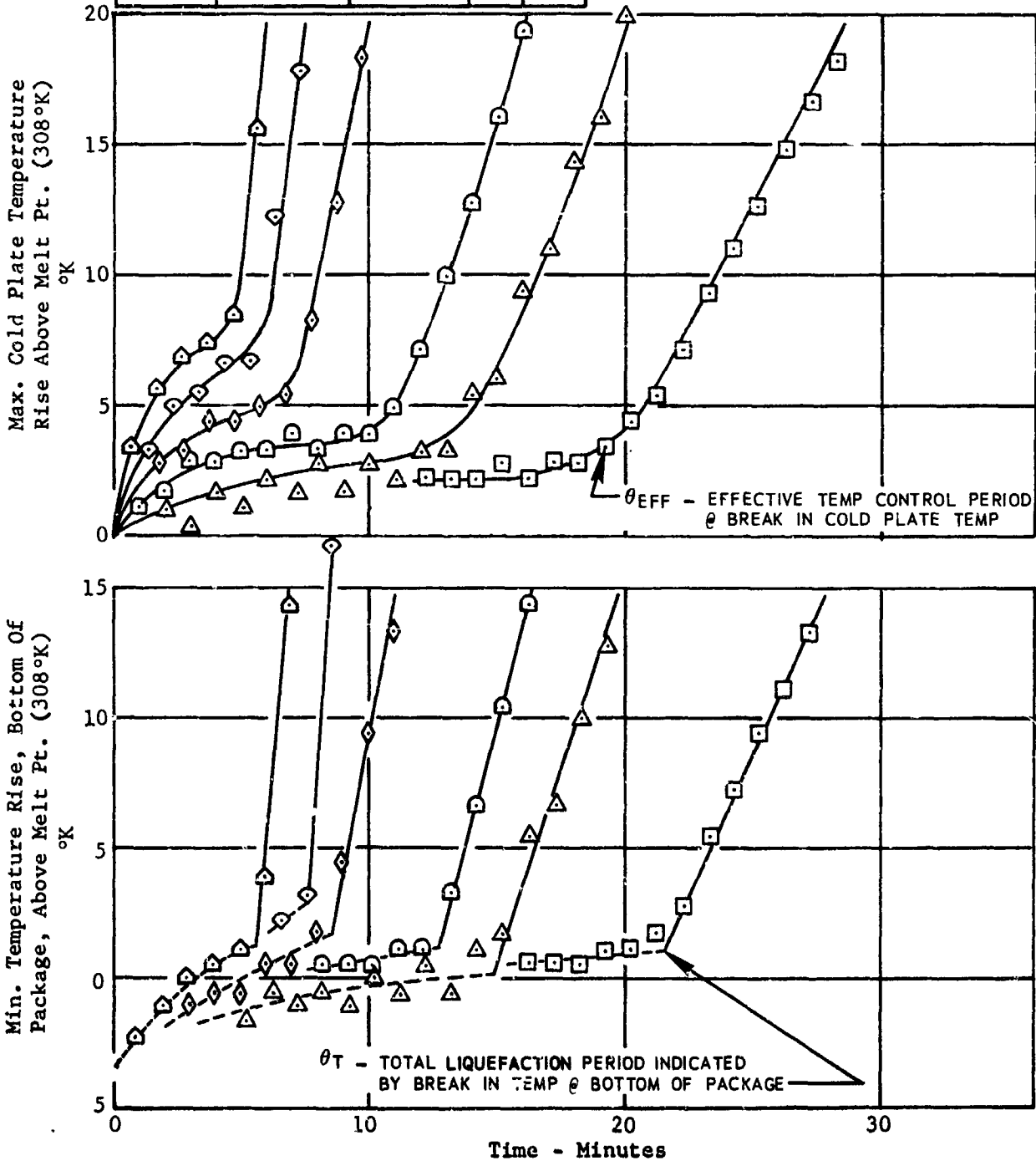


FIGURE 7-38 SYSTEM IMPROVEMENT ADIABATIC TEST RESULTS, FUSIBLE MATERIAL - EICOSANE, MODEL 126-00100-15, MOD 1

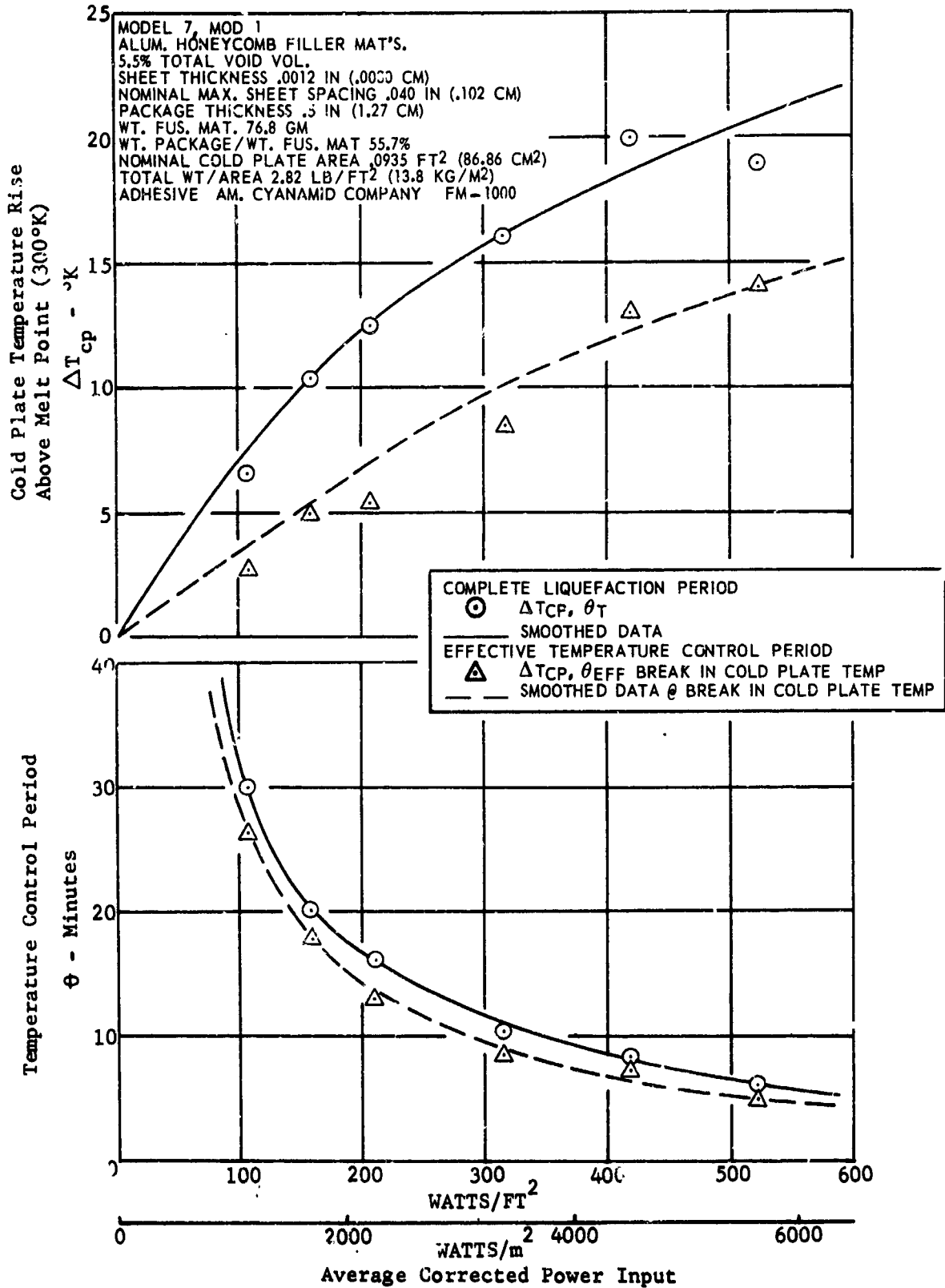


FIGURE 7-39 CORRELATION OF TEST RESULTS - SYSTEM IMPROVEMENT - ADIABATIC MODEL - FUSIBLE MATERIAL OCTADECANE, MODEL 126-00100-7, MOD 1

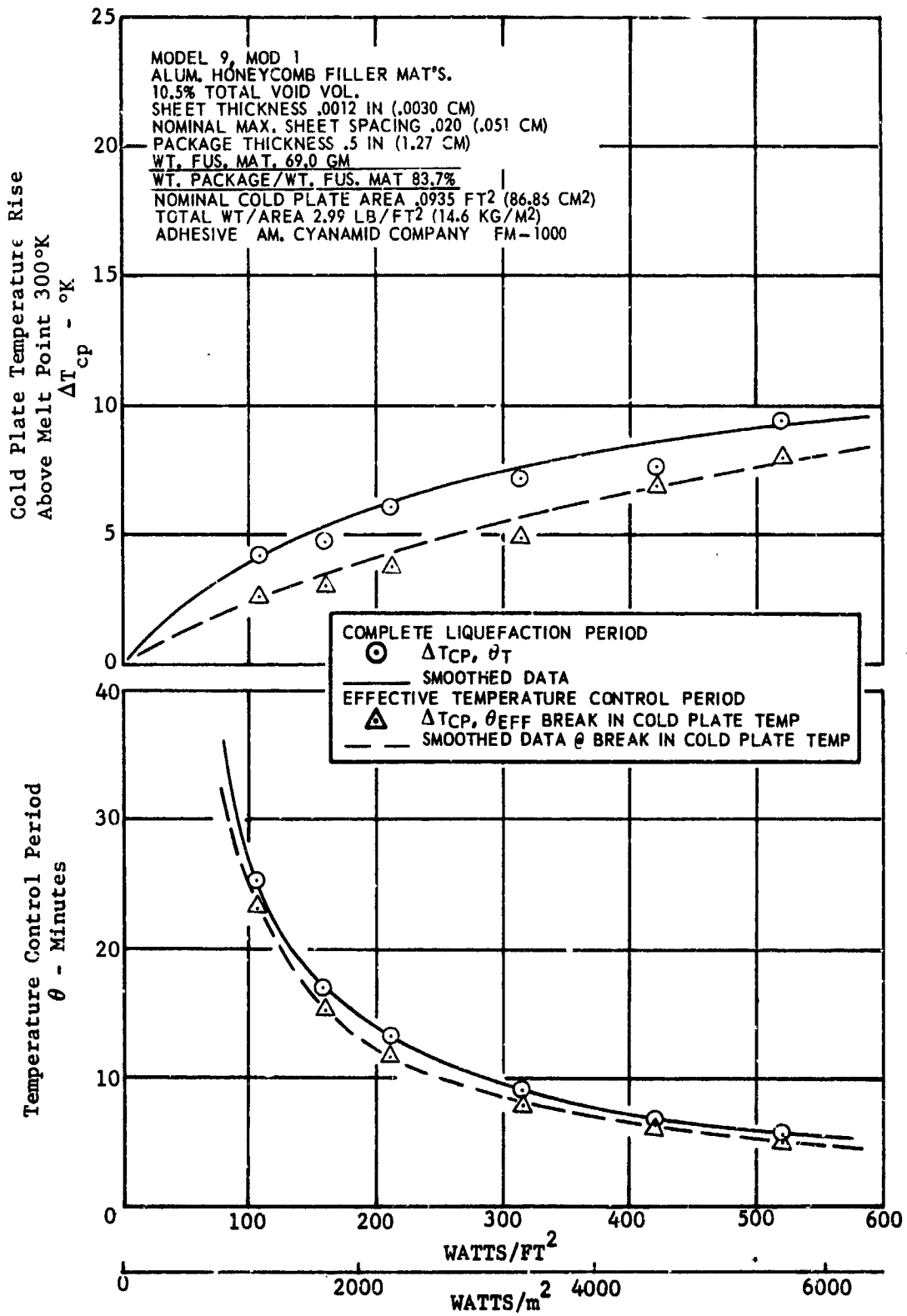


FIGURE 7-40 CORRELATION OF TEST RESULTS - SYSTEM IMPROVEMENT - ADIABATIC MODEL - FUSIBLE MATERIAL OCTADECANE, MODEL 126-00100-9, MOD 1

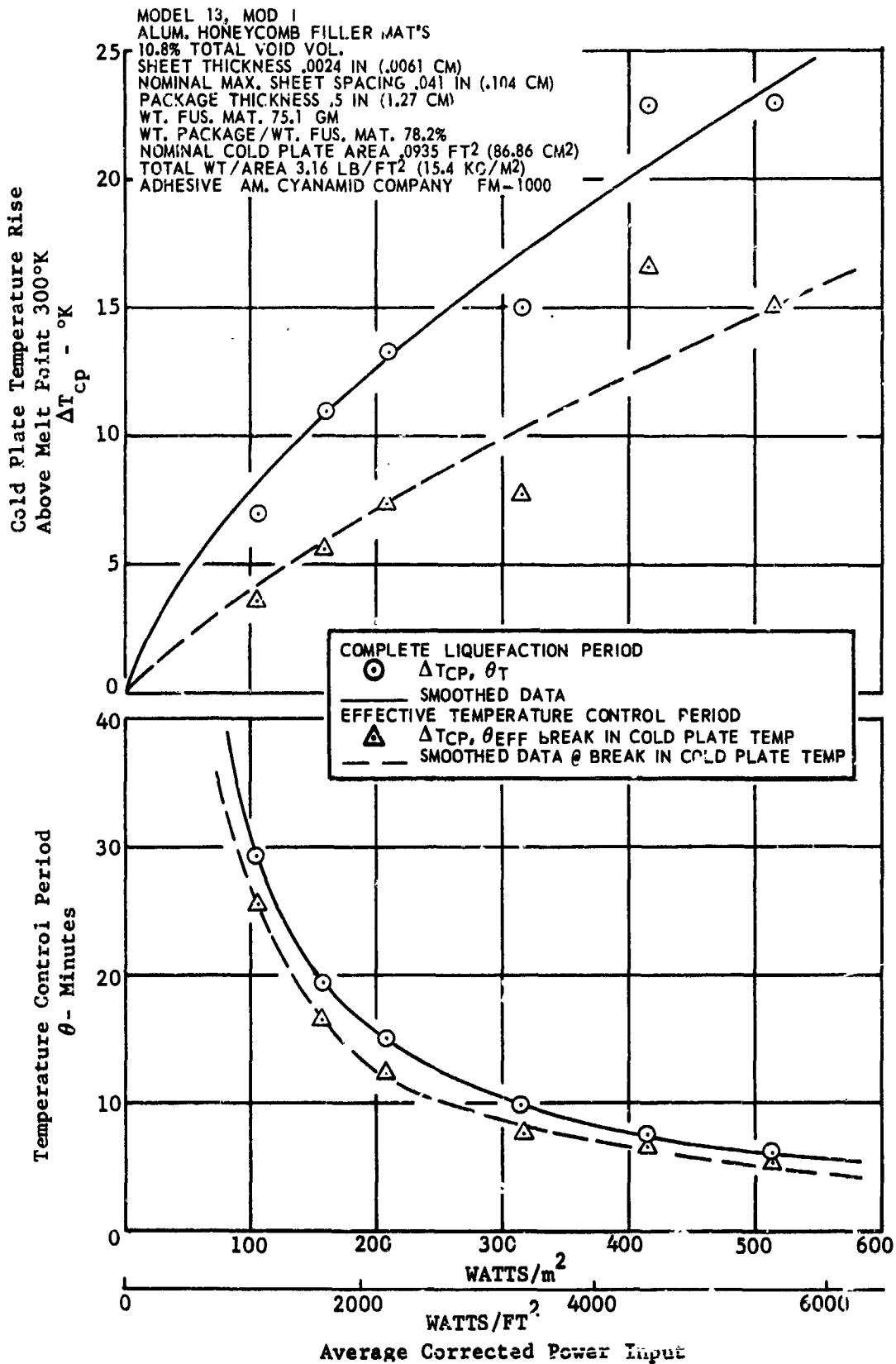


FIGURE 7-41 CORRELATION OF TEST RESULTS - SYSTEM IMPROVEMENT - ADIABATIC MODEL - FUSIBLE MATERIAL OCTADECANE, MODEL 126-00100-13, MOD 1

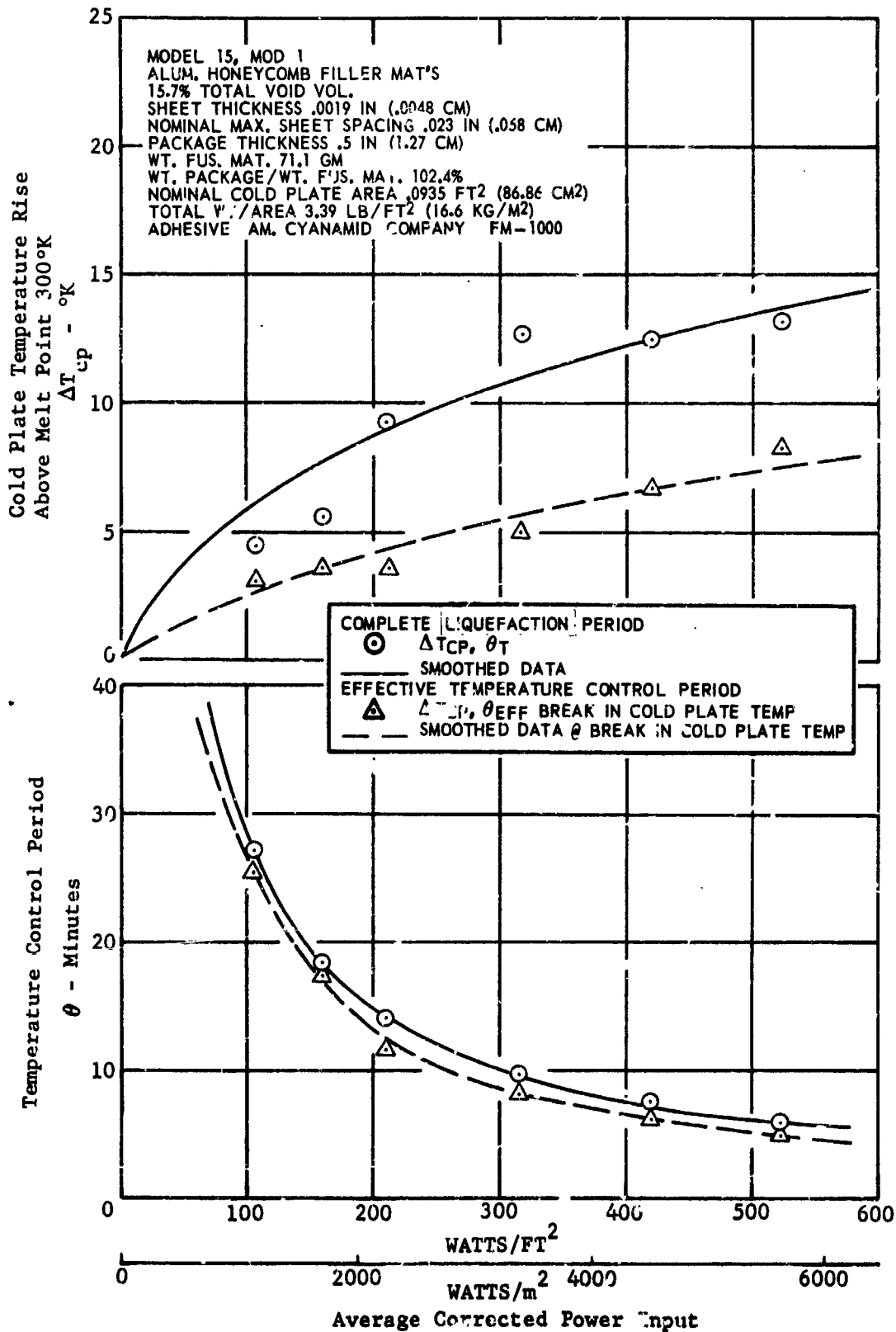


FIGURE 7-42 CORRELATION OF TEST RESULTS - SYSTEM IMPROVEMENT - ADIABATIC MODEL - FUSIBLE MATERIAL OCTADECANE, MODEL 126-00100-15, MOD 1

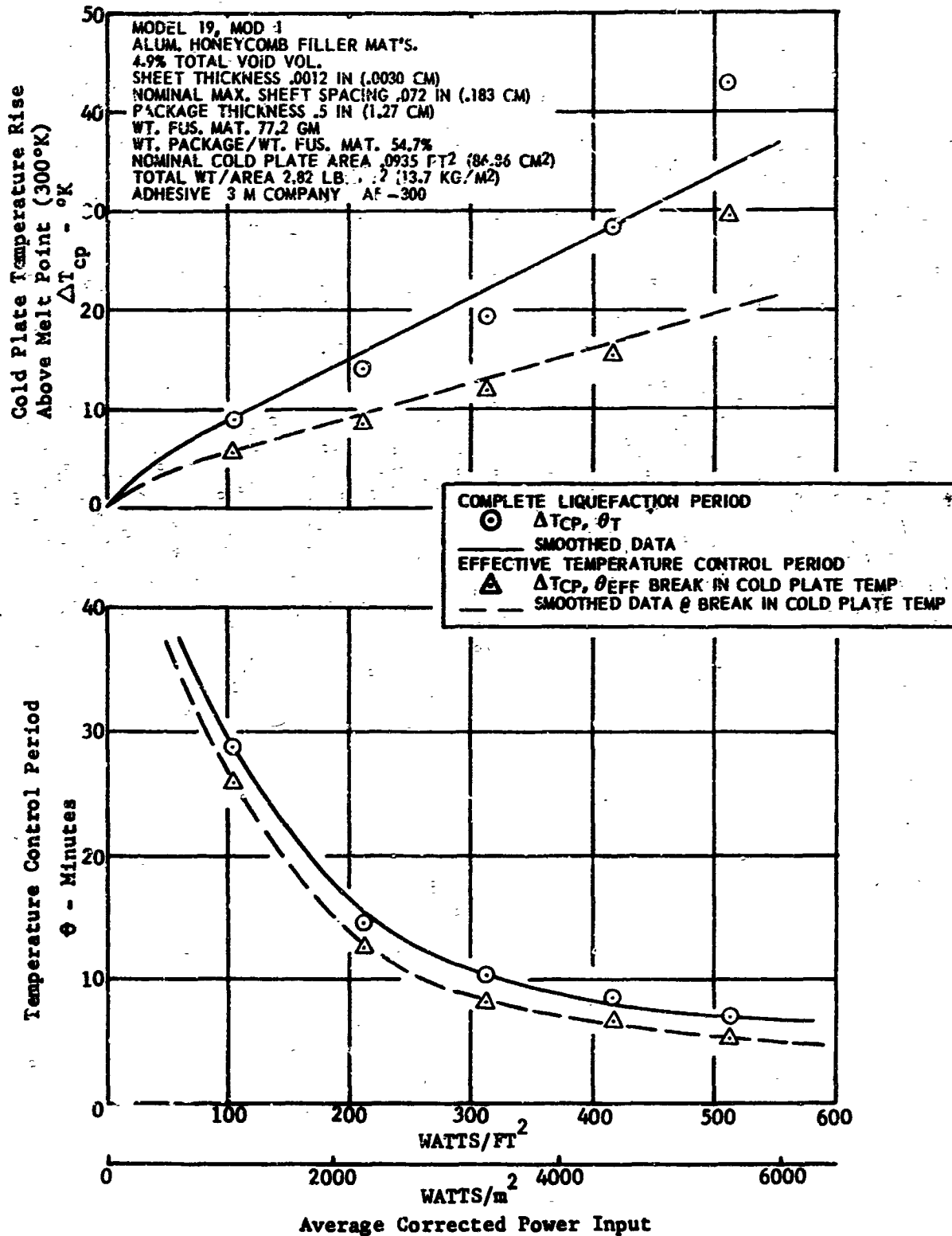


FIGURE 7-43 CORRELATION OF TEST RESULTS - SYSTEM IMPROVEMENT - ADIABATIC MODEL - FUSIBLE MATERIAL OCTADECANE, MODEL 126-00100-19, MOD 1

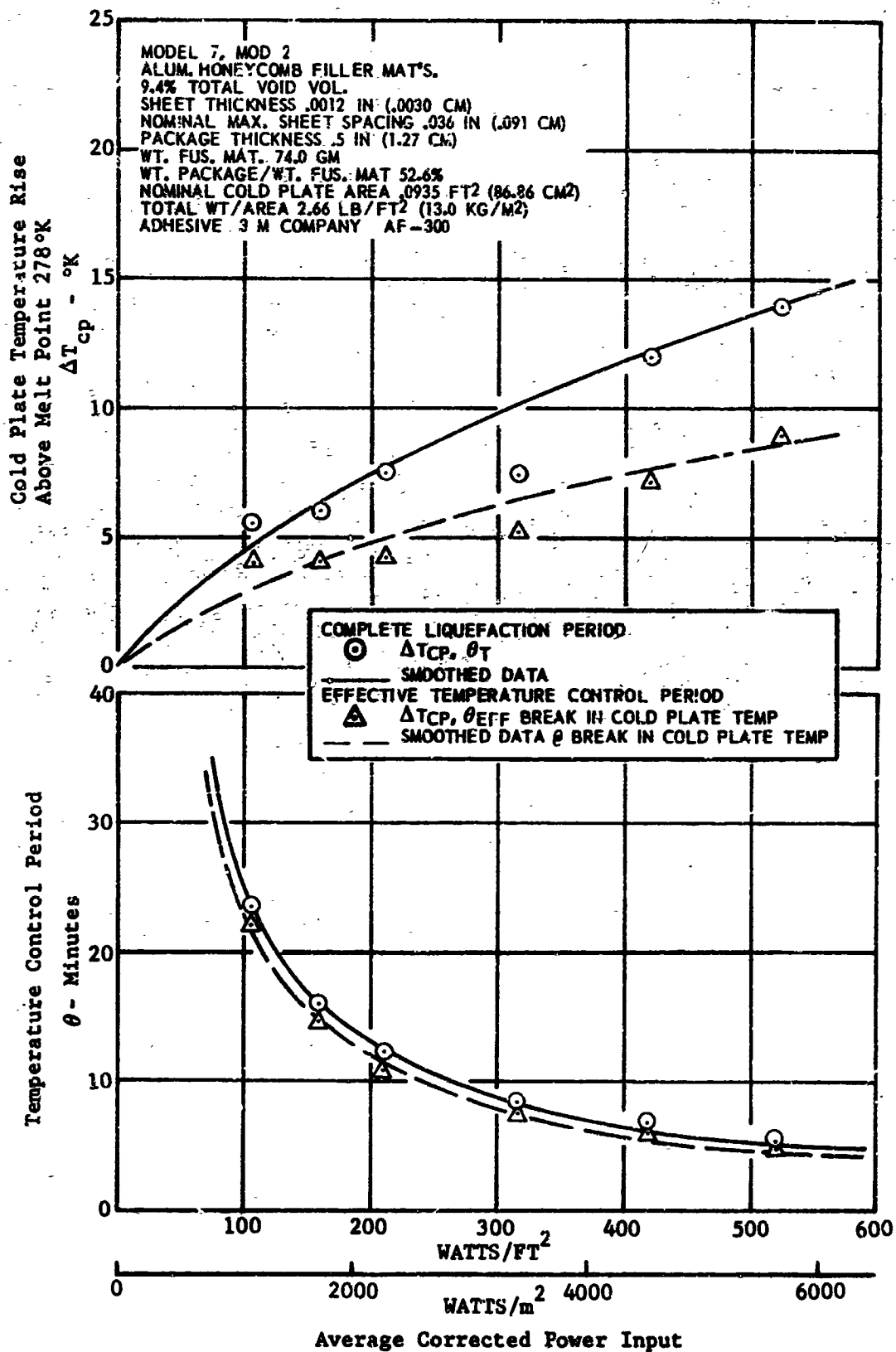


FIGURE 7-44 CORRELATION OF TEST RESULTS - SYSTEM IMPROVEMENT - ADIABATIC MODEL - FUSIBLE MATERIAL TETRADECANE, MODEL 126-00100-7, MOD 2

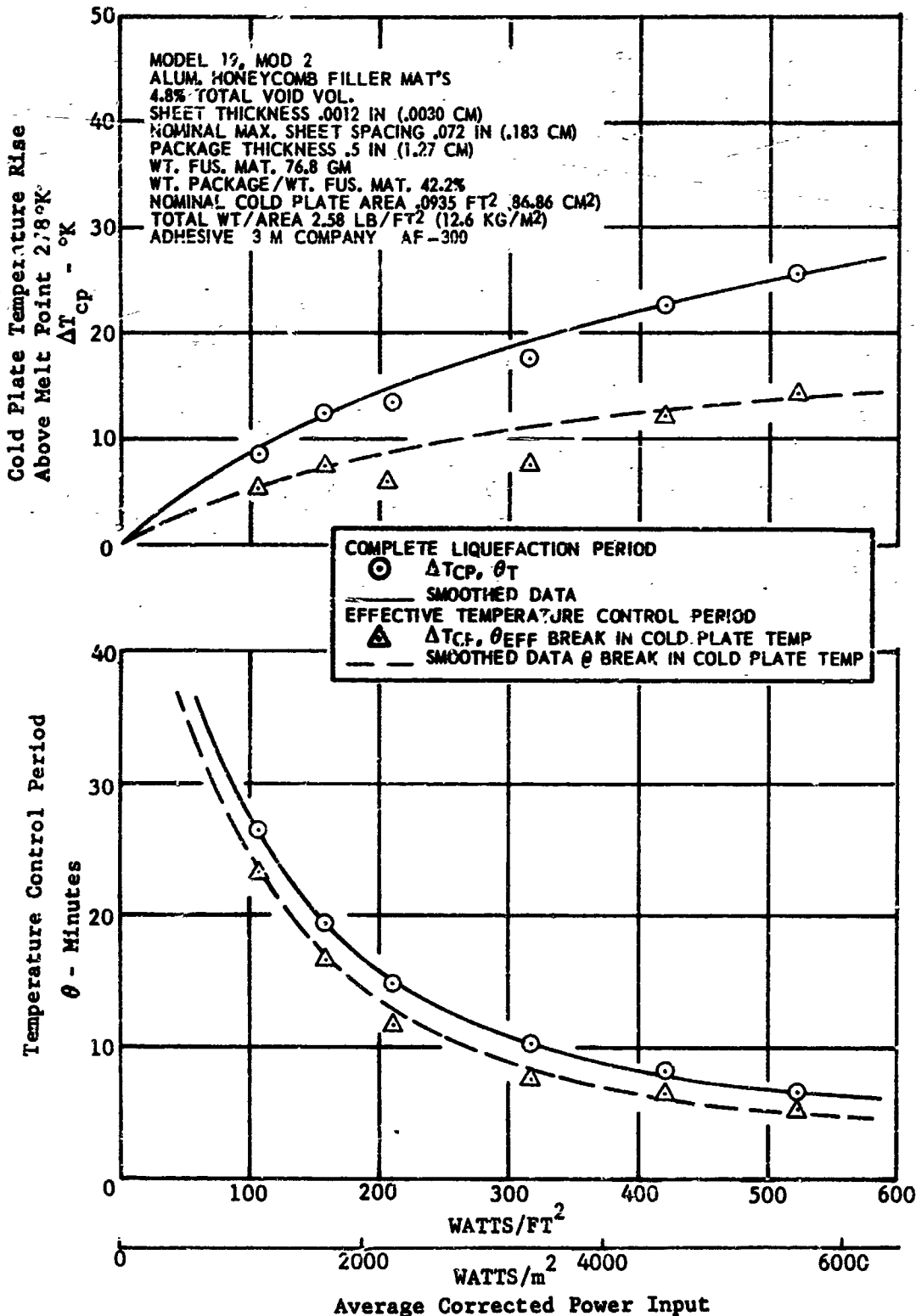


FIGURE 7-45 CORRELATION OF TEST RESULTS - SYSTEM IMPROVEMENT - ADIABATIC MODEL - FUSIBLE MATERIAL TETRADECANE, MODEL 126-00100-19-MOD 2

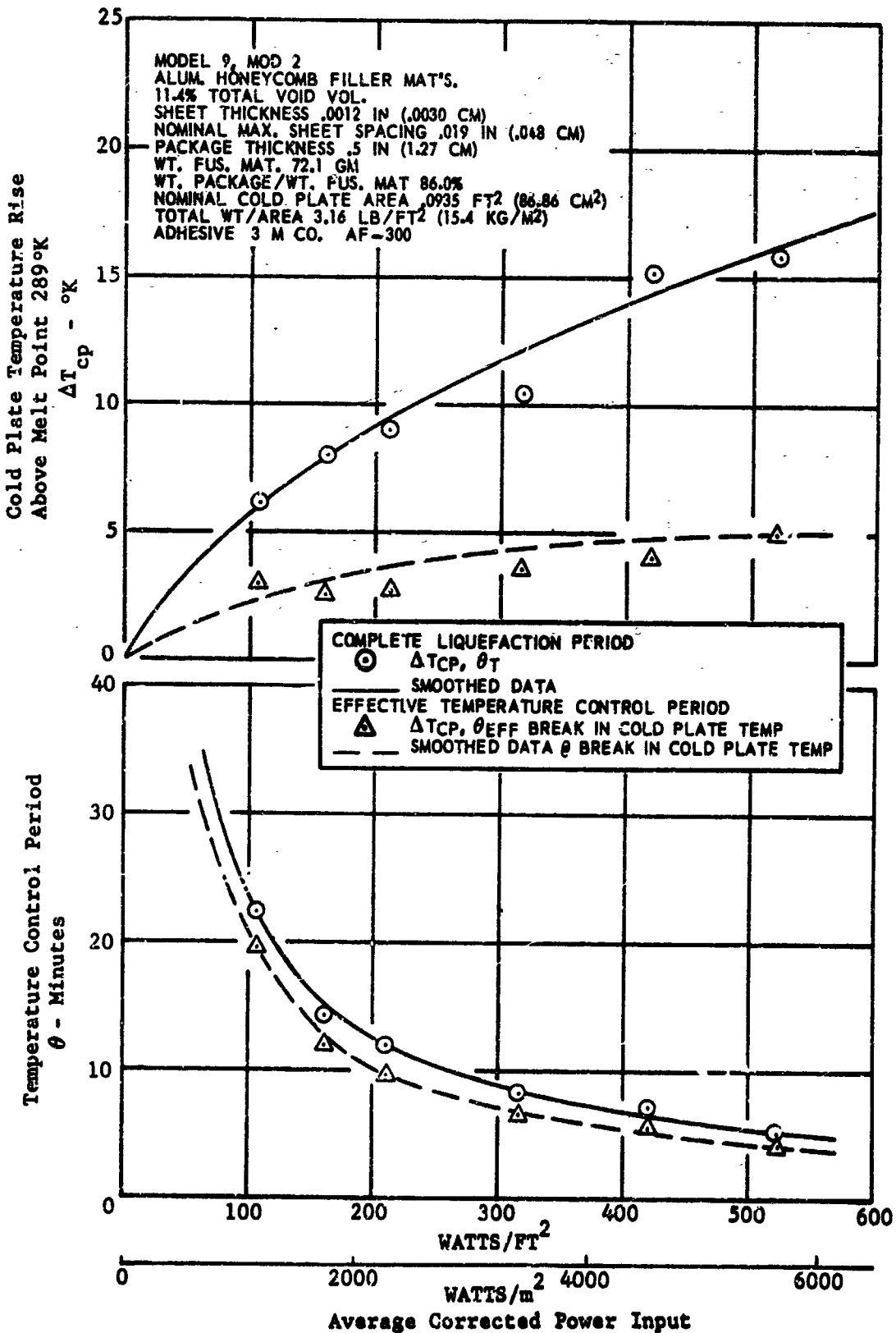


FIGURE 7-46 CORRELATION OF TEST RESULTS - SYSTEM IMPROVEMENT - ADIABATIC MODEL - FUSIBLE MATERIAL HEXADECANE, MODEL 126-00100-9, MOD 2

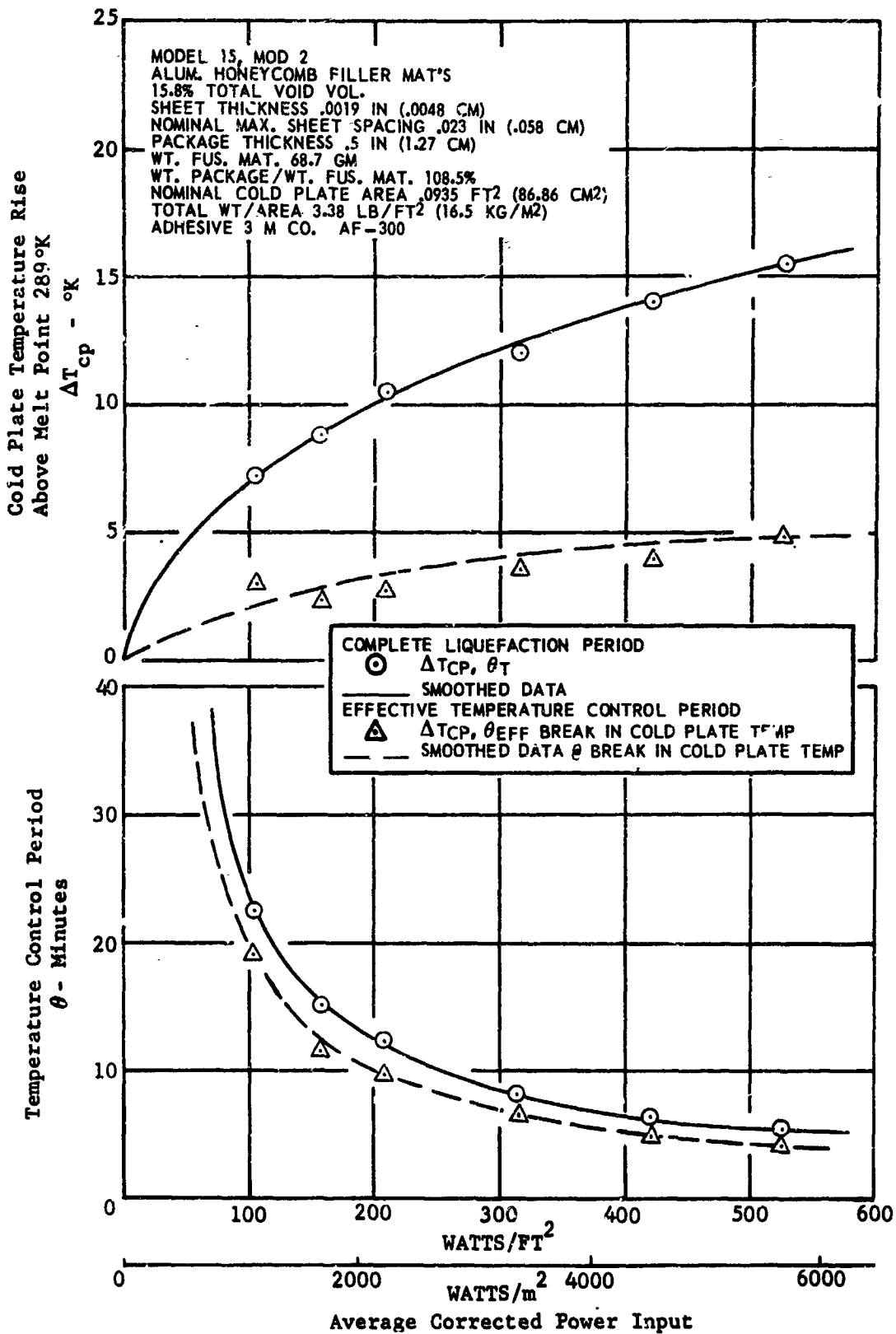


FIGURE 7-47 CORRELATION OF TEST RESULTS - SYSTEM IMPROVEMENT - ADIABATIC MODEL - FUSIBLE MATERIAL HEXADECANE, MODEL 126-00100-15, MOD 2

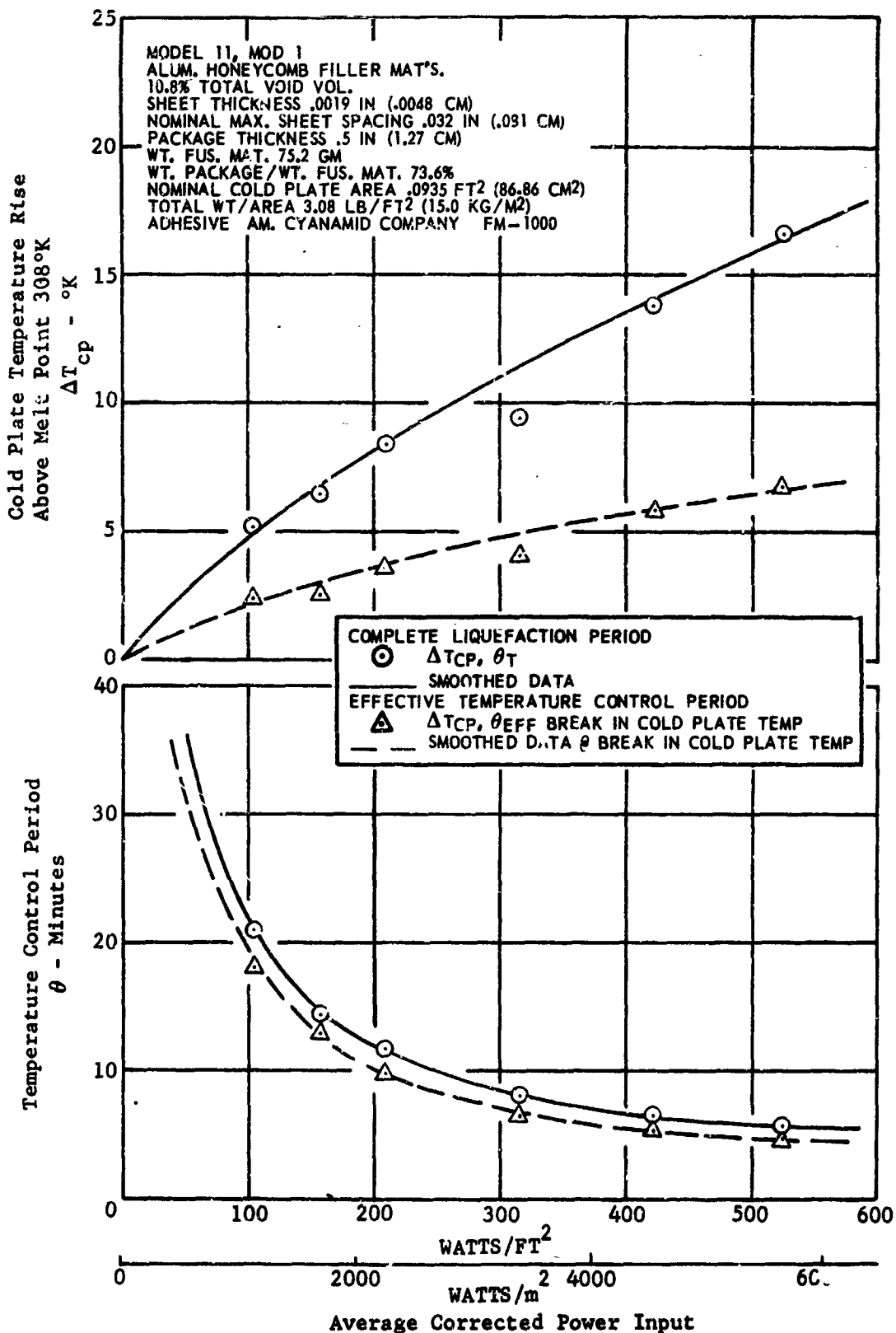


FIGURE 7-48 CORRELATION OF TEST RESULTS - SYSTEM IMPROVEMENT - ADIABATIC MODEL - FUSIBLE MATERIAL EICOSANE, MODEL 126-00100-11, MOD 1

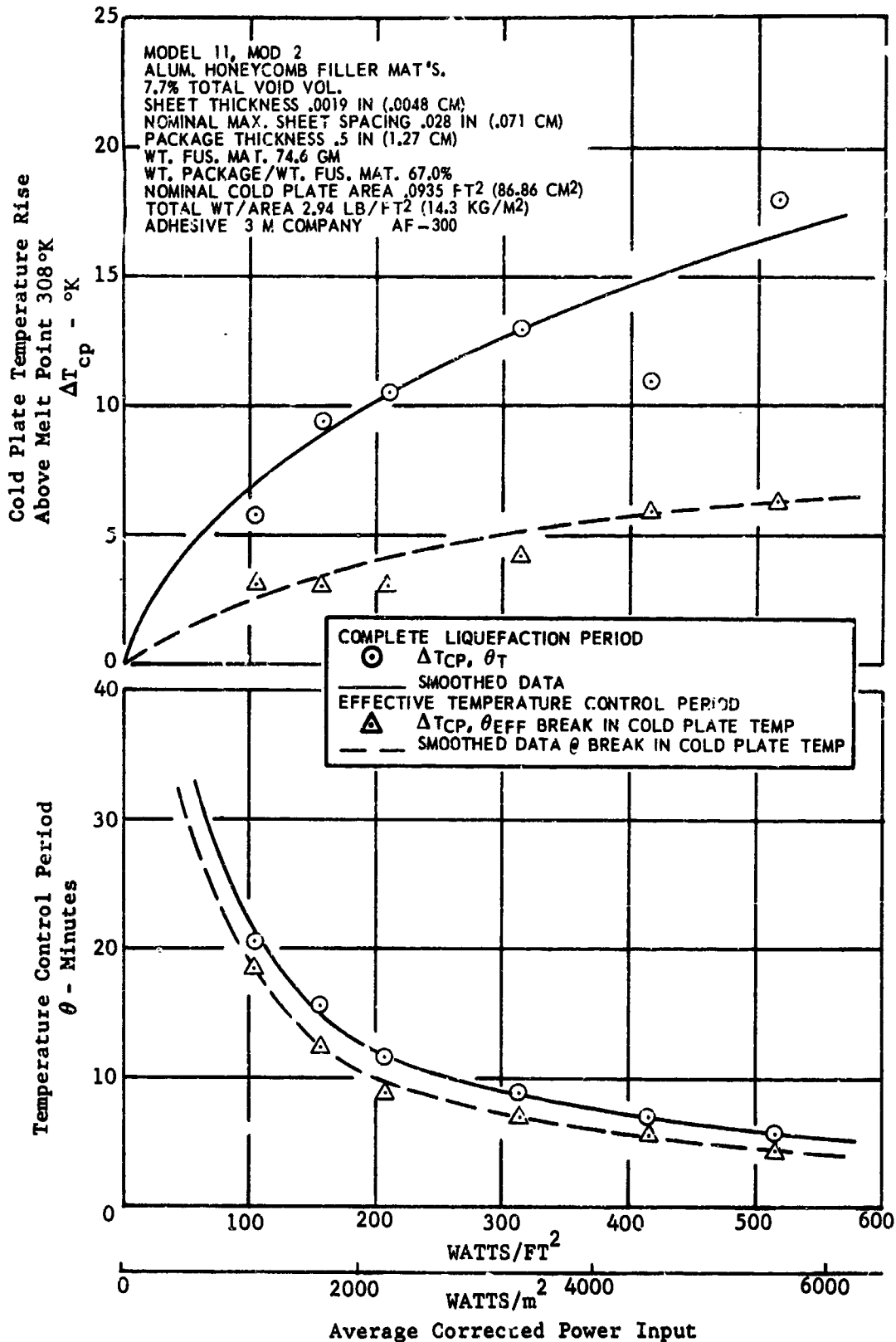


FIGURE 7-49 CORRELATION OF TEST RESULTS - SYSTEM IMPROVEMENT - ADIABATIC MODEL - FUSIBLE MATERIAL EICOSANE, MODEL 126-00100-11, MOD 2

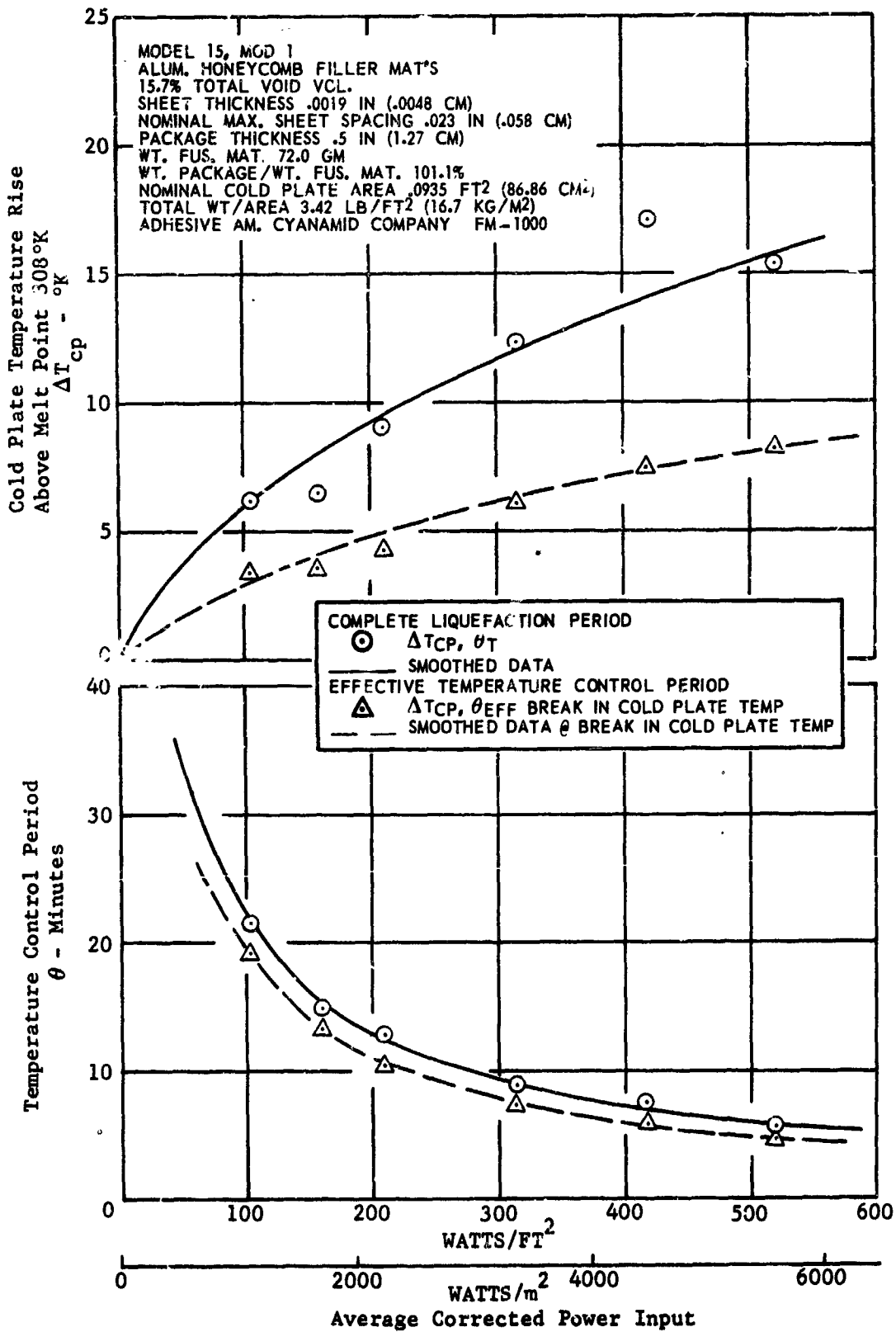
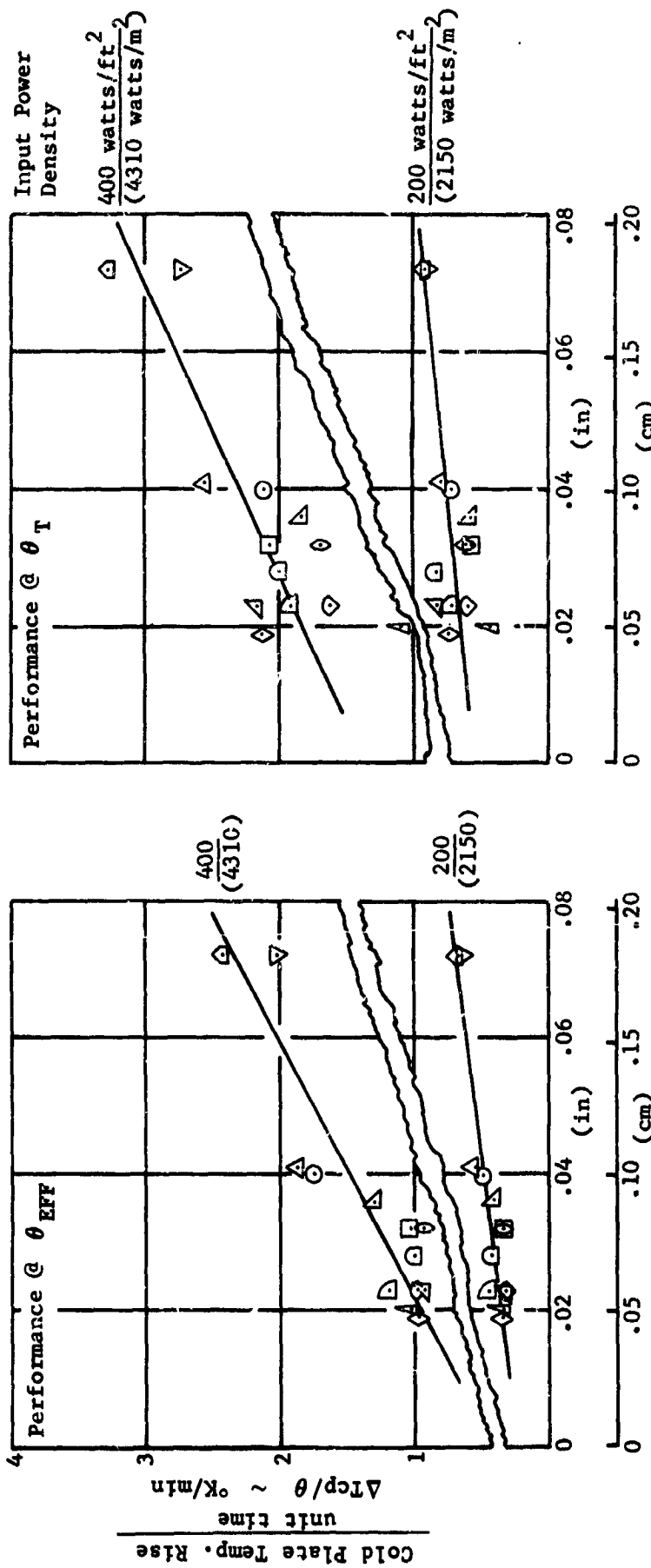
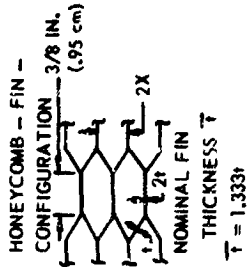


FIGURE 7-50 CORRELATION OF TEST RESULTS - SYSTEM IMPROVEMENT - ADIABATIC MODEL - FUSIBLE MATERIAL EICOSANE, MODEL 126-00100-15, MOD 1

DATA FROM CORRELATED TEST RESULTS (SMOOTHED DATA)

MODEL DASH NO.	-7	-9	-11	-13	-15	-19	-11	-11	-15	-9	-15	-7	-19
MODIFICATION NO.	1	1	1	1	1	1	1	2	1	2	2	2	2
HONEYCOMB SHEET	IN	.0012	.0019	.0024	.0019	.0019	.0019	.0012	.0019	.0012	.0019	.0019	.0019
THICKNESS -t-	cm	.0030	.0048	.0061	.0048	.0048	.0046	.0030	.0048	.0030	.0048	.0048	.0048
% CORE VOL FILLED BY FINS		6.2	11.7	11.9	12.0	17.5	5.4	11.9	8.6	17.5	12.7	17.6	10.5
% TOTAL VOL FILLED BY FINS		5.5	10.5	10.8	10.8	15.7	4.9	10.8	7.7	15.7	11.4	15.8	9.4
SYMBOL	○	△	○	△	◇	◇	○	□	□	◇	◇	△	△
TEST FUSIBLE MAT'S MELT PT.	OCTADECANE 308° K			EICOSANE 308° K			HFRADECANE 288° K			TETRADECANE 278° K			

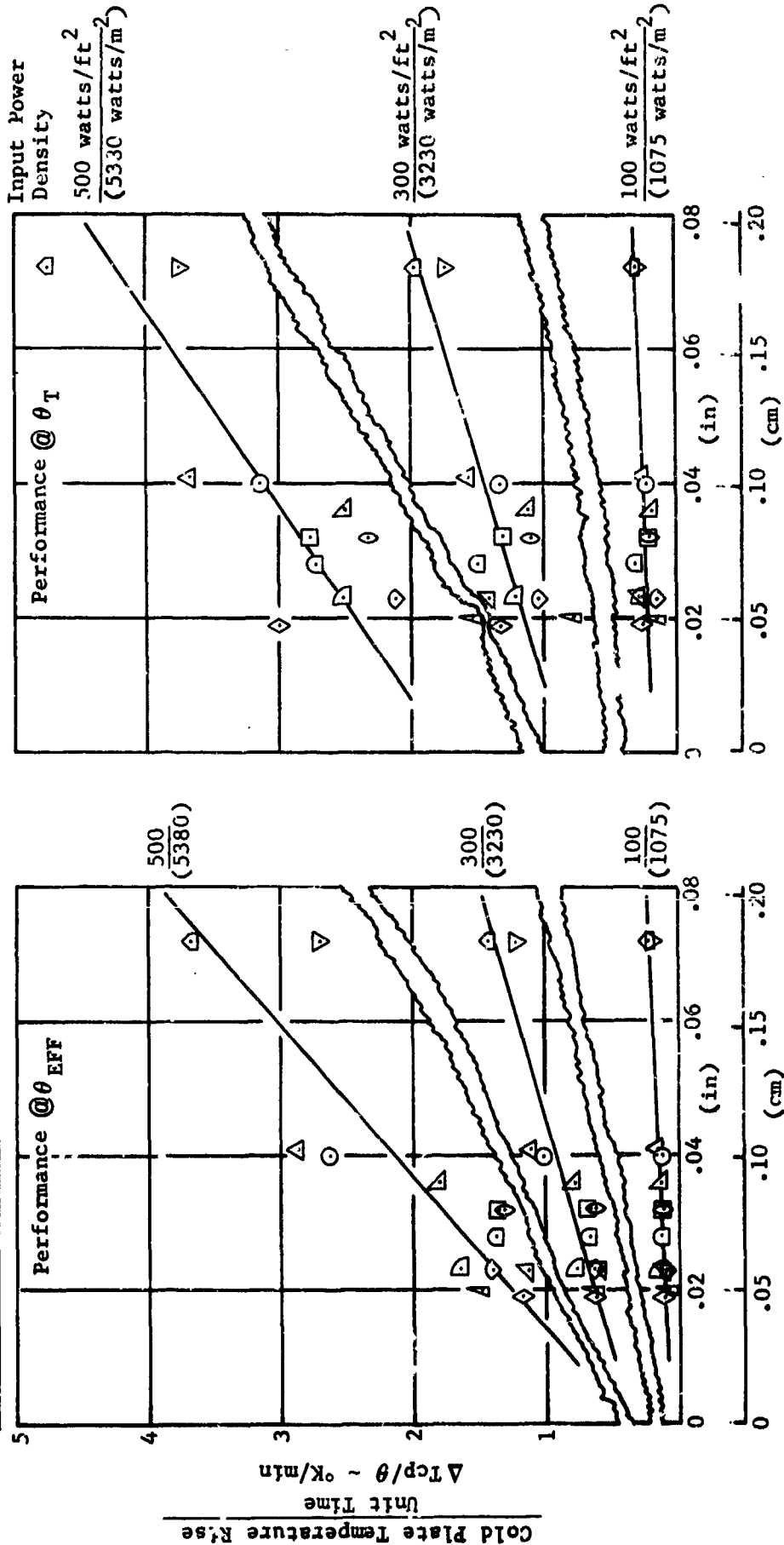
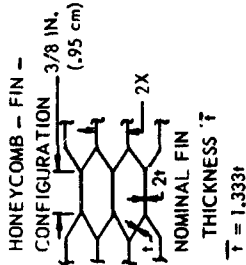


Max Fin (Honeycomb Sheet) spacing ~ 2x

FIGURE 7-51 PERFORMANCE COMPARISON OF THE SYSTEM IMPROVEMENT - ADIABATIC TEST MODELS (Sheet 1 of 2)

DATA FROM CORRELATED TEST RESULTS (SMOOTHED DATA)

MODEL DASH NO.	MODIFICATION NO.	EICOSANE 308° K						TETRADECANE 278° K				
		-7	-9	-11	-13	-15	-19	-11	-15	-19		
HONEYCOMB SHEET	IN	.0012	.0012	.0019	.0024	.0019	.0019	.0019	.0012	.0019	.0019	.0019
THICKNESS -t-	cm	.0030	.0030	.0048	.0061	.0048	.0048	.0048	.0030	.0048	.0048	.0048
% CORE VOL FILLED BY FINS		6.2	11.7	11.9	12.0	17.5	5.4	11.9	8.6	17.5	12.7	17.6
% TOTAL VOL FILLED BY FINS		5.5	10.5	10.8	10.8	15.7	4.9	10.8	7.7	15.7	11.4	15.8
SYMBOL		○	△	○	△	○	△	○	△	○	△	○
	TEST FUSIBLE MAT'S MELT PT.	OCTADECANE 330° K						TETRADECANE 278° K				



Max Fin (Honeycomb Sheet) Spacing - 2 X  
 FIGURE 7-51 PERFORMANCE COMPARISON OF THE SYSTEM IMPROVEMENT ADIABATIC - TEST MODELS (Sheet 2 of 2)

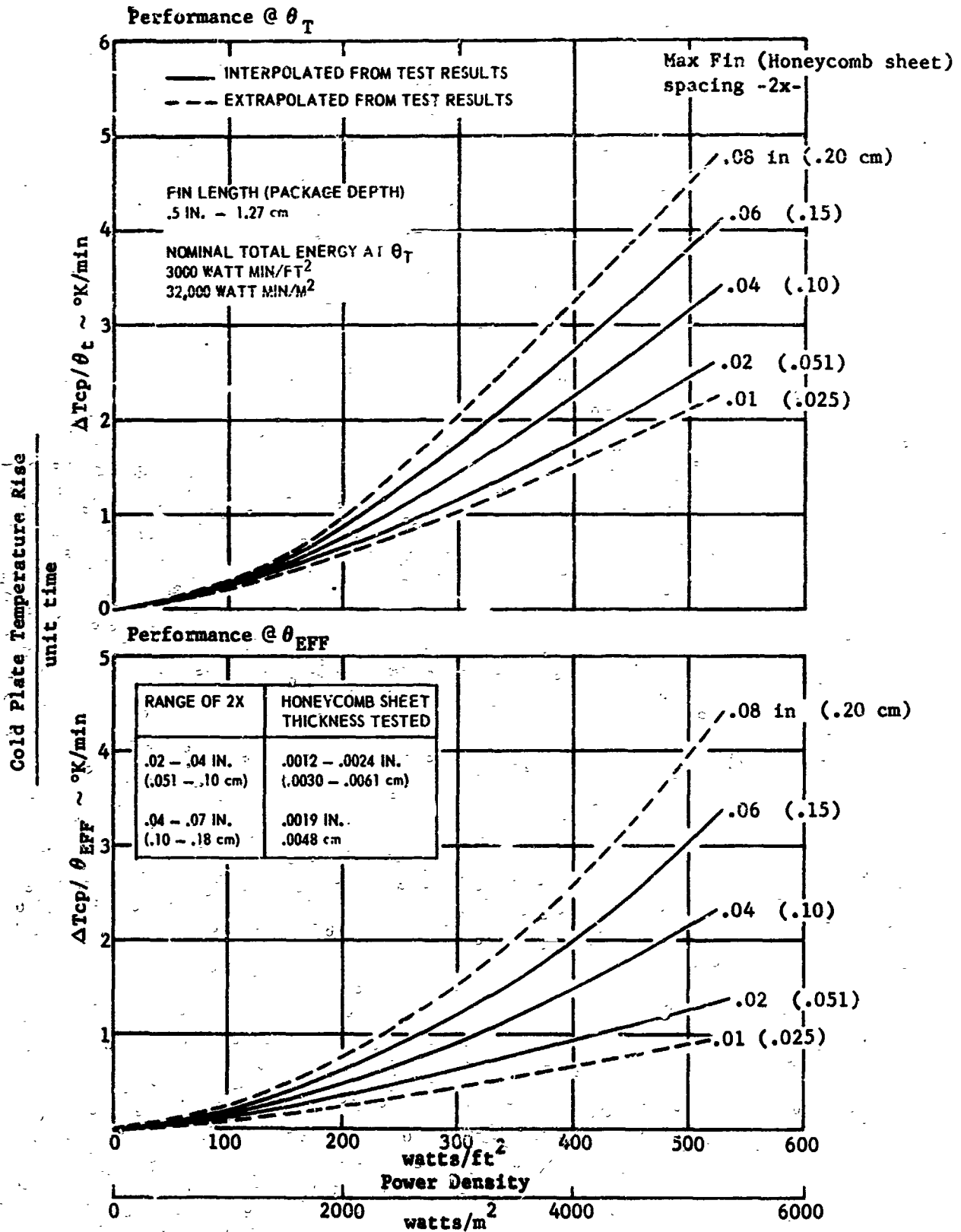


FIGURE 7-52 ADIABATIC SYSTEM PERFORMANCE OF THE IMPROVED PACKAGE WITH ALUMINUM HONEYCOMB CORE AND n-PARAFFIN FUSIBLE MATERIALS

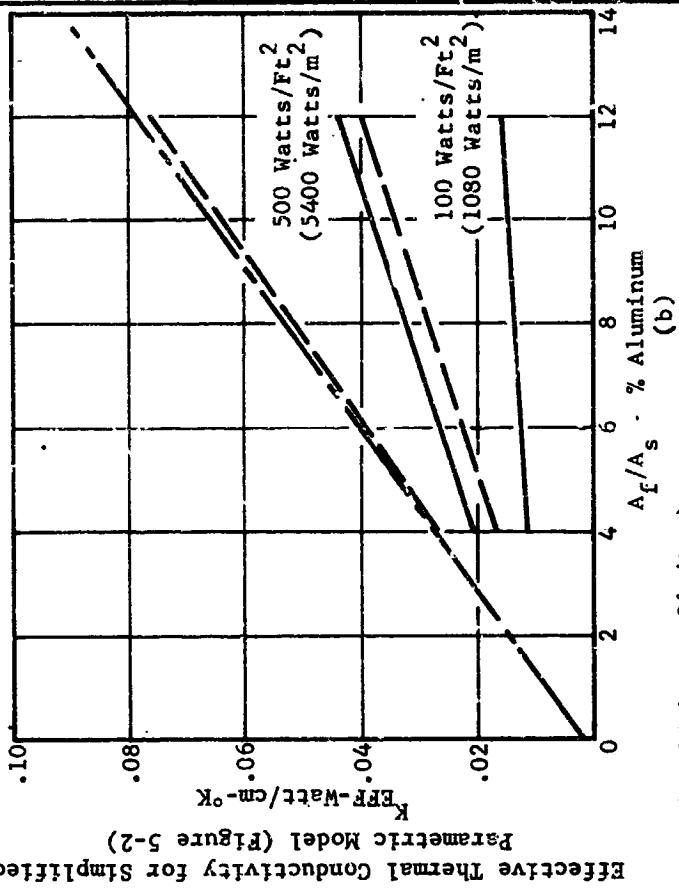
Analytical  $K_{EFF} = f(A_f/A_s)$ , Figure 7-9

Test  $K_{EFF} = .733 \left[ \frac{(q/A)^2}{\bar{p} \bar{H} .944 \bar{C}_p} \right]^{1.056} (\Delta T_{cp})^{1.056}$  (Figure 5-2)

Where  $q/A, \theta$  - From Test Results for Selected Honeycomb-Total Energy Configuration Figure 7-52

$\rho, \bar{H}$  - Fig. 7-9

$\bar{C}_p = .036 \frac{\text{Watt-min}}{\text{gm-c}^\circ\text{K}}$



— Test Results @  $\theta_T$

- - - Test Results @  $\theta_{EFF}$

--- Results and Data for Simplified Analysis - Aluminum Foam + Octadecane

Honeycomb Configuration Selected for Comparison

Depth of Package: .5in (1.27 cm)

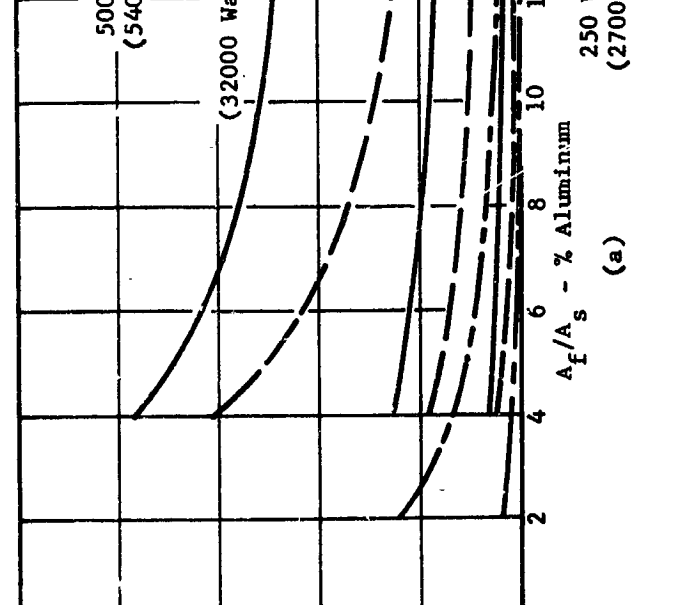
Sheet Thickness (t): .0012in. (.0030cm)

Max. Sheet Spacing (2X): .02-.06in. (.051-.15cm),

Figure 7-52  $A_f/A_s = f(t, 2X)$

Effective Thermal Conductivity for Simplified Parametric Model (Figure 5-2)

$K_{EFF}$ -Watt/cm-c<sup>o</sup>K



Melt Thickness  $f(q/A, )$

Analytical (Figure 7-6)

$\Delta X = .45 \pm .06 \text{in.} (.114 \pm .15 \text{cm})$

Experimental (Eq. on Figure 5-2)

$\Delta X = .44 \pm .0 \text{in.} (.112 \pm .13 \text{cm})$

From Nominal Fill Temp. and Density (Figure 3-2)

$\Delta X = .43 \text{in.} (.109 \text{cm})$

Fusible Material - Octadecane

Total Energy - 3000 Watt Min/Ft<sup>2</sup>

(32000 Watt Min/M<sup>2</sup>)

FIGURE 7-53 COMPARISON OF TEST RESULTS AND SIMPLIFIED ANALYTICAL MODEL FOR THE SYSTEM IMPROVEMENT STUDY

**BLANK PAGE**

## SECTION 8

### SUPERCOOLING

In order to achieve a basic understanding of the thermodynamics and kinetics of nucleation and supercooling, as they affect this area of thermal control, it has been instructive to examine (1) the fundamental theories of nucleation and supercooling, and (2) the effect which weightlessness might have upon mechanisms derivable from these theories. Once a working knowledge of various theories had been achieved, methods and techniques of preventing excessive supercooling were investigated experimentally. Consequently, this study will assist in providing an insight into (1) alleviating possible problems encountered in space which are not observed in the laboratory, (2) utilizing materials previously rejected because of supercooling, and (3) presenting methods which allow flexibility in design capability.

Experimental data concerning supercooling in fusible materials were obtained by studying aqueous droplet dispersions of n-octadecane and n-hexadecane using dilatometric techniques. The materials were investigated both as dispersions of the pure material and as dispersions doped with substances which should improve the thermal conductivity and/or reduce supercooling. Dopants investigated (aluminum wool, colloidal silica, and silica gel) differed widely in their effectiveness.

The results of this investigation are presented in the following subsections. The fundamental theories of nucleation and supercooling are described. General recommendations are made regarding studies of the effects of weightlessness. The experimental data are tabulated and discussed. Conclusions regarding the importance of supercooling in thermal control applications are presented in Section 10.

#### Fundamental Nucleation Theory

The nucleation of crystal growth in a supercooled solution can occur by a variety of processes, which can be categorized for convenience as (1) homogeneous nucleation, (2) heterogeneous nucleation, (3) dynamically stimulated nucleation, and (4) breeding from existing crystals.

In homogeneous nucleation, the nuclei are formed by random statistical configurational fluctuations in an otherwise homogeneous liquid. The nuclei are thus very small clusters of atoms or molecules which are spontaneously forming and dissociating. Their rates of formation and dissociation do not depend on the presence or absence of surfaces, such as container walls or foreign particles.

Heterogeneous nucleation is the process by which nuclei are formed in a liquid by configurational fluctuations which occur at a container wall or upon a foreign particle. This type of nucleation does not take place wholly within a single phase and is therefore designated as heterogeneous.

Dynamically stimulated nucleation (or nucleation by cavitation) depends upon the opening of small cavities in the liquid by negative pressures. Very large local pressures are produced when these cavities collapse. In certain cases, the high pressures lower the melting temperature according to the Clapeyron equation,  $\frac{dp}{dt} = \frac{\Delta H}{T\Delta V}$ ; they can then cause enough supercooling to allow homogeneous nucleation.

Breeding of new crystals from existing crystals depends upon fracture, partial melting, etc., of growing crystals to produce nuclei which spontaneously initiate the growth of new crystals. After fracture occurs, each new particle itself can grow in the supercooled melt.

Many excellent review articles and books have appeared which discuss the thermodynamics and kinetics of nucleation in condensed phases (References 15-18). In this report, we will present a brief summary of these ideas as they apply to nucleation and supercooling of materials used for thermal control purposes.

Homogeneous nucleation. - The stability of nuclei in supercooled liquids depends upon two factors, namely, the free energy difference between the liquid and solid phases and the surface free energy of the solid phase. For nuclei smaller than a certain critical size, the surface area is large relative to the volume; hence, the surface free energy term predominates and enables these nuclei to decrease the total free energy of the system by shrinking and lowering their surface area. Nuclei larger than this critical size can reduce the total free energy by simply growing into more crystal. The balance existing between these two factors defines the critical size.

As long as the clusters of atoms or molecules are all below the critical size corresponding to the temperature of the liquid, they cannot grow to form crystals. Conversely, if the temperature is such that the critical size is less than the largest cluster size, nucleation takes place, and the nuclei grow into crystals.

The number  $n_i$  of nuclei of  $i$  atoms is given by the expression

$$n_i = n \exp(-\Delta F/kT) \quad (1)$$

where 
$$\Delta F = \frac{4}{3} \frac{\pi r^3}{V} \frac{\Delta H \Delta T}{T_E} + 4\pi r^2 \sigma \quad (2)$$

$\Delta H$  = latent heat of fusion

$\Delta T = T_E - T$  = supercooling

$T_E$  = equilibrium temperature of fusion

$\sigma$  = specific surface free energy

and the radius of the critical nucleus is obtained as

$$r^* = \frac{2\sigma T_E}{L\Delta T} \quad (3)$$

by maximizing  $\Delta F$  with respect to  $r$  in (2).

From (1) it follows that, since  $\Delta F$  cannot be infinite,  $n_i/n$  cannot be zero; hence, there is always a finite probability of the existence of a cluster of any particular size. Whether a given sample nucleates and grows at a given temperature is therefore dependent upon the probability of a nucleus reaching critical size during the time in which the sample is to be observed.

We must therefore consider the rate of formation of nuclei of critical size. This subject has been discussed by several authors (References 19-22). The treatment applied by Turnbull and his co-workers to solidification is appropriate for our present purpose.

Their rate of nucleation can be stated approximately as

$$I = \frac{nkT}{h} \exp(-Q_D/kT) \exp(-\Delta F^*/kT) \quad (4)$$

where  $n$  = number of molecules in the system

$Q_D$  = activation energy for diffusion in the liquid

$\Delta F^*$  = free energy of the cluster of atoms of critical size, from equation (2)

The above equation may be rewritten as

$$I = I_0 \exp\left[-b/T_r (\Delta T_r)^2\right] \quad (5)$$

where  $I_0 = \frac{nkT}{h} \exp(-Q_D/kT)$  and  $b = \frac{16}{3}\pi \left(\frac{\sigma}{\Delta H}\right)^3 \left(\frac{\Delta H}{kT_E}\right)$

with  $T_r = \frac{T}{T_E}$  and  $\Delta T_r = \frac{T_E - T}{T_E} = \frac{\Delta T}{T_E}$

The rate of nucleation thus shows a strong exponential dependence upon  $\Delta T_r$  and hence upon the amount of supercooling  $\Delta T$ . Further refinements in the definition of  $I_0$ , such as consideration of crystal growth kinetics or time lag effects, would have to affect  $I_0$  greatly to overwhelm the effect of the exponential.

Heterogeneous nucleation. - The heterogeneous nucleus can be visualized as a spherical section or cap of nucleating solid situated upon a flat substrate (Reference 15). Its stability depends both upon its radius of curvature and contact angle  $\theta$ , where  $\theta$  is defined by

$$\sigma_{SL} - \sigma_{SC} = \sigma_{LC} \cos \theta$$

and S, L, and C refer to substrate, liquid, and crystal respectively.

The substrate enables the critical radius to be reached in a nucleus which contains far fewer atoms than a sphere. In essence, the substrate changes the nucleation frequency, as follows:

$$I = I_0 \exp \left[ -b(\theta)/T_f (\Delta T_f)^2 \right]$$

Note that in this expression the constant  $b$  is determined by the unknown surface energy parameters,  $c$  and  $\theta$ .

Dynamically stimulated nucleation. - Although the basic mechanisms of dynamic nucleation are not very well understood, experimental data concerning this phenomenon have been obtained (Reference 23). A variety of dynamic conditions in the liquid were found to cause the appearance of crystals which would have not been observed in the corresponding static experiment. There are three distinct types of disturbances which cause nucleation in a supercooled solution, namely, friction, vibration, and pressure pulse.

Nucleation by friction is well known in organic chemistry. A supercooled melt of an organic substance will often solidify if the inner surface of the beaker containing it is "stroked" with a stirring rod. The explanation proposed is that the vibration inherent in "stick-slip" friction has the same effect as vibration which causes cavitation.

It has been shown by various authors that ultrasonic vibration causes nucleation in supercooled water (Reference 15). It is believed that nucleation occurs as a result of the change of equilibrium temperature which occurs when a cavity collapses.

Chalmers mentions that, for water and for nickel, cobalt, and iron, a single pressure pulse can cause nucleation (Reference 15). It was found that the intensity of the pulse required depends upon the amount of supercooling and the surface characteristics of the material in contact with the supercooled liquid.

Breeding of new crystals. - Other authors have found that grain refinement can be brought about by introducing vibration while a metal is solidifying (References 24 and 25). It is hence difficult to distinguish whether this observation is due to cavitation or to the fracture of growing crystals, since ultrasonically produced cavitation can cause extensive fracturing of growing crystals.

Jackson mentions that when fracture occurs in a brittle material such as ice, many small fragments are produced (Reference 16). Each small particle formed then grows in the supercooled melt.

#### Effect of Weightlessness

Under conditions of normal gravity, nucleation and the resultant crystal growth are indeed complex phenomena which cannot be explained completely by one single theory. At best, conditions of homogeneous environment, which are the most convenient to treat theoretically, are sometimes approximated experimentally but are never perfectly realized. Nucleation

and growth always involve some transport process, i. e. , transport of matter or heat or both, and homogeneous conditions for the transport process can only exist for such ideal cases as spherically symmetric, circularly cylindric, or infinite plane surfaces; therefore, most nucleation and growth effects are not amenable to detailed theoretical analysis, even under conditions of normal gravity.

Because of the complexity of the phenomena under normal gravity, it is impossible to calculate a priori the effect of weightlessness on nucleation and growth mechanisms pertaining to a particular material. We must therefore rely upon empirical observations to furnish us with information regarding the effect of weightlessness.

At present, however, experimental data concerning crystal growth under weightless conditions are totally lacking; therefore, any data whatsoever not only would assist in clarifying our fundamental ideas regarding mechanisms of crystal growth under various conditions, but also would assist in developing useful design concepts for space hardware applications. Indeed, the physical basis of solidification should be studied on the atomic, the microscopic, and the macroscopic scales in order to provide a complete, broad picture of the effect of weightlessness upon crystallization. In such studies at the atomic level, one is concerned with the atomic processes by which a crystal grows, or because of which it does not grow; similarly, one is equally interested in supercooling and the nucleation processes which actually initiate the growth of a crystal. Events at the microscopic level are controlled by the local flow of heat and by the diffusion of solute within a solidifying liquid; likewise, on the macroscopic scale the flow of heat in and out via the container walls is significant. Weightlessness has an effect on all these processes, and this effect should be evaluated.

Specifically, crystallization is governed by the laws of chemical thermodynamics and kinetics. The change in phase from liquid to solid is accompanied by a release of heat; consequently, this release of heat causes a local temperature rise which results, under conditions of normal gravity, in convection currents. These currents have several effects, e. g. , they create turbulence in the liquid; they move nuclei through the liquid spreading the loci of crystallization; in addition, they have an effect on the size and morphology of the crystals. Under weightless conditions they are absent.

Being transport processes, convection currents are a function of time; hence, the time required to reach an equilibrium or steady state configuration varies widely over several orders of magnitude depending upon the presence or absence of convection and the particular material under investigation. It is thus highly desirable to select representative samples for investigation and to attain thermal steady state or equilibrium heat transfer conditions in order to obtain meaningful data (a) for comparison with sophisticated theoretical calculations on basic models, and (b) for design of space hardware and verification of various thermal control concepts.

Although we have been discussing nucleation and growth, crystal morphology should be considered as the keystone of the subject, since it is closely related to all the aspects of crystal growth with which we are concerned. We obviously must observe under earth-g and zero-g conditions (a) the morphology of crystals obtained, (b) the kinetics and thermodynamics of crystal growth, and (c) the mechanical properties, since as often happens when we have understood the mechanism which brings about the morphology, we also have the basis for interpreting the mechanical behavior. An example of this is the morphological phenomenon of high strength in whiskers; some whiskers seem to correlate well, others do not, as explained by the various different growth mechanisms which are known to produce fibrous morphology.

Indeed, the interdependence of morphology, chemical kinetics, chemical thermodynamics, and mechanical properties requires the presence of a trained observer during the zero-g studies. This observer is needed to perform several functions, the most important of which include (a) the preparation of supercooled solutions after the establishment of a stable orbit to prevent initiation of growth during launch by vibration, (b) the observation of the size and habit of the growing crystals, and (c) the recovery of crystals grown in zero-g for later determination of their mechanical properties and for comparison of their morphology and physical properties (i. e., index of refraction, thermal conductivity, specific heat, etc.) with crystals grown under influence of the earth's gravity. The physical and mechanical properties of a crystal depend strongly upon the concentration of defects and type of defects incorporated; thus, intelligent selection of representative crystal samples is quite necessary to ensure meaningful postflight data. In addition, observations made during the actual growth of the crystals will assist in providing a broad range of experimental information upon which conclusions regarding the thermodynamic and kinetic mechanisms can be based. Of course, the temperature, time, initiation of growth, and rate of growth data will be obtained instrumentally; however, the presence of a trained observer will ensure that these instrumental measurements are performed in a meaningful manner on the particular samples which are recovered and studied in detail at some later time.

#### Experimental Investigation of Supercooling and Nucleation in Paraffins

The supercooling of aqueous dispersions of n-octadecane and n-hexadecane was studied using dilatometric techniques developed by Turnbull (Reference 26). Melting-freezing hysteresis loops were obtained for the pure materials under experimental conditions which approximated homogeneous nucleation. The use of a highly dispersed sample assisted in circumventing the effects of foreign surfaces on nucleation and enabled the maximum amount of supercooling to be achieved in a reproducible manner. Figures 8-2 through 8-11 present these data.

The same samples were also investigated under controlled conditions of heterogeneous nucleation. In this case, various dopants (aluminum wool, colloidal silica, and silica gel)

were added to the pure dispersions previously investigated. Figures 8-3, 8-4, 8-6, 8-9, 8-10, and 8-11 show the interesting effects observed during the experiments on doped dispersions. Changes in the nucleation mechanism and in the thermal conductivity are proposed to account for these results.

Experimental procedures. - Two Pyrex glass dilatometers (capacity: 3.5 cm to 13.7 cm<sup>3</sup>), shown in Figure 8-1, were constructed and placed in a thermostated water bath which was controlled to  $\pm 0.002^\circ\text{C}$ . The coefficient of thermal expansion of water was measured from  $25^\circ\text{C}$  to  $40^\circ\text{C}$  to evaluate our experimental techniques. The results agreed within a few percent of the handbook values.

Aqueous dispersions of the hydrocarbons were prepared using a wetting agent, Igepal No. CO-880, and a Waring Blendor. The mixture consisted of, in all cases, 100 cc distilled water, 7 cc hydrocarbon, and 2 gm Igepal. The mean droplet size was kept at 6 microns in all dispersions investigated. Turnbull describes these techniques in Reference 26.

The height of the meniscus in the dilatometer capillary was recorded as a function of temperature as the temperature of the bath was changed at a rate of one degree every five minutes with stabilization periods of 30 minutes at the upper and lower temperatures. Duplicate measurements performed in both the large and small dilatometers showed that the thermal equilibration time of the small dilatometer was much more advantageous. Data obtained on both pure materials are quite similar to those reported by Turnbull (Reference 26).

Experimental results. - The melting-freezing hysteresis loops are presented in Figures 8-2 through 8-11. The temperatures observed and the supercooling resulting are tabulated below for each determination.

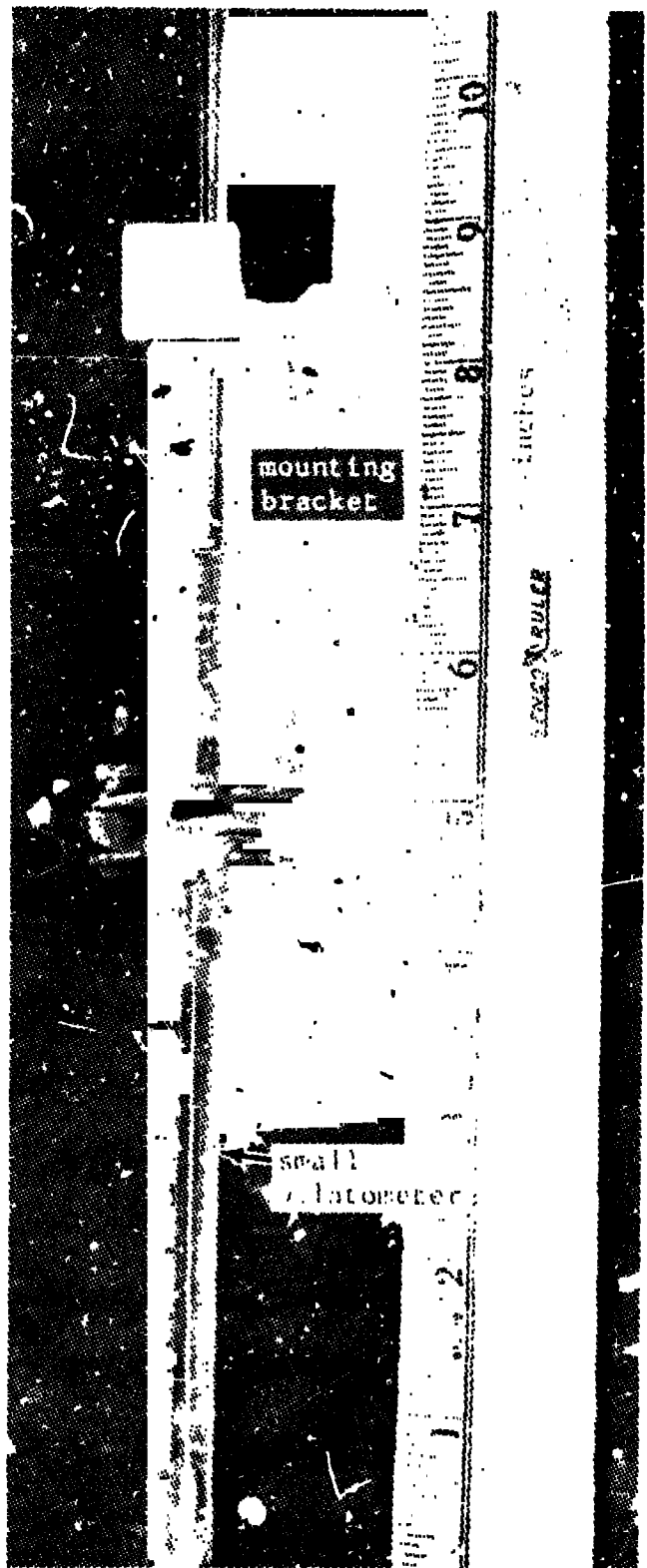
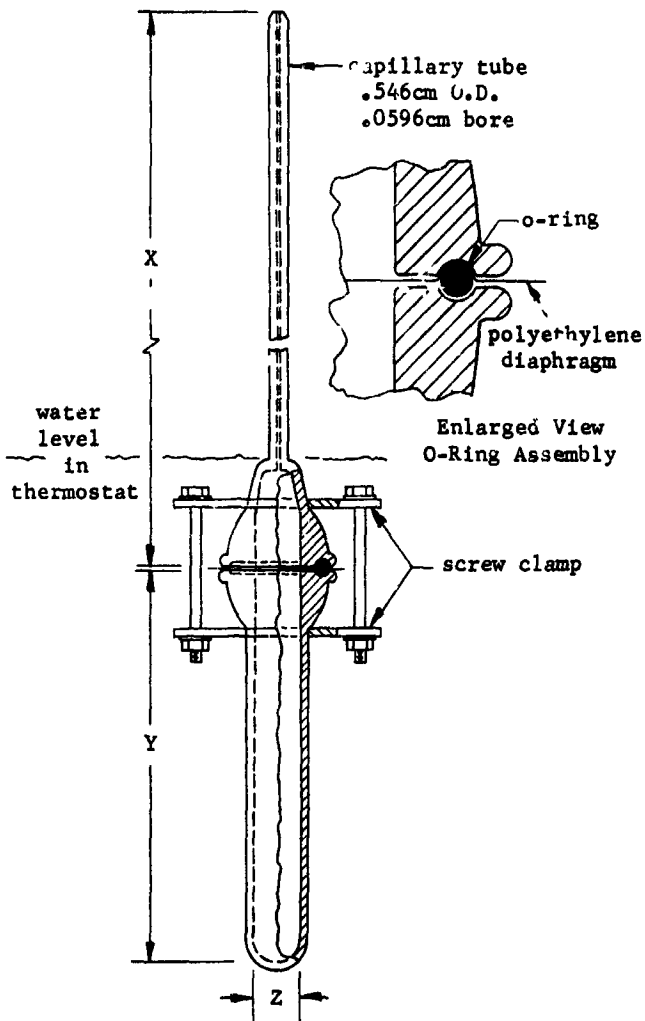
Figure No.	Dilatometer Size	Material	Temperatures		
			Melting	Freezing	Supercooling
8-2	Large	n-Octadecane	$27^\circ\text{C}$	$13^\circ\text{C}$	$14^\circ\text{C}$
8-3	Large	n-Octadecane + Al wool	?	?	?
8-4	Large	n-Octadecane + Al wool	?	?	?
8-5	Large	n-Hexadecane	$17^\circ\text{C}$	$7^\circ\text{C}$	$10^\circ\text{C}$
8-6	Large	n-Hexadecane + Al wool	?	?	?
8-7	Small	n-Octadecane	$27^\circ\text{C}$	$13^\circ\text{C}$	$14^\circ\text{C}$
8-8	Small	n-Octadecane	$28^\circ\text{C}$	$15^\circ\text{C}$	$13^\circ\text{C}$
8-9	Small	n-Octadecane + Al wool	?	?	?
8-10	Small	n-Octadecane + Coll. $\text{SiO}_2$	$27^\circ\text{C}$	?	?
8-11	Small	n-Octadecane + Silica Gel	$28^\circ\text{C}$	$26^\circ\text{C}$	$2^\circ\text{C}$

Discussion of the results. - The most striking observation was the effect upon the shape of the hysteresis loops caused by the addition of 1% (by volume) aluminum whiskers. This material obviously changed the thermal conductivity of the nucleating dispersion drastically, while altering the kinetic mechanism at the same time. The general effect was to smear the melting and freezing phenomena over a wide temperature range for samples investigated in both dilatometers. It was therefore not possible to determine the melting and freezing temperatures or the amount of supercooling for this case.

A solution of 1% silica gel appears to be best of the three additives in reducing the amount of supercooling in n-octadecane. A solution of 1% colloidal silica produced an anomalous heat effect, which caused some scatter in the observed data.

Use of a material like silica gel to assist in the nucleation of crystal growth may very well be useful in allowing flexibility in the design of the thermal control packages. Chopped aluminum wool (whiskers) seems to complicate the simple processes of melting and freezing to such a degree that their use cannot be recommended. Colloidal silica suffers from the same disadvantages as aluminum whiskers and also appears to have a heat effect of its own to complicate the process further.

Obviously, these observations can only be extrapolated to the weightless situation with great caution. To be meaningful, steps taken toward alleviation of thermal control problems dependent upon nucleation and growth under zero-g must be based upon actual experimental data obtained in space experiments.



	X (cm)	Y (cm)	Z (cm)	Volume (cm <sup>3</sup> )
Large dilatometer	69.85	9.65	1.14	13.7
Small dilatometer	50.11	12.06	.61	3.5

FIGURE 8-1 DILATOMETERS (2) USED IN SUPERCOOLING EXPERIMENTS

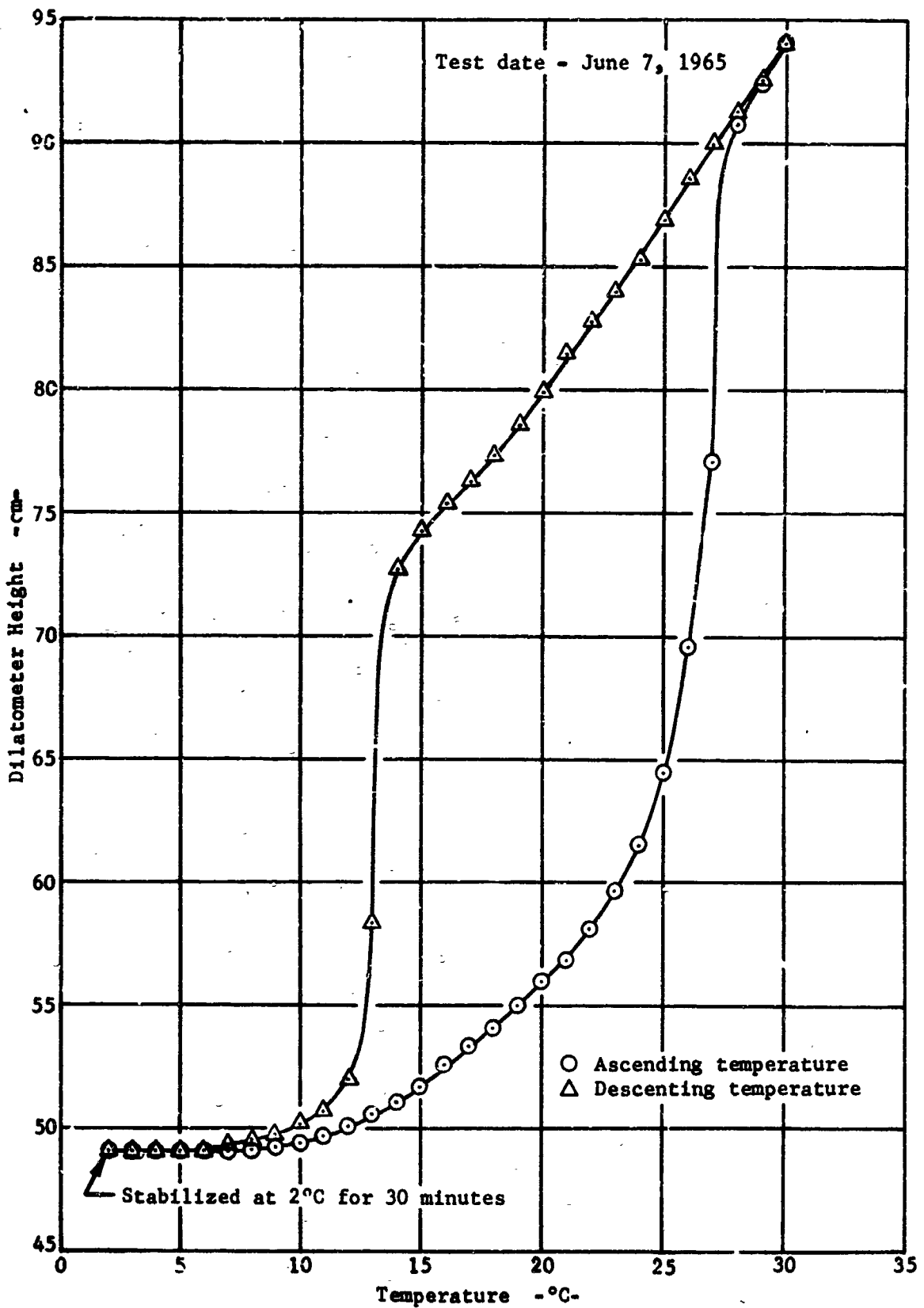


FIGURE 8-2 COOLING-HEATING CYCLE ILLUSTRATING SUPERCOOLING IN AN AQUEOUS n-OCTADECANE DISPERSION (LARGE DILATOMETER).

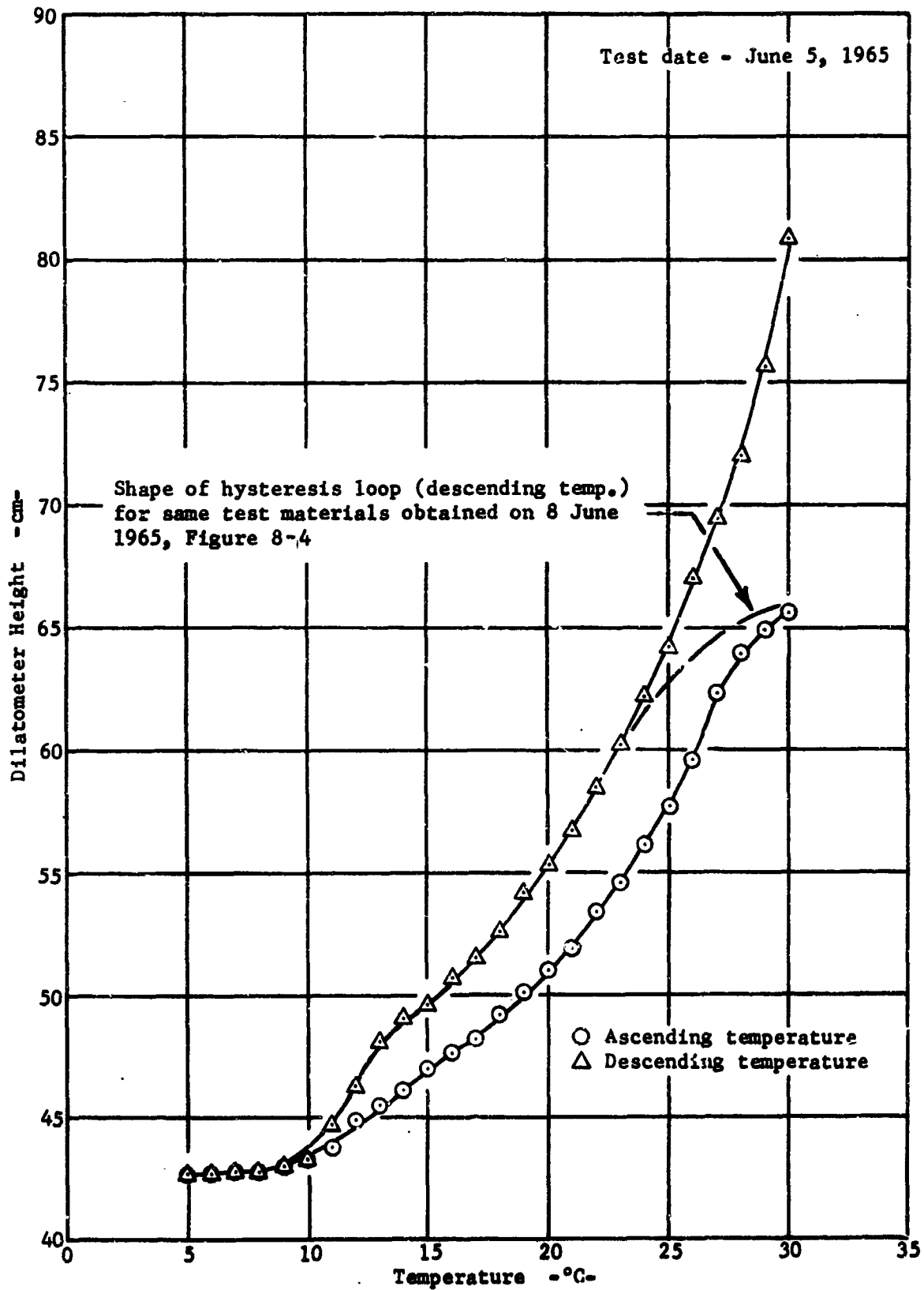


FIGURE 8-3 COOLING-HEATING CYCLE ILLUSTRATING SUPERCOOLING IN AN AQUEOUS n-OCTADECANE + ALUMINUM WOOL DISPERSION (LARGE DILATOMETER).

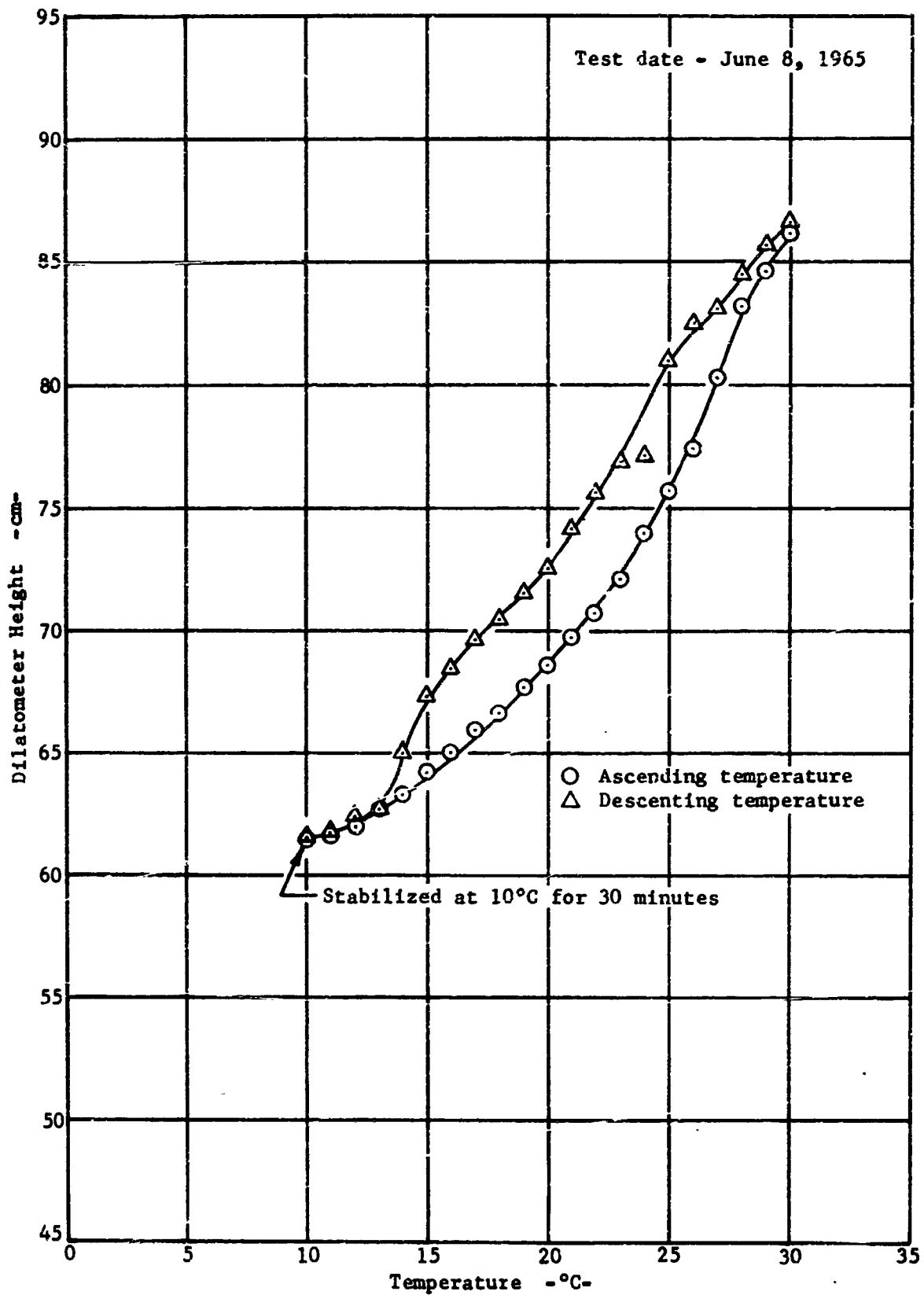


FIGURE 8-4 COOLING-HEATING CYCLE ILLUSTRATING SUPERCOOLING IN AN AQUEOUS n-OCTADECANE + ALUMINUM WOOL DISPERSION (LARGE DILATOMETER).

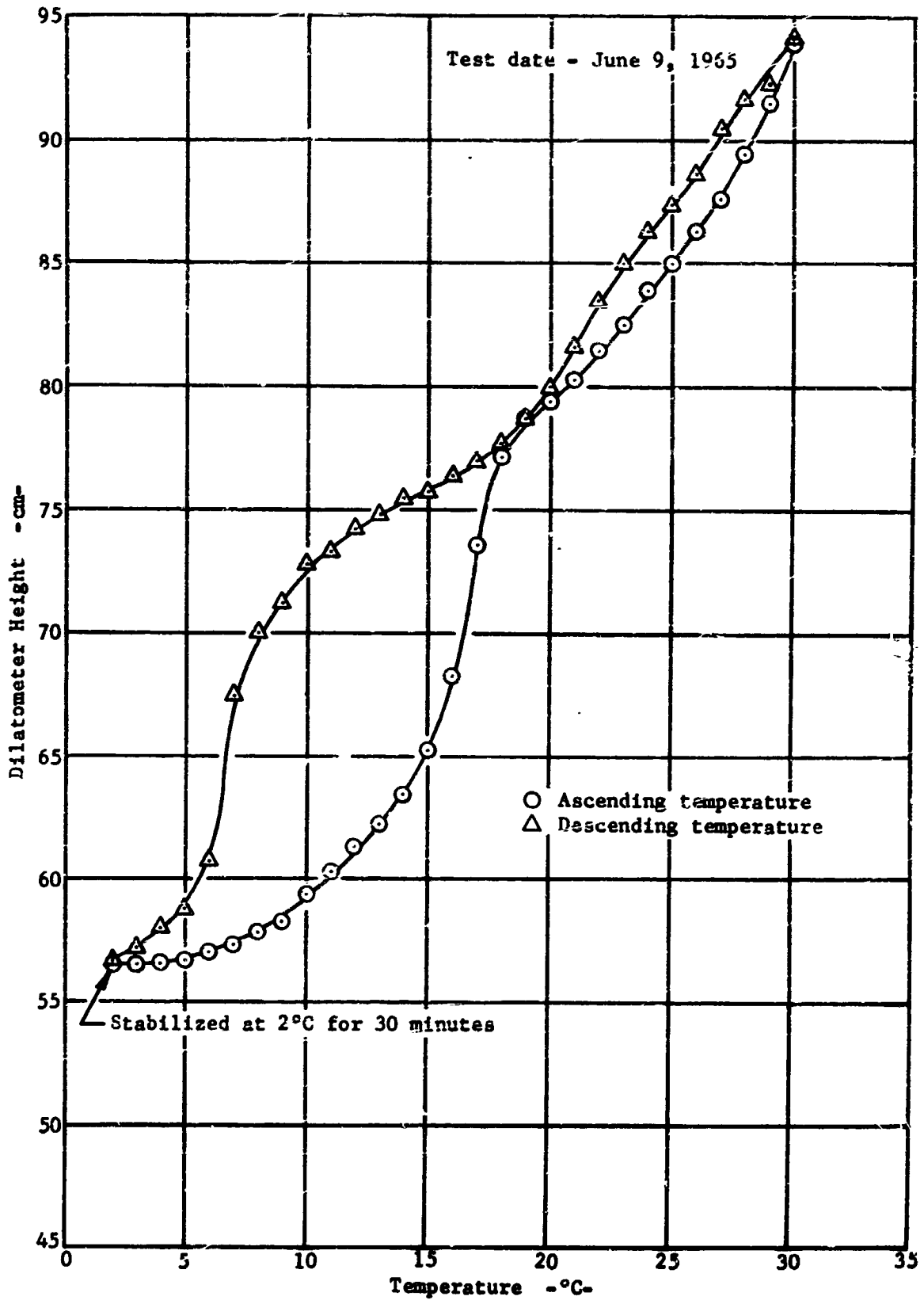


FIGURE 8-5 COOLING-HEATING CYCLE ILLUSTRATING SUPERCOOLING IN AN AQUEOUS n-HEXADECANE DISPERSION (LARGE DILATOMETER).

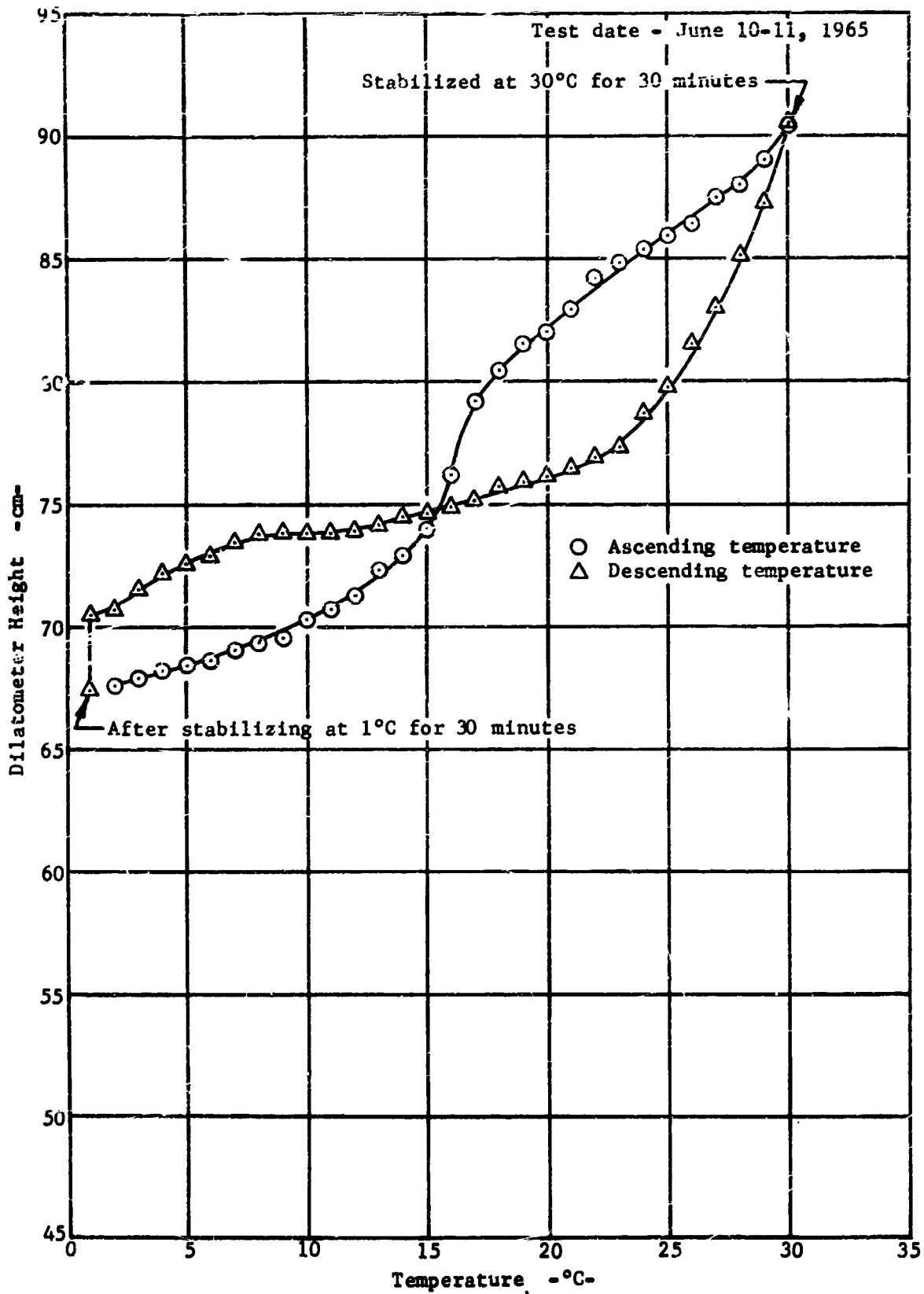


FIGURE 8-6 COOLING-HEATING CYCLE ILLUSTRATING SUPERCOOLING IN AN AQUEOUS n-HEXADECANE + ALUMINUM WOOL DISPERSION (LARGE DILATOMETER).

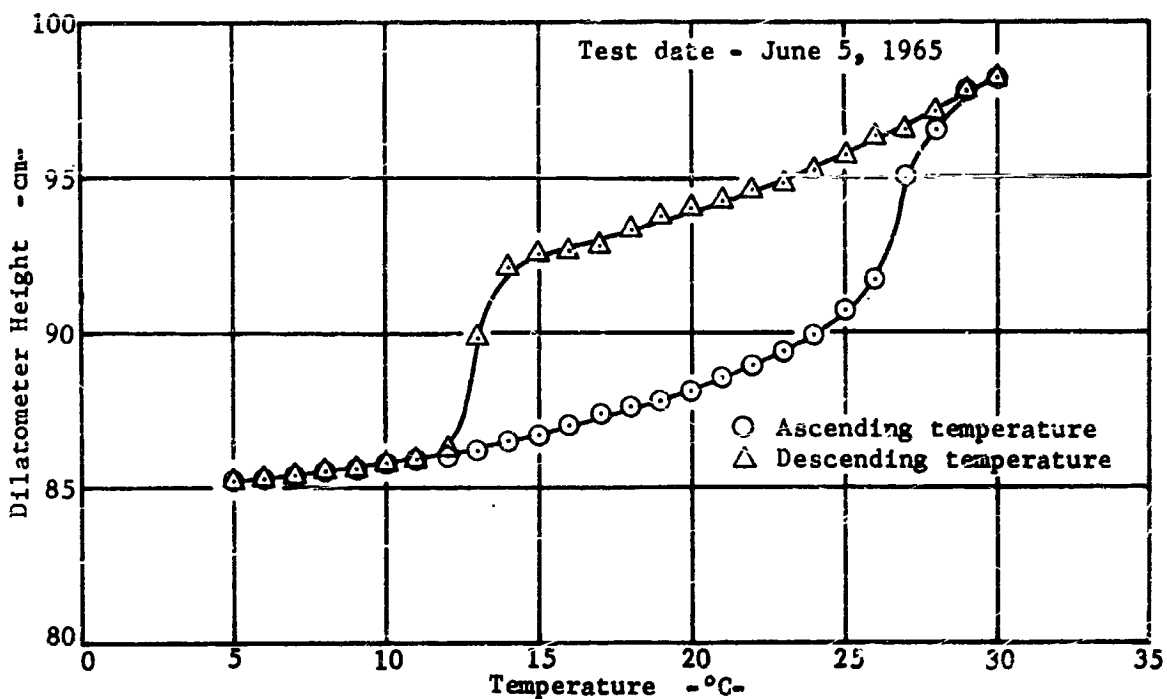


FIGURE 8-7 COOLING-HEATING CYCLE ILLUSTRATING SUPERCOOLING IN AN AQUEOUS n-OCTADECANE DISPERSION (SMALL DILATOMETER).

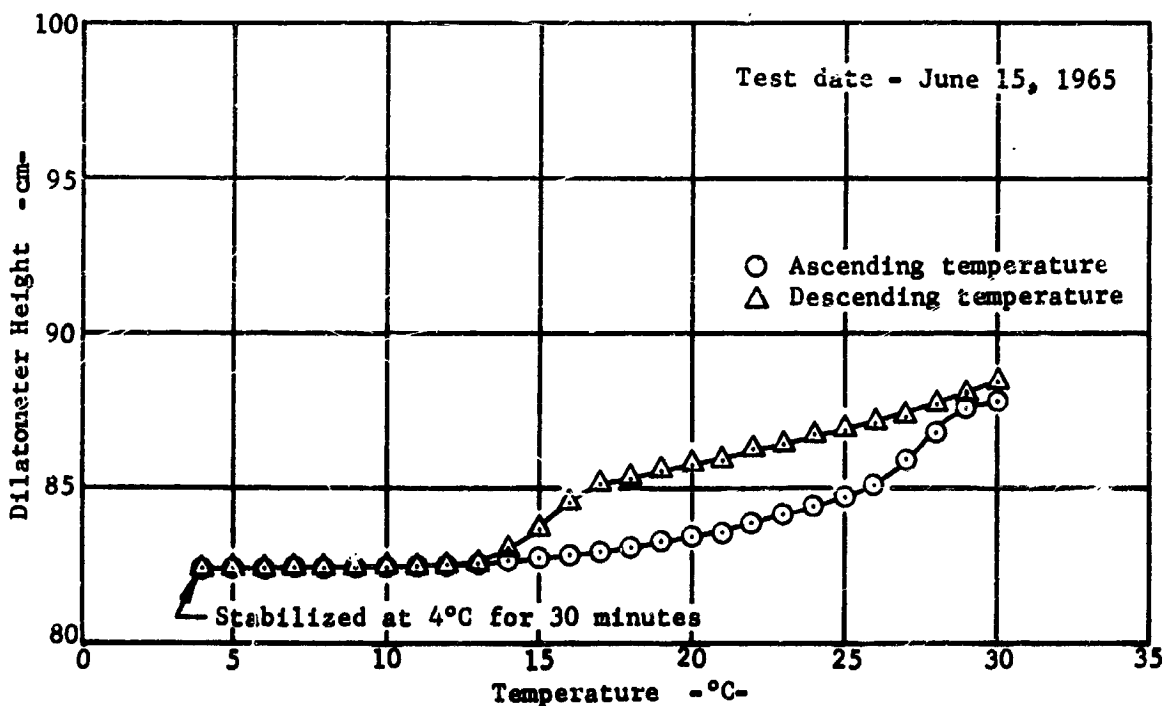


FIGURE 8-8 COOLING-HEATING CYCLE ILLUSTRATING SUPERCOOLING IN AN AQUEOUS n-OCTADECANE DISPERSION (SMALL DILATOMETER). TEST RERUN(FIGURE 8-7)

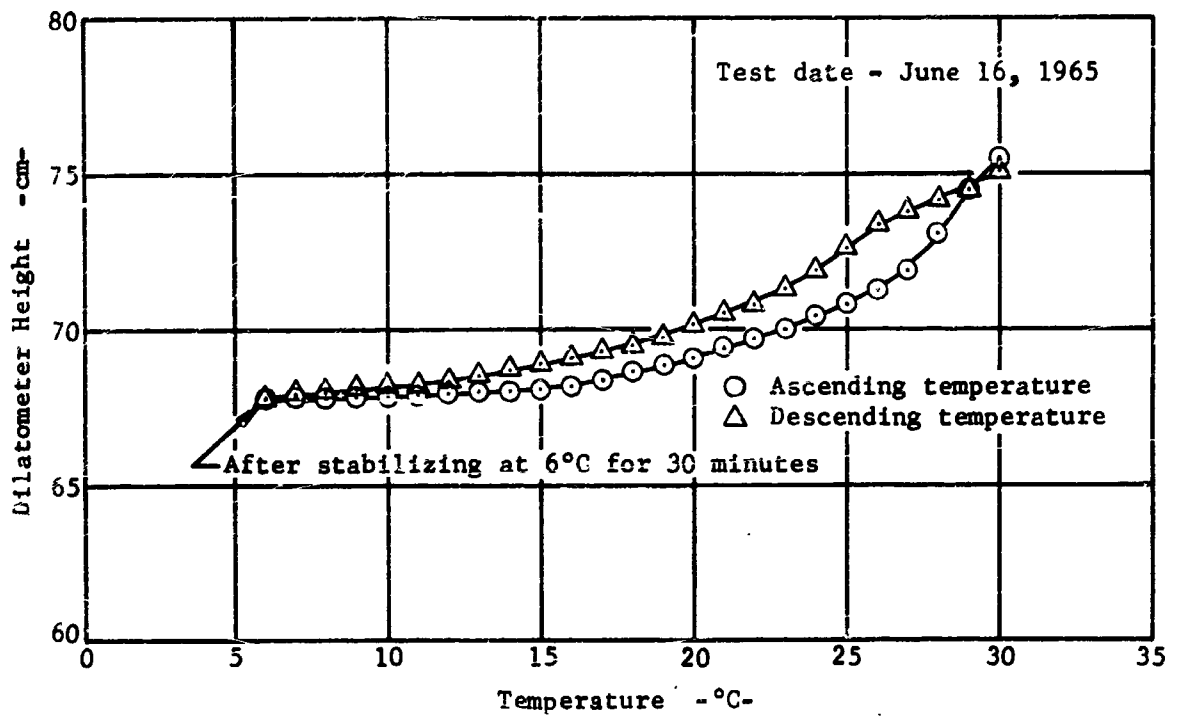


FIGURE 8-9 COOLING-HEATING CYCLE ILLUSTRATING SUPERCOOLING IN AN AQUEOUS n-OCTADECANE + ALUMINUM WOOL DISPERSION (SMALL DILATOMETER).

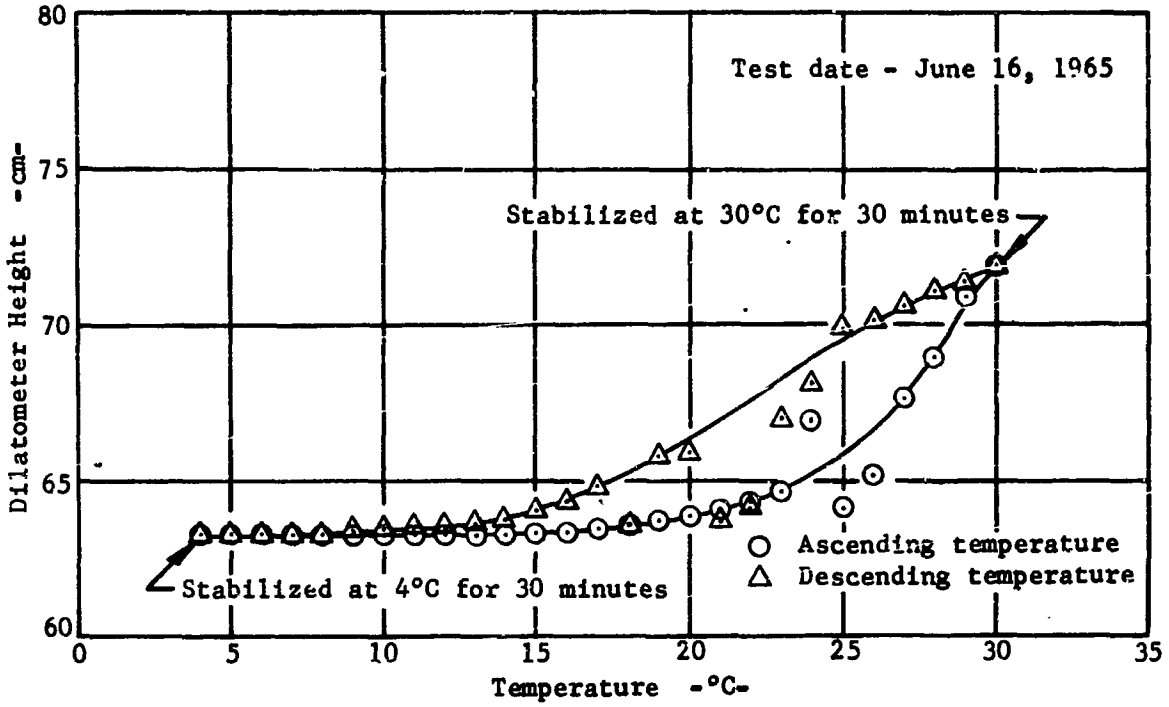


FIGURE 8-10 COOLING-HEATING CYCLE ILLUSTRATING SUPERCOOLING IN AN AQUEOUS n-OCTADECANE + COLLOIDAL SILICA DISPERSION (SMALL DILATOMETER).

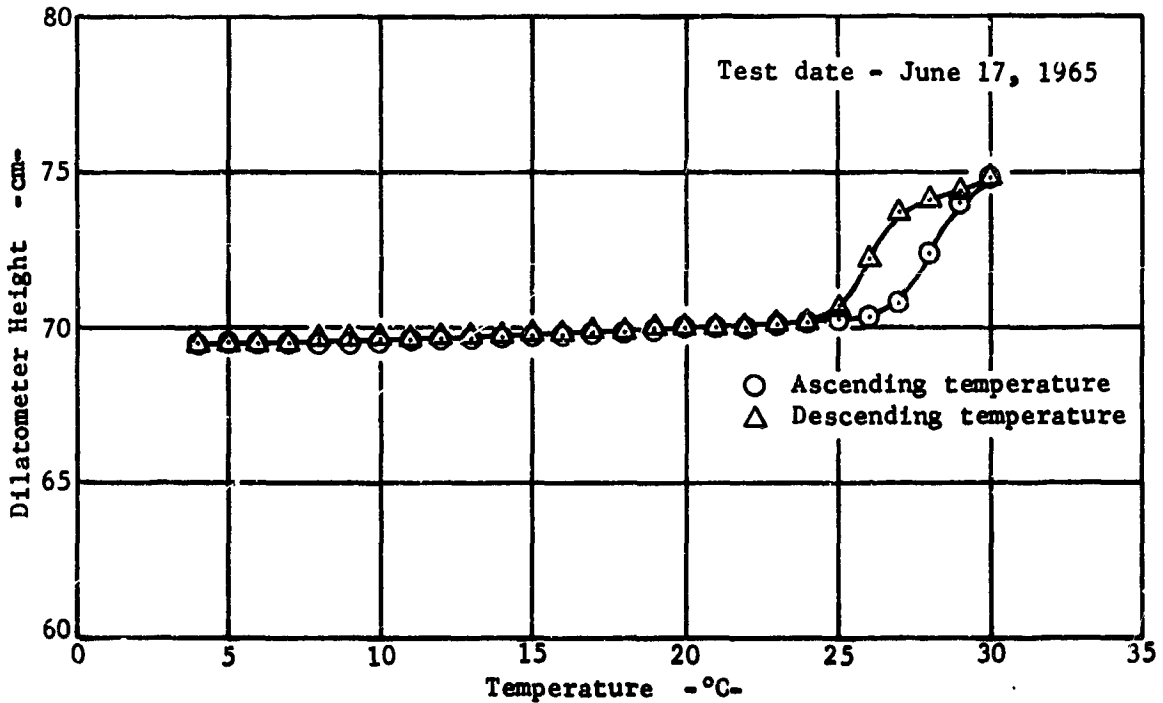


FIGURE 8-11 COOLING-HEATING CYCLE ILLUSTRATING SUPERCOOLING IN AN AQUEOUS n-OCTADECANE + SILICA GEL DISPERSION (SMALL DILATOMETER)

**BLANK PAGE**

## SECTION 9

### PHASE EQUILIBRIA STUDY OF BINARY NORMAL ALIPHATIC HYDROCARBON SYSTEMS

The applicability of the fusible materials concept to thermal control was demonstrated during the analytical and packaging studies. Therefore, an extension of the concept was sought based upon the behavior of binary systems of the normal aliphatic hydrocarbons (paraffins). Hopefully, such binary systems would demonstrate eutectic behavior, thus extending the selection of melting points available in the homologous series of hydrocarbons. For example, a blend of eicosane (m. p. 309°K) and octacosane (m. p. 334°K) in eutectic proportions might give a paraffin mass with a melt point somewhere in the vicinity of 303° - 304°K, thus filling in the melting point gap between octadecane (m. p. 301°K) and eicosane (m. p. 309°K). This same principle could be extended to other binary mixtures of the aliphatic series to give a more inclusive choice of melt points for specific design purposes.

A secondary purpose of such a study would be a better insight into the time-temperature history of such binary systems, with increased understanding of the manner in which thermal energy is released and absorbed during the solid-liquid phase transformation. This information would provide a feeling for the thermal response to be expected from the various mixtures.

#### Experimental Procedure

The system selected for this study was a binary mixture of octacosane ( $C_{28}H_{58}$ ) and eicosane ( $C_{20}H_{42}$ ). It was decided that the behavior of this system would be best illustrated by construction of a temperature-composition phase diagram. If pressure is held constant, this system becomes bivariant in composition and temperature. Since the pressure was constant (atmospheric), it is allowable to represent the system as a two-dimensional figure.

An apparatus was assembled (Figure 9-1) which consists of round glass tubes into which 40-gage thermocouples were introduced through capillary tubes. This allowed positioning of the thermocouples at a fixed height and equidistant from the walls of the glass tubes. The tubes were positioned in a circular pattern in a wooden holder which allowed the array of sample holding tubes to be introduced into a constant temperature bath while being firmly held in position. Thermocouples were provided to monitor the bath temperature at levels in close approximation to the sample levels in the bath.

Binary mixtures of the two component systems at various concentrations were introduced into the glass sample holder tubes in the liquid state after thorough mixing. The

thermocouple junctions were positioned as close to the center of the paraffin mixture as possible, and the melt was allowed to solidify. In all cases, visual observation indicated complete miscibility of the two components in the liquid state at all concentrations and no segregation of components upon solidification.

The binary mixtures were compounded on a percent-by-weight basis, with the total mass of the sample being on the order of  $0.820 \pm 0.005$  grams. It must be stated at this point that when the expression "pure" components is used, it means the composition of the materials as received. No attempt was made to purify the materials, because this study was directed towards an understanding of the engineering applicability of the commercially available even carbon paraffins rather than a detailed investigation of the scientific phenomena surrounding the behavior of very pure materials. As stated previously in Table 3-2, the eicosane used is approximately of 97% purity, while the octacosane is approximately of 96% purity.

Based upon this observation, it should also be noted that the description of the systems as "binary" is also a misnomer, because there are small amounts of materials (neighboring hydrocarbon homologues) in the mixtures other than octacosane and eicosane.

The array of filled sample tubes (Figure 9-1) was lowered into the water bath and heated at a steady rate until all mixtures had completely melted. The temperature of each sample was monitored continuously during the entire heating cycle with a multipoint recorder giving readings at one minute intervals. Once complete melting for all samples had occurred, the bath was cooled at a steady rate to below room temperature with continuous temperature monitoring.

The heating-cooling history of each sample was plotted versus time from the data developed. These curves were the first indication that the behavior of the binary system was complex, rather than being characterized by simple solubility in all proportions in both the solid and liquid state.

### Experimental Results

The cooling curve for pure octacosane (Figure 9-2) exhibits the behavior expected of a pure component. A gradual decline in temperature is noted until the freezing point is reached (approximately  $333^{\circ}\text{K}$ ), at which point a halt in the cooling occurs due to the release of the heat of fusion. Once the heat of fusion has been dissipated, the solid material cools in a linear manner, with the exception of a slight halt attributed to a solid-solid transition point. This phenomenon is more obvious upon examination of the heating curve than it is on the cooling curve.

In like manner, the sharp solidification point of eicosane is illustrated by the cooling curve for eicosane presented in Figure 9-3. No solid-solid transition point is obvious for

the pure eicosane. The liquid eicosane cools until its melting point is reached (approximately 309°K), at which time a halt in the cooling curve is observed. Once the heat of fusion is dissipated, the cooling again resumes its linear relationship to the water bath.

Close examination of the heating curve for octacosane in Figure 9-2 illustrates a halt which occurs at approximately 328°K. As the sample is heated further, a second halt is observed at 333°K. The lower halt has been characterized (Reference 6) and is ascribed to a solid-solid transition in which solid octacosane in the monoclinic crystal form reverts to solid octacosane in the hexagonal crystal form (Reference 7). The heat associated with this transition is on the order of 8.47 kcal/mole. Further heating to 333°K results in the hexagonal crystal form being melted to the liquid state. This is exhibited by the halt at 333°K on the heating curve of Figure 9-2. This heat of fusion is reported to be 15.45 kcal/mole. It is interesting to note that the heat associated with the combined transition and fusion in this relatively small temperature range of about 5°K involves approximately 23.9 kcal/mole of fusible material, while the even numbered carbon paraffins with 20 carbons or less involve only heats on the order of 17 kcal/mole or less to pass from the solid to liquid form in the vicinity of their melting points.

All of the even carbon paraffins between 20 carbons and 32 carbons are known to exhibit this solid-solid transition within 5°K of the melting point. Thus, the ability of these materials to absorb and release heat is based upon both a heat of fusion at the melting point and a transition heat several degrees below the melting temperature. The halt due to the solid-solid transition is not as obvious in the cooling cycle of Figure 9-2, but close examination of the curve occurring after the melting halt shows a "bowed out" configuration, rather than a sharp decline. This is attributed to the solid-solid transition.

If the solid-solid transition is occurring in the series of even carbon paraffins, including eicosane and shorter chain homologues, it has not been observed and does not exhibit itself as an increased heat associated with the transition in the liquid state. Inspection of Figure 9-3 illustrates that the reported absence of a solid-solid transition for eicosane is confirmed by this work.

Once the sensitivity of the described heating-cooling method had been established by comparison of the data obtained from the pure materials with literature values, the method was extended to mixtures of octacosane and eicosane to determine the behavior of this system at various temperatures and concentrations.

Figure 9-4 illustrates the behavior of an 80% octacosane-20% eicosane system when it is cycled through heating and cooling at the same rate as the pure components. Further discussion of the remaining curves will refer to the cooling curves and ignore the heating cycle because the halts are much more consistent and easily distinguished on the cooling curves. The heating curves are more useful for illustrating the heat transfer effects experienced by this class of compounds.

Figure 9-4 shows the upper halt has dropped from 333°K to approximately 330°K. This halt is characteristic of the temperature at which solid octacosane separates from the melt for the concentration under consideration. A less intense halt can also be distinguished at approximately 307°K. This lower halt is due to solidification of solid octacosane plus solid eicosane at the eutectic composition. It is interesting to note the increased area under the lower halt as the composition of the binary system approaches the eutectic composition. The heating curve data confirm the position of both halts, but these data are much more difficult to interpret due to the lack of definition of the halt.

Figure 9-5 shows the curves for a 50% octacosane-50% eicosane binary system. The upper halt has dropped to approximately 323°K, which is the temperature at which the solid octacosane begins to separate from the melt. The eutectic is again obvious at 307°K, and the area under this halt has increased, showing that a larger amount of eutectic mixture is separating at the 50%-50% composition. That more heat is released from the system at 307°K and less at 323°K is illustrated by the relative areas under the halts in Figure 9-5, compared with those in Figure 9-4. A third halt appears at approximately 300°K. This effect is real, because it is evident in subsequent experiments where the composition of the binary mixture contains 30% or more eicosane in the system. The origin of this phenomenon is unknown, but it is thought that it is due to either a solid-solid transition in the solid mixture or the solidification of octadecane impurity in the eicosane. The effect is more pronounced with increasing concentration of eicosane, and occurs at approximately the 301°K melt point of octadecane.

Figure 9-6 illustrates the behavior of a 20% octacosane-80% eicosane composition. Close inspection shows that the upper halt occurs at approximately 311°K and that its area has decreased to practically nothing, while the eutectic is again at 307°K and its area has increased appreciably, indicating the separation of a large amount of the eutectic mixture. The third halt at approximately 300°K is again obvious, and its area has increased.

Figure 9-7 is an illustration of the cooling curve of what appears to be the best approximation to the true eutectic composition. The upper halt has completely disappeared and the eutectic at 307°K is a sharply defined flat curve with an appreciable area under it. The halt at 300°K is again obvious and of appreciable area.

#### Discussion of Results

The heating-cooling technique was repeated in three separate experiments on approximately 30 different compositions of the octacosane-eicosane binary system. Several different heating and cooling rates were tried to determine their effect on the reliability and ease of interpretation of the data developed. A graphic comparison of the effect of heating and cooling rates on the display of the experimental data is illustrated in Figure 9-8. It can be seen that the rate of heating and cooling does not affect the temperature at which the halts appear, but can be an aid in defining the position of halts.

The data obtained from the 30 samples were interpreted in the manner just described for Figures 9-2 through 9-7. The points obtained were used to construct the temperature-composition phase diagram for the octacosane-eicosane binary system presented in Figure 9-9. This phase diagram indicates that a eutectic composition is formed at a composition of approximately 8% octacosane and 92% eicosane. The binary system with this composition melts at approximately 307°K, and this is the lowest that a melt point can be decreased by blending these two paraffins. Thus, the indication is that blending the two components at a eutectic composition will result in a lowering of the melt point by only several degrees. This change of several degrees in the melting point is small justification for using a binary system to adjust the melt point.

Any mixture of the two components, other than the eutectic composition, would tend to absorb and release heat at other than one sharply defined melt point. For applications where it is desirable to have a heat sink over a wide range of temperatures, the binary system may be put to practical use.

An interesting application can be illustrated by examination of the cooling curve of Figure 9-5 (50% octacosane-50% eicosane). In an application where it is desirable to limit the temperature of a system to a relatively narrow temperature range (such as between 307°K and 322°K), a 50% octacosane-50% eicosane mixture might be used. Figure 9-5 illustrates that approximately equivalent total quantities of heat are absorbed or released at both 307°K (eutectic) and 322°K (solid octacosane plus solution halt). A system packaged with such a composition would tend to be bracketed between these temperature limits due to the halts and associated heats of fusion and transition which are exhibited at these temperatures. By proper choice of paraffins and compositional mixtures, an infinite number of upper and lower limits can be selected for control by the fusible materials concept. It is realized, of course, that applications to high heat impulse systems will be proportionally reduced due to the "splitting up" of the available heats of fusion and transition between two halt temperatures. This reduced efficiency can be circumvented by increasing the mass of the fusible material mixture, if feasible from the heat transfer aspect. One advantage of this system that becomes immediately obvious is the elimination of multiple packaging techniques to effect the same results.

Whether a binary system of the other normal paraffins in the series under consideration would behave in a like manner could not be deduced from the results of the octacosane-eicosane binary system. Knowledge of the chemical and physical behavior of the paraffins would indicate that the same behavior should predominate over a wide range of homologues (with the exception of solid-solid transitions observed in members above  $C_{20}$ ). This observation is based upon the assumption that there are no chemical reactions between components of the binary systems thus forming ternary systems.

To confirm the prediction that other systems should behave in a similar manner, a binary system of eicosane ( $C_{20}H_{42}$ ) and octadecane ( $C_{18}H_{38}$ ) was studied in less detail,

using the heating-cooling curve method for various concentrations of the two components. This system again exhibited a eutectic at a composition of approximately 10% eicosane to 90% octadecane, with a melting point of approximately 299°K.

Based upon observation of the two binary system studied, it appears that other combinations of the series of even carbon paraffins should yield eutectics displayed towards the side of the phase diagram richer in the lower melting component. It is doubtful that any eutectic composition of this series will yield more than a 2 to 3°K reduction in melting point below the melt point of the lower melting component.

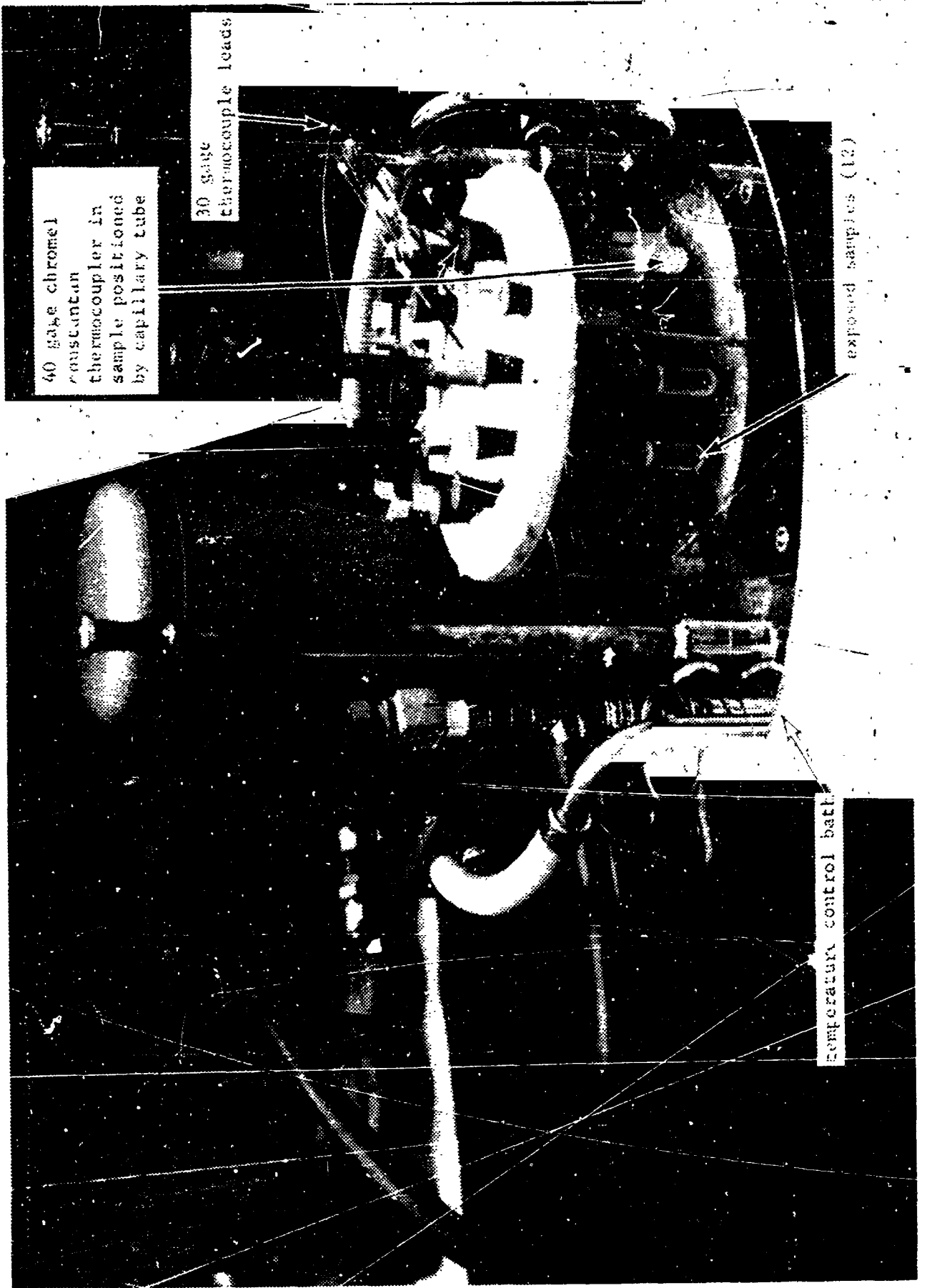


FIGURE 9-1. EXPERIMENTAL APPARATUS FOR SOLUTION AND PHASE EQUILIBRIA STUDY

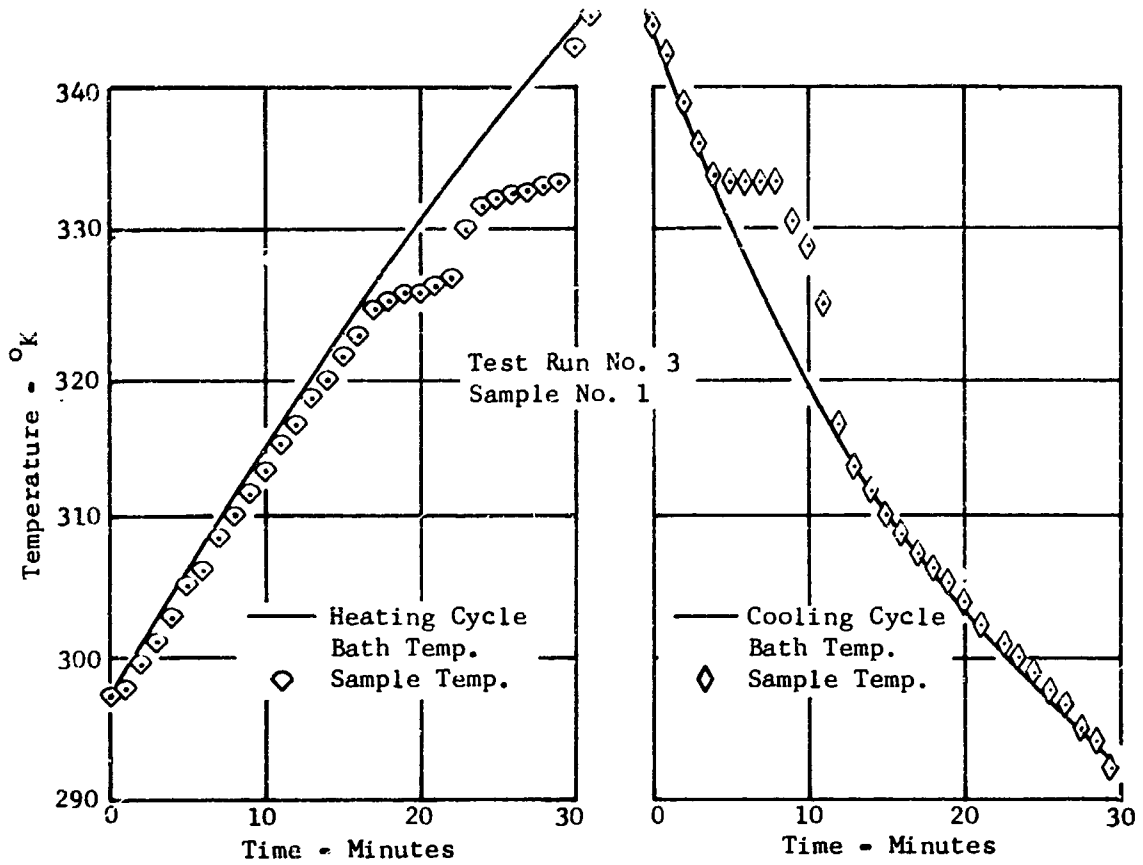


FIGURE 9-2 HEATING-COOLING CURVES FOR PURE OCTACOSANE

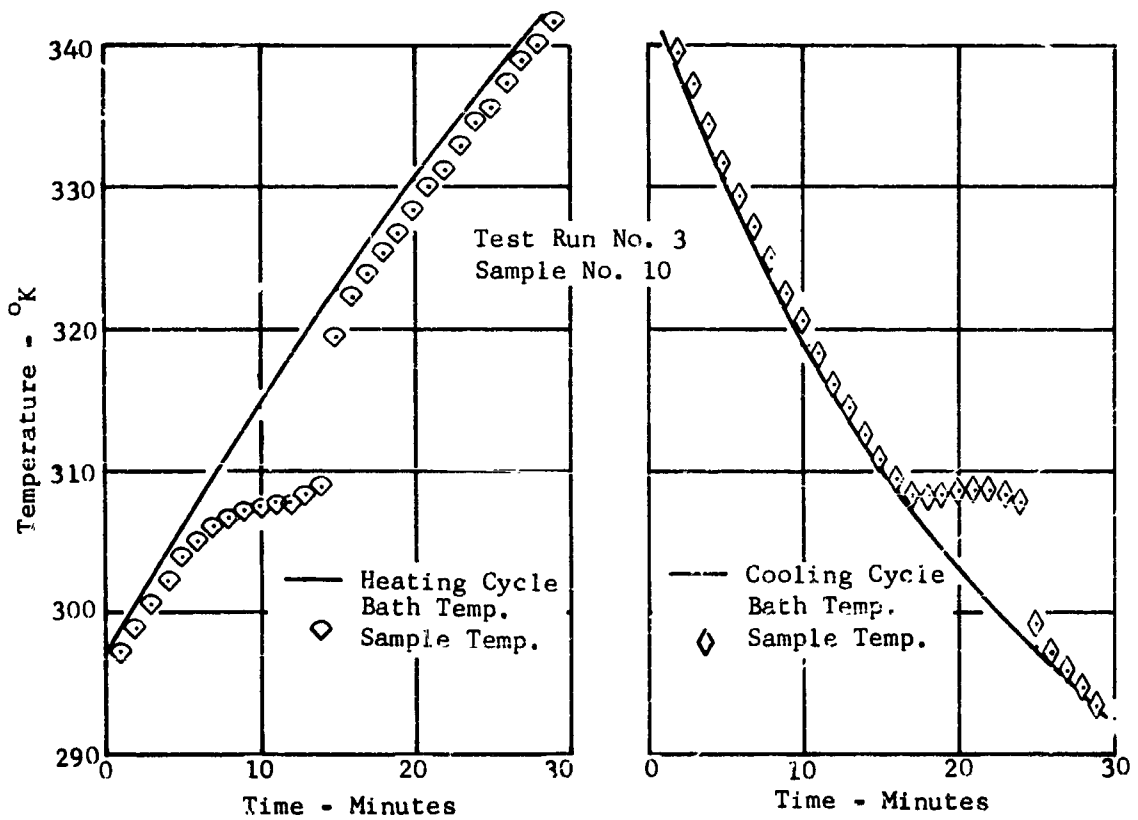


FIGURE 9-3 HEATING-COOLING CURVES FOR PURE EICOSANE

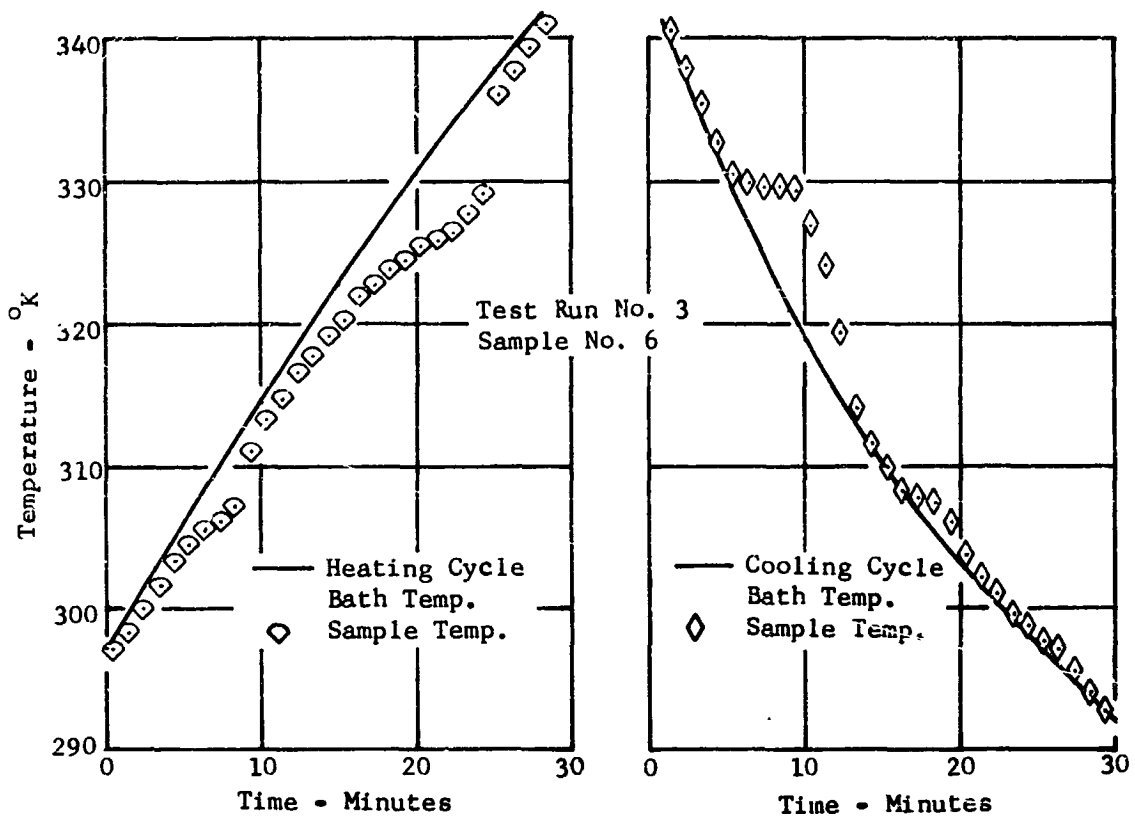


FIGURE 9-4 HEATING-COOLING CURVES FOR 80% OCTACOSANE-20% EICOSANE BINARY SYSTEM

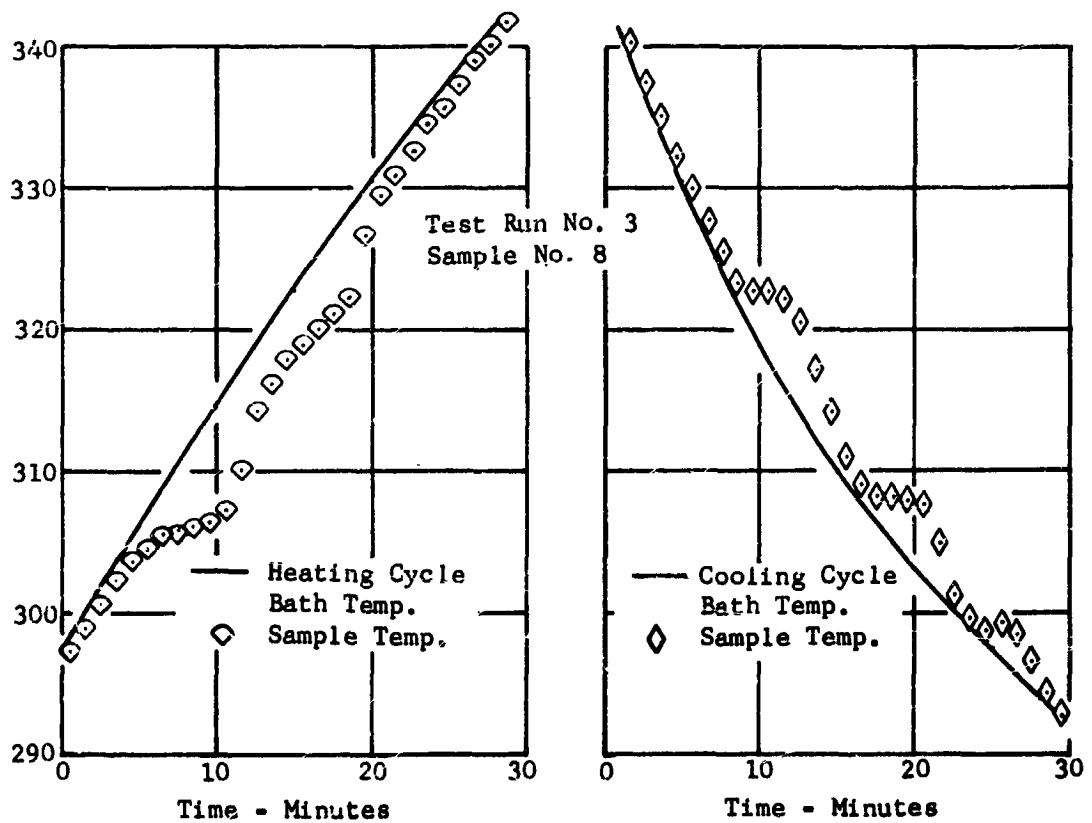


FIGURE 9-5 HEATING-COOLING CURVES FOR 50% OCTACOSANE - 50% EICOSANE BINARY SYSTEM

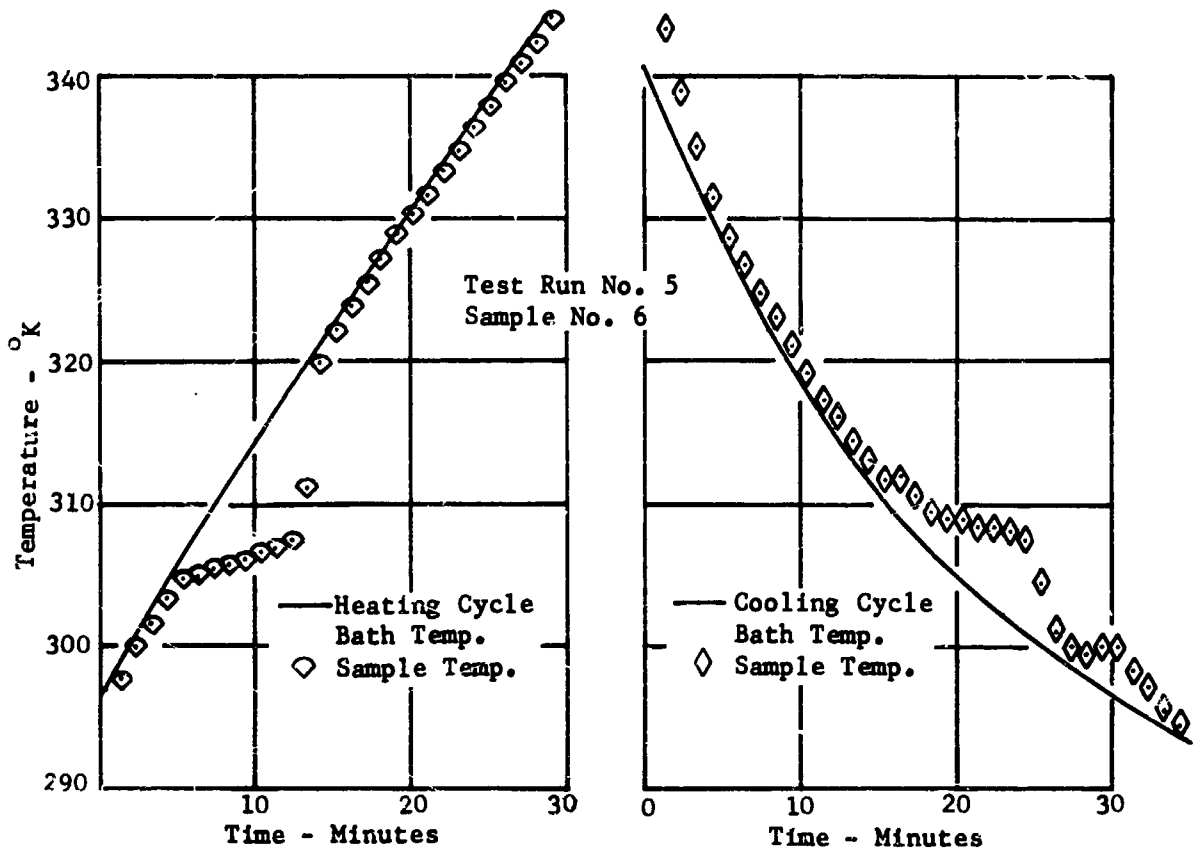


FIGURE 9-6 HEATING-COOLING CURVES FOR 20% OCTACOSANE-80% EICOSANE BINARY SYSTEM

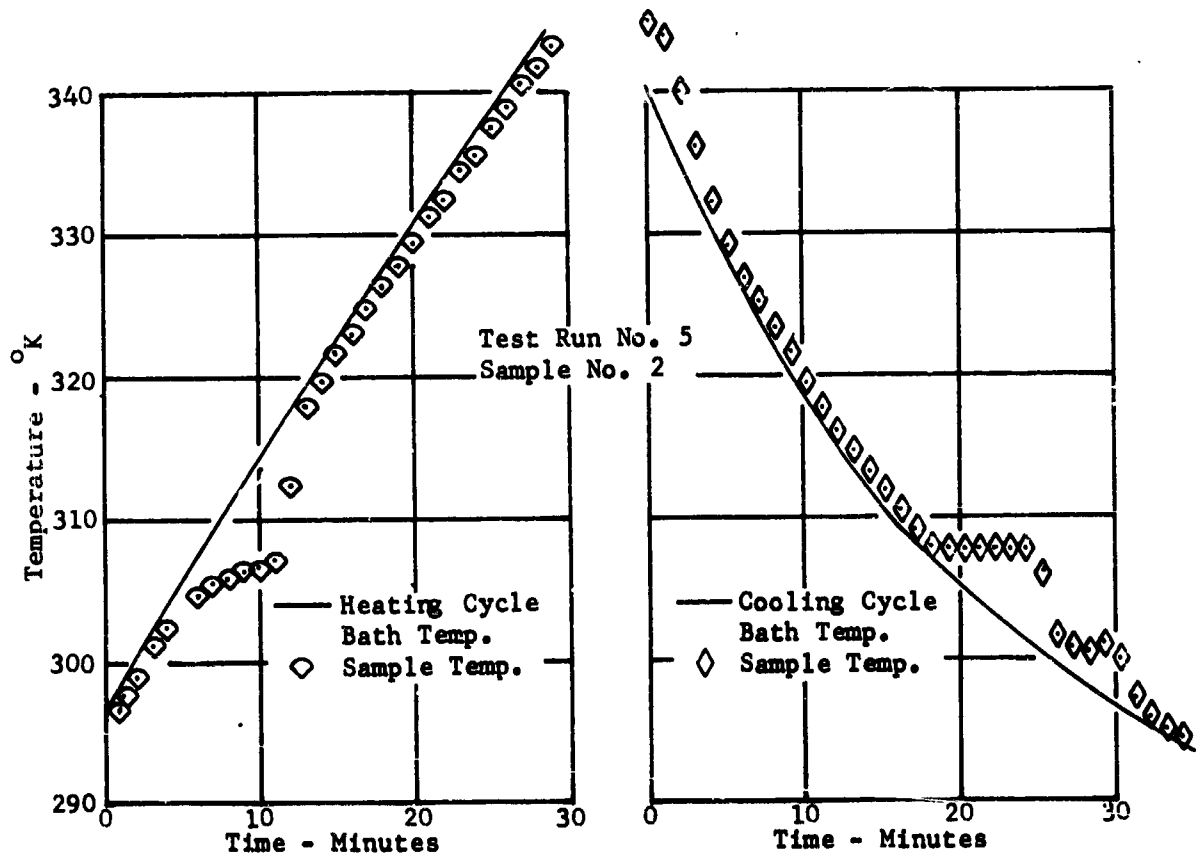


FIGURE 9-7 HEATING-COOLING CURVES FOR 8% OCTACOSANE - 92% EICOSANE BINARY SYSTEM

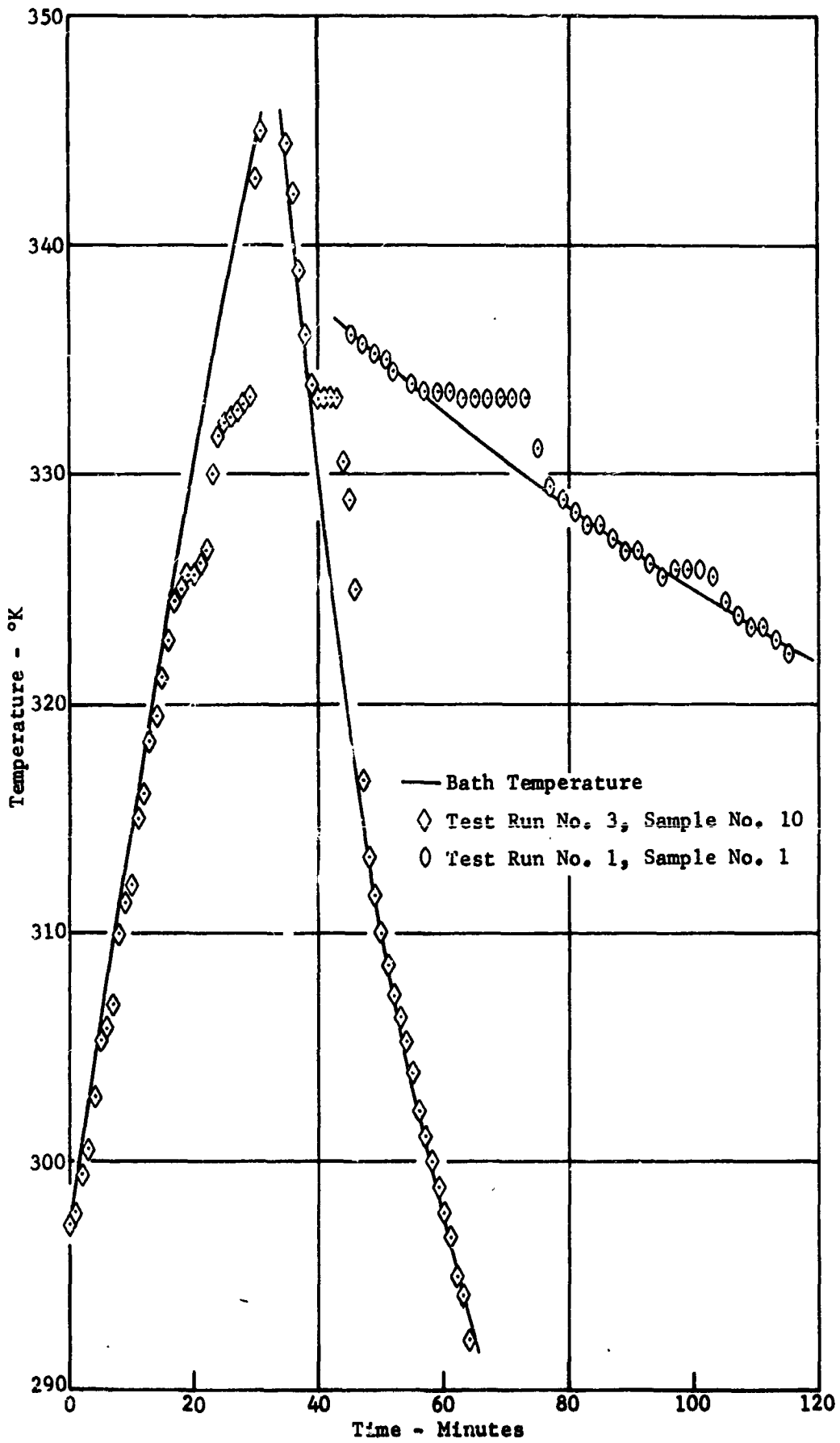


FIGURE 9-8 BEHAVIOR OF PURE OCTACOSANE AT ONE HEATING RATE AND TWO COOLING RATES

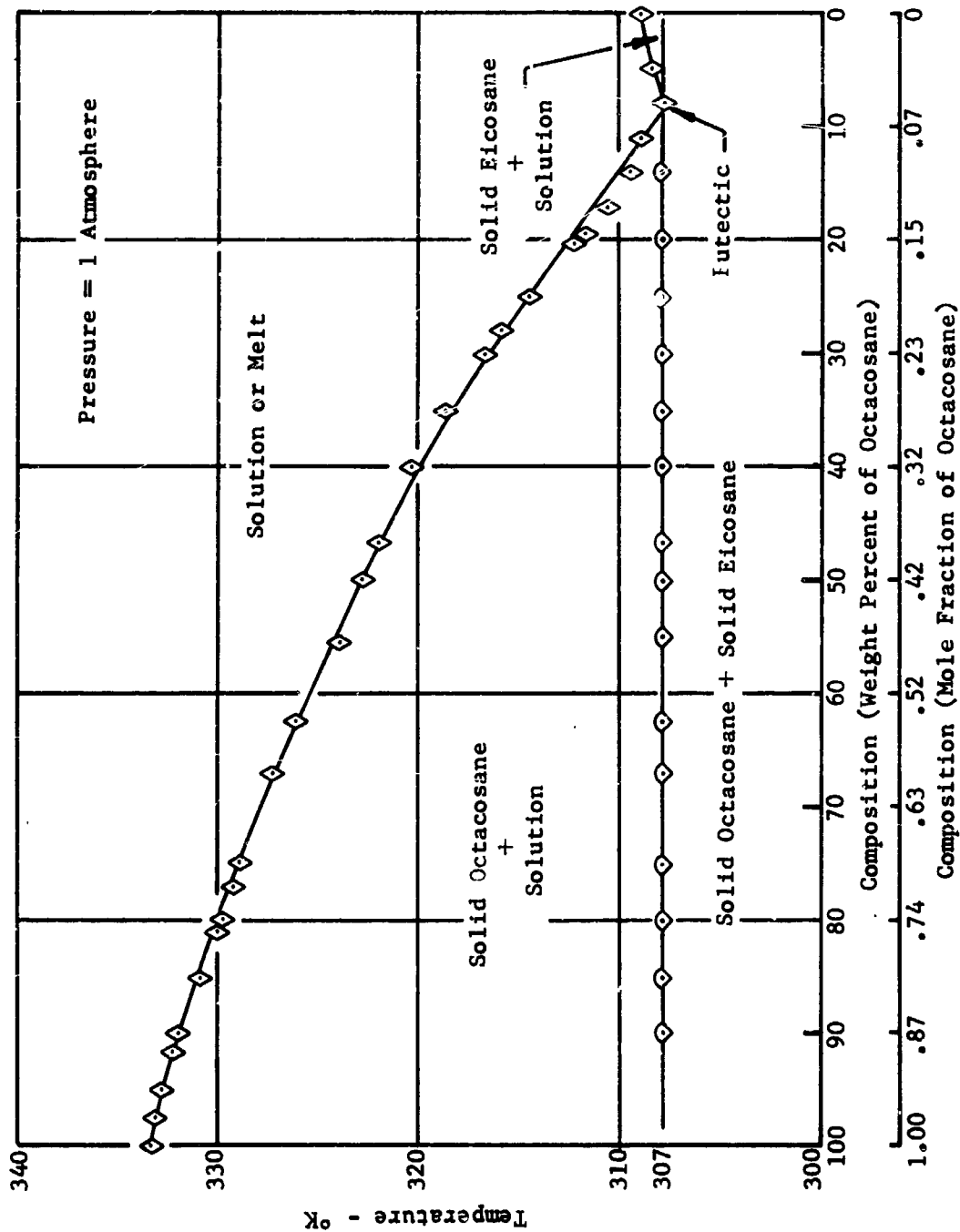


FIGURE 9-9 TEMPERATURE-COMPOSITION PHASE DIAGRAM FOR THE OCTACOSANE-EICOSANE BINARY SYSTEM

## SECTION 10

### CONCLUSIONS AND RECOMMENDATIONS

The feasibility of using fusible materials for spacecraft subsystem temperature control has been demonstrated. Incorporation of fusible material heat sinks in temperature control systems can greatly increase the systems' thermal inertia and reduce temperature excursions caused by high density power pulses. When a sufficient regeneration time period and an ultimate heat sink (i. e., dark space) are available, the use of fusible materials could eliminate the requirement for an active temperature control system. When an active system is required, the use of fusible materials can reduce the temperature excursion so that the active system can be sized for a nominal power profile.

#### Temperature Control Systems

The developed adiabatic packaging techniques should be extended to higher total energy levels, greater package depths, and greater heat transfer fin lengths. The limit of useful total energy absorption by this technique depends on the allowable weight penalties, temperature rise, and power density. In this study, a total energy absorption level of 3,000 watt-min/ft<sup>2</sup> (32,000 watt-min/m<sup>2</sup>) has been demonstrated with a cold plate temperature rise of 10°K. With a cold plate rise of less than 15°K, a total energy of 10,000 watt-min/ft<sup>2</sup> (108,000 watt-min/m<sup>2</sup>) at 100 watts/ft<sup>2</sup> (1,080 watts/m<sup>2</sup>) and of 5,000 watt-min/ft<sup>2</sup> (53,900 watt-min/m<sup>2</sup>) at 500 watts/ft<sup>2</sup> (5,390 watt/m<sup>2</sup>) appears feasible. The experimental results presented in this report should be analyzed in an attempt to fit the data to an analytical fin-effectiveness model. This model should be used to predict effective fin geometries at greater fin lengths, and these geometries should be verified by experimental models.

The incorporation of the developed packaging techniques should be applied to additional passive temperature control techniques, as shown in Figure 10-1. The system with the fusible material package between the radiator and the heat dissipating equipment appears feasible and practical with a honeycomb filler material.

The incorporation of the fusible material-honeycomb package to active temperature control systems (Figure 10-2) shows promise and should be investigated.

Space-quality hardware should be developed and flight-tested so that the technique can be incorporated in spacecraft design with a high level confidence. The system with the fusible material-honeycomb package between the heat source and a thermal radiator appears

to be the most practical for a flight experiment. This system (Figure 10-1) will regenerate by thermal radiation. Therefore, numerous test runs can be made with no support functions except a programmed heat source (power supply for a heater) and temperature monitoring and telemetry services.

The tests should be programmed so that the first test runs do not cause complete liquefaction, but leave crystals to assist in resolidification. The final tests should cycle through the complete liquefaction period to determine the effect of zero g on the liquefaction and resolidification cycle of the particular fusible material and packaging system. A temperature-controlled power shutoff switch could override the programmed power schedule in case the fusible material did not resolidify. A normal paraffin is recommended as the test fusible material.

The system performance can be determined from the power and temperature history if the spacecraft orbit and attitude history are known with reasonable accuracy. The data would have to be telemetered to a ground station.

#### Crystal Growth Phenomena and the Effects of Zero Gravity

For thermal control with the use of fusible materials to be reliable, crystal growth must be obtained each time sufficient heat is removed from a melt. Some degree of supercooling is inherently necessary for the nucleation and growth of crystals. The amount of supercooling required depends upon the particular fusible material and the environment surrounding the material. Many materials under normal gravity supercool so very slightly that no problem exists for thermal control applications. Others (e. g., gallium) supercool to such a degree that their efficiency as a thermal control medium is reduced.

The best method to reduce supercooling in a material which normally tends to supercool to a large degree is to ensure that the original crystalline material never completely melts; thus, crystalline "seeds" will be present in the melt to nucleate the solid, crystalline phase again as heat is removed.

However, one cannot be sure that in an actual space application only partial melting of the solid will occur, and thus, a priori one should choose materials which supercool only slightly as a result of their inherent nature or from seeding with substances which will assist in initiating the nucleation and growth of crystals.

As explained in Section 8, nucleation and the growth of crystals are complex phenomena whose mechanisms under weightless conditions are difficult to predict intelligently. The obvious way to determine which materials supercool excessively is through the performance of actual flight experiments. Experiments at weightless conditions should be performed in such a way that the actual size and habit of the growing crystals can be witnessed by a trained observer.

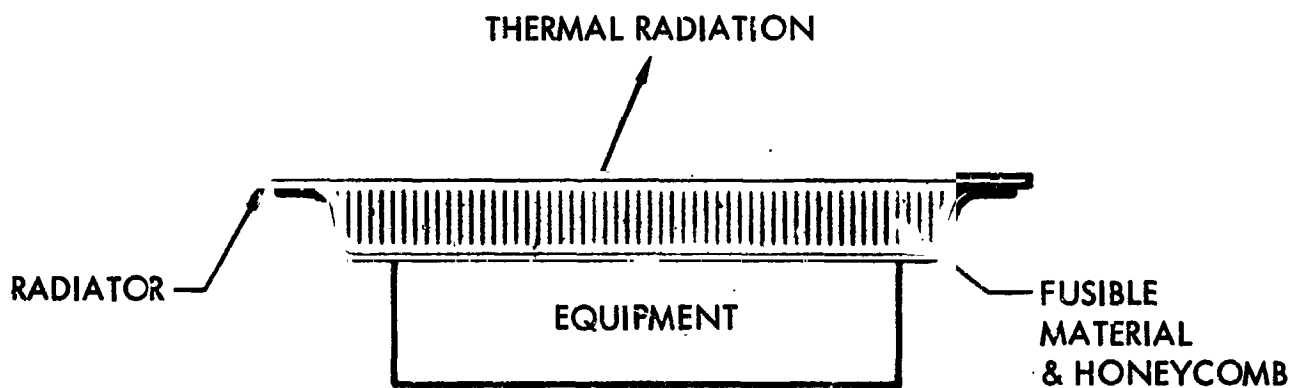
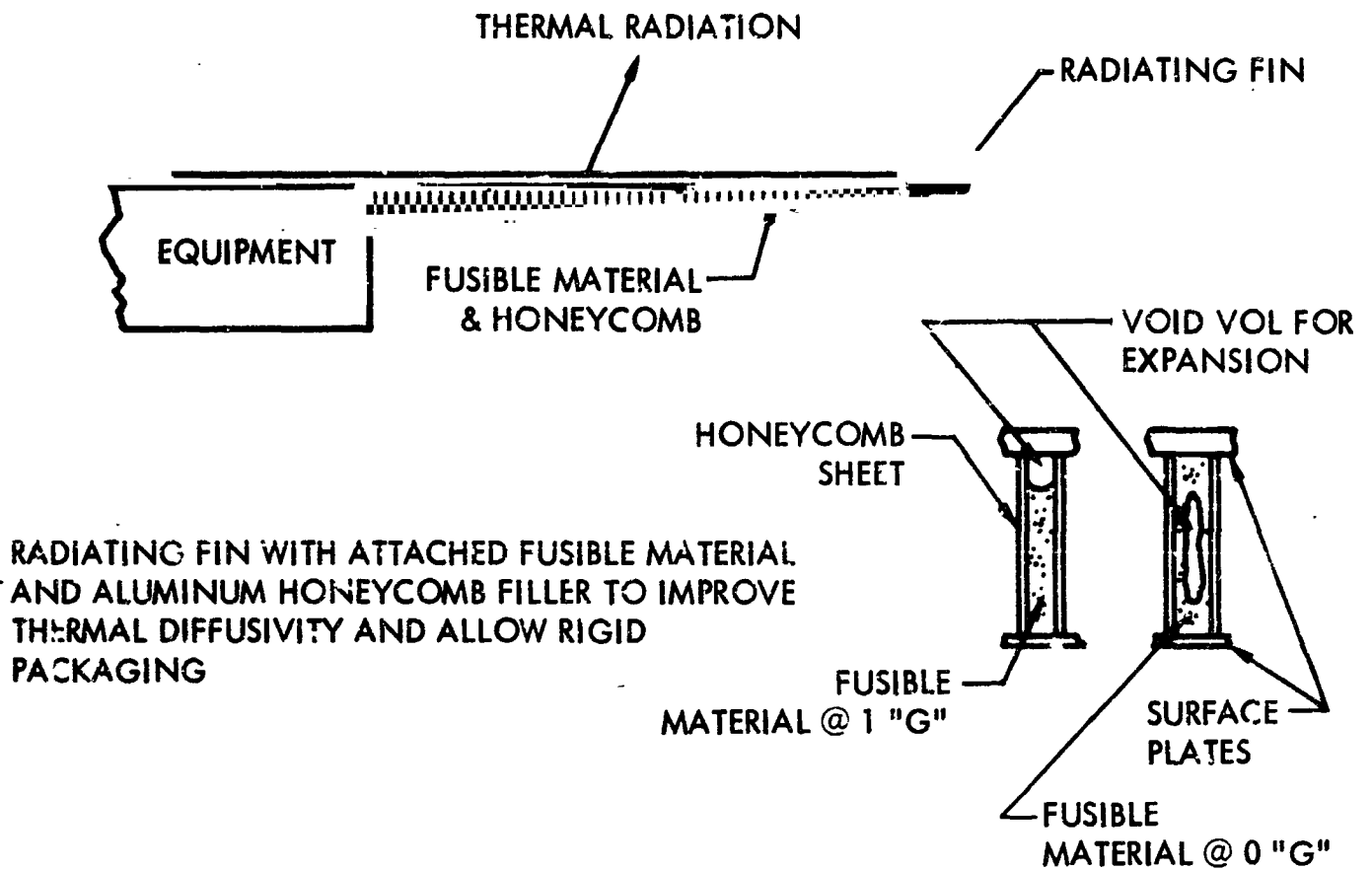
## Applicable Fusible Materials

The applicability of the normal paraffins to passive thermal control systems in both the pure form and as mixtures has been demonstrated by phase equilibria studies. These materials demonstrate a eutectic temperature several degrees below the melting point of the lowest melting component and a variable temperature of maximum heat absorption and release dependent upon the composition of the mixtures. This variable heat release temperature and eutectic can be put to practical use in both passive thermal control in space applications, such as temperature control of electronic components, and in commercial applications, such as the control of shipping packages and reaction vessels which are subjected to rapid exotherms during chemical reactions.

Availability of technical grade paraffin mixtures (Atlantic Refining Company) can be put to practical use if the effects of the presence of neighboring homologues on the thermophysical properties of the paraffins are characterized. Since the pure paraffins are quite expensive, large quantities of technical grade material that has been appropriately doped to achieve the desired properties can be used to reduce the cost of applying this concept.

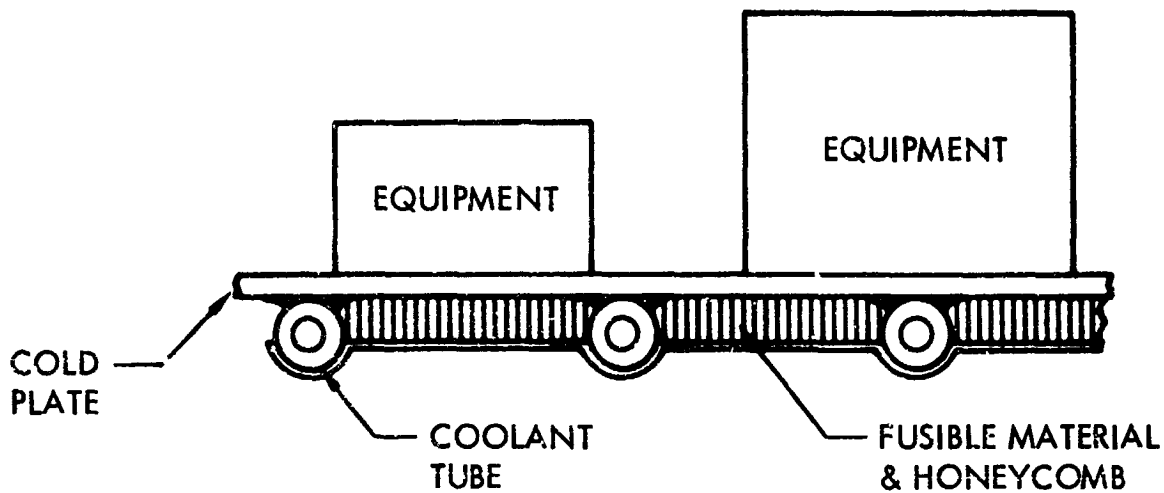
Studies of paraffin mixtures must be conducted to establish the behavior of these materials when they are compounded in different proportions. The selection of fusible materials should be extended to a study of the possible inorganic compounds which may be applicable and, if feasible, extended to mixtures of organics and inorganics. Other series of homologous organics may also find application to specific requirements.

Since the fusible materials concept shows promise for passive thermal control in space, the effects of zero gravity upon both the pure components and the mixtures should be investigated.

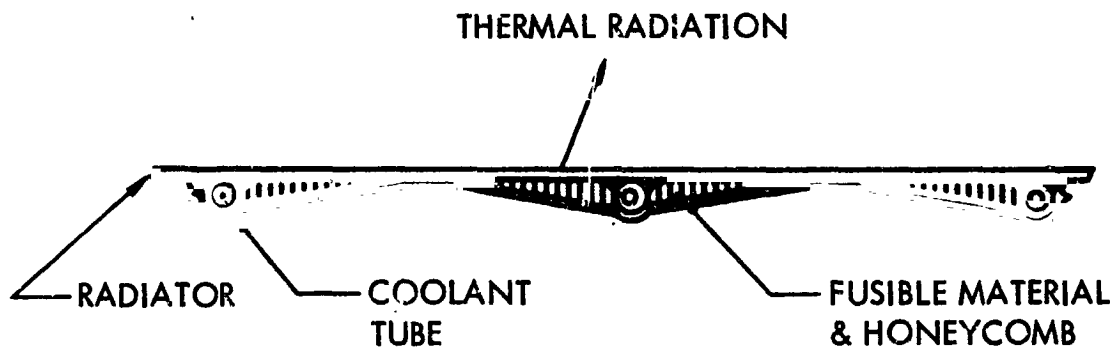


**RADIATOR WITH EQUIPMENT MOUNTED DIRECTLY UNDER FUSIBLE MATERIAL LAYER. HONEYCOMB SHEET THICKNESS IS SLIGHTLY OVERSIZED TO ALLOW GOOD HEAT TRANSFER TO THE THERMAL RADIATOR. THE FUSIBLE MATERIAL GREATLY INCREASES THE SYSTEM'S THERMAL INERTIA.**

**FIGURE 10-1 APPLICATIONS OF THE IMPROVED FUSIBLE MATERIAL - HONEYCOMB - ADIABATIC - PACKAGE TO OTHER PASSIVE TEMPERATURE CONTROL TECHNIQUES**



LIQUID COOLED EQUIPMENT COLD PLATE WITH ATTACHED FUSIBLE MATERIAL TO ABSORB HIGH ENERGY POWER PULSATIONS



ACTIVE THERMAL SPACE RADIATOR, THE FUSIBLE MATERIAL SUPPLEMENTS THERMAL RADIATION DURING HIGH HEAT DISSIPATION PERIODS. THIS MINIMIZES VARIATION IN COOLANT OUTLET TEMPERATURE.

FIGURE 10-2 APPLICATIONS OF THE IMPROVED FUSIBLE MATERIAL - HONEYCOMB - ADIABATIC PACKAGE TO ACTIVE TEMPERATURE CONTROL SYSTEMS TO DECREASE TEMPERATURE EXCURSIONS AND ALLOW SYSTEMS TO BE DESIGNED FOR NOMINAL POWER LEVELS

**BLANK PAGE**

## REFERENCES

1. Shlosinger, A. P.; and Bentilla, E. W.: Research and Development Study on Thermal Control by Use of Fusible Materials, Interim Report. Report NSL 65-16, Northrop Space Laboratories, Feb. 1965.
2. Kaye, J.; Fand, R. M.; Nance, W. G.; and Nickerson, R. J.: Final Report on Heat Storage Cooling of Electronic Equipment. WADC TR 56-473, MIT, Feb., 1957.
3. Development of High Capacity Heat Storage Materials. Report 380, MIT, Instrument Lab/Cryo. Therm., Inc.
4. Selected Values of Physical and Thermodynamic Properties of Hydrocarbons and Related Compounds. American Petroleum Institute Research Project 44, Carnegie Press, Pittsburgh, Pa., 1953.
5. Hodgman, C. D., ed.: Handbook of Chemistry and Physics. Forty-second ed., The Chemical Rubber Publishing Co., Cleveland, Ohio, 1960-61.
6. Broadhurst, M. G., Jr.: An Analysis of the Solid Phase Behavior of the Normal Paraffins. Vol. 66A, No. 3, J. Res. Natl. Bur. Std., May-June 1962.
7. Schaerer, A. A.; Basso, C. J.; Smith, A. E.; and Skinner, L. B.: Properties of Pure Normal Alkanes in the C<sub>17</sub> to C<sub>36</sub> Range. Chemical Society 77, 1955.
8. International Critical Tables of Numerical Data, Physics and Technology. McGraw-Hill Book Co., Inc., New York, 1933.
9. Sakiadis, B. C.; and Coates, J.: Studies of Thermal Conductivity of Liquids, Part III. A. I. Ch. E. J. 3, 1957.
10. Frick, J. L.: SHARE Program, MLETHAN-LMSC Thermal Network Analyzer, 7090 Fortran. Lockheed Missiles and Space Company, 1962.
11. Thomas, L. J.; and Westwater, J. W.: Microscopic Study of Solid-Liquid Interfaces During Melting and Freezing. Chem. Eng. Progress Symposium Series, U59-No49, 1963.
12. Mackay, D. P.; and Bacha, C. P.: Space Radiator Analysis and Design. ASD TR 61-30, Part 1, October, 1961.
13. Tatom, J. W.: Steady-State Behavior of External Surfaces in Space. ARS Journal, Jan. 1960.

14. Eckert, E. R. G.; and Drake, R. M., Jr.: Heat and Mass Transfer. McGraw-Hill Book Co., New York, 1959.
15. Chalmers, B.: Principles of Solidification. John Wiley & Sons, Inc., New York, 1964.
16. Jackson, K. A.: Nucleation From the Melt. Ind. Eng. Chem. 57 (12), 28-32 (1965).
17. Uhlmann, D. R.; and Chalmers, B.: The Energetics of Nucleation. Ind. Eng. Chem. 57 (9), 18-31 (1965).
18. Turnbull, D.: The Undercooling of Liquids. Sci. Am. 212 (1), 28-46 (1965).
19. Turnbull, D.: Phase Changes. Solid State Physics 3, 225-306 (1956).
20. Avrami, M.: Kinetics of Phase Change: I. General Theory. J. Chem. Phys. 7, 1103-1112 (1939).
21. Avrami, M.: Kinetics of Phase Change: II. Transformation-Time Relations for Random Distribution of Nuclei. J. Chem. Phys. 8, 212-224 (1940).
22. Turnbull, D.; and Fisher, J. C.: Rate of Nucleation in Condensed Systems. J. Chem. Phys. 17, 71-73 (1949).
23. Jackson, K. A.; and Chalmers, B.: Unpublished work. Ultrasonics applied to solidification and solid state transformation
24. Jones, J. B.: Ultrasonics Applied to Solidification and Solid State Transformation, AF-TR 6675 (1951).
25. Rostoker, W.; and Berger, M. J.; Effects of Vibration during Solidification of Castings, Foundry 81 (7), 100 (July 1963)
26. Turnbull, D.; and Cormia, R. L.: Kinetics of Crystal Nucleation in Some Normal Alkane Liquids, J. Chem. Phys. 34, 820-831 (1961).